UNIVERSITY OF BERGAMO

Department of Engineering and Applied Sciences

Ph.D. Program in "Engineering and Applied Sciences"

XXIX CYCLE

ICAR/09

Evaluation of the Expected Annual Loss for Precast Concrete Industrial Structures

Fabrizio Cornali

Advisor:
Prof. Paolo Riva

Co-advisor:
Andrea Belleri, Ph.D.

2017

UNIVERSITY OF BERGAMO
PhD Program in "Engineering and Applied Sciences"
XXIX cycle
ICAR/09

UNIVERSITÀ DEGLI STUDI DI BERGAMO
Dottorato di ricerca in Ingegneria e Scienze Applicate
XXIX ciclo
ICAR/09

Prof. Valerio Re (Coordinator)

Author: Fabrizio Cornali
Title: Evaluation of the Expected Annual Loss for Precast Concrete Industrial Structures

SYNOPSIS

During the last few years, several analyses and scientific studies were conducted on existing buildings in terms of economic damages and losses on the affected buildings. These studies showed the importance of the rate of recovery costs associated to the damages of the non-structural elements (or secondary elements) and/or the contents of the building. Especially in the industrial field, in almost all cases the monetary value of the facilities and the internal installations is far greater than the value of the bare structure. Just think about the damages suffered by many companies spread in the Emilian territory following the recent earthquakes that occurred in May, 2012.

The main purpose of the current research is framed in this scenario. To achieve this goal, a simple and reliable method capable of allowing an accurate estimation of the economic losses linked to the damage caused by earthquakes on precast reinforced concrete industrial buildings is developed.

Within this project, different models of computation are critically studied and analysed. All of these methods are based fundamentally on a probabilistic and interdisciplinary approach, which incorporates: the hazard analysis of the site, the structural analysis, the damage analysis and the loss analysis suffered by each vulnerable component. Starting from the most refined PEER PBEE methodology, this research has led to the development of two more simplified and speedy procedures, one based on a displacement method for performing the structural analysis and the second method uses a closed formula as an alternative to the refined PEER PBEE methodology.

The use of such procedures requires the identification of the most common vulnerabilities detectable in precast reinforced concrete buildings, as well as the knowledge of the fragility and the cost curves for all the vulnerable elements which can give rise to possible damages and then the monetary losses.

Actually, the seismic response of the non-structural elements in precast reinforced concrete buildings and the interaction of the same with the global response of the structure is not completely defined and in some cases, it has never been investigated. Therefore, very often the fragility and the cost curves of the elements are not available: this is one of the reason why it is the subject of the most recent research studies. From this, the interest to inquire about the seismic response of the out-of-plane performance of the horizontal cladding panels was born. In addition, the

influence of the overhead crane in the seismic response of precast buildings is also analysed.

SOMMARIO

Nel corso degli ultimi anni sono state condotte analisi e ricerche scientifiche riguardanti l'effetto che i fenomeni sismici hanno in termini di danni economici sulle opere colpite. Da questi studi è emersa l'importanza rivestita dall'aliquota di costo relativa al ripristino de i danni associati agli elementi non-strutturali (o secondari) e/o al contenuto dell'edificio. Questo vale specialmente nel settore industriale in cui, nella quasi totalità dei casi, il valore monetario degli impianti e delle installazioni interne è di gran lunga maggiore rispetto al valore della nuda struttura. Si pensi ad esempio ai danni subiti dalle numerose aziende diffuse nel territorio Emiliano a seguito dei recenti eventi sismici avvenuti nel Maggio del 2012.

In questo scenario si inserisce lo scopo principale della presente ricerca, ossia quello di sviluppare una metodologia semplice e affidabile in grado di consentire una stima precisa delle perdite economiche legate ai danni subiti dai terremoti, con particolare riferimento agli edifici prefabbricati industriali.

All'interno di questo progetto sono analizzati differenti modelli basati su un approccio probabilistico interdisciplinare che accorpa in sé: l'analisi della pericolosità del sito su cui sorge l'edificio, l'analisi della risposta strutturale, l'analisi del danno subito e la valutazione del costo associato per ogni componente vulnerabile. Partendo dai modelli di calcolo più raffinati, quali il PEER PBEE, si è giunti infine alla messa a punto di due procedure più semplificate e rapide, l'una basata su un approccio agli spostamenti per l'analisi strutturale e l'altra sull'impiego di una formulazione in forma chiusa in alternativa alla procedura raffinata.

L'impiego di tali procedure, richiede dapprima l'identificazione delle più comuni vulnerabilità caratterizzanti e riscontrabili negli edifici prefabbricati industriali e successivamente la conoscenza delle curve di fragilità e di costo per tutti gli elementi che possono dare origine ad eventuali perdite economiche.

Ad oggi però, la risposta sismica degli elementi non strutturali in edifici prefabbricati e l'interazione degli stessi con la risposta globale della struttura non è completamente definita ed in alcuni casi non è mai stata indagata, per tale motivo è attualmente oggetto di numerosi studi di ricerca. Molto spesso quindi le curve di fragilità e di costo non sono disponibili. Da qui nasce l'interesse d'indagare la risposta sismica nel fuori piano dei pannelli prefabbricati di tamponamento esterno, nonché l'entità delle forze nelle connessioni metalliche pannello-struttura. Oltre a questo è indagata pure

l'influenza del carroponte e l'interazione dello stesso con la risposta sismica globale della struttura in edifici prefabbricati industriali in calcestruzzo armato.

With love

to Graziella, Rosario, Clarita

and Carolina who always remain in my heart.

ACKNOWLEDGEMENTS

At the end of these three long years of my Ph.D., my thanks goes to all those who were able to stay close to me day after day, who helped me through all the difficult moments and who have been able to give me the necessary support to continue with perseverance and devotion that led to the culmination of this thesis successfully.

I would like to give my sincere gratitude to my advisor Prof. Paolo Riva since he gave me the opportunity to apply for this Ph.D. program in the University of Bergamo. I wish to thank him for the significant role he played by providing me with his experienced advice and inspiration during this journey.

A special thank you to my co-advisor Andrea Belleri for his continuous presence during the development of my research throughout the years. He helped me with his rich knowledge and experience, his valuable advice, time spent and his strong interest on the topic of my research.

I like to express my great appreciation to Prof. Babak Moaveni, who was always available to me and who provided to me his precious and continuous support during my research at Tufts University in Boston (MA, USA).

I wish to thank in particular, all of my friends and Ph.D. colleagues in the University of Bergamo, who helped me through all the hardships that I faced in this time.

I am grateful to all the friends I met during the period I spent far from my home. I would to remember the friends I met in Pavia and Naples: Mehmetcan Atakul, Bledar Kalemi, David Welch, Gerard O'Reilly, Giorgio Proestos, Matthew Fox, Stefano Barone, Cigdem Yilmaz, Marc Tatarsky, Riccardo Milanesi, Matteo Peruch.

A heartfelt and a special thanks to those friends I met in Boston, who were able to share with me a lot of unforgettable moments. I am thinking of: Srismitha Modem, Giacomo Sciarra and Evan Makris.

Lastly but most importantly, my biggest gratitude and thanks go to my mother, my father and my sister who have shared with me every single thing that happened in my life, especially during this journey. They helped me a lot to survive and go through all the difficulties that I went through my whole life. All of this has made me stronger and more confident of myself. I would like to dedicate this big achievement to you and I hope from the deepest part of my heart that today I will make you proud of me.

Thank You!

Fabrizio

CONTENTS

EVALUATION OF THE EXPECTED ANNUAL LOSS FOR PRECAST CONCRETE INDUSTRIAL STRUCTURES

LIST OF FIGURES

LIST OF TABLES

1. INTRODUCTION

The recent experiences of well documented seismic events have revealed that in the recovery of the buildings saved from destruction and/or for those that can be saved from a subsequent demolition, the higher costs are mainly due to the damages suffered by non-structural elements and the inner content of the buildings. In terms of economic value, this concerns particularly industrial facilities, hospital complexes and offices as well as residential buildings in general. It was observed that the cost of the installations and the contents is far greater than the value of the bare structure.

A striking example from the past has been the case of the Olive View Hospital built in 1970 in Sylmar, California. This represented an important milestone regarding the design phase of new buildings. This hospital was hit by the San Fernando earthquake and it experienced a widespread and significant structural damage that required the complete demolition of the entire building complex (Figure 1.1).

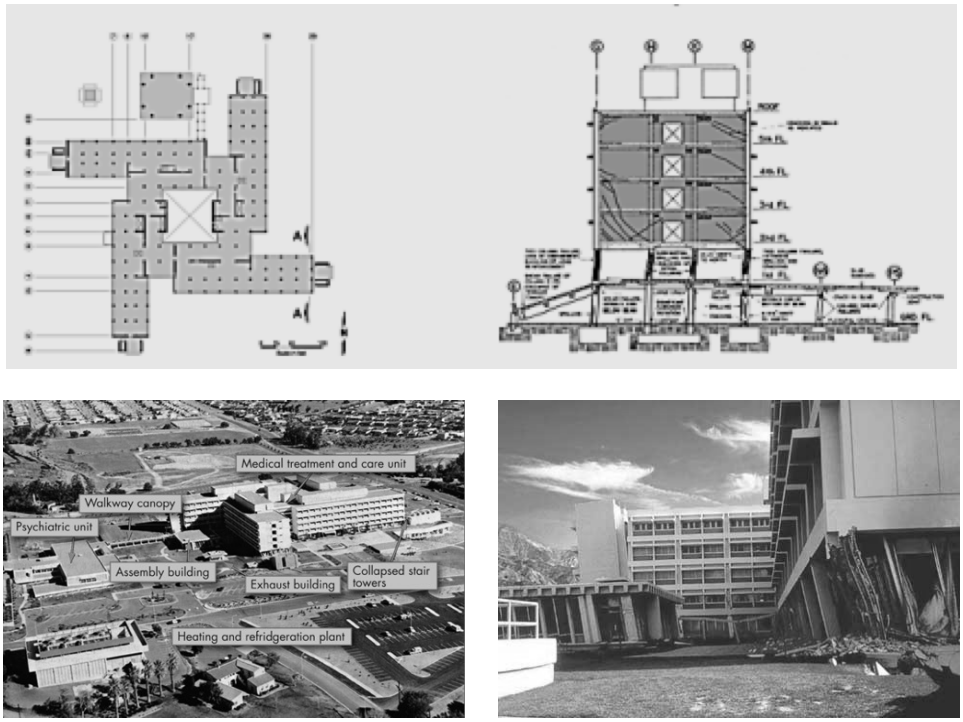

Figure 1.1 View in plant and cross section of the Olive View Hospital (above); structural damage experienced after the San Fernando earthquake: collapse of the parking, collapse due to soft-storey mechanism and overturning of the stairwell (below).

After this event, it was commissioned for the designers to design a new hospital, according to the latest anti-seismic regulations. The new building complex was completed in 1988. In 1994, however, the Northridge earthquake came and hit again the new hospital. This gave birth to a new problem: the structure responded very well to seismic stress but this time the real damage concerned the contents and non-structural elements inside the building. The result was that the hospital was once again unfit to use. From this moment, engineers and researchers began to focus on how important the design of the internal systems is and how they can interact with the seismic response of the structure. In addition to this, it has been perceived for the first time, that the amount of the total economic losses was related for the most part to the damage suffered by non-structural elements (Figure 1.2) and the inaccessibility of the building (in terms of economic losses caused by the downtime of a company).

Figure 1.2 Olive View Hospital immediately after the Northridge earthquake in 1994 (left) and damage of the non-structural elements (right).

As shown by recent studies [Taghavi and Miranda, 2003], these components represent the largest share of the total investments in typical buildings estimated around 80-90% of the total cost of construction (Figure 1.3).

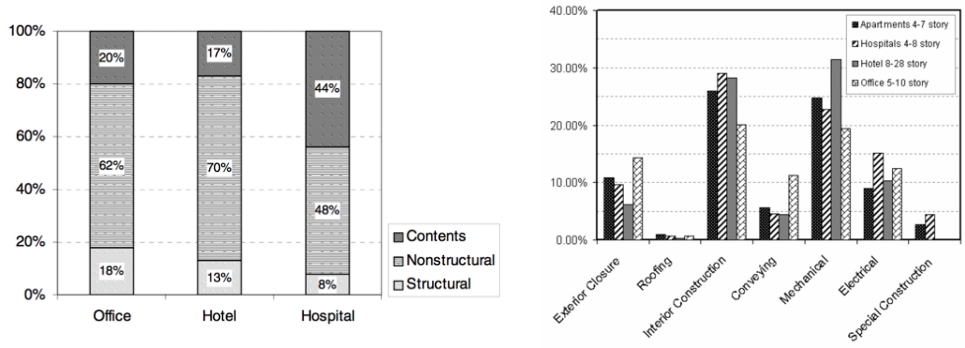

Figure 1.3 Investments in constructions [Taghavi and Miranda, 2003].

Now it is no longer enough to design a building that has only a good seismic response. Besides this, the new goal of engineers during the design phase has become to prevent, or at least minimize, the damage of the internal components such as: furniture, interior partitions, water systems, air conditioning systems, stored materials, internal machineries or equipment with a high value, etc. This had led the designers to guide the design of new buildings towards a Performance-Based Design approach.

Table 1.1 highlights the indicative amount of the economic losses that have occurred for several companies located in Chile as a result of recent earthquakes that hit the Chilean territory.

Table 1.1 Extent to the damage at the premises of the largest industrial companies affected by recent earthquakes in Chile.

Company	Industry	Estimated Loss (USD millions)	Type of Loss
Grupo Arauco	Pulp, Plywood Producer and Saw Mill.	400 to 600	Approximately 65% of the loss is from business interruption
Grupo Quinienco	Brewery, Winery and Manufacturing	300	60% from business interruption
CMPC	Pulp and Paper Manufacturer	170	60% from business interruption
D&S (WalMart Chile)	Retail Stores	150	Primarily physical damage
ENAP	Oil and Gas	150	Evenly distributed between physical damage and business interruption
CAP	Steel Mill (Huachipato Plant)	140	60% from business interruption
Viña Concha y Toro	Winery	110	Evenly distributed between physical damage and business interruption
Telefónica	Communications	100	Primarily physical damage
Grupo Claro	Winery, Communications, TV channel, Bottler	84	Evenly distributed between physical damage and business interruption
Censosud	Retail	72	Primarily physical damage
Carozzi	Food Manufacturer	60	Primarily physical damage
SCL - Santiago Airport	Infrastructure	40	Primarily physical damage
Falabella	Retail - Largest chain of retail stores in Chile	42	Primarily physical damage

Most recent research studies are more and more directed towards the development of a methodology that is able to compute, during the design phase of a building, the annualized economic losses defined as Expected Annual Loss (EAL), both in terms of direct losses and indirect losses (production downtime, out of order of portion of the building etc.).

Much of the research in this direction has been developed and finalized by the Pacific Earthquake Engineering Research (PEER) Center at the University of California, Berkeley, through the development of the Performance-Based Earthquake Engineering methodology (PBEE) [Porter, 2003], [Günay and Mosalam, 2012].

This methodology incorporates in itself four main phases: the hazard analysis, the structural analysis, the damage analysis and the loss analysis. The entire evaluation is mainly based on a probabilistic calculation that combines the four analyses and related uncertainties, such as the uncertainties of the components defining the earthquake hazard; the uncertainties in the response of the structure to the earthquake hazard; the uncertainties in the pattern and history of the structural response; the uncertainties in the distribution of damage throughout the structure, such as the variation of components resulting in the same damage level and also the uncertainties in economical values such as market prices (Figure 1.4).

The entire PEER PBEE methodology is based on a probabilistic approach, because the uncertainty nature linked to the seismic intensity, the structural response, the damage corresponding to the assessed structural response and the economic losses related to the damage state cannot be defined by a deterministic value; they can be expressed by various values with different probabilities.

To solve this, the PEER PBEE methodology combines all of these probabilities in a consistent manner using the total probability theorem, where the final result is the probability of exceedance (POE) of various values of a decision variable (DV) during the lifecycle of the building due to earthquake hazard. DV is typically a system performance measuring the direct interest of various stakeholders, such as monetary losses, downtime, or casualties.

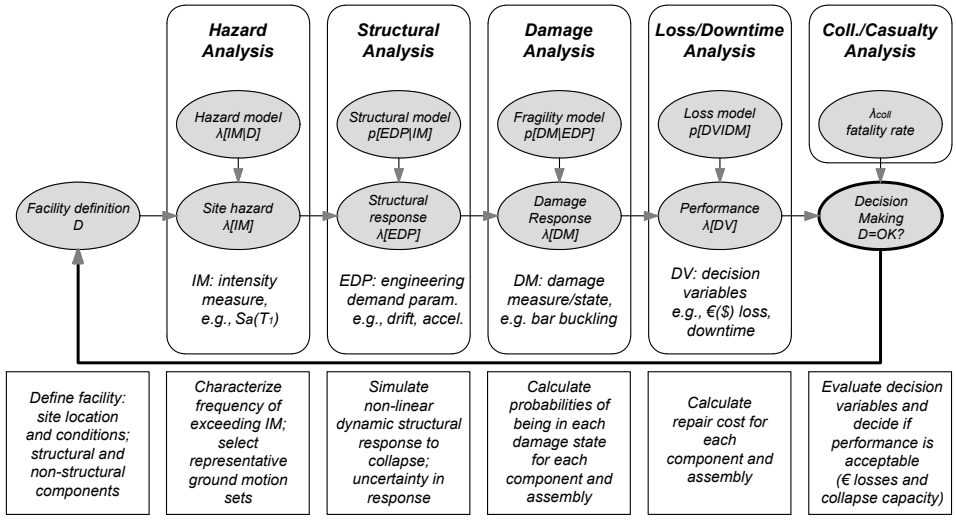

Figure 1.4 PEER-PBEE framework [Porter, 2003].

Currently in Italy and in Europe there are not laws or guidelines providing guidance for the determination of the expected annual monetary losses due to earthquakes. Actually the only international reference about this is the PEER PBEE methodology, which has been recently implemented by the Applied Technology Council (ATC) for Federal Emergency Management Agency (FEMA) in an American standard [FEMA P-58, 2012a, FEMA P-58, 2012b].

1.1 Research significance

The main purpose of this research is to check the suitability of the PEER PBEE procedure when applied to one-storey precast reinforced concrete industrial buildings. It is intended to investigate what are the critical aspects and issues related to the application of this procedure.

The potential related to the use of this application is immediately clear: it can give to engineers a reliable tool for assessing the EAL, in order to evaluate the convenience in terms of monetary savings and economic return of a seismic improvement or a retrofit of an existing building.

Due to the peculiarities linked to the building construction tradition of precast reinforced concrete buildings in Italy, it is required to give special attention to local vulnerabilities which can lead to partial collapses. Some examples are the rupture of forks at the top of columns, the lack of connections between structural components, the breaking of the connections between cladding panels and the structure. This research also aims at investigating the main vulnerabilities and how to consider those inside the PEER PBEE framework.

Nowadays the PEER PBEE methodology is applicable only to academic research, because of its complexity linked to the determination of the many input data needed to carry out all the phases. Another goal of the current research is to find a simpler method than the PEER PBEE for the determination of the EAL, so it can be used even by professional engineers. The Direct Displacement Based Design (DDBD) [Priestly *et al.*, 2007] and the SPO2IDA tool based on Vamvatsikos and Cornell (2006) are adopted as alternative methods to the Incremental Dynamic Analysis (IDA) [Vamvatsikos and Cornell, 2002] for carrying out the structural analysis. A further effort is performed to simplify the whole procedure for the evaluation of the EAL, by applying a closed formula according to the latest study [Sullivan, 2016] from which certain considerations and critical comments were made. Afterwards, an alternative

curve in the "monetary loss-seismic intensity measure" graph is proposed for a better evaluation of the expected annual loss.

For each of these methods the pros and cons as well as the deficiencies and limits are illustrated in order to make further improvements to the methodologies that can be applied to precast reinforced concrete industrial structures.

1.2 Outline of the research

A general overview of the PEER PBEE framework consisting of all four phases is shown in Chapter 2, where each individual phase is illustrated in a comprehensive manner. This chapter discusses the individual inputs and data necessary for carrying out the assessment of the EAL; in addition to this, other simplified methods for performing the structural analysis alternative to IDA such as DDBD method and SPO2IDA tool are shown.

The evaluation of the economic losses of precast reinforced concrete one-storey structures is closely linked to the consideration of local vulnerabilities that characterize this family of buildings. This is the reason why in Chapter 3 the main local vulnerabilities that can lead to partial collapse when an earthquake occurs are described and analysed. Beyond this, special attention has been given to the assessment of the out-of-plane seismic response of cladding panels and the values of the forces in the connections between these elements and the structure. A new formulation for the evaluation of such forces in substitution to the formula proposed by the current Italian standard is proposed. A comparison of the results is shown. Within this chapter, the influence of the overhead crane in the seismic response of the structure is also investigated. Besides this, a sensitivity analysis is conducted on the connections between the structural elements based on the friction forces generated at element interface only.

In Chapter 4, the applicability of the refined PEER PBEE methodology for assessing the EAL of precast reinforce concrete one-storey structure is explored, as well as the applicability of some simplified procedures as SPO2IDA tool and DDBD method for carrying out the structural analysis in a time efficient manner. In addition to this, the possibility to adopt a new formula for the calculation of the EAL as an alternative to the PEER PBEE is analysed. An alternative to the curve in the "monetary loss-seismic intensity measure" graph is also proposed. Some comparisons about these different procedures and a critical analysis are made.

The conclusions and future developments of the current research are shown in Chapter 5.

1.3 References

FEMA P-58. [2012a] Seismic Performance Assessment of Buildings, Volume 1 - Methodology.

FEMA P-58. [2012b] Seismic Performance Assessment of Buildings, Volume 2 - Implementation Guide.

Günay, M., Mosalam, K. [2012] "PEER Performance Based Earthquake Engineering Methodology, Revisited", Journal of Earthquake Engineering, Lisboa, Vol. 17, No.6, pp. 829–858.

Porter, K.A. [2003] "An Overview of PEER's Performance-Based Earthquake Engineering Methodology", Ninth International Conference on Applications of Statistics and Probability in Civil Engineering (ICASP9), San Francisco.

Priestley, M.J.N., Calvi, G.M., Kowalsky, M.J. [2007] Displacement-Based Seismic Design of Structures, IUSS Press.

Sullivan, T.J. [2016] "Use of Limit State Loss versus Intensity Models for Simplified Estimation of Expected Annual Loss", Journal of Earthquake Engineering, Vol. 2469, No. May, pp. 1–21.

Taghavi, S., Miranda, E. [2003] "Response Assessment of Nonstructural Building Elements".

Vamvatsikos, D., Cornell, C.A. [2002] "Incremental Dynamic Analysis", Earthquake Engineering and Structural Dynamics, Vol. 20, No.2, p. 23.

Vamvatsikos, D., Cornell, C.A. [2006] "Direct Estimation of the Seismic Demand and Capacity of Oscillators with Multi-linear Static Pushovers Through IDA", Earthquake Engineering and Structural Dynamics, Vol. 35, No.9, pp. 1097–1117.

2. ASSESSMENT OF THE EXPECTED ANNUAL LOSS

As a result of what was experienced in the past, such as the Olive View Hospital, and of the impact observed after the recent Italian (Emilia 2012, L'Aquila 2009) and international (Tohoku, Japan, 2011; Christchurch, NZ, 2011; Maule, Chile, 2010; Kobe, Japan, 1995; Northridge, USA, 1994; San Fernando, USA, 1971) earthquakes, the bad economic effects caused by a seismic event cannot be neglected anymore. Given the huge impact that the earthquakes had on the affected area [Daniell *et al.*, 2012] (see Figure 2.1 and Table 2.1), especially for the economic losses related to non-structural components and building contents [Taghavi and Miranda, 2003], the civil engineering community has realized and understood the necessity and the importance of having to develop a new approach for the design phase of a building (or a general construction) and for preventing unnecessary future losses.

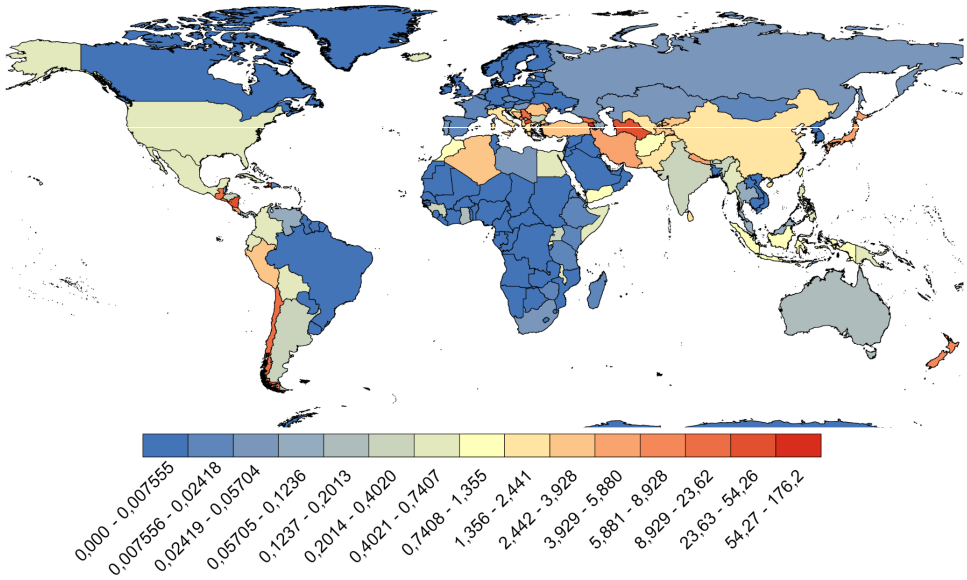

Figure 2.1 Cumulative net capital stock loss (in %) from earthquakes over 112 years from 245 nations [Daniell, 2012].

As a replacement of the classical load-and-resistance-factor design (LRFD) seismic approach, the new performance-based earthquake engineering (PBEE) seismic design approach was undertaken. A clear difference in the approach between these two design procedures is given by the fact that the LRFD design method aims to ensure the performance in terms of probability of damage and collapse of the structural elements (considering some design aspects that are unique to the principle

of capacity design to ensure the development of plastic hinges in specific areas of the facility, such as strong-column-weak-beam), while the PBEE addresses the seismic design trying to ensure the performance to the entire system, which can be expressed in economic terms and/or post-earthquake loss function, or as risk of collapse and/or in terms of casualties.

Table 2.1 List of the highest insured losses from 1900 to 2012, the values are expressed in 2012 CPI adjusted $ international [Daniell et al., 2012].

Rank	Earthquake	Country	Date	Insured Loss Range	Pref. Source for Loss
1	Tohoku	Japan	11.03.2011	$33,9bn-$38,75bn	Industry Estimates
2	Northridge	USA	17.01.1994	$23,53bn	Industry Estimates
3	Christchurch	New Zealand	21.02.2011	$10,97bn-$16,46bn	Industry Estimates
4	Great Kanto	Japan	01.09.1923	$8,46bn-$14,58bn	[Daniell et al., 2010]
5	Maule	Chile	27.02.2010	$8,39bn-$13,30bn	Industry Estimates
6	Kobe	Japan	16.01.1995	$6,56bn	Industry Estimates
7	San Francisco	USA	18.04.1906	$6,14bn	[Daniell, 2012]
8	Izmir	Turkey	17.08.1999	$3,63bn-$8,46bn	Industry Estimates
9	Darfield	New Zealand	03.09.2010	$2,19bn-$4,94bn	Industry Estimates
10	Sumatra	Many	26.12.2004	$2,375bn-$4,224bn	[Daniell, 2012]
11	Loma Prieta	USA	18.10.1989	$2,58bn	[Daniell, 2012]

Therefore, the PBEE method can be defined as the assessment of the expected performance of a system as a result of a seismic excitation, as well as the detailed design of its structural and non-structural characteristics in order to achieve the described performance objectives. These performance objective goals are relevant to various types of stakeholders. They might be interested in the estimation of the losses as a result of an earthquake because the repair costs are not the only costs suffered by the owners of the building but there are also costs due to the interruption of the business, building closure taken as a post-earthquake safety precaution, and human casualties caused by building failures during the seismic event.

The current technical standards at national [NTC, 2008], European [EN 1998-1, 2004], American [ASCE/SEI 7-10, 2010] and international [International Code Council (ICC), 2003] level provide design guidelines intended to achieve a specific performance objective with specific effects (near collapse, life safety and different levels of damage) given a particular hazard. Recently published documents aim to provide more-robust performance-based seismic design.

In the following, an overview of the documents published in recent years is reported as written and illustrated by [Mitrani-Reiser, 2007].

The first of these was [SEAOC Vision 2000, 1995], written by Structural Engineers Association of California (SEAOC) and academics with the intention to "embrace a broader scope of design and construction quality assurance issues and yield more predictable seismic performance over a range of earthquake demands". For the first time, within Vision 2000, different levels of the hazard, were talked about and distinguished as: the *frequent* intensity level with a probability of exceedance (POE) of 50% in 30 years (43-year return period), the *occasional* intensity level with a POE of 50% in 50 years (72-year return period), the *rare* intensity level with a POE of 10% in 50 years (475-year return period) and the *very rare* intensity level with a POE of 10% in 100 years (975-year return period).

For each of these levels of hazard, Vision 2000 also associated a specific performance level (or limit state) in terms of damage experienced by structural and non-structural elements and in terms of effects to the operability of the building and the occupants. Ordered with an increasing level of damage, these performance levels were defined as: *fully operational*, *operational*, *life safe* and *near collapse*. As shown in Figure 1.3, a graphical representation of this correspondence between the levels of hazard and the performance levels for different buildings types was offered by Vision 2000. In this figure, the diagonal lines in the matrix correspond to different typologies of building, for each of these is specified the acceptable and non-acceptable damage level.

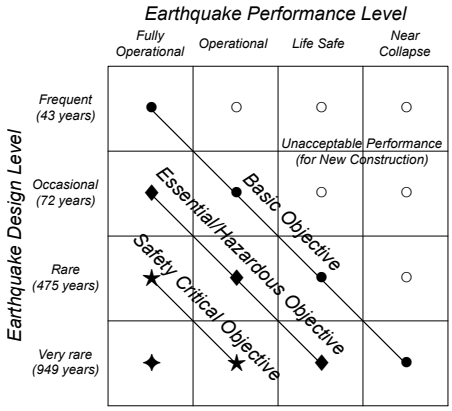

Figure 2.2 Vision 2000 recommended seismic performance objectives for buildings. Mean recurrence intervals of 43yrs, 72yrs, 475yrs and 949yrs correspond to Poisson arrival events with 50% probability of exceedance in 30yrs (Fully Operational limit state), 50% in 50yrs (Operational limit state), 10% in 50yrs (Life Safe limit state), and 10% in 100yrs (Near Collapse limit state), respectively (after SEAOC, 1995).

For example: a building which contains a large quantity of pollutants, dangerous substances and/or toxic materials that has a large impact if damaged after an earthquake is categorized as *safety critical objective*; a hospital, a facility necessary for

first aid, a fire station or a police station are all considered as *essential objective*; a building with hazardous materials, pollutants that has a limited impact if damaged after an earthquake is classified as *hazardous objective*; most common residential and commercial building are included in the *basic objective* category.

Others important documents published after Vision 2000 were the *Seismic Evaluation and Retrofit of Concrete Buildings* developed by the Applied Technology Council (ATC) in 1996 [ATC-40, 1996] and the *National Earthquake Hazards Reduction Program (NEHRP) Guidelines for the Seismic Rehabilitation of Buildings* and its *Commentary* developed by the Federal Emergency Management Agency (FEMA) in 1997 ([FEMA 273, 1997]; [FEMA 274, 1997]). The documents mentioned above acted as the main reference for the rehabilitation and retrofitting of buildings and led to the drafting of the next and most comprehensive guidelines for the PBEE procedure entitled *Prestandard and Commentary for the Seismic Rehabilitation of Buildings* [FEMA 356, 2000].

The FEMA 356 report was designed to promote broader use of FEMA 273 by converting it into mandatory language, and to provide a basis for a future, nationally recognized, ANSI-approved standard that incorporates its approaches and technologies into a traditional design and construction practice.

The FEMA 356 report was written with the aim to provide professional engineers a useful tool for the design of seismic rehabilitation measures to existing buildings.

In accordance with the desires of the customer, the engineer can choose a target building performance between the different choices offered within the FEMA 356 (established on the basis of Vision 2000) and he can decide to design the building according to the standard as laid down in the FEMA 356 itself. This report also provides multiple tables for structural (e.g., steel moment frames, steel braced frames, steel plate shear walls, concrete frames, precast concrete frames, concrete frames with infills) and non-structural (e.g., for partitions, interior veneers, ceilings, plumbing, cladding, glazing) components aimed to express different performance levels in a qualitative way, and these levels are open to a wide range of interpretations (Table 2.2 and Table 2.3). In some of these tables, engineering limit states may correspond to the various performance levels, for example drift values. These limit states should not be intended as a criterion of acceptance or in the assessment of the damage after an earthquake, but are indicative of the range that typical structures go through.

Even if FEMA 356 relates component-level damage states to life safety and post-earthquake operability, it does not permit to quantify the probability of achieving a

selected performance level or to quantify the repair costs, the number or the probability of the casualties, or the post-earthquake loss function of the building. Such a qualitative approach was not enough to proceed in the development of a probabilistic and quantitative methodology for the assessment of the damage and the economic losses, especially considering that for some special buildings, the tables provided by FEMA 356 are missing or unsuitable. These tables needed a better definition and quantification of the limit states for individual components and they needed appropriate fragility functions for the estimation of the probabilities of these damage states. These fragility functions are used to assess the probability that a particular type of component will reach or exceed a clearly defined damage state as a function of the structural response which act on the component itself.

Efforts of many research studies developed over recent years have been oriented to a clear definition of the damage states and the corresponding fragility functions, the repair efforts and costs associated for every damageable building components considered in the damage assessment ([Mitrani-Reiser, 2007], [Haselton *et al.*, 2008], [Lee and Grigoriu, 2012] and other [NEES] projects), but much work is still required in the future to cover the wide range of these damageable components. An important contribution for the development of a new and complete methodology of performance-based earthquake engineering within a probabilistic framework was carried out by the Pacific Earthquake Engineering Research Center (PEER) at the University of California (Berkeley, CA, USA).

The results and the methodology from PEER research have been used as a main reference in the development of the project n.58 developed by Applied Technology Council (ATC-58). The FEMA sponsored this project which was realized for the development of a new generation of guidelines for the application of PBEE and it can be considered as the main current reference guide for the evaluation of the economic losses. Developed by an advisory committee composed of experts from various fields including engineers, architects, government officials, social scientists, and researchers, the final result of this project is incorporated within the FEMA P-58 - *Seismic Performance Assessment of Buildings*, this code is composed by three parts: *Vol.1 – Methodology* [FEMA P-58, 2012a]; *Vol.2 - Implementation Guide* [FEMA P-58, 2012b]; *Vol.3 - Supporting Electronic Materials and Background Documentation* [FEMA P-58, 2012c]. In the third volume, different electronic supports are provided for the implementation of the PEER PBEE methodology, i.e. the PACT software (Performance Assessment Calculation Tools) and others electronic sheets useful for the implementation of the assessment.

Therefore, the goal of the ATC-58 project [Whittaker *et al.*, 2004] was to create a standard for the design of new structures and the upgrade of existing ones that incorporates the building performance level desired by the stakeholders into the design process, using clear and quantitative definitions for building performance (i.e., life safety, building operability, and economic losses). For achieving this, FEMA P-58 provides three different assessment types: the intensity based, the scenario-based, and the time-based assessments. The intensity- based assessment determines the probability of loss for a given hazard level; the scenario-based assessment addresses the probability of loss for a specified seismic event; the time-based assessment defines the probability of loss over a given time period, such as the design life of the structure. Each of these assessments addresses different concerns that stakeholders are likely to have.

Table 2.2 Damage control and building performance levels from Table C1-2, [FEMA 356, 2000].

	Target Building Performance Levels			
	Collapse Prevention Level (5-E)	*Life Safety Level (3-C)*	*Immediate Occupancy Level (1-B)*	*Operational Level (1-A)*
Overall Damage	*Severe*	*Moderate*	*Light*	*Very Light*
General	*Little residual stiffness and strength, but load- bearing columns and walls function. Large permanent drifts. Some exits blocked. Infills and unbraced parapets failed or at incipient failure. Building is near collapse.*	*Some residual strength and stiffness left in all stories. Gravity-load- bearing elements function. No out-of- plane failure of walls or tipping of parapets. Some permanent drift. Damage to partitions. Building may be beyond economical repair.*	*No permanent drift. Structure substantially retains original strength and stiffness. Minor cracking of facades, partitions, and ceilings as well as structural elements. Elevators can be restarted. Fire protection operable.*	*No permanent drift. Structure substantially retains original strength and stiffness. Minor cracking of facades, partitions, and ceilings as well as structural elements. All systems important to normal operation are functional.*
Nonstructural components	*Extensive damage.*	*Falling hazards mitigated but many architectural, mechanical, and electrical systems are damaged.*	*Equipment and contents are generally secure, but may not operate due to mechanical failure or lack of utilities.*	*Negligible damage occurs. Power and other utilities are available, possibly from standby sources.*
Comparison with performance intended for buildings designed under the NEHRP Provisions, for the Design Earthquake	*Significantly more damage and greater risk.*	*Somewhat more damage and slightly higher risk.*	*Less damage and lower risk.*	*Much less damage and lower risk.*

Within the FEMA P-58, some fragility specifications, a large fragility database and a guidance on how to sort the damageable components of a building into what are termed "performance groups" are also provided. In FEMA P-58, each performance

group is defined by the type of building component (e.g., columns, curtain walls, ceilings, partitions) that experience similar demands (e.g., storey drift ratio, floor acceleration, peak ground acceleration) and will have similar damage patterns ([NISTIR 6389, 1999], [FEMA P-58, 2012b]). FEMA P-58 also proposed three ways to assess the building performance: direct economic losses (e.g., repair costs), downtime (e.g., interruption of building functions), and casualties given a selected distribution of the population for the typology of the building considered (e.g. number of deaths or serious injuries).

Table 2.3 Structural performance levels and damage for vertical elements from Table C1-3, [FEMA 356, 2000].

		Structural Performance Levels		
Elements	*Type*	*Collapse Prevention S-5*	*Life Safety S-3*	*Immediate Occupancy S-1*
Concrete Frames	*Primary*	*Extensive cracking and hinge formation in ductile elements. Limited cracking and/or splice failure in some non-ductile columns. Severe damage in short columns.*	*Extensive damage to beams. Spalling of cover and shear cracking (<1/8" width) for ductile columns. Minor spalling in non-ductile columns. Joint cracks <1/8" wide.*	*Minor hairline cracking. Limited yielding possible at a few locations. No crushing (strains below 0.003).*
	Secondary	*Extensive spalling in columns (limited shortening) and beams. Severe joint damage. Some reinforcing buckled.*	*Extensive cracking and hinge formation in ductile elements. Limited cracking and/or splice failure in some non-ductile columns. Severe damage in short columns.*	*Minor spalling in a few places in ductile columns and beams. Flexural cracking in beams and columns. Shear cracking in joints <1/16" width.*
	Drift	*4% transient or permanent*	*2% transient; 1% permanent*	*1% transient; negligible permanent*
Steel Moment Frames	*Primary*	*Extensive distortion of beams and column panels. Many fractures at moment connections, but shear connections remain intact.*	*Hinges form. Local buckling of some beam elements. Severe joint distortion; isolated moment connection fractures, but shear connections remain intact. A few elements may experience partial fracture.*	*Minor local yielding at a few places. No fractures. Minor buckling or observable permanent distortion of members.*
	Secondary	*Same as primary.*	*Extensive distortion of beams and column panels. Many fractures at moment connections, but shear connections remain intact.*	*Same as primary.*
	Drift	*5% transient or permanent*	*2.5% transient; 1% permanent*	*0.7% transient; negligible permanent*

2.1 Overview of the refined PEER PBEE framework

The PEER PBEE methodology has been developed to estimate the performance of structures in seismic zones in terms of mean annual frequency with which a particular performance metric will be exceeded for a given location. This methodology has been summarized in various publications [Cornell and Krawinkler, 2000], [Krawinkler, 2002], [Moehle, 2003], [Porter, 2003], [Krawinkler and Miranda, 2004], [Moehle and Deierlein, 2004], [Günay and Mosalam, 2012] and different studies have been conducted [Comerio, 2005], [Krawinkler, 2005], [Goulet *et al.*, 2006], [Mitrani-Reiser *et al.*, 2006], [Kunnath, 2006], [Kunnath *et al.*, 2006], [Bohl, 2009], [Haselton *et al.*, 2008]. This revisited procedure led to several new improvements over the first generation of the PBEE method through the introduction of the calculation of the performances in a rigorous probabilistic method, which allows to consider the uncertainties, and the assessment of the performance with decision variables expressed as parameters of interest for various stakeholders.

The PEER PBEE revisited procedure consists of four main steps: the hazard analysis, the structural analysis, the damage analysis, and the loss analysis. According with [Günay and Mosalam, 2012], the framework and the mathematical expression of the PEER PBEE methodology are shown in Figure 2.3 and in Eq. 2.1.

In the following, a summary of the entire PEER PBEE framework and the four phases is reported as explained and illustrated by [Günay and Mosalam, 2012].

In both the figure and the equation, $p[X|Y]$ denotes the probability density of X conditioned on Y, $\lambda[X|Y]$ denotes the mean occurrence rate of X given Y, IM denotes the intensity measure (e.g. spectral acceleration considered at the period of the first mode shape $S_a(T_1)$), EDP denotes the engineering demand parameters (e.g. drift, peak floor acceleration, peak floor velocity), DM denotes the damage measures (e.g. cracking and spalling of the concrete, buckling of the rebars, collapse of the elements), and DV denotes the decision variables (e.g., repair costs, casualties and downtime).

Based on the total probability theorem, the combination of the analyses within the PEER PBEE methodology can be expressed with the integral in Eq. 2.1:

$$\lambda[DV|D] = \iiint p[DV|DM,D]\,p[DM|EDP,D]\,p[EDP|IM,D]\,\lambda[IM|D]\,dIM\,dEDP\,dDM \quad \text{Eq. 2.1}$$

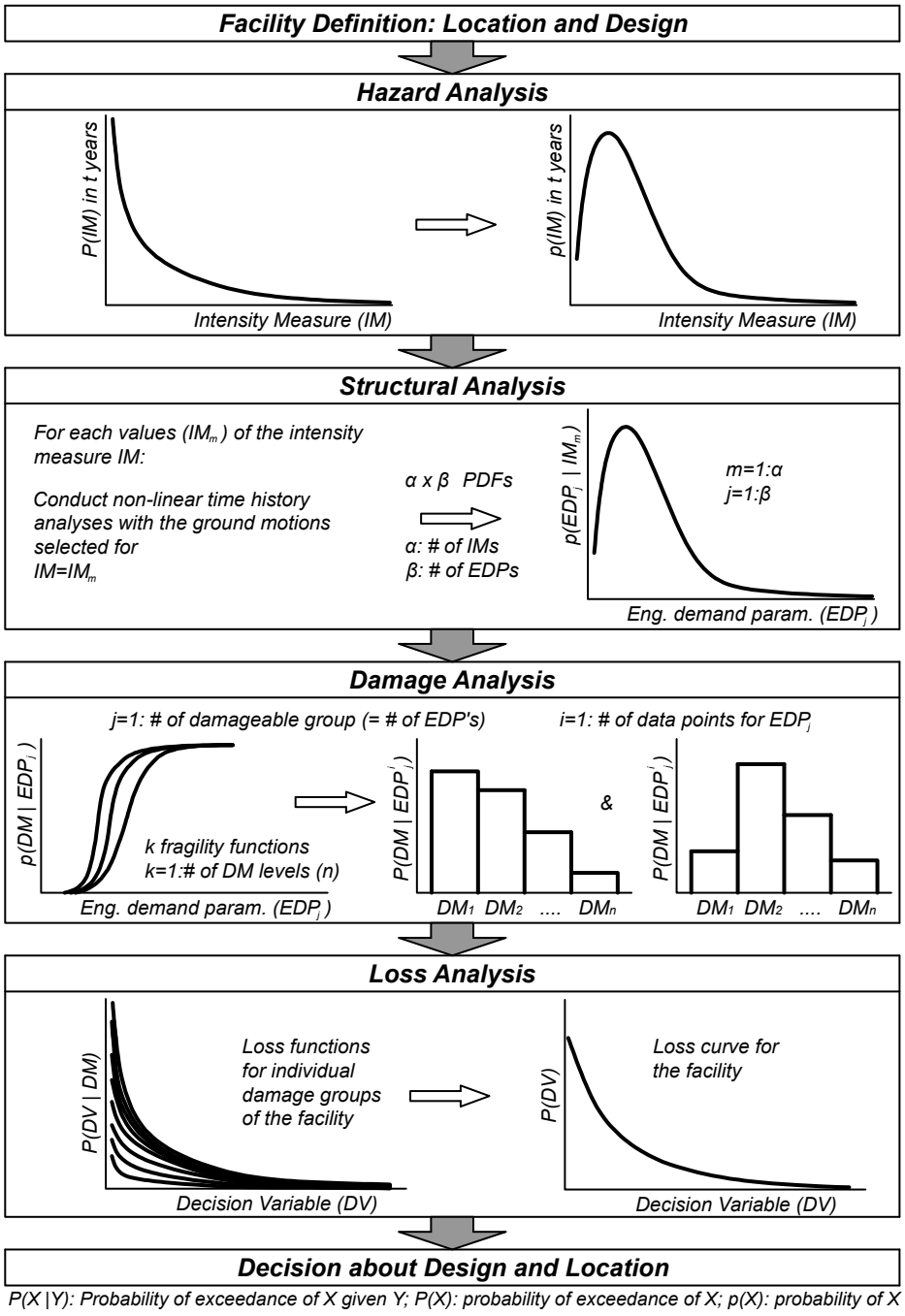

Figure 2.3 Diagram of the PEER PBEE framework, from [Günay and Mosalam, 2012].

Considering a defined number in the values of intensity measure (IM), damageable group (DG), engineering demand parameter (EDP) and damage measure (DM), the integral in Eq. 2.1 can be expressed as a defined sum of the phases instead of using the triple integral as shown in Eq. 2.2:

$$P\left(DV^n\right)=\sum_m P\left(DV^n \mid IM_m\right)p\left(IM_m\right)$$

$$P\left(DV^n \mid IM_m\right)=P\left(DV^n \mid NC, IM_m\right)p\left(NC \mid IM_m\right)+P\left(DV^n \mid C\right)p\left(C \mid IM_m\right)$$

$$P\left(DV^n \mid NC, IM_m\right)=\sum_j P\left(DV_j^n \mid NC, IM_m\right) \qquad \text{Eq. 2.2}$$

$$P\left(DV_j^n \mid NC, IM_m\right)=\sum_i P\left(DV_j^n \mid EDP_j^i\right)p\left(EDP_j^i \mid IM_m\right)$$

$$P\left(DV_j^n \mid EDP_j^i\right)=\sum_k P\left(DV_j^n \mid DM_k\right)p\left(DM_k \mid EDP_j^i\right)$$

where m is the index for intensity measure (IM), j is the index for damageable groups (DG), i index for engineering demand parameter (EDP), k is the index for damage measure (DM).

The PEER PBEE procedure assesses the losses in a probabilistic manner considering the hazard of the site $p(IM_m)$ (as a result from the hazard analysis) and two post-earthquake scenarios. PEER PBEE framework takes into account the losses in the cases of no-collapse $P(DV^n \mid NC, IM_m)$ and of collapse $P(DV^n \mid C)$ of the structure and it considers the probabilities of no-collapse $p(NC \mid IM_m)$ and of collapse $p(C \mid IM_m)$ of the facility obtained as a result from the structural analysis. In the case of collapse of the structure, the economic losses are evaluated combining the loss function for collapse, $P(DV^n \mid C)$, with the probability of collapse, $p(C \mid IM_m)$, obtained from the loss analysis and from the structural analysis respectively. Whereas in the case of no-collapse of the facility and for a given probabilistic distribution of the seismic response of the structure $p(EDP_j{}^i \mid IM_m)$ (as a result of the structural analysis), the assessment of the economic losses is possible through the combination of the damage and loss analysis phases using the probabilities $p(DM_k \mid EDP_j{}^i)$ and $P(DV_j{}^n \mid DM_k)$ respectively (Eq. 2.2).

A different formulation of the Eq. 2.2 is available if there will be the necessity to determine the expected value of the n^{th} value of a particular decision variable (DV). In this case, the previous sum become:

$$E\left(DV^n\right)=\sum_m E\left(DV^n \mid IM_m\right)p\left(IM_m\right)$$
$$E\left(DV^n \mid IM_m\right)=E\left(DV^n \mid NC, IM_m\right)p\left(NC \mid IM_m\right)+E\left(DV^n \mid C\right)p\left(C \mid IM_m\right)$$
$$E\left(DV^n \mid NC, IM_m\right)=\sum_j E\left(DV_j^n \mid NC, IM_m\right) \qquad \text{Eq. 2.3}$$
$$E\left(DV_j^n \mid NC, IM_m\right)=\sum_i E\left(DV_j^n \mid EDP_j^i\right)p\left(EDP_j^i \mid IM_m\right)$$
$$E\left(DV_j^n \mid EDP_j^i\right)=\sum_k E\left(DV_j^n \mid DM_k\right)p\left(DM_k \mid EDP_j^i\right)$$

where the *m*, *j*, *i*, *k* indexes are the same as in the previous integral and the probability of exceedance (POE) is replaced with the expected value (E).

The following paragraphs show the single phases of the PEER PBEE framework specifying the meaning of each term within the formula in Eq. 2.2.

2.1.1 Hazard analysis

The first stage in the PEER PBEE formulation is the hazard analysis, which is conducted to describe the earthquake hazard for a particular facility in a probabilistic manner, considering nearby faults, their mechanism and magnitude-recurrence rates, site distance, source-to-site conditions, facility location, etc. probabilistic seismic hazard analysis (PSHA) leads to create a hazard curve, this curve is used to show in a chart the variation of a selected intensity measure (IM) versus the mean annual frequency of exceedance (MAFE). Then the probability of exceedance (POE) in "*t*" years corresponding to a given MAFE is calculated using Eq. 2.4, where "*t*" can be selected as the duration of lifecycle of the considered facility:

$$P\left(IM\right)=1-e^{-\lambda(IM)t} \qquad \text{Eq. 2.4}$$

where *IM* is the intensity measure, $\lambda(IM)$ is the MAFE of the *IM*, and *P(IM)* is the POE of *IM* in "*t*" years (Figure 2.4). The formula in Eq. 2.4 is valid considering the temporal occurrence of an earthquake as described by a Poisson's model. The probability of each value of IM, i.e., $p(IM_m)$, is calculated algorithmically using the Eq. 2.5 from the POE of IM:

$$\begin{aligned} &for\ \ m=1:\#\ of\ IM\ data\ points \\ &p(IM_m)=P(IM_m)\quad if\ m=\#\ data\ points \\ &p(IM_m)=P(IM_m)-P(IM_{m+1})\quad otherwise \end{aligned} \qquad \text{Eq. 2.5}$$

Some examples of parameters which can be adopted as intensity measure are the peak ground acceleration (PGA), the peak ground velocity (pgv) and the spectral acceleration at the period of the first mode $S_a(T_1)$. The hazard analysis also includes the selection of an adequate number of ground motion time histories compatible with the hazard analysis which allows to carry out the next structural analysis in a meaningful statistical way. In order to be consistent with the PSHA, the ground motions should be compatible with the magnitude and the distance which dominates the hazard for a particular value of the IM and it is important to use the ground motions recorded in sites consistent with the site class of the considered structure. Whenever possible the selection of the ground motions for each IM is preferred and beneficial instead of using scaled ground motions, this is because the use of a scaled set of accelerograms to simulate earthquakes with different IM might lead to unrealistic ground motions when large scales are needed. Scaling one single set of ground motions, it is possible to obtain a higher magnitude (see 3rd chapter "Hazard Analysis" in [Comerio, 2005]), then a higher $S_a(T_1)$ but this does not change the duration of the ground motion which may make the ground motion unrealistic.

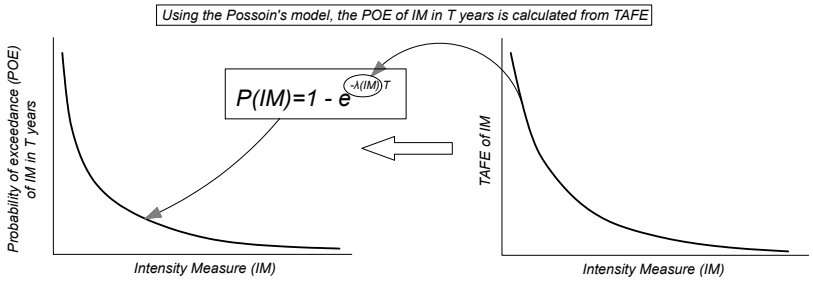

Figure 2.4 Hazard analysis: correspondence between total annual frequency of exceedance (TAFE) and probability of exceedance (POE) of the intensity measure (IM), from [Günay and Mosalam, 2012].

2.1.2 Structural analysis

The second stage of the PEER PBEE formulation is the structural analysis, which is conducted in order to estimate the uncertain structural response to various levels and characteristics of earthquake hazard. This phase requires the development of the structural model of the building which should accurately capture the behaviour of the building for low-intensity and high-intensity seismic events, since the damage at all IMs contributes to total loss.

For each IM of earthquake hazard, the structural analysis is carried out performing non-linear time histories and the estimation of the structural response in terms of

EDP conditioned on the IM and the structural design is then achieved. Open-source software programs such as [Ruaumoko, 2007] and [OpenSees, 2007] can be used for carrying out this phase. A wide range of element and material types are provided inside the libraries of these software programs, so it is possible to select the desired object between several choices, facilitating a better modelling of the building. The result of the structural analysis is a probabilistic distribution of the selected EDPs which can be expressed with a value of median and dispersion (PEER PBEE requires a single value for EDP, then for each time history performed, the peak value of the considered EDP is generally assumed). A suitable probability distribution can be the lognormal distribution (EDP_j in Figure 2.8). The selected EDPs may be expressed in terms of force (e.g.: axial or shear forces) or deformation (plastic hinge rotation, peak curvature at the base of the columns) related to the elements, or global parameters such as interstorey drift, floor displacement and acceleration. The EDPs of interest should be selected depending on the type of building component and the PEER PBEE allows to use different EDPs for different damageable components (EDP_j in Figure 2.8).

The structural analysis can be performed in a refined way with the incremental dynamic analysis (IDA) according to [Vamvatsikos and Cornell, 2002a] and [Vamvatsikos and Cornell, 2002b] (Figure 2.5), but also other simplified methods can be adopted as an alternate to the IDA such as SPO2IDA tool (see Chapter 2.2.1) and the DDBD method (see Chapter 2.2.2).

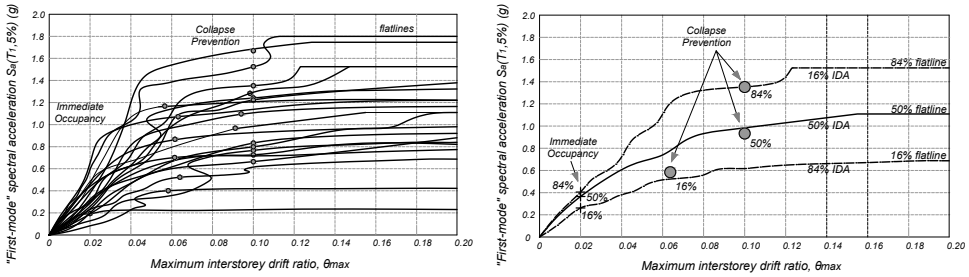

Figure 2.5 Example of the results obtained from an incremental dynamic analysis (IDA), from [Vamvatsikos and Cornell, 2002b].

The determination of the global collapse of the facility for higher intensity levels plays an important role within the structural analysis since its probability does not change from a damageable group to another. When a representative set of ground motions is selected and then the ground motions are scaled for each intensity level, the global collapse can be determined in correspondence to an infinite increase of

response for small increases in the input intensity (Figure 2.6, on the left). In case of using unscaled ground motions, or when the intensity level of the ground motions is not adequate to accurately determine the beginning of the collapse mechanism, a practical method might be to calculate a value of a representative response parameter corresponding to global collapse from a prior analysis (e.g. a push-over analysis) and compare this value with the peak values obtained from non-linear analyses (Figure 2.6, on the right).

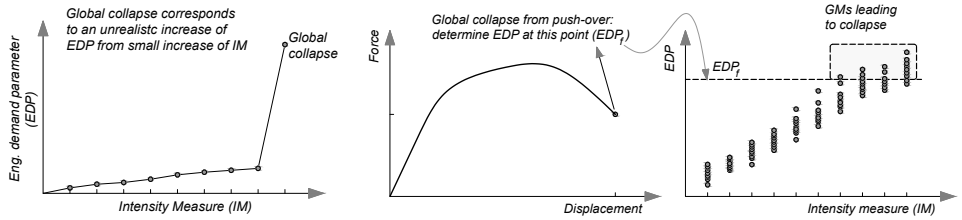

Figure 2.6 Methods for the determination of the global collapse: using scaled ground motions (left) or with a push-over analysis (right).

The probability $p(C|IM)$ can be approximately determined as the number of simulations leading the global collapse divided by the total number of the analyses performed at the considered intensity level (Figure 2.7).

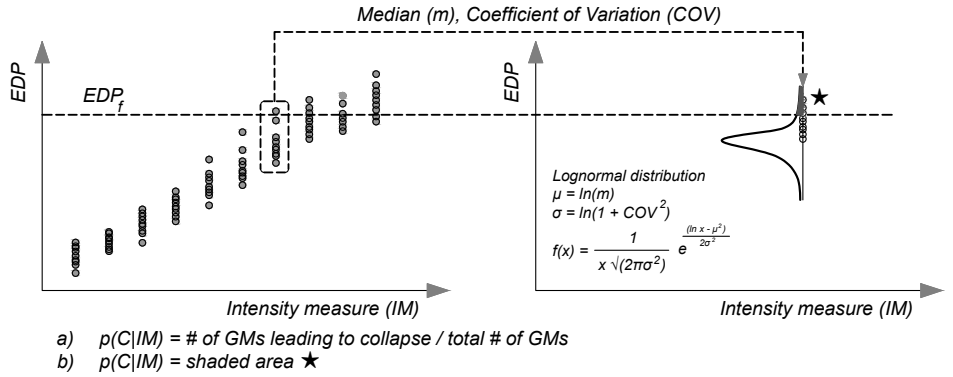

Figure 2.7 Determination of the probability of collapse for each IM considered for performing the structural analysis.

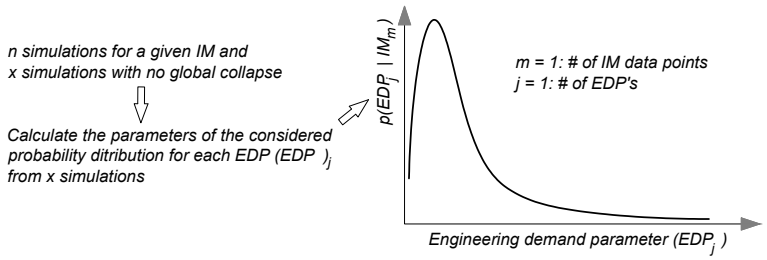

Figure 2.8 Structural analysis: determination of the probability density function (PDF) of an engineering demand parameter (EDP) from structural analysis, [Günay and Mosalam, 2012].

2.1.3 Damage analysis

The third stage of the PEER PBEE formulation is the damage analysis, the purpose of which is to estimate physical damage at the component or system levels as a function of the structural response in terms of a specified EDP. The damage measures are typically defined in terms of damage levels corresponding to different measures and efforts necessary to repair and restore the element to its original undamaged condition. Some examples of repair measures corresponding to damage level are given by [Mitrani-Reiser *et al.*, 2006]. The uncertainties linked to the material characteristics (that lead to a specific damage level for a corresponding EDP) and the differences in the pattern and history of the structural response can be taken into account through the use of the "fragility functions", which express the probability that a facility component (structural and/or non-structural) is in or exceeds a particular damage state (DS) as a function of a selected reference EDP (Figure 2.9). Usually, the fragility functions for both structural and non-structural elements can be obtained by experimental or analytical models, whereas when there is no data (as it happens for many facility components), they can be built based on expert opinion.

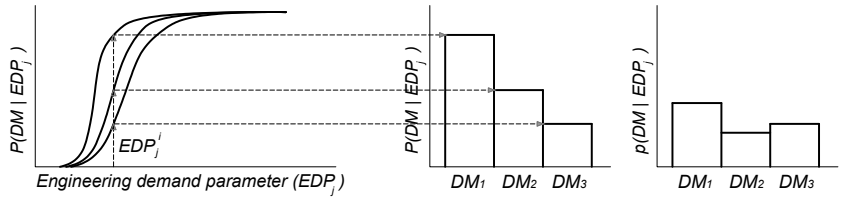

Figure 2.9 Damage analysis: probability of exceedance, P, and probability, p, of a damage level from fragility curves, from [Günay and Mosalam, 2012].

Components which are affected by the same EDP in a similar manner and have the same fragility function can be considered in the same damageable group. According to [Günay and Mosalam, 2012], for each damageable group (index *j*) and each EDP

(index *i*) data point ($EDP_j{}^i$), the POE of a DM is available as a point on the related fragility curve (Figure 2.9). The probability of a DM is calculated from the POE using Eq. 2.6:

$$for \;\; k = 1 : \#\ of\ DM\ levels$$

$$p(DM_k \mid EDP_j^i) = P(DM_k \mid EDP_j^i) \quad if\ k = \#\ of\ DM\ levels \qquad \text{Eq. 2.6}$$

$$p(DM_k \mid EDP_j^i) = P(DM_k \mid EDP_j^i) - P(DM_{k+1} \mid EDP_j^i) \quad otherwise$$

2.1.4 Loss analysis

The last phase of PEER PBEE methodology is the loss analysis which evaluates in a probabilistic way the facility performance conditioned on the damage state of all components. The information obtained from the damage analysis is converted to the final DVs that can be directly used by engineers in the design and the decision-making process with the stakeholders. Performance metrics include economic loss (monetary loss for the repair cost of the damaged components and/or the replacement of the facility), repair duration (time spent for the realization of the repair measures), casualties and injuries (number of deaths and/or injured people). Usually within PEER PBEE framework and in the recent literature the three DVs identified as economic loss, repair duration and casualties are commonly known as dollars, downtime and deaths (the 3Ds). According to the Eq. 2.2, the POE of the losses for different damageable groups at different DMs (loss functions) is determined.

The outcome of the PEER PBEE framework is the loss curve, which is obtained by applying the total probability theorem to the combination of all four phases. The result is graphically shown in Figure 2.10.

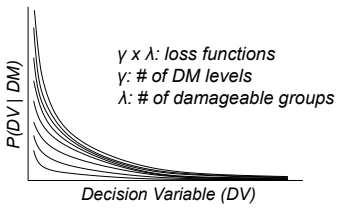

Figure 2.10 Loss analysis: POE of a DV for different damageable groups and DMs, from [Günay and Mosalam, 2012].

2.2 Simplified methods for carrying out the structural analysis

The PEER PBEE framework does not prescribe the type of structural analysis that must be undertaken within the performance evaluation process. As said before, most applications typically involve the use of IDA [Vamvatsikos and Cornell, 2002b], but for most practicing engineers, the structural analysis can be carried out by performing two simplified non-linear analyses methods: the former consists of using the SPO2IDA tool provided within [FEMA P-58, 2012c] and the latter consists of the application of direct displacement-based design (DDBD) according to [Priestley *et al.*, 2007].

2.2.1 Static pushover to incremental dynamic analysis (SPO2IDA) tool

Static push-over to incremental dynamic analysis (SPO2IDA) is an Excel workbook application that was originally developed by [Vamvatsikos and Cornell, 2006]. This tool uses empirical relationships from a large database of incremental dynamic analysis results to convert static push-over curves into probability distribution of building collapse as a function of ground shaking intensity, from which the collapse fragilities of the building can be generated.

To use the SPO2IDA application, a push-over analysis should be performed first according to the non-linear static procedure shown in [ASCE/SEI 41-06, 2007] and its result should be generated as a normalized force-displacement relationship (usually expressed as a global shear, V, versus roof displacement, Δ, relationship). SPO2IDA transforms the force-displacement relationship into a normalized spectral acceleration versus global displacement ductility relationship (Figure 2.11, left).

Given the global shear, the 5% damped spectral acceleration is evaluated as in Eq. 2.7:

$$S_a = V / \left(C_m W / g \right) \qquad \text{Eq. 2.7}$$

where V is the global shear at the base of the structure, C_m is the effective mass factor as defined in [ASCE/SEI 41-06, 2007], W is the effective seismic weight and g is the acceleration of gravity. The normalization is computed as the ratio of the spectral acceleration, S_a, to the spectral acceleration at the first control point, S_y, i.e. where S_a / S_y is equal to 1 (yielding point). The global displacement ductility, μ, is the ratio of the roof displacement, Δ, to the roof yield displacement, Δ_y. The control point

(yielding point) is then defined in SPO2IDA graph with the coordinates (μ, S_a / S_y), or (*1,1*).

An example of the result from SPO2IDA application is shown in Figure 2.11 (on the right) where it is possible to see the push-over curve used as input.

The total dispersion of the collapse fragility should be computed considering record-to-record variability and modelling uncertainty, but without any information on this, a minimum default dispersion of 0,6 is recommended by [FEMA P-58, 2012a] to derive collapse fragility functions based on SPO2IDA results.

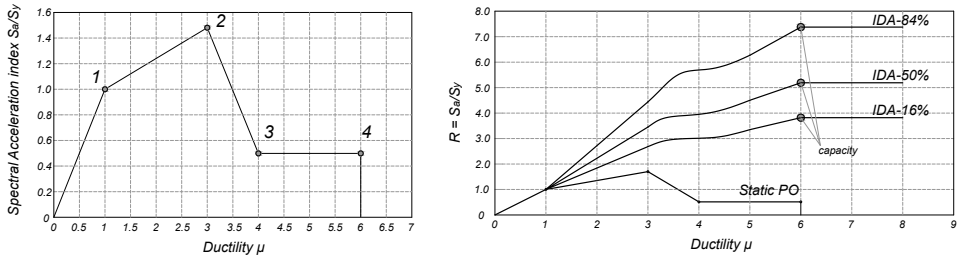

Figure 2.11 Normalized spectral acceleration-global ductility relationship used in SPO2IDA (left) and an example of SPO2IDA result (right).

Regarding the using of the SPO2IDA application, it should be limited to low-rise buildings that are regular in both plant and elevation dominated by first mode translational behaviour, with independent response along each principal axis, and negligible torsion.

2.2.2 *Direct displacement-based design (DDBD)*

The Direct Displacement-Based Design (DDBD) is a procedure developed and suggested by [Priestley *et al.*, 2007] (Figure 2.12). Several publications have been produced recently such as [Calvi *et al.*, 2008], [Welch *et al.*, 2012], [Welch *et al.*, 2014], [Sullivan *et al.*, 2014] and different research works have been conducted in order to verify the application of this procedure on different type of buildings as in [Haselton *et al.*, 2008], [Belleri, 2009], [Torquati, 2014].

The DDBD procedure is aimed at computing the demand-capacity ratio for a given earthquake intensity level based on the likely sway mechanism (Figure 2.12, above on the right) determined with the guidelines provided by [Priestley *et al.*, 2007]. Once that the likely mechanism is assessed, the displaced shape and the storey shear profile can be obtained and made through rational assumptions. Specifically, the

effects due to the higher mode shape (e.g. influence of the higher mode effects on the displacement and drifts) should be taken into account. Instead of this hand-calculation process, it is possible to develop a numerical model of the building and undertake a push-over analysis of the structure according to [EN 1998-1, 2004], [ASCE/SEI 7-10, 2010].

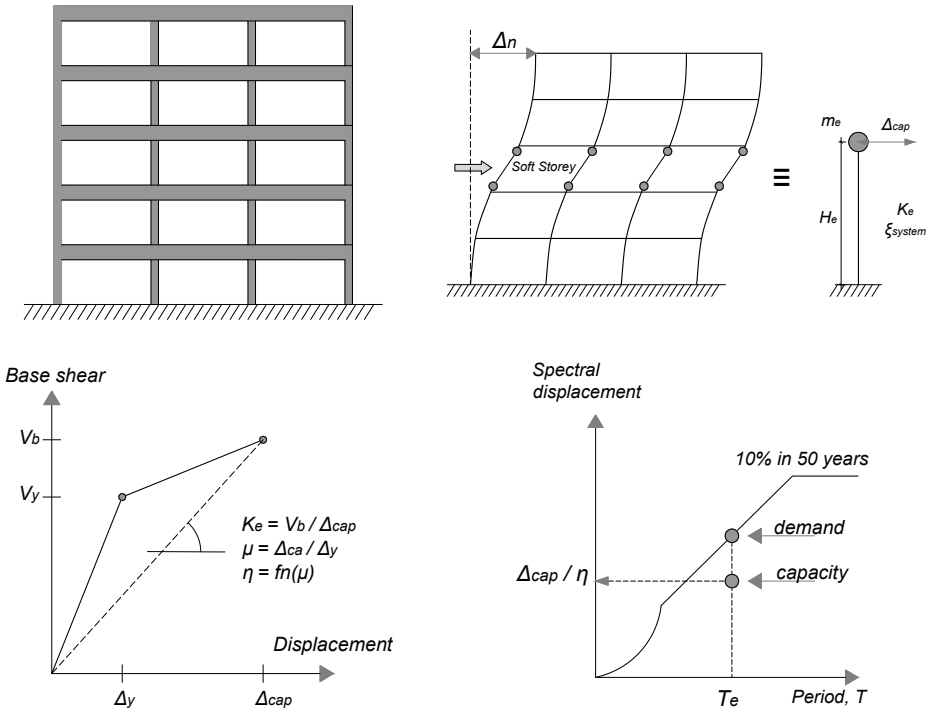

Figure 2.12 Displacement-based assessment procedure from [Priestley et al., 2007]: an example of a multi-storey building (above on the left); the assessment of the likely mechanism and equivalent single degree of freedom system (above on the right); effective stiffness, displacement and ductility capacity (below on the left); demand-capacity ratio identified from displacement spectrum (below on the right).

The assessed shear-force displacement response of the multiple degree of freedom (MDOF) system can be converted into an equivalent single degree of freedom (SDOF) system as shown in Figure 2.12 (above on the right), which is characterized by a system displacement capacity, Δ_{cap} (for each limit state of interest), effective mass, m_e, effective stiffness, K_e, and effective height, H_e, via the Eq. 2.8 to Eq. 2.11:

$$\Delta_{cap} = \frac{\sum m_i \Delta_i^2}{\sum m_i \Delta_i} \qquad \text{Eq. 2.8}$$

$$m_e = \frac{\left(\sum m_i \Delta_i\right)^2}{\sum m_i \Delta_i^2} \qquad \text{Eq. 2.9}$$

$$K_e = \frac{V_b}{\Delta_{cap}} \qquad \text{Eq. 2.10}$$

$$H_e = \frac{\sum m_i \Delta_i h_i}{\sum m_i \Delta_i} \qquad \text{Eq. 2.11}$$

where Δ_i, m_i, and h_i, are the displacement, seismic mass and height associated with *i*-level of the structure. V_b is the base shear resistance of the equivalent SDOF at the system displacement value of Δ_{cap} (Figure 2.12, below on the left).

The DDBD procedure utilizes an empirical spectral scaling factor, η, as shown in Figure 2.12 (below, on the right) determined as suggested by [Sullivan *et al.*, 2014] in order to take into account the effects of energy dissipation and non-linear response of the structure. The equivalent SDOF system characteristic displacement capacity, Δ_{cap}, is divided by the spectral scaling factor, η, to give the equivalent elastic spectral displacement capacity at the same effective period, $S_{d,\,cap}$:

$$S_{d,\,cap} = \frac{\Delta_{cap}}{\eta} \qquad \text{Eq. 2.12}$$

The final step of the displacement-based assessment procedure is then to compute the spectral displacement demand at the effective period, and compare it to the assessed spectral displacement capacity from Eq. 2.12.

2.3 *Precast buildings*

The aim of this research is to study the applicability of the PEER PBEE methodology to one-storey precast reinforced concrete industrial buildings, widespread on the Italian national territory.

Over the last few years, multiple studies concerning the enforceability of the PEER PBEE methodology to different building typology were carried out and they are still in a development phase [Haselton *et al.*, 2008], [Ottonelli *et al.*, 2015], [Cardone and Perrone, 2015], [Cardone, 2016], but nothing has been done regarding precast reinforced concrete industrial buildings.

The particularity solely related to this type of buildings is given by the necessities of the owners. Industries are very sensitive about possible damage of the production process and/or production losses as a consequence of a seismic event. The importance to study the enforceability of this procedure seems obvious, especially due to the opportunity to predict this kind of expected losses during the design phase. The main advantage of the new refined PEER PBEE methodology compared to the first-generation PBEE method is the determination of DVs meaningful to stakeholders in terms of monetary losses, downtime and casualties and/or injuries.

Nowadays, however, there are many limitations for the application of the PEER PBEE methodology to precast industrial buildings. In order to allow the applicability of the procedure in a comprehensive and reliable way, several aspects need to be improved and/or (re)defined.

One of the main limitations is the lack of fragility curves related to the structural and non-structural elements, such as installations and the inner content. In the last few years, there has been much advancements in the development of fragility and cost distribution functions for damageable building components, but much work is still needed in this area to cover the wide range of damageable components present in real buildings, especially with regards to precast reinforced concrete industrial buildings. Depending on the business activity for which the building is intended, the internal components are usually heterogeneous and in some cases, unique. For this reason, it is unthinkable to realize fragility curves by means of experimental results.

Another critical point is the fact that the current PEER PBEE methodology does not consider the indirect economic losses in the short, intermediate and long periods due to downtime. This is a crucial point because in most cases the higher losses for a

company are represented by indirect losses and stakeholders may be very interested in the prediction of these kind of consequences.

Before proceeding to an assessment of the expected annual loss, it is essential to know the typical failure mechanisms of precast structures which can influence the structural response, such as the rupture of the forks at the top of the columns, the failure of the cladding-structure connections, the loss of support, etc. The achievement of this step is essential because the evaluation of the losses can be affected by the presence or not of local collapse mechanisms.

The implications of a local collapse are unpredictable and depend on both the type of local collapse and the layout position of the structural elements collapsed. Let's think for instance to the different effects related to the rupture of a fork at the top of a column with the following out-of-plane overturning of the beam and then the collapse of roof element supported by the beam itself, compared to the collapse of a single roof element due to the loss of support. In the former case (the overturning of the beam) the economic losses would be substantial, given the damage to structures and everything which was installed inside the building (expensive machinery, special equipment, etc.); in the latter case (loss of support of the single roof element) the economic losses will be lower since they are restricted to the damage suffered solely by the components under the roof element collapsed.

In Chapter 3, this research investigates the main vulnerabilities in precast industrial buildings that can lead to local and/or global collapse. A special focus is given to the cladding-structure connections, the loss of support and the effects of the overhead crane in the seismic response of precast one-storey buildings.

Subsequently, Chapter 4 investigates the application of PEER PBEE framework highlighting the potential, problems and missing aspects required to get a better estimation of the expected annual loss.

2.4 References

ASCE/SEI 41-06. [2007] Seismic Rehabilitation of Existing Buildings, American Society of Civil Engineers, Reston, Virginia, USA, pp. 1–428.

ASCE/SEI 7-10. [2010] Minimum Design Loads for Buildings and Other Structures, American Society of Civil Engineers, Reston, Virginia, USA, pp. 1–658.

ATC-40. [1996] "Seismic Evaluation and Retrofit of Concrete Buildings", Redwood City, CA, United States of America.

Belleri, A. [2009] Displacement Based Design for Precast Concrete Structures, Starrylink Editrice, Brescia, Italy.

Bohl, A. [2009] "Comparison of Performance Based Engineering Approaches," The University of British Columbia, Vancouver, Canada.

Calvi, G.M., Priestley, M.J.N., Kowalsky, M.J. [2008] "Displacement – Based Seismic Design of Structures", 3rd Greek Conference on Earthquake Engineering and Engineering Seismology.

Cardone, D. [2016] "Fragility Curves and Loss Functions for RC Structural Components with Smooth Rebars", Earthquake and Structures, Vol. 10, No.5, pp. 1181–1212.

Cardone, D., Perrone, G. [2015] "Damage and Loss Assessment of Pre-70 RC Frame Buildings with FEMA P-58: A Case Study", Journal of Earthquake Engineering, No. September, pp. 363–375.

Comerio, M.C. [2005] "PEER Testbed Study on a Laboratory Building: Exercising Seismic Performance Assessment", Pacific Earthquake Engineering Research Center, University of California, Berkeley, United States of America.

Cornell, C.A., Krawinkler, H. [2000] "Progress and Challenges in Seismic Performance Assessment", PEER Center News, Vol. 3, No.2, pp. 1–4.

Daniell, J.E. [2012] "The CATDAT Damaging Earthquakes Database. Searchable Integrated Historical Global Catastrophe Database", Digital Database, updates v1.0 to latest update v5.1001 – nb. v0.0-v0.99 refers to all work and updates done 2003 to 2007.

Daniell, J.E., Daniell, K.A., Daniell, T.M., Khazai, B. [2010] "a Country Level Physical and Community Risk Index in the Asia-Pacific Region for Earthquakes and Floods", 5th CECAR Conference Proceedings, Sydney, Australia, pp. 1–8.

Daniell, J.E., Khazai, B., Wenzel, F., Vervaeck, A. [2012] "The Worldwide Economic Impact of Historic Earthquakes", WCEE Lisboa 2012, p. 10.

EN 1998-1. [2004] Design of Structures for Earthquake Resistance - Part 1: General Rules, Seismic Actions and Rules for Buildings, Brussels, Belgium.

FEMA 273. [1997] NEHRP Guidelines for the Seismic Rehabilitation of Buildings, Washington, D.C., United States of America, p. 435.

FEMA 274. [1997] NEHRP Commentary on the Guidelines for the Seismic Rehabilitation of Buildings, Washington, D.C., United States of America, p. 488.

FEMA 356. [2000] Seismic Rehabilitation of Buildings, Washington, D.C., United States of America, p. 519.

FEMA P-58. [2012a] Seismic Performance Assessment of Buildings, Volume 1 - Methodology.

FEMA P-58. [2012b] Seismic Performance Assessment of Buildings, Volume 2 - Implementation Guide.

FEMA P-58. [2012c] Seismic Performance Assessment of Buildings, Volume 3 - Supporting Electronic Materials and Background Documentation.

Goulet, C., Haselton, C.B., Mitrani-Reiser, J., Stewart, J.P., Taciroglu, E., Deierlein, G.G. [2006] "Evaluation of the Seismic Performance of a Code-Conforming Reinforced-Concrete Frame Building - Part 1: Ground Motion Selection and Structural Collapse Simulation", 8th National Conference on Earthquake Engineering (100th Anniversary Earthquake Conference), San Francisco, CA.

Günay, M., Mosalam, K. [2012] "PEER Performance Based Earthquake Engineering Methodology, Revisited", Journal of Earthquake Engineering, Lisboa, Vol. 17, No.6, pp. 829–858.

Haselton, C.B., Goulet, C.A., Mitrani-Reiser, J., Beck, J.L., Deierlein, G.G., Porter, K.A., Stewart, J.P., Taciroglu, E. [2008] "An assessment to benchmark the seismic performance of a code-conforming reinforced concrete moment-frame building", Pacific Earthquake Engineering Research Center Report.

International Code Council (ICC). [2003] ICC International Building Code (IBC 2003), United States of America.

Krawinkler, H. [2002] "A General Approach to Seismic Performance Assessment", Proceedings of International Conference on Advances and New Challenges in Earthquake Engineering Research, ICANCEER, Hong Kong.

Krawinkler, H. [2005] "Van Nuys Hotel Building Testbed Report: Exercising Seismic Performance Assessment", Pacific Earthquake Engineering Research Center, Stanford University, CA, United States of America.

Krawinkler, H., Miranda, E. [2004] "Performance-Based Earthquake Engineering",

Earthquake Engineering, International Code Council (ICC), ed., CRC PRESS, Boca Raton London New York Washington, D.C., pp. 560–635.

Kunnath, S.K. [2006] "Application of the PEER PBEE Methodology to the I-880 Viaduct", Pacific Earthquake Engineering Research Center, Davis, CA, United States of America.

Kunnath, S.K., Larson, L., Miranda, E. [2006] "Modelling Considerations in Probabilistic Performance-based Seismic Evaluation: Case study of the I-880 viaduct", Earthquake Engineering and Structural Dynamics, Vol. 35, No.1, pp. 57–75.

Lee, C.H., Grigoriu, M.D. [2012] Bayesian Fragility for Nonstructural Systems, p. 82.

Mitrani-Reiser, J. [2007] "An Ounce of Prevention: Probabilistic Loss Estimation for Performance-Based Earthquake Engineering."

Mitrani-Reiser, J., Haselton, C., Goulet, C., Porter, K., Beck, J., Deierlein, G. [2006] "Evaluation of the Seismic Performance of a Code-conforming Reinforced-concrete Frame Building - Part 2: Loss Estimation", 8th National Conference on Earthquake Engineering (100th Anniversary Earthquake Conference), San Francisco, CA.

Moehle, J. [2003] "A Framework Methodology for Performance-based Earthquake Engineering", Proceedings of ATC-15-9 Workshop on the Improvement of Building Structural Design and Construction Practices, Maui, HI.

Moehle, J., Deierlein, G.G. [2004] "A Framework Methodology for Performance-based Earthquake Engineering", 13th World Conference on Earthquake Engineering, Canada.

NEES. "The George E. Brown, Jr. Network for Earthquake Engineering Simulation (NEES)", <https://nees.org/about>.

NISTIR 6389. [1999] "UNIFORMAT II Elemental Classification for Building Specifications, Cost Estimating, and Cost Analysis".

NTC. [2008] Decreto Ministeriale del 14 Gennaio 2008: Norme Tecniche per le Costruzioni.

OpenSees. [2007] "Open System for Earthquake Engineering Simulation", University of California, Berkeley, California.

Ottonelli, D., Cattari, S., Lagomarsino, S. [2015] "A Seismic Loss Assessment Procedure for Masonry Buildings", Improving the Seismic Performance of Existing Buildings and Other Structures. ATC & SEI 2015, No.1, pp. 447–458.

Porter, K.A. [2003] "An Overview of PEER's Performance-Based Earthquake

Engineering Methodology", Ninth International Conference on Applications of Statistics and Probability in Civil Engineering (ICASP9), San Francisco.

Priestley, M.J.N., Calvi, G.M., Kowalsky, M.J. [2007] Displacement-Based Seismic Design of Structures, IUSS Press.

Ruaumoko. [2007] "Athol J. Carr, Ruaumoko - The Maori God of Volcanoes and Earthquakes", University of Canterbury, Christchurch, New Zealand.

SEAOC Vision 2000. [1995] Performance-based Seismic Engineering of Buildings, Sacramento, CA, United States of America.

Sullivan, T.J., Welch, D.P., Calvi, G.M. [2014] "Simplified seismic performance assessment and implications for seismic design", Earthquake Engineering and Engineering Vibration, Vol. 13, No. Suppl. 1, pp. 95–122.

Taghavi, S., Miranda, E. [2003] "Response Assessment of Nonstructural Building Elements".

Torquati, M. [2014] "Displacement Based Assessment for Precast Structures," University of Brescia, Brescia, Italia.

Vamvatsikos, D., Cornell, C.A. [2002a] "Incremental Dynamic Analysis", Earthquake Engineering and Structural Dynamics, Vol. 20, No.2, p. 23.

Vamvatsikos, D., Cornell, C.A. [2002b] "The Incremental Dynamic Analysis and Its Application to Performance-Based Earthquake Engineering", European Conference on Earthquake Engineering, p. 10.

Vamvatsikos, D., Cornell, C.A. [2006] "Direct Estimation of the Seismic Demand and Capacity of Oscillators with Multi-linear Static Pushovers Through IDA", Earthquake Engineering and Structural Dynamics, Vol. 35, No.9, pp. 1097–1117.

Welch, D.P., Sullivan, T.J., Calvi, G.M. [2012] "Towards a Direct Displacement-Based Loss Assessment Methodology for RC Frame Buildings".

Welch, D.P., Sullivan, T.J., Calvi, G.M. [2014] "Developing Direct Displacement-Based Procedures for Simplified Loss Assessment in Performance-Based Earthquake Engineering", Journal of Earthquake Engineering, Vol. 18, No. April 2014, pp. 290–322.

Whittaker, A., Hamburger, R., Comartin, C., Mahoney, M., Bachman, R., Rojahn, C. [2004] "Performance Based Engineering of Buildings and Infrastructure for Extreme Loadings", Technical paper submitted to ATC-58 project.

3. LOCAL VULNERABILITIES IN PRECAST BUILDINGS

In this Chapter, the research focuses its attention to examine and investigate some of the main typical vulnerabilities that characterized RC precast industrial buildings in order to provide suggestions and considerations which can be helpful in the assessment of the damages and thus of the monetary losses due to earthquake. Knowing the correct seismic response of the structure is one of the most important requirement to perform a proper evaluation of the EAL. In particular, a study to determine the out-of-plane seismic forces acting on horizontal cladding panels and then the structure-to-cladding panel connections is carried out through a parametric study performed by linear and non-linear analyses. A new formulation able to predict such seismic forces is proposed as an alternative to those formulations provided by current standards for non-structural elements. Furthermore, the interaction between the overhead crane and the structure is investigated on both 2D portal and 3D building model and conclusions are given based on the results observed. Lastly, a preliminary sensitivity analysis is carried out on a single 2D portal having connections between structural elements relying only on friction with the aim to inquire how the variability of different parameters can affect the loss of support.

Recent earthquakes in Italy (L'Aquila 2009 and Emilia 2012) highlighted the vulnerability of precast reinforced concrete (RC) structures not designed according to modern seismic codes ([Toniolo and Colombo, 2012], [Marzo *et al.*, 2012], [Savoia *et al.*, 2012], [Liberatore *et al.*, 2013], [Magliulo, Ercolino, Petrone *et al.*, 2014], [Belleri, Brunesi *et al.*, 2014], [Bournas *et al.*, 2014], [Casotto *et al.*, 2015] and [Minghini *et al.*, 2016]). The main vulnerabilities, which caused both local and global collapses, are related to the inefficiency of the horizontal load transfer mechanism between precast elements and to the displacement and rotation compatibility among structural elements and between structural and non-structural elements ([Belleri, Torquati *et al.*, 2014], [Belleri and Marini, 2016], [Belleri *et al.*, 2015], [Brunesi *et al.*, 2015] and [Colombo *et al.*, 2016]).

The structural layout of the precast concrete structures considered herein ([Bellotti *et al.*, 2009] and [Negro *et al.*, 2013]), typical of industrial and commercial buildings, is composed of cantilever columns pin-connected ([Psycharis and Mouzakis, 2012], [Magliulo, Ercolino, Cimmino *et al.*, 2014] and [Zoubek *et al.*, 2015]) to prestressed RC beams spanning in one direction, which support prestressed concrete roof elements spanning in the transverse direction. The columns are placed inside cup footings [Osanai *et al.*, 1996] or connected to the foundation by means of mechanical devices or grouted sleeves ([Metelli *et al.*, 2011] and [Belleri and Riva, 2012]). The static

structural scheme assumed in the design phase is constituted by a frame fixed at the base of the columns and hinge connections between the remaining structural elements. The structural layout typology is characterized by a higher flexibility compared to traditional reinforced concrete structures, owing to the higher storey height, lower structural indeterminacy, and roof flexibility, being the latter associated to the absence of mechanical connections between adjacent roof elements and to the presence of numerous skylights.

In order to proceed to the assessment of the expected annual loss (EAL) for precast reinforced concrete industrial buildings, it is necessary to carry out the identification and classification of those vulnerabilities and fragilities which characterize this family of structures. Based on the observations and experience gained after the collapses occurred in the recent earthquakes on Emilian territory, this chapter will highlight the main structural vulnerabilities in precast industrial buildings.

This chapter will investigate the issues concerning the out-of-plane seismic response of the horizontal cladding panels and the vulnerability of the panel-to-column connections; the vulnerability due to the connections between structural elements which rely only on the friction forces generated at the elements interface; and the influence of the overhead crane in the global seismic response of the structure.

3.1 Main vulnerabilities of precast buildings

A large part of the industrial facilities built in the Emilian region and inspected after the earthquake of May 2012 did not show an acceptable seismic behaviour: the damage and the economic losses have been exaggerated compared to the intensity of the earthquake. Many of the observed damage are closely related to a delay in the adoption of the current seismic provisions and by the mistrust on seismically efficient but more complex solutions. The beam-to-column and roof-to-beam connections are the most vulnerable points in precast industrial buildings given that they inhibit the rational exploitation in terms of strength and ductility reserves of precast elements. The observed behaviour of the structural elements is typically elastic until the sudden failure of the undersized connections or loss of support.

In the following, the main vulnerabilities in existing industrial buildings will be shown and described as well as a photographic documentation of the observed collapses will be provided.

Horizontal structural elements: beams and roof elements

The lack of connections between the roof elements leads to a higher global flexibility of the roof system and it does not allow the development of a rigid diaphragm behaviour of the roof itself. Due to this lack, there is an inefficiency in transferring and redistributing the horizontal seismic forces to the vertical elements. This can lead to the development of mechanisms due to relative movements between structural elements. Furthermore, given the different distribution of the participating mass and the stiffening effect provided by the cladding panels, the flexibility of the floor causes differences in the seismic response between the internal and external frames. In this way, the main damage is mainly linked with the fall of the horizontal structural elements (roof elements and beams) and the lack or reduced ability of the mechanical connections to achieve a proper restraint leads to the loss of support (Figure 3.1).

Many partial collapses with no obvious damage to the columns have occurred during the Emilian seismic sequence in 2012, in particular to those roofs equipped with skylights, which have contributed to increase the in-plane flexibility of the roof itself. This means that the horizontal seismic forces acting on the roof elements were transferred directly to the beams, with a consequent achievement of the maximum out-of-plane resistance capacity or facilitation of the overturning.

Figure 3.1 Fall of roof elements (left) and fall of I-shaped beams due to loss of support (right). The lack of support at the end of the beam led to a changing of the real static scheme and the beam is collapsed since it has not been designed for the new constraint configuration.

Precast lateral cladding panels

The absence of mechanical devices able to allow displacements and/or relative rotations between precast panels and the structure and the absence of appropriate restraints to prevent the overturning of the masonry wall have caused extensive damage to the external cladding. Regarding the brick infill, the collapse is mainly

associated to their high slenderness, out-of-plane flexibility and the lack of restraints to prevent tilting.

The top part of the cladding walls is often surmounted by strip windows without the presence of an overlying beam connected to the columns. This implies a collapse mechanism characterized by a rigid overturning of the wall as a rigid body; the consequence is a reduction of the value of the collapse multiplier factor for horizontal loads. In the case of masonry infill walls regularly distributed along the perimeter of the buildings without significant openings, it was noted that the walls can give a sufficient in-plane resistance for supporting the horizontal seismic loads, especially in the presence of a rigid floor diaphragm.

In some cases, also the structures with highly flexible roof showed undamaged masonry infill, especially in the case of a single portal structure. Despite this, the contribution provided by the external infill walls in terms of resistance to horizontal seismic stress is difficult to quantify, given the simultaneous in-plane and out-of-plane actions due to the earthquake.

Regarding the horizontal and vertical precast cladding panels, the fall of them is mainly due to the failure of the panel-structure connections.

It is known that in past building techniques, such connections were designed to withstand the gravitational load of the panel itself and to prevent its overturning due to small horizontal actions, such as wind pressure. However, the flexibility of the herein considered industrial buildings causes large lateral displacements, leading to an increase of relative displacement demand in the connections. Given the configuration of the static scheme as a hinged frame, an acceptable behaviour of these connections during an earthquake should allow non-negligible relative displacements and rotations between panels and structure.

The Emilian seismic sequence of 2012 has shown that the complex panel-structure interaction often induced the collapse of precast cladding panels, especially in case of irregularities along the height of the structure. As for the horizontal cladding panels, the displacement demand has mainly involved the upper rows (Figure 3.2), which are subjected to a greater relative displacement demand.

Figure 3.2 Failure of the support of the cladding panel with consequent fall of the panel itself (left and middle); out-of-plane overturning of the masonry infill in a single-storey industrial building (right).

It was noted that the vertical cladding panels have a better behaviour once they are fixed to the foundation beam.

Columns and top column forks

In the single-storey precast industrial buildings, the columns are generally placed inside cup footings and the modelling of the boundary at the base is assumed as a fixed node while the modelling of the beam-to-column connection at the top of the column is usually assumed as a hinged connection.

The bending and shear demand induced by the earthquake on the forks at the top of the column have generally exceeded the capacity of the fork itself, causing the consequent inability to control the sliding and/or the out-of-plane overturning of the beam (Figure 3.3).

Figure 3.3 Failure of the column due to the presence of infill panels and strip windows (left); failure of the fork at the top of the column due to the out-of-plane stress of the beam (right).

More rarely, it was observed the formation of plastic hinges at the base of the columns, since they are more vulnerable to damage caused by the shear forces acting

on the corresponding structural irregularities along the height of the construction, as in the case of strip windows (short column behaviour).

In limited cases, damage was also detected at the base of the columns, such as spalling of concrete cover and/or instability of longitudinal rebars due to the absence of the anti-seismic construction details in those zones where the formation of a plastic hinge is expected (for example the high distance between the transverse reinforcement and the bending at 90 degrees of the stirrups).

Visual surveys conducted after the Emilian earthquake sequence in 2012 showed that in many cases, the damage was caused by the impact of the columns with horizontal elements, such as beams and roof elements collapsed due to loss of support.

The vulnerability linked to the reinforced concrete fork at the top of the columns deserves particular attention. In fact, in the next chapter concerning the assessment of the EAL, different configurations will be analysed, such as the presence or not of a retrofit intervention (provided with two lateral steel profiles) and the different solutions in modelling the reinforced concrete fork at the top of the column.

Figure 3.4 and Figure 3.5 show the scheme of the retrofit intervention and the procedure for the evaluation of the acting forces that allow the correct design of the resistant elements, such as the two lateral UPN steel profiles, the retaining bolts and the passer steel dowel.

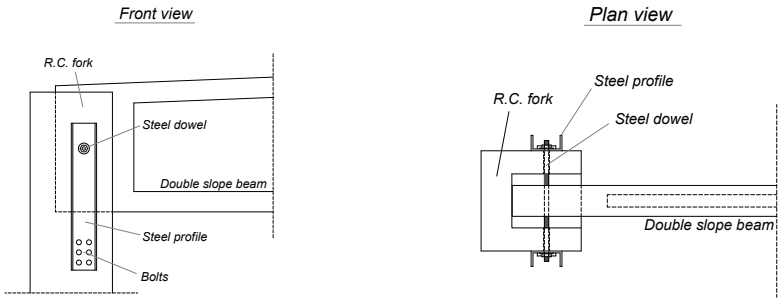

Figure 3.4 Beam-to-column hinged connection realized by a passing steel dowel and two lateral steel profiles: front view (left) and plan view (right) of the solution.

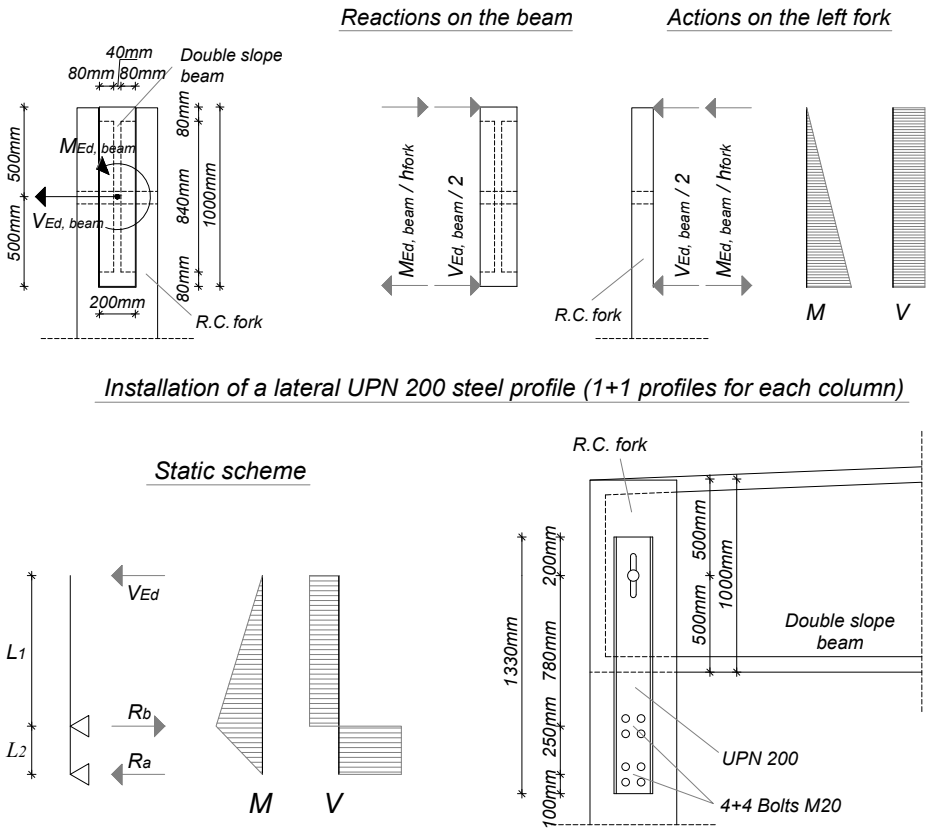

Figure 3.5 Actions and reaction acting respectively on the fork and on the double slope beam (above); the static scheme adopted for the determination of the forces (below on the left) and an example of a reinforcing retrofit on the fork provided by a double UPN 200 steel profile (below on the right).

Foundations

As previously mentioned, the typical design practice of foundations for precast industrial buildings provides the use of cup footings. These types of foundations have been widely adopted in the past, and regarding the eccentricity due to the horizontal load, they were sized to prevent the overturning induced by the wind and/or by the overhead cranes movement.

The main issues observed are related to the loss of verticality of the columns (Figure 3.6) mainly due to the rigid rotations and/or relative permanent displacements of the foundations. This problem is especially obvious with the absence of horizontal connections between the different isolated elements of the foundations.

Figure 3.6 Permanent loss of verticality: the presence of a gap in the lower side between the column and the external infills blocks can be observed (left); permanent rigid rotation of the columns in the isolated cup foundations (right).

3.2 Horizontal cladding panels: out-of-plane seismic response

In this section, the out-of-plane seismic response of the horizontal cladding panels and its interaction with the structure is investigated through a parametric study performed by linear and non-linear analyses. The formulas provided by current standards ([EN 1998-1, 2004] and [ASCE/SEI 7-10, 2010]) are compared with the results assessed through analyses carried out with fem models in order to show the inadequacy if these formulas in the estimation of the forces acting on the structure-to-cladding panel connection. The results observed from the parametric study allowed to develop a new formulation that is able to predict the value of these forces as an alternative to those formulations provided by current standards for non-structural elements. A direct application of this new formula is shown in a step-by-step example.

The cladding system is typically constituted by horizontal or vertical heavy precast RC panels, mainly reinforced with steel welded wire meshes [Riva *et al.*, 2001], installed on the outside of the building and connected to the main structural elements. The in-plane interaction between cladding and structural systems is distinguished in [Arnold, 1989]: completely separated cladding, accidentally participating cladding [Belleri *et al.*, 2016], controlled participating cladding ([Ferrara *et al.*, 2011] and [Scotta *et al.*, 2015]) and fully participating cladding ([Biondini *et al.*, 2013] and [Magliulo *et al.*, 2015]). In high seismicity regions [NIST GCR 95-681, 1995], connections enabling relative movements between the elements are commonly adopted, i.e. completely separated cladding according to [Arnold, 1989].

In the past Italian construction practice, the cladding system was considered as part of the non-structural elements, and it was primarily designed for vertical gravity loads and to avoid panel overturning due to out-of-plane wind or, more recently, seismic loads. Displacement compatibility associated to the interaction with the supporting structure was neglected. The relative displacements and rotations between the cladding panels and the supporting structure needed to be accommodated by the connecting system, owing to the lower stiffness of the connection devices compared to the connected RC precast elements: the cladding panel failure assessed after the Emilia earthquake was clearly related to the failure of the mechanical connections, such as anchor channels, C-shape or L-shape steel profiles ([Bournas *et al.*, 2014], [Belleri *et al.*, 2016] and [Colombo *et al.*, 2016]).

In recent years, experimental campaigns have been carried out to investigate the performance of cladding-to-structure subassemblies ([Colombo *et al.*, 2014],

[Fischinger *et al.*, 2014], [Isaković *et al.*, 2014] and [Pantoli *et al.*, 2016]), and design recommendations have been derived accordingly ([Belleri *et al.*, 2016] and [Colombo *et al.*, 2016]), mainly concerning the in-plane behaviour of such systems. Noteworthy, in the case of out-of-plane loading, the seismic demand on cladding elements and connections is still determined based on building code formulas associated to non-structural elements (clause 4.3.5 in EN 1998-1, 2004; clause 13.3 in ASCE 7-10, 2010), thus disregarding cladding-to-structure interaction and without accounting for displacement compatibility issues.

The current research evaluates the out-of-plane vulnerability and performance of horizontal cladding panels typical of industrial and commercial precast reinforced concrete buildings (Figure 3.7). Starting from the available formula on seismic loads in non-structural elements ([EN 1998-1, 2004] and [ASCE/SEI 7-10, 2010]), a new procedure is investigated to account for the influence of the mass, the fundamental period and the vertical position of the cladding system. The formulation is validated by means of non-linear time history analyses on selected reference structures. The proposed formulation is suitable for the design of new cladding panels and for the assessment of existing systems.

Figure 3.7 Examples of precast industrial buildings with horizontal precast cladding panels. Undamaged panels (left); damaged panels after Emilia earthquake (right).

3.2.1 Existing design practice

In the current design practice, cladding panels are regarded as non-structural elements and are typically included as lumped masses in finite element models. The out-of-plane seismic loads acting on the panel-to-column connections are evaluated from simplified formulations, typically related to response spectra associated to the supporting structure. The main reference codes adopted in the design practice are [EN 1998-1, 2004] and [ASCE/SEI 7-10, 2010].

In [EN 1998-1, 2004], the inertia load acting on the panel centroid (F_i) takes into account the dynamic amplification associated to parameters such as the relative vertical position of the panel centroid (h_p) compared to the building height (H) and the ratio between the fundamental period of the panel (T_p) and the fundamental period of the building (T_s):

$$F_i = PGA \cdot \left[\frac{3\left(1+h_p/H\right)}{1+\left(1-T_p/T_s\right)^2} - 0{,}5 \right] \frac{W_p}{q_a} \qquad \text{Eq. 3.1}$$

where W_p is the panel weight, PGA is the peak ground acceleration as a fraction of g, and q_a is a behaviour factor, which is taken equal to 2, according to what is suggested by [EN 1998-1, 2004] - "*§ 4.3.5.4 - Behaviour factors" - Table 4.4* for facade elements and equal to 1 in order to assess the elastic response in case the designer wants to assess the elastic response.

A similar formulation, independent by the panel to structure period ratio, is provided in [ASCE/SEI 7-10, 2010]:

$$F_i = 0{,}4 \cdot S_{DS} \left[1+2\frac{h_p}{H} \right] \frac{I_p \cdot a_p}{R_p} W_p \qquad \text{Eq. 3.2}$$

where S_{DS} is the spectral acceleration at short period, a_p and R_p are the component amplification and response modification factors respectively; a_p = 1, R_p = 2,5 for exterior non-structural wall elements and a_p = 1,25, R_p = 1 for the fasteners of the connecting system. I_p is the component importance factor, ranging from 1 to 1,5. Other formulations are available in the literature based on the derivation of floor spectra for multi-storey buildings, either accounting for or disregarding the inelastic behaviour of the lateral force resisting system ([Medina *et al.*, 2006], [Politopoulos, 2010], [Sullivan *et al.*, 2013] and [Petrone *et al.*, 2015]). However, these formulations do not investigate the case of non-structural elements at heights below the first storey, such as in the case of horizontal cladding in single-storey industrial buildings.

It is worth noting that [EN 1998-1, 2004] (§ 4.3.5.1.2) claims that in the case of non-structural elements of great importance or of a particularly dangerous nature, the seismic analysis shall be based on a realistic model of the relevant structures and on the use of appropriate response spectra associated to the supporting structure. The use of modal analysis is also considered in [ASCE/SEI 7-10, 2010] as an alternative to Eq. 3.2.

In the following, a parametric analysis is conducted to check the validity of the aforementioned formulations (see Chapter 3.2.2), and a new simplified procedure that best fits the analysis results is proposed and validated in order to have a more accurate estimation of the out-of-plane loads on the horizontal cladding panels (Chapter 3.2.4).

3.2.2 Parametric analysis

To investigate the out-of-plane seismic loads acting on horizontal cladding panels, an elastic parametric analysis is conducted taking as reference a structural system constituted by 2D multi-bay frames, in which columns are pinned to roof beams and each panel is modelled as a single degree of freedom system (SDOF) with mass m_p and stiffness k_p (Figure 3.8).

The results of the parametric analysis are rearranged as a function of three main dimensionless parameters governing the out-of-plane inertia loads on each cladding panel:

- m_r: ratio between the total mass of the panels on the two frame ends (mass of each panel, m_p, times the total number of panels, 2 n_p) and the roof mass (m_{roof});
- T_r: ratio between the fundamental period of the panel (T_p) and the fundamental period of the system (T_s); T_p is obtained considering the panel as a simply supported beam; T_s is obtained modelling each panel as a lumped mass on the supporting column at a height corresponding to the panel centroid (the spring representing the panel stiffness in Figure 3.8 is here removed);
- h_r: ratio between the vertical position of each panel centroid (h_p) and the column height (H); this ratio identifies the single panel.

The analyses consider: frames with 2, 4 or 8 columns with fixed stiffness and different roof masses (m_{roof}) distributed at the top of each column as tributary masses (m_{top}); 3 or 5 horizontal cladding panels along the height of each column (being n_p the number of panels on each column, Figure 3.8); different periods (T_p) and masses (m_p) of the

panels. The roof mass is selected in order to have a fundamental period of the system in the constant velocity region of the pseudo-acceleration spectrum, being the fundamental period of typical precast industrial and commercial buildings in that range cause the slenderness and large height of this type of structures. Previous studies have shown that the selection of the values for the period of the system in the constant velocity region of the pseudo-acceleration spectrum well correlates with maximum displacement demand [Akkar *et al.*, 2005] [Akkar and Özen, 2005] [Senel and Kayhan, 2010]. 7 values of T_s equally spaced between T_C and T_D [EN 1998-1, 2004] are considered; 4 spectra [EN 1998-1, 2004] type 1 spectrum are taken into account by changing the soil conditions (A, B, C and D); the value of the PGA is not relevant being the results presented in dimensionless terms. The panel period (T_p) is selected in the range 0-2s with 0,02 intervals; four values of mass ratio (m_r) are selected and assumed equal to 0,05, 0,1, 0,5 and 1. It is worth noting that the selected parameters T_r and m_r fall in the ranges 0–1,5 and 0,025–1,00 respectively for the considered combination of structure and panel characteristics. However, for the geometry distribution of Italian precast concrete industrial buildings, the ranges 0,1-0,7 and 0,05-1 should be better considered for T_r and m_r respectively [Casotto *et al.*, 2015]; other values of T_r and m_r could be associated to different structural typologies and cladding systems. In this way, a total of more than 33'000 dynamic analyses are performed. The range of interest for the considered structural typology as previously defined is represented in each figure with the un-shaded area.

Figure 3.8 shows an example of the considered structural system: three-bay frame with four columns and five panels at each side of the frame.

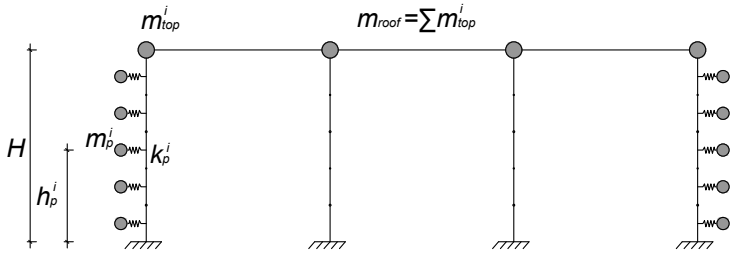

Figure 3.8 Structural system considered for the evaluation of the out-of-plane loads on cladding panels.

The results of the response spectrum analyses are expressed in terms of α (Figure 3.9), which is defined as the ratio between the panel inertia load obtained from the analyses and the load obtained from a linear load distribution (F_a) with top ($F_{a,\,top}$) and bottom ($F_{a,\,bot}$) value equal to:

$$F_{a,top} = S_a\left(T_s\right)m_p \qquad \text{Eq. 3.3}$$

$$F_{a,bot} = S_a\left(T_p\right)m_p \qquad \text{Eq. 3.4}$$

$S_a(T)$ is the pseudo-acceleration spectral value for a period T, considering a spectrum with 5% relative damping. It should be noted that the choice to refer to this linear distribution is an arbitrary choice just aimed at simplifying calculations.

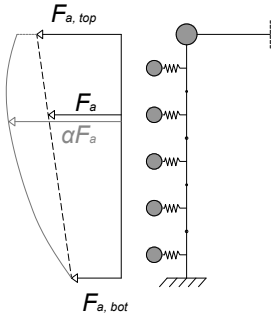

Figure 3.9 Actual load distribution on the panels and linear distribution considered for the evaluation of the dimensionless load parameter α.

Figure 3.10 and Figure 3.11 show the out-of-plane loads on each panel as a function of m_r and T_r in terms of α; the significance of the dashed line will be explained later. In these figures, the sole results considering 5 panels and selected values of m_r in the range of interest are presented. As expected, a peak value of α in proximity of $T_r = 1$ is observed; such peak is higher for panels placed at the top of the column and lower for increasing values of the mass ratio (m_r). For T_r lower than 0,5, an increase of α is observed, especially for central panels and for increasing values of m_r. Similar results are obtained in the case of 3 panels. The influence of the number of columns is already accounted for by T_r and m_r. The type of the considered spectra leads to differences for low values of T_r.

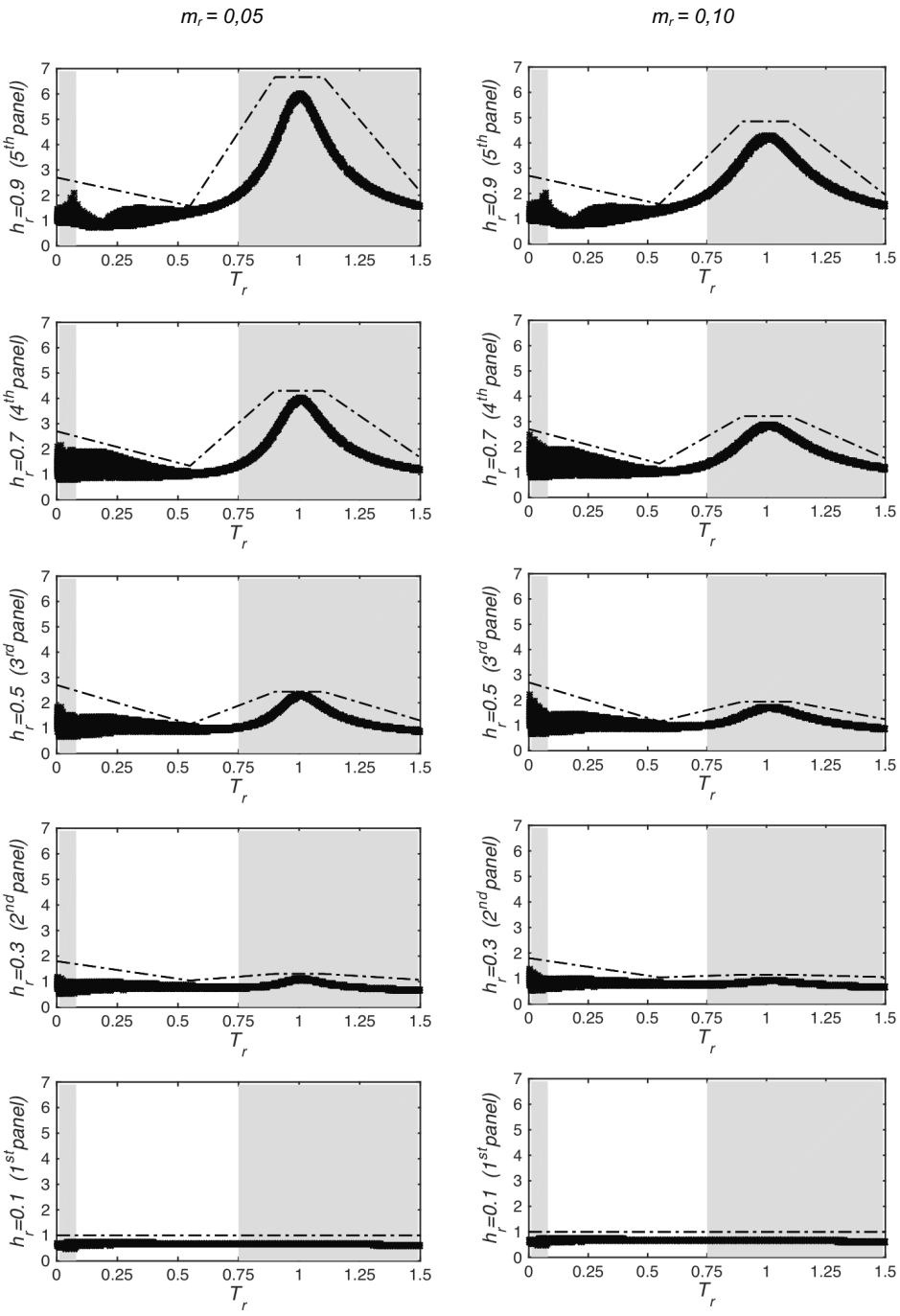

Figure 3.10 Loads on each panel in terms of α value in the cases of m_r equal to 0,05 and 0,10. Note: range of interest for the considered structural typology in the un-shaded area.

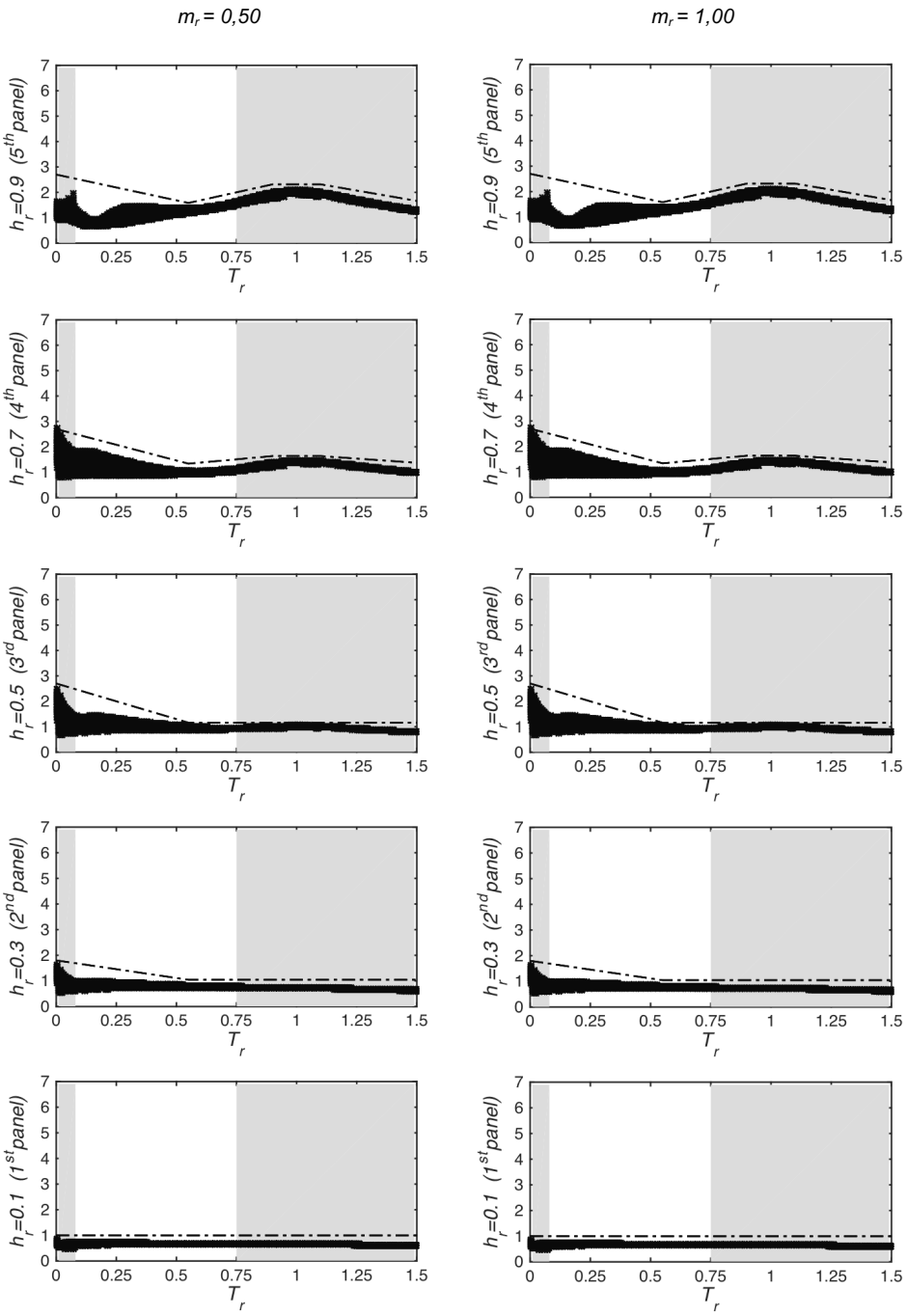

Figure 3.11 Loads on each panel in terms of α value in the cases of m_r equal to 0,50 and 1,00. Note: range of interest for the considered structural typology in the un-shaded area.

3.2.3 *Comparison with current design formulation*

The formulations suggested by the codes are compared to the results of the parametric analysis. The same characteristics of the multi-bay frames are considered in order to estimate the seismic load on each cladding panel with the code equations and the response spectrum analysis.

Figure 3.12 and Figure 3.13 show the minimum values of the ratio between the panel out-of-plane load computed with [EN 1998-1, 2004] (Eq. 2.1) or [ASCE/SEI 7-10, 2010] (Eq. 3.2) and the corresponding load obtained from the response spectrum analyses. Values below the unity represent conditions in which the equations of the codes provide unsafe results. In these figures, EN_1 and EN_2 consider [EN 1998-1, 2004] formula (Eq. 2.1) with q_a=1 and q_a=2 respectively as specified in this standard itself; AS_f and AS_w consider [ASCE/SEI 7-10, 2010] formula (Eq. 3.2) for wall element and fasteners respectively, both with I_p=1 range of interest for the considered structural typology in the un-shaded area.

In the range of interest, the best predictions are provided by Eq. 3.2 ([ASCE/SEI 7-10, 2010]) in the case of fasteners of the connecting system, especially for the lower panels, while Eq. 2.1 ([EN 1998-1, 2004]) is always unsafe when considering q_a=2, which is quite commonly adopted in the design practice. Outside the range of interest, it is worth observing how both formulations could provide unsafe results for panels in the higher rows in the case of low m_r and for T_r close to unity. In general Eq. 2.1 ([EN 1998-1, 2004]) with q_a=1 provides higher values than Eq. 3.2 ([ASCE/SEI 7-10, 2010]).

The current design formulations are not always conservative, hence a more refined procedure is investigated here to better capture the seismic load demand on precast cladding panels of single-storey buildings.

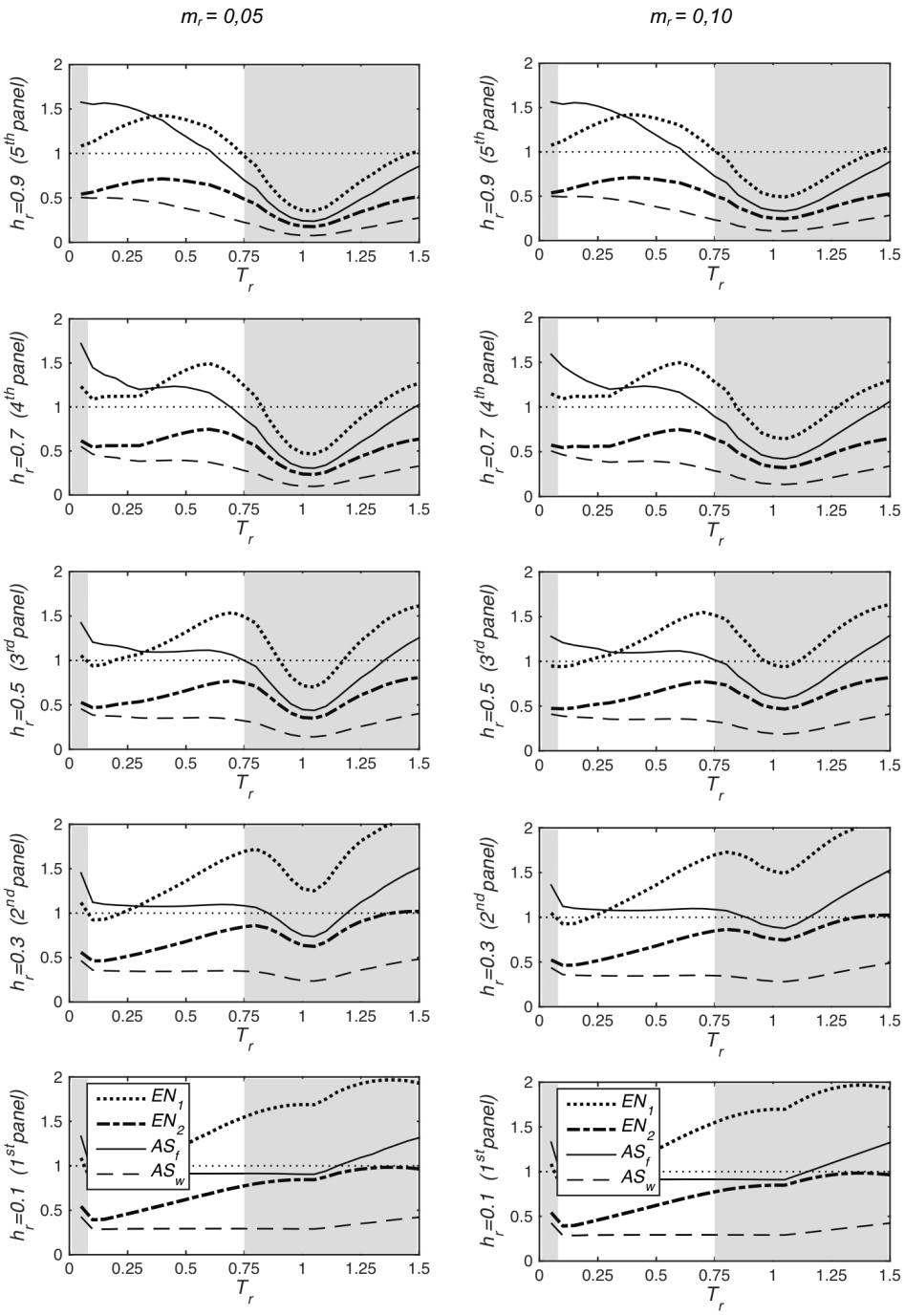

Figure 3.12 Minimum ratio between design practice formula and parametric analysis results in the cases of m_r equal to 0,05 and 0,10.

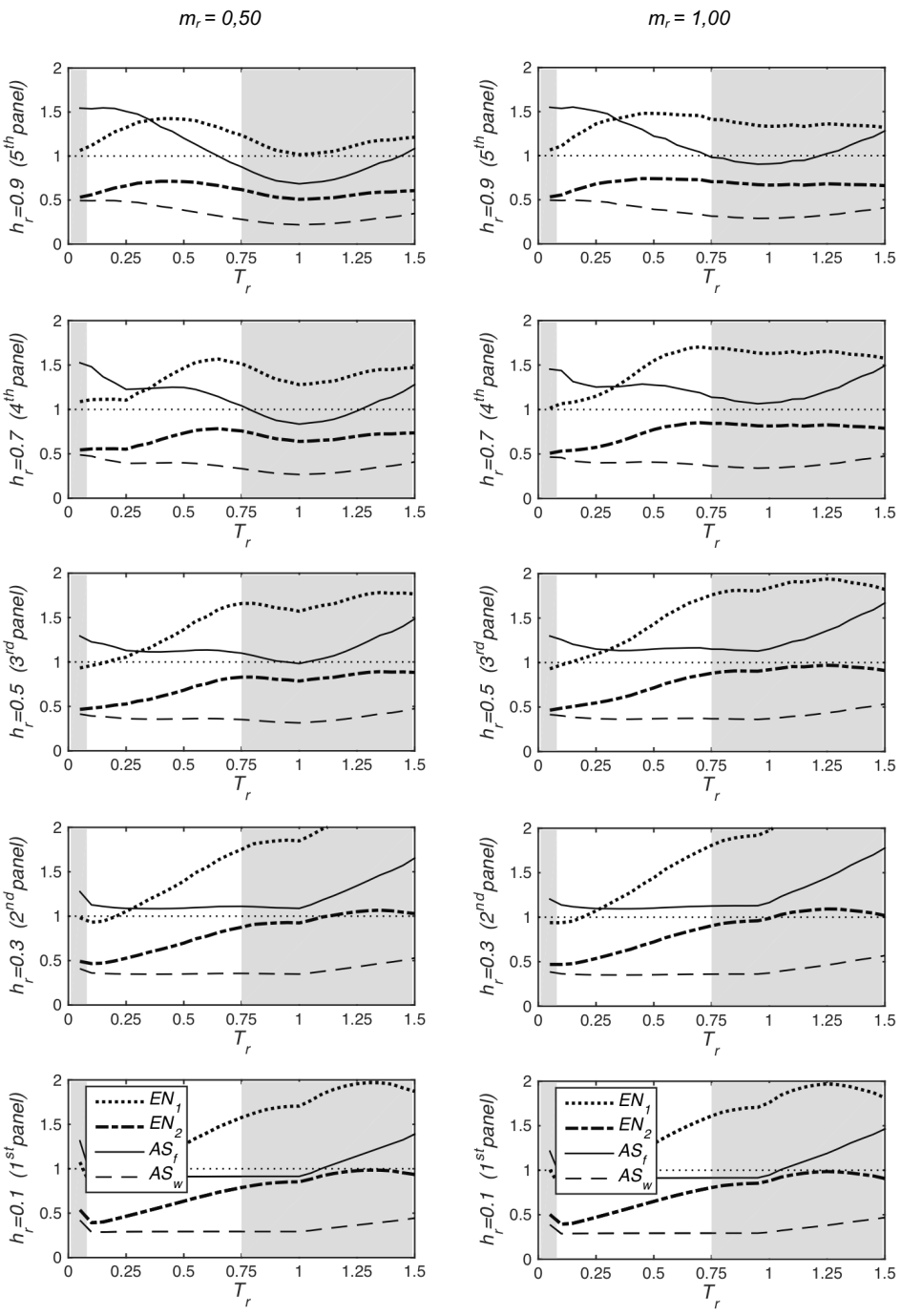

Figure 3.13 Minimum ratio between design practice formula and parametric analysis results in the cases of m_r equal to 0,50 and 1,00.

3.2.4 *Refined design formulation proposed*

A refined simplified procedure for the evaluation of the out-of-plane seismic loads on horizontal cladding panels in precast one-storey structures is here defined based on the results of the parametric analysis. The results of the elastic response spectrum analyses are fitted (dashed lines in Figure 3.10 and Figure 3.11), and a new formulation of α fitting the results is provided.

Four regions are identified (Figure 3.14) delimited by five values of T_r ($T_{r\,1}$=0, $T_{r\,2}$ =0,55, $T_{r\,3}$=0,9, $T_{r\,4}$=1,1 and $T_{r\,5}$=1,55). The α-value is assumed to vary linearly as a function of T_r in each region j:

$$\alpha = \alpha_j + T_r \cdot \frac{\alpha_{j+1} - \alpha_j}{T_{r\,j+1} - T_{r\,j}} \qquad \text{Eq. 3.5}$$

The values of α delimiting each region (α_j and α_{j+1}) are obtained by means of linear least squares and are expressed as a function of h_r in order to determine the force on each panel:

$$\alpha_1 = \begin{cases} 1{,}00 & for \quad h_r < 0{,}1 \\ 3{,}75 \cdot h_r + 0{,}63 & for \quad 0{,}1 \le h_r < 0{,}5 \\ 2{,}5 & for \quad 0{,}5 \le h_r < 0{,}9 \end{cases} \qquad \text{Eq. 3.6}$$

$$\alpha_2 = \alpha_5 = 1 + 0{,}83 \cdot h_r^2 - 0{,}1 \cdot h_r$$

$$\alpha_3 = \alpha_4 = c \cdot m_r^d$$

where

$$c = 1{,}87 \cdot h_r^2 - 0{,}68 \cdot h_r + 0{,}78$$

and

$$d = 0{,}64 \cdot h_r^2 - 1{,}23 \cdot h_r + 0{,}12$$

The minimum α allowed in all the regions corresponds to α_2.

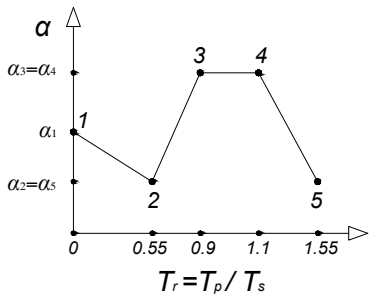

Figure 3.14 Proposed linearization of α-value.

The inertia load (F_i) on each panel is obtained by the following simplified 6-step procedure:

1. evaluate $m_r = (2\ n_p\ m_p)/m_{roof}$, $T_r = T_p/T_s$ and $h_r = h_p/H$;
2. select the region (Figure 3.14) which T_r belongs to;
3. evaluate α_j and α_{j+1} corresponding to the delimiting points of the selected region (Eq. 3.6);
4. get the appropriate α from Eq. 3.5;
5. calculate the inertia load on the panel (F_i) as:

$$F_i = \alpha\left[F_{a,bot} + h_r\left(F_{a,top} - F_{a,bot}\right)\right] \qquad \text{Eq. 3.7}$$

6. calculate the out-of-plane load on each connection ($F_{i,c}$) as:

$$F_{i,c} = F_i / 4 \qquad \text{Eq. 3.8}$$

A step-by-step example shows here a direct application of the formulation and procedure proposed. The characteristics of the assumed case study are reported in Table 3.1.

Table 3.1 Descriptive characteristics of the assume case study.

Description	Symbol	Value
Fundamental period of the system	T_s	1,3s
Fundamental period of the cladding panel	T_p	0,2s
Column height, total height of the structure	H	7,2m
Mass of the cladding panel	m_p	10300kg
Roof mass	m_{roof}	67300kg
Number of horizontal cladding panels	n_p	3
Vertical position of each panel centroid	h_p	1,18, 3,58 and 5,95m
Spectral acceleration at the top	$S_a(T_s)$	0,210g
Spectral acceleration at the bottom	$S_a(T_p)$	0,875g

By using the aforementioned procedure, it follows that:

1. mass ratio (m_r), ratio between the fundamental periods (T_r) and ratio between heights (h_r) are respectively equal to:

$$m_r = \frac{2 \cdot n_p \cdot m_p}{m_{roof}} = 0,9183$$

$$T_r = \frac{T_p}{T_s} = 0,1583$$

$$h_{r\ 1^{st}\ panel} = \frac{h_{p\ 1^{st}\ panel}}{H_s} = \frac{1,18m}{7,2m} = 0,1619; \qquad h_{r\ 2^{nd}\ panel} = \frac{h_{p\ 2^{nd}\ panel}}{H_s} = \frac{3,58m}{7,2m} = 0,4972;$$

$$h_{r\ 3^{rd}\ panel} = \frac{h_{p\ 3^{rd}\ panel}}{H_s} = \frac{5,95m}{7,2m} = 0,8264;$$

2. given T_r equal to 0,1538, the selected region of the Figure 3.14 is the range between $T_{r\,1} = 0$ and $T_{r\,2} = 0,55$;

3. from the formula provided by Eq. 3.6, the values of α_j and α_{j+1} corresponding to the delimiting points of the selected region are calculated:

1st panel	$\alpha_1 = 3,75 \cdot h_{r\ 1^{st}\ panel} + 0,63 = 1,2446$	$\alpha_2 = 1 + 0,83 \cdot h^2_{r\ 1^{st}\ panel} - 0,1 \cdot h_{r\ 1^{st}\ panel} = 1,0059$
2nd panel	$\alpha_1 = 3,75 \cdot h_{r\ 2^{nd}\ panel} + 0,63 = 2,4946$	$\alpha_2 = 1 + 0,83 \cdot h^2_{r\ 2^{nd}\ panel} - 0,1 \cdot h_{r\ 2^{nd}\ panel} = 1,1555$
3rd panel	$\alpha_1 = 2,5$	$\alpha_2 = 1 + 0,83 \cdot h^2_{r\ 3^{rd}\ panel} - 0,1 \cdot h_{r\ 3^{rd}\ panel} = 1,4842$

4. α can now be evaluated for each panel according to Eq. 3.5, the values are:

1st panel	$\alpha_{1^{st}\ panel} = \alpha_1 + T_r \cdot \frac{\alpha_2 - \alpha_1}{T_{r\,2} - T_{r\,1}} = 1,2446 + 0,1538 \cdot \frac{1,0059 - 1,2446}{0,55 - 0} = 1,1778$
2nd panel	$\alpha_{2^{nd}\ panel} = \alpha_1 + T_r \cdot \frac{\alpha_2 - \alpha_1}{T_{r\,2} - T_{r\,1}} = 2,4946 + 0,1538 \cdot \frac{1,1555 - 2,4946}{0,55 - 0} = 2,1200$
3rd panel	$\alpha_{3^{rd}\ panel} = \alpha_1 + T_r \cdot \frac{\alpha_2 - \alpha_1}{T_{r\,2} - T_{r\,1}} = 2,5 + 0,1538 \cdot \frac{1,4842 - 2,5}{0,55 - 0} = 2,2159$

5. the inertia load on the panel (F_i) are equal to:

1st panel $$F_{1^{st}\ panel} = a_{1^{st}\ panel} \cdot \left[F_{a,bot} + h_{r\ 1^{st}\ panel} \cdot \left(F_{a,top} - F_{a,bot} \right) \right] = 91{,}13kN$$

2nd panel $$F_{2^{nd}\ panel} = a_{2^{nd}\ panel} \cdot \left[F_{a,bot} + h_{r\ 2^{nd}\ panel} \cdot \left(F_{a,top} - F_{a,bot} \right) \right] = 64{,}76kN$$

3rd panel $$F_{3^{rd}\ panel} = a_{3^{rd}\ panel} \cdot \left[F_{a,bot} + h_{r\ 3^{rd}\ panel} \cdot \left(F_{a,top} - F_{a,bot} \right) \right] = 38{,}72kN$$

6. and then the out-of-plane load on each of the four connections ($F_{i,c}$) are equal to:

1st panel $$F_{1^{st}\ panel,c} = \frac{F_{1^{st}\ panel}}{4} = 22{,}78kN$$

2nd panel $$F_{2^{nd}\ panel,c} = \frac{F_{2^{nd}\ panel}}{4} = 16{,}19kN$$

3rd panel $$F_{3^{rd}\ panel,c} = \frac{F_{3^{rd}\ panel}}{4} = 9{,}68kN$$

3.2.5 *Further considerations: influence of plastic hinge development at the base of the columns*

The influence of the development of a plastic hinge at the column base is investigated by means of non-linear time history analyses considering one of the configurations used in the parametric elastic analyses: a single-portal frame with five panels along the height of each column with fixed T_s and m_{roof}. The plastic hinge is modelled according to the Takeda hysteresis rule [Takeda *et al.*, 1970] by considering an approximate length equal to the dimension of the cross-section of the column and the yield moment is chosen in order to obtain a behaviour factor q equal to 1,5, 2,5 and 4; q is taken as the ratio between the bending moment obtained from an elastic analysis and the yield moment. The ground acceleration is provided by an artificial record spectrum-compatible with [EN 1998-1, 2004] type 1 spectrum, soil type A, and a_g=0,35g (ground acceleration on rock), generated with the SIMQKE-1 algorithm [Vanmarcke and Gasparini, 1976].

Figure 3.15 and Figure 3.16 show the results of the analyses in terms of load ratio between the inelastic and elastic case. The influence of the behaviour factor is relevant especially for the panels in the higher rows and for T_r closed to unity. In the considered range of T_r, un-shaded area in both Figure 3.15 and Figure 3.16, and for low values of m_r, the difference between the various behaviour factors is not so relevant.

It is worth mentioning that the considered type of structures is characterized by higher flexibility compared to traditional RC structures, both for the high inter-storey height and for the lateral force resisting system, i.e. cantilever columns fixed at the base. The high flexibility leads to low values of the displacement ductility demand, hence low values of the behaviour factor. As a safety measure, it is therefore suggested to evaluate the out-of-plane loads on cladding panels without accounting for the load reduction due to the development of column plastic hinges. In the case of response spectrum analyses this condition is accomplished by taking the behaviour factor equal to unity in the cladding out-of-plane load evaluation; this condition is a possible choice is in [ASCE/SEI 7-10, 2010] but not in [EN 1998-1, 2004].

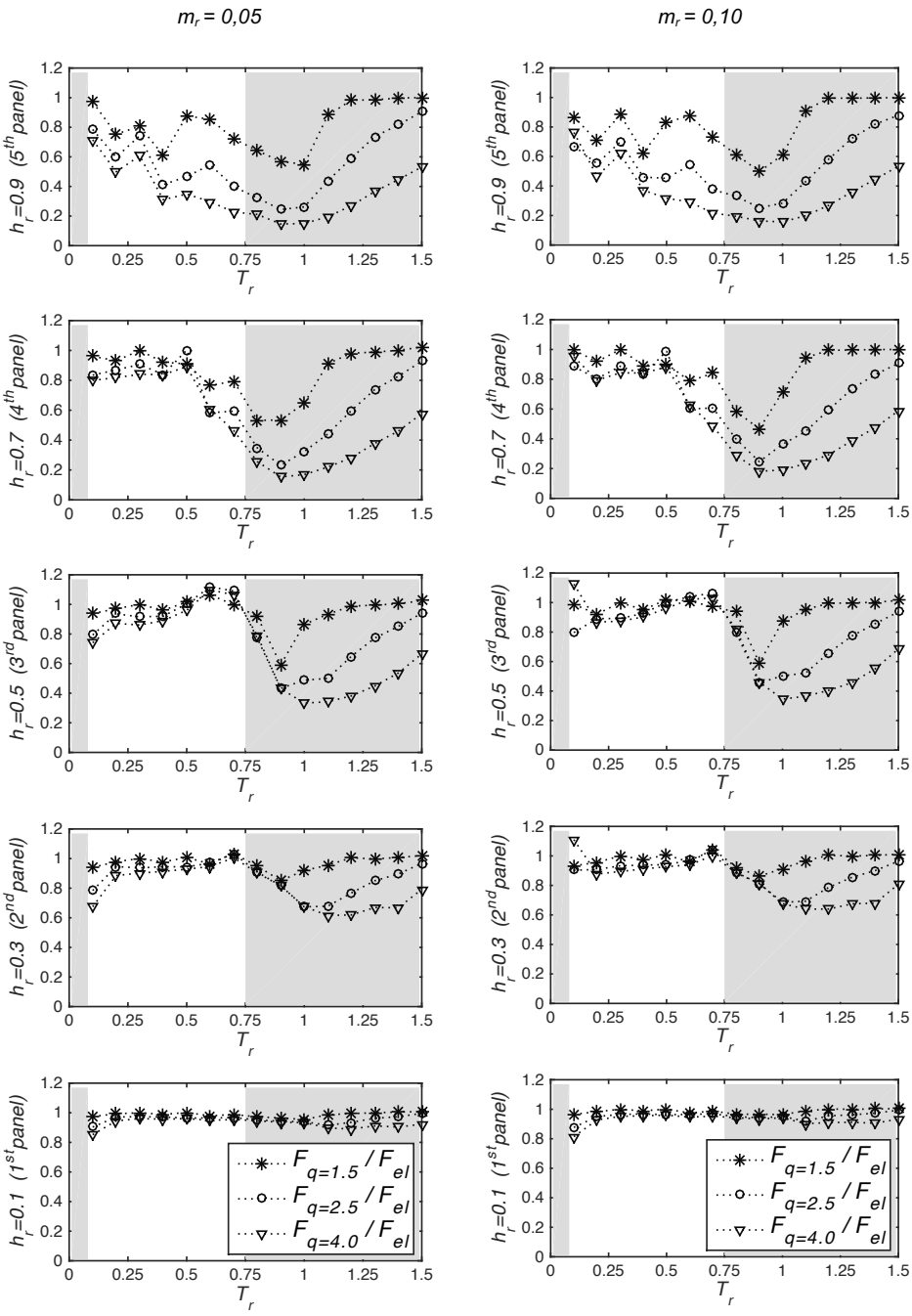

Figure 3.15 Ratio between the inertia load in the panel in the inelastic and elastic case with m_r equal to 0,05 and 0,10. Note: range of interest for the considered structural typology in the un-shaded area.

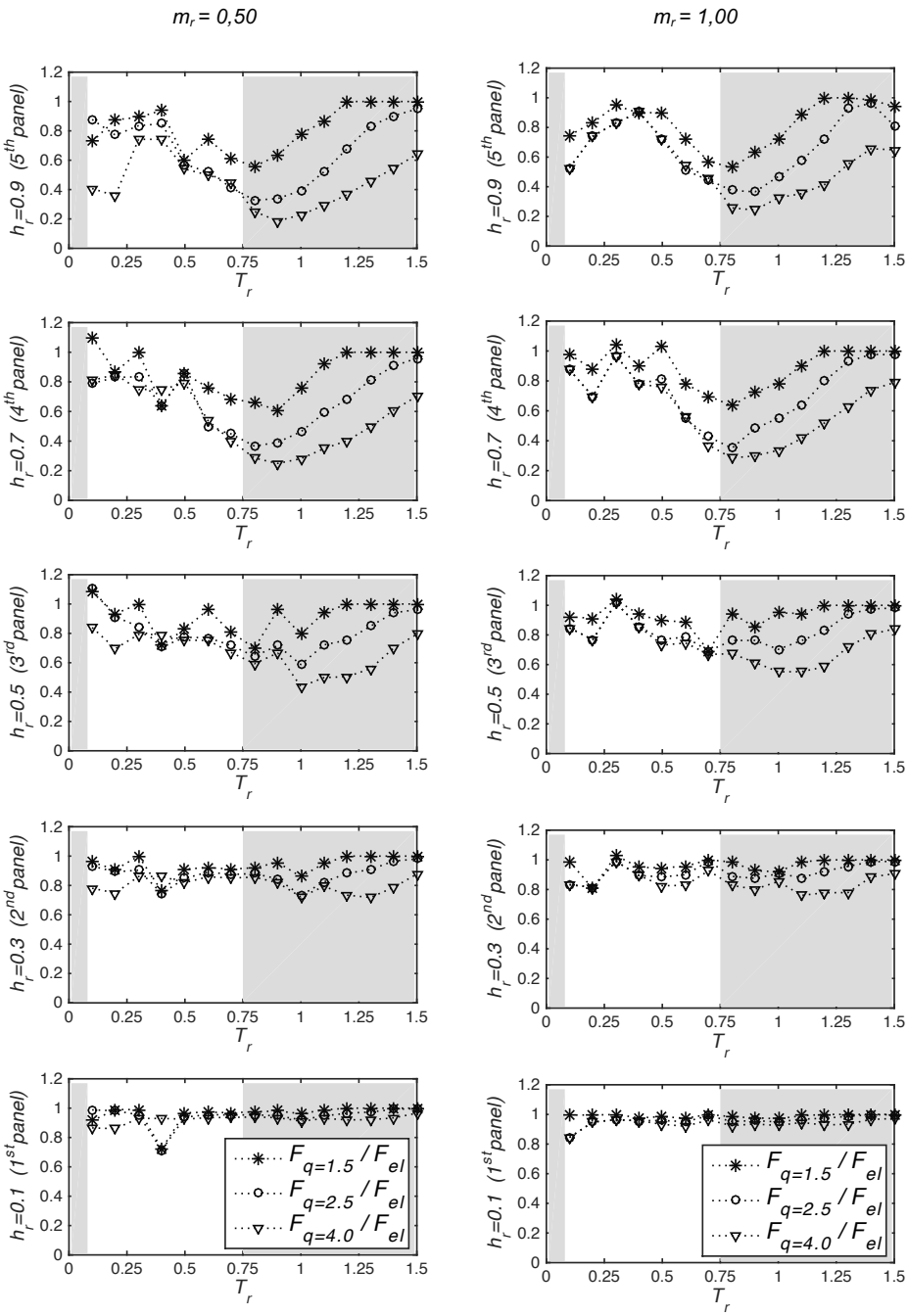

Figure 3.16 Ratio between the inertia load in the panel in the inelastic and elastic case with m_r equal to 0,50 and 1,00. Note: range of interest for the considered structural typology in the un-shaded area.

3.3 *Influence of the overhead crane in the seismic response of precast one-storey buildings*

The purpose of the current Chapter is to investigate the influence of the overhead crane in the seismic response of a typical RC precast industrial building in terms of difference on both top displacements and curvature at the base of the column. Possible differences in values of these engineering demand parameters might affect the value of EAL, for this reason it is important to understand how the presence of the overhead crane in a RC precast industrial building can influence the seismic response of the structure. At first, the equations of motion are analysed in order to define the combined model structure with overhead crane as well as the equivalent stiffness and equivalent coefficient of damping parameters which are essential in the modelling. Laboratory tests are also conducted on the overhead crane to determine the damping factor considering different configurations of the overhead crane. Afterwards, once defined these parameters, different modelling solutions are taken into account and compared among themselves as well as hints for optimal modelling are suggested. In the end, the influence of the overhead crane is analysed in a 3D model and observed results are discussed.

Most of the industrial buildings that were damaged during the recent earthquakes in the Emilia region in May 2012, were characterized by the presence of overhead crane. This is a dynamic element connected to the structure of the building with fundamental importance for the phases of moving and/or lifting loads with high weight such as the inner content of typical industrial buildings.

Although this component is normally classified as a non-structural element, its presence cannot be overlooked if we want to analyse the structural seismic response. For this reason, the necessity to investigate the influence of the overhead crane in the global and local seismic response of the structure was born ([CNR 10021-85, 1985] and [EN 1993-6, 2007]).

The contribution of the crane to the seismic response of the structural system is affected by the swinging suspended load. This suspended load cannot be directly entered as a mass rigidly connected to the structure since its behaviour is closer to a pendulum.

For this reason, the approach used to perform the seismic analysis has been to consider the whole system as a combination between the frame structure and the crane connected to it. The next chapter will explain the procedure adopted for obtaining the equations of motions and then the formula for assessing the damping factor ζ.

Starting from the equations of motion of a system with two degrees of freedom with a pendulum behaviour subjected to the motion of the support, it is possible to find the analogy with a classical two degrees of freedom system. This allowed defining how to model the pendulum system in the finite element analyses: the behaviour of the hanging load is comparable to a single degree of freedom system with mass equal to the hanging mass and horizontal stiffness equal to mg/L where L is the length of the cables that connect the load hanging from the crane.

3.3.1 Equation of motions

3.3.1.1 Structure model

The main structural model representing a one-bay industrial building can be represented as a single degree of freedom (SDOF) model as shown in Figure 3.17 (left). In this scheme, the discrete lumped mass M is connected to the global fixed reference system through an ideal spring characterized by a constant stiffness k and a viscous damper with a damping coefficient b. The energy within the system is dissipated by this viscous damper. On this system is also applied an external time varying force.

Figure 3.17 Single degree of freedom scheme adopted for the structure (to the left) and the free body diagram of the structure model (on the right).

The equation of motion of the aforementioned system is obtained applying the D'Alembert's principle of dynamic equilibrium which argues that the sum of the different forces acting on the system must be equal in each time period t considered.

Imposing the equilibrium of the forces shown in the previous figure is possible to obtain:

$$\ddot{x}(t)+\frac{b}{M}\dot{x}(t)+\frac{k}{M}x(t)=\frac{1}{M}F(t) \qquad \text{Eq. 3.9}$$

with the possibility to replace k and b with ζ and ω, which represent the structure's damping factor and the natural frequency:

$$\zeta=\frac{b}{b_{cr}}=\frac{b}{2\sqrt{kM}} \qquad \omega=\sqrt{\frac{k}{M}} \qquad \text{Eq. 3.10}$$

3.3.1.2 Pendulum tuned mass damper (PTMD) model

The crane can be modelled as a simple pendulum tuned mass damper (PTMD) with a point mass m supported by a massless rod of length L which has a pivot point at the other end (Figure 3.18, left). The coefficient c represents the pendulum friction constant. The damping between the pendulum and the structure is represented by a viscous damper with damping coefficient d constrained to move only along the horizontal direction. The free body diagram of the pendulum is shown in Figure 3.18, on the right.

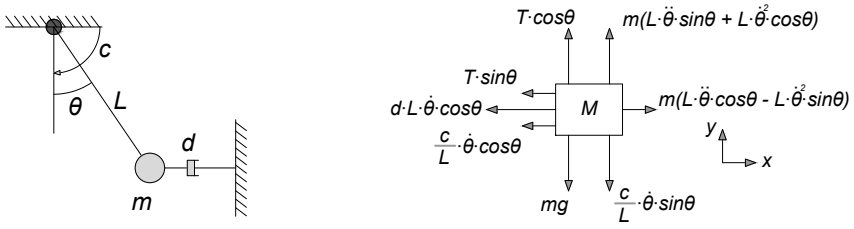

Figure 3.18 PTMD system adopted for the crane (left) and free body diagram of the pendulum (right).

Also in this case, the D'Alembert principle of dynamic equilibrium is used to evaluate the equation of motion of the pendulum which is equal to:

$$\ddot{\theta}(t) = -\frac{1}{mL}\left(\frac{c}{L} + dL\cos^2\theta(t)\right)\dot{\theta}(t) - \frac{g}{L}\sin\theta(t) \qquad \text{Eq. 3.11}$$

Since in the typical configurations of use, the crane is not perturbed much from its stable equilibrium configuration, it is possible to consider small values of the rotation at the pivot point of the pendulum, then Eq. 3.11 can be linearized by assuming that the two harmonic terms $cos\theta(t)$ and $sin\theta(t)$ are approximated to 1 and $\theta(t)$ respectively.

The equation of motion becomes:

$$\ddot{\theta}(t) = -\frac{1}{mL}\left(\frac{c}{L} + dL\right)\dot{\theta}(t) - \frac{g}{L}\theta(t) \qquad \text{Eq. 3.12}$$

3.3.1.3 Combined model

The combined final model consists of a PTMD model mounted to the structure. The resulting dynamic system brings together the dynamic response of the individual structure and PTMD systems considering the coupling dynamic response between the two models (see Figure 3.19, left) [Lourenco, 2011].

The representation of an equivalent translational tuned mass damper (TMD) system, as illustrated in the Figure 3.19 on the right, is useful to express the motion of the pendulum mass m in terms of its horizontal displacement instead of its rotational displacement. With this modelling assumption, it is possible to include the contribution of the crane by adding a mass m equal to the suspended load connected to the structure via an elastic ideal spring with an equivalent stiffness k_{eq} and a viscous damper with an equivalent coefficient of damping b_{eq}.

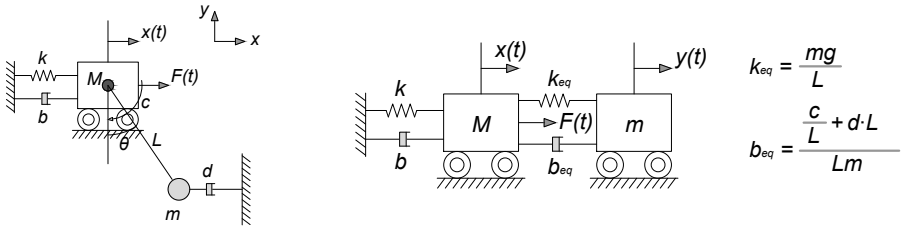

Figure 3.19 Structure and pendulum combined model (left) and equivalent translational TMD model (right).

For small values of angular rotations, the horizontal displacement, the velocity and the acceleration of the pendulum can be expressed as:

$$y(t) = L\theta \qquad \dot{y}(t) = L\dot{\theta} \qquad \ddot{y}(t) = L\ddot{\theta} \qquad \text{Eq. 3.13}$$

Replacing these last expressions Eq. 3.13 in Eq. 3.12, it is possible to obtain:

$$\frac{\ddot{y}}{L} = -\frac{1}{mL}\left(\frac{c}{L} + dL\right)\frac{\dot{y}}{L} - \frac{g}{L}\cdot\frac{y}{L} \qquad \text{Eq. 3.14}$$

then

$$m\ddot{y} + d\dot{y} + \frac{mg}{L}y = 0 \qquad \text{Eq. 3.15}$$

Eq. 3.15 is similar to the equation of motion of a SDOF system, where the coefficients c and k used to describe the SDOF are in this case equal to d and mg/L respectively.

According to equation Eq. 3.15, the equivalent stiffness k_{eq} and the equivalent coefficient of damping b_{eq} are then equal to:

$$k_{eq} = \frac{mg}{L} \qquad b_{eq} = \frac{\frac{c}{L} + dL}{L} \qquad \text{Eq. 3.16}$$

By expressing the equivalent coefficient of damping b_{eq} as a function of the only viscous damping d, thus neglecting the damping given by the friction component c, we have:

$$k_{eq} = \frac{mg}{L} \qquad b_{eq} = \frac{dL}{L} \qquad \text{Eq. 3.17}$$

where the coefficient of damping d is evaluated by Eq. 3.18 according to the dynamic of structures theory:

$$d = 2\zeta m\sqrt{\frac{g}{L}} \qquad \text{Eq. 3.18}$$

where ζ is the damping factor assessed with laboratory tests as reported in Chapter 3.3.2, m is the mass of the hook of the crane, g is the gravity acceleration and L is the length of the rope which is the distance between the crane and the centroid of the hook.

3.3.2 Laboratory tests for the determination of the damping factor ζ

Before proceeding with the modelling of the entire system in a finite element software, such as shown in the previous Chapter 3.2, it's necessary to determine the value of the damping factor ζ through laboratory tests. This damping factor is calculated by measuring the damping in the oscillations of the crane hook in a specific time period, both with the logarithmic decrement method [Paultre, 2011] and the Half-Bandwidth method [Chopra, 2012].

The damping factor ζ is thus evaluated by considering multiple and different configurations of the crane layout, both in terms of the direction of the oscillation of the hook (in the two orthogonal directions in the horizontal plane, Figure 3.20) and in terms of the applied load at the hook of the crane (Figure 3.21).

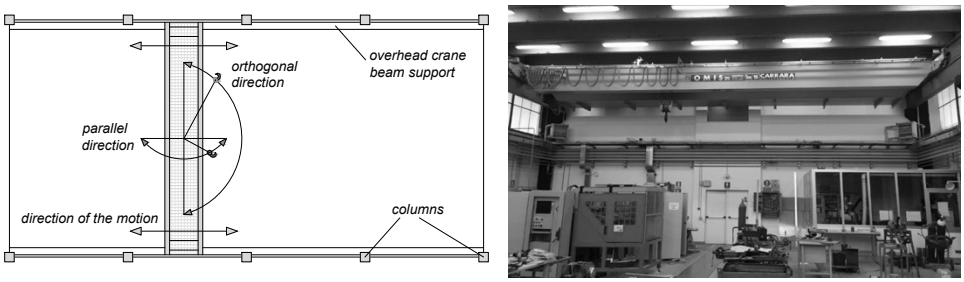

Figure 3.20 Plan view of the precast shed with an indication of the directions when the hook was raised (left) and one example of an overhead crane in a precast reinforced concrete industrial building (right).

The measurement of the oscillations and the displacements is conducted using a linear position transducer (Figure 3.22) appropriately installed along the two orthogonal directions in the horizontal plane, in addition to this the accelerations experienced by the hook of the crane were monitored using accelerograms (Figure 3.23).

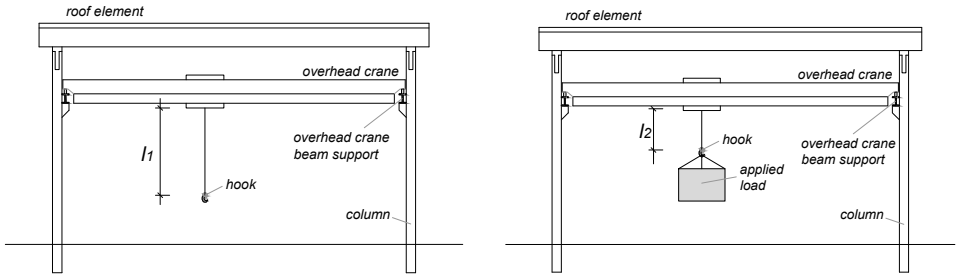

Figure 3.21 Configurations of the crane considered during the tests: without applied load at the hook (left) and with applied load at the hook equal to 16,3kN (right).

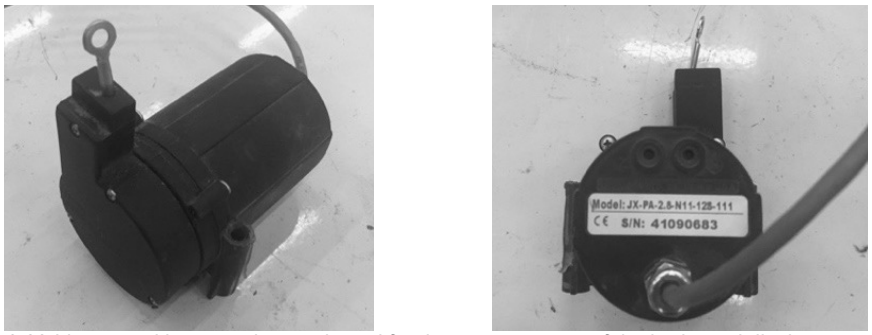

Figure 3.22 Linear position transducer adopted for the measurement of the horizontal displacement in the both directions of the horizontal plane: x-direction and y-direction.

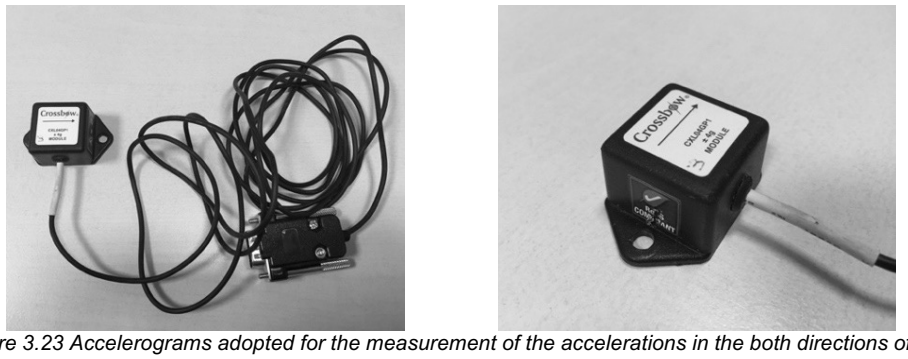

Figure 3.23 Accelerograms adopted for the measurement of the accelerations in the both directions of the horizontal plane: x-direction and y-direction.

From Figure 3.24 to Figure 3.27, it is possible to see the results in term of oscillation of the hook of the crane both without an applied load at the hook and with an applied load at the hook equal to 16,3kN.

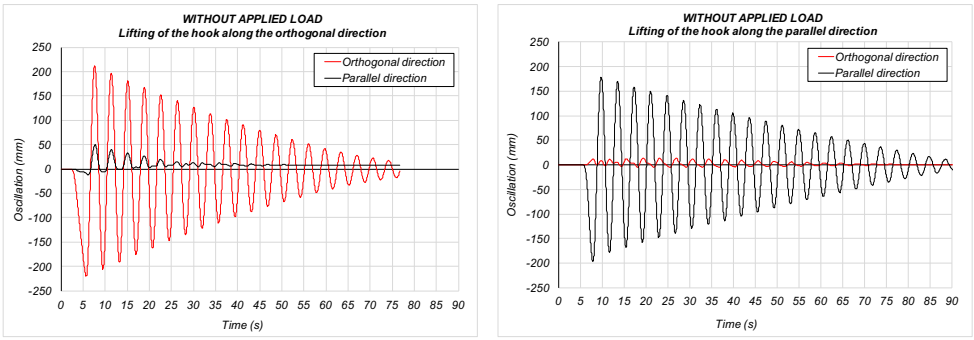

Figure 3.24 Oscillation of the hook in the configuration without the applied load in the case of: lifting along the orthogonal direction in referring to the development of the crane (left); lifting along the parallel direction in referring to the development of the crane (right).

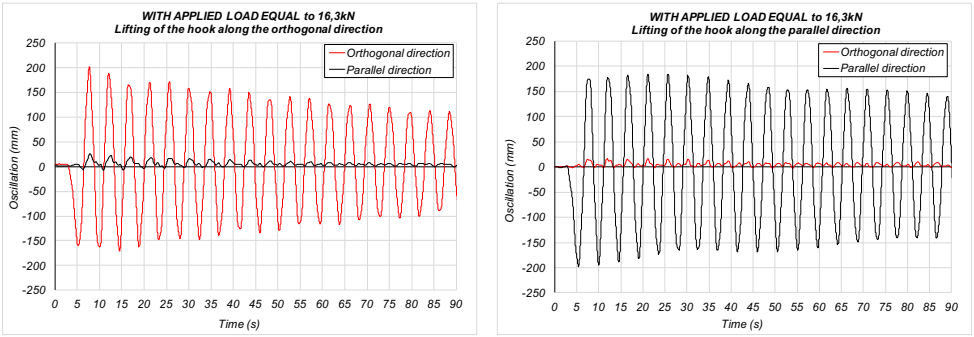

Figure 3.25 Oscillation of the hook in the configuration with an applied load equal to 16,3kN in the case of: lifting along the orthogonal direction in referring to the development of the crane (left); lifting along the parallel direction in referring to the development of the crane (right).

In the Figure 3.26 and Figure 3.27 it's possible to see the results in terms of acceleration for both the test without any applied load and the test with an applied load at the bottom of the crane equal to 16,3kN.

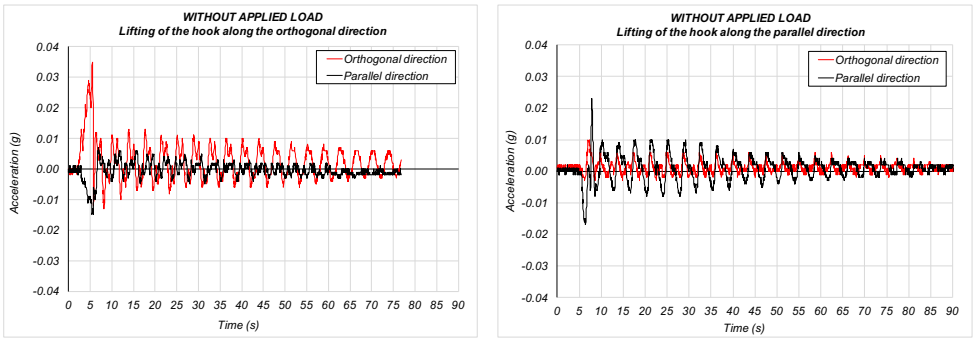

Figure 3.26 Acceleration of the hook in the configuration without the applied load in the case of: lifting along the orthogonal direction in referring to the development of the crane (left); lifting along the parallel direction in referring to the development of the crane (right).

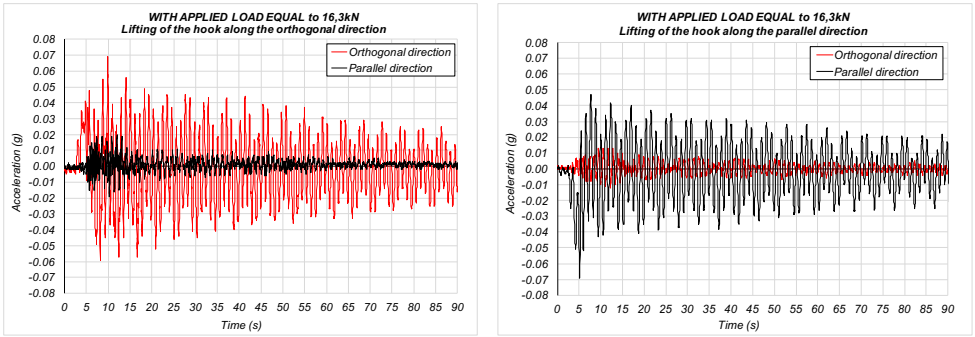

Figure 3.27 Acceleration of the hook in the configuration with an applied load equal to 16,3kN in the case of: lifting along the orthogonal direction in referring to the development of the crane (left); lifting along the parallel direction in referring to the development of the crane (right).

3.3.2.1 Logarithmic decrement method for the evaluation of the damping factor ζ

The application of the logarithmic decrement method avoids to determine the real value of the damping factor ζ from the free vibration response tests such as the same performed and shown in Chapter 3.3.2.

This method applies the following formulation as shown in [Paultre, 2011], the logarithmic decrement can be expressed as:

$$\delta = \frac{1}{b}\ln\frac{u_a}{u_{a+b}} \qquad \text{Eq. 3.19}$$

where b is the number of cycles considered that being an integer, u_a and u_{a+b} are the amplitudes at time t_a and $t_a + b\,T_D$.

Figure 3.28 shows the displacements $u(t)$ and $u(t+b\,T_D)$ measured at the ends of one-cycle interval during free vibration.

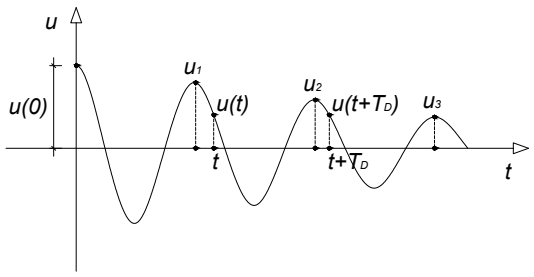

Figure 3.28 Evaluation of the logarithmic decrement based on the free vibration test.

Since for small values of damping, an approximation of δ is given by:

$$\delta \approx 2\pi\zeta \qquad \text{Eq. 3.20}$$

it's possible to deduce that the damping factor is equal to:

$$\zeta \approx \frac{\delta}{2\pi} = \frac{1}{2b\pi}\ln\frac{u_a}{u_{a+b}} \qquad \text{Eq. 3.21}$$

Where the assumed ratio u_n/u_{n+m} is equal to:

$$\frac{u_a}{u_{a+b}} = e^{b\zeta\omega T_D} \qquad \text{Eq. 3.22}$$

The damping coefficient d for a pendulum system is evaluated with the previous Eq. 3.18. In this equation, the mass m is assumed equal to the weight of the hook and the sum of the weight of the hook and the weight of the applied load at the hook in the cases of the test without an applied load and with an applied load of 16,3kN

respectively. The length L, equal to the distance considered between the crane and the hook, is assumed equal to 4,1m and 3,74m for the tests without and with an applied load respectively. The values of the damping factor ζ and the damping coefficient d obtained for each test performed in different configurations are shown in Table 3.2.

Table 3.2 Values of the damping factor ζ and then the damping coefficient δ obtained for each configuration considered during the test with the logarithmic decrement method. The direction is referred to the development in plan of the overhead crane.

	b	**Wihtout applied load**		**With applied load (16,3kN)**	
		Ortho. direc.	*Paral. direc.*	*Ortho. direc.*	*Paral. direc.*
Damping Factor ζ (%)	*17*	*2,10*	*1,49*	*0,54*	*0,17*
Damping Coefficient d (Ns/m)	*17*	*8,63*	*6,12*	*31,14*	*9,74*

3.3.2.2 Half-power bandwidth method for the evaluation of the damping factor ζ

For completeness, the evaluation of the damping factor ζ is carried out also with the half-power bandwidth method [Chopra, 2012, pg. 83:84]. This method is based on an important property of the frequency response curve for the deformation response factor R_d defined according to the formulation in Eq. 3.23:

$$R_d = \frac{u_0}{(u_{st})_0} = \frac{1}{\sqrt{\left[1-(\omega/\omega_n)^2\right]^2 + \left[2\zeta(\omega/\omega_n)\right]^2}} \qquad \text{Eq. 3.23}$$

The property of this curve and then the half-power bandwidth method is shown in Figure 3.29.

Determined ω_a and ω_b, as the forcing frequencies evaluated on either side of the resonant frequency at which the amplitude u_0 is $1/\sqrt{2}$ times the resonant amplitude, the damping factor is given by:

$$\zeta = \frac{\omega_b - \omega_a}{2\omega_n} \qquad \text{Eq. 3.24}$$

where ω_n is the frequency determined at the peak of the curve.

For brevity, the value of the damping factor computed is carried out with the half-power bandwidth method only for the configuration of the overhead crane without an applied load and providing the lifting of the hook along the orthogonal direction. The result obtained confirms the value of the damping factor achieved with the logarithmic decrement method. Precisely the damping factor ζ evaluated with the

half-power bandwidth method is equal to 2,18%, only 3,67% more than the value obtained with the logarithmic decrement method.

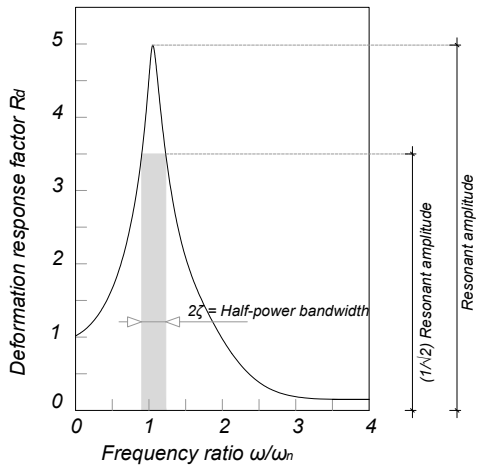

Figure 3.29 Definition of the half-power bandwidth method in the frequency-R_d plot.

3.3.3 Seismic analysis and modelling

3.3.3.1 Modelling of the 2D pendulum

As shown in the previous chapters, the results obtained from the laboratory test performed allow to determine the damping factor ζ for the different configurations considered, then the damping coefficient d.

After this, different 2D finite element models of the combined model structure plus pendulum are provided to study the interaction in the global and local seismic response ([CNR 10021-85, 1985] and [EN 1993-6, 2007]).

The analysis and the fem models is implemented within the [Ruaumoko, 2007] software. At the beginning, the aim is to investigate how the different assumptions in the pendulum modelling (hence the crane) could affect the variability of the results in terms of the oscillation of the pendulum itself. Initially, the 2D-model of the single pendulum is analysed. The response of the system is studied with the application of an impulsive lateral forcing input (Figure 3.30, left). The results observed show that there are no differences in the horizontal displacements of the node at the end of the pendulum (Figure 3.30, right). The effects due to a variation of the applied load at the end of the pendulum is also investigated in terms of rotations observed at the pivot of the pendulum.

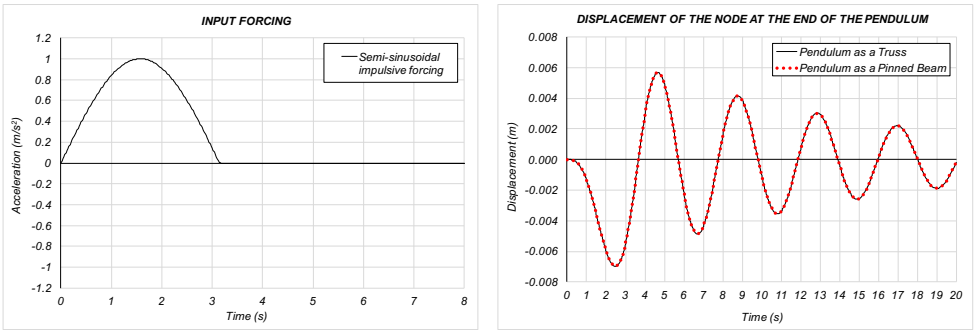

Figure 3.30 Forcing input considered (left) and comparison of the results in terms of the displacement of the node at the end of pendulum for the two models considered: pendulum modelled ad a truss and pendulum modelled as a pinned beam (right).

Two values of the applied load are assumed: 16,3kN in accordance to the applied load considered during the laboratory tests and 30kN, almost double of the previous value. As expected, there are no differences in the results (Figure 3.31) because the value of the first period of vibration is the same (4s), due to the fact that the length of the pendulum is the same, as determined by the Eq. 3.25:

$$T = 2\pi\sqrt{\frac{l}{g}} \qquad \text{Eq. 3.25}$$

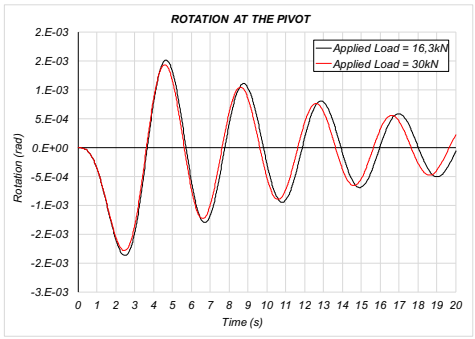

Figure 3.31 Comparison of the rotations at the pivot of the pendulum obtained considering two different values of the applied load.

3.3.3.2 Modelling of the 2D combined model

The variability of the 2D combined model relatively to the type of system adopted for the connection between the hanging mass of the overhead crane and the structure model is also investigated. Two models are considered: the model in which the pendulum is modelled as a point mass connected with a beam element to the structure and the model in which the pendulum is modelled as a point mass connected to the structure with a spring and a damper element using the values of k_{eq} and b_{eq} evaluated according with the Eq. 3.17 (Figure 3.32).

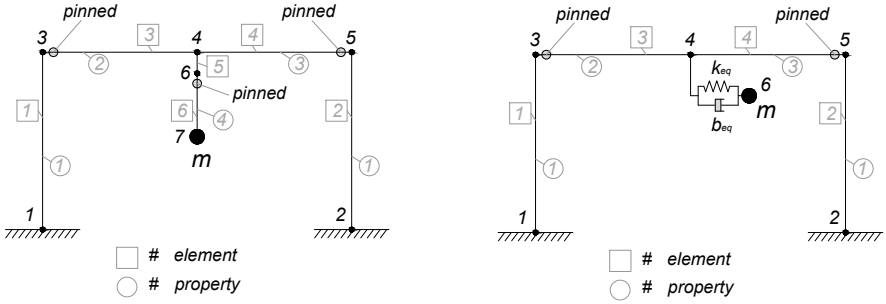

Figure 3.32 Model with pendulum as a pinned beam (left) and with pendulum as a spring and damper element (right).

As in the previous chapter, the variability of the results is investigated considering the two models shown in Figure 3.32. Two different configurations of the applied load at the end of the pendulum are considered, the applied load is assumed equal to 16,3kN and 155kN. The results for both of these assumptions are compared in terms of the shear force in the beam element (element number 5 in the Figure 3.32, on the left) versus the axial force in the spring. Figure 3.33 shows how the differences in the results are really small, the trends are pretty much similar as well as the maximum values observed. The observed results allow to say that, during the modelling of the entire precast building, it is possible to consider the overhead crane with the most convenient and fast spring plus damper modelling solution without getting substantial differences in terms of the acting forces.

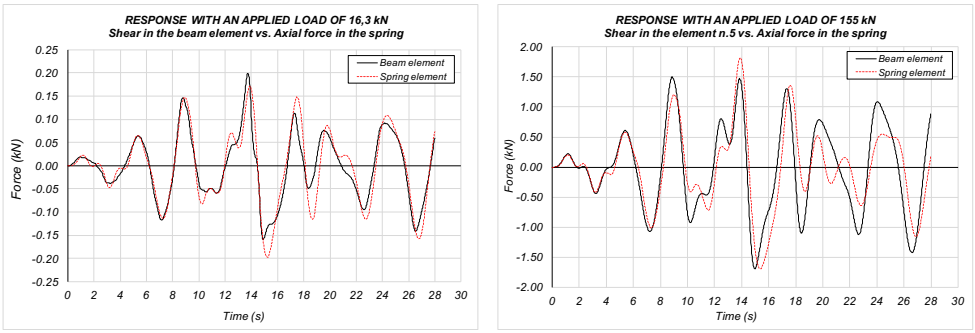

Figure 3.33 Comparison of the forces obtained in the cases of an applied load of 16,3kN (left) and 155kN (right).

The results in terms of the shear at the base of the column are assessed performing the analysis considering three different configurations: the frame without an overhead crane and the combined model (crane and pendulum) with an applied load of 16,3kN and 155kN considered at the hook of the crane. In Figure 3.34, the results depending on time for these three models are plotted on a same graph. The results obtained performing an analysis with an accelerogram show that the introduction of the hanging load leads to a reduction of the shear at the base of the column. In case of an impulsive forcing function, the first peak of the shear value confirms this trend but it is not possible to say the same for the other part of the response.

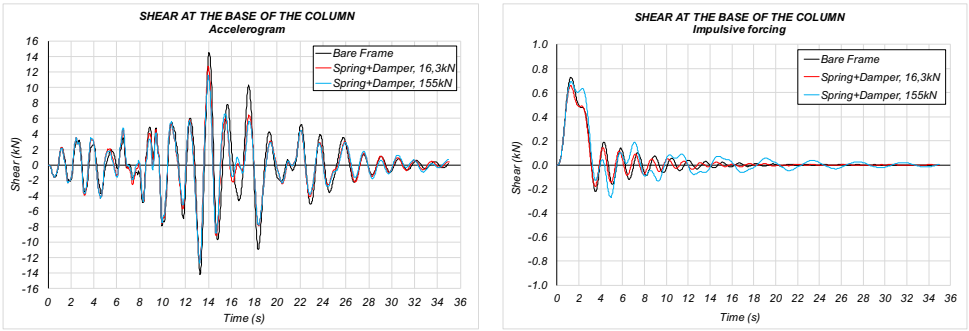

Figure 3.34 Comparison of the shear forces at the base of the column for the three models considered in cases of an accelerogram applied as an external forcing (left) and impulsive forcing (right).

3.3.3.3 Influence of the overhead crane in a 3D-model

The last step of this study investigates the influence of the overhead crane in the seismic response of RC precast industrial building selected according to the typical characteristics of the precast industrial buildings widespread on the Italian territory and equipped with an overhead crane (Figure 3.35). In particular, this case study represents a portion consisting of one portal and four bays of the facility shown in Chapter 4 that is characterized by two portals and ten bays.

The structure is modelled as a fem 3D-model within the [Midas GEN (v1.2), 2014] software. The building is characterized by a rectangular plan with dimensions 32x15m. The size of the cross sections of the columns are 45x45cm and the longitudinal reinforcement consists in 12ϕ18 equally distributed; the type of the model used to describe the non-linear behaviour of the columns is characterized by fiber elements. The structural materials used are C50/60 for concrete and B450 for steel. The characteristic values of such materials are considered to describe the non-linear behaviour of the plastic hinges. The weight of the overhead crane is estimated to be equal to 184kN while the hanging load is considered equal to 300kN. The connection between the hanging load and the overhead crane is modelled with an elastic spring with a stiffness equal to $k = mg/L$ =120'035N/m.

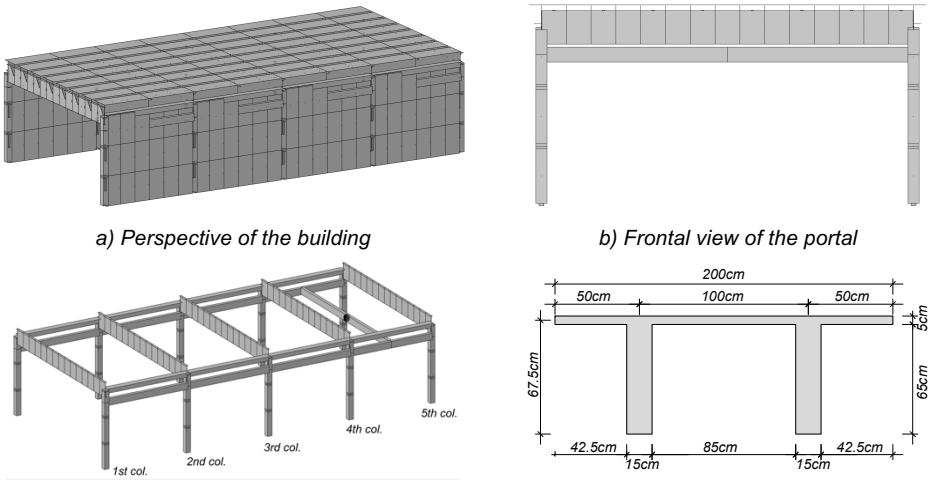

a) Perspective of the building *b) Frontal view of the portal*

c) Perspective of the main structure and the crane *d) Cross section of the roof element*

Figure 3.35 Three-dimensional model as a case study used for performing the analysis. Perspective view (above on the left); cross section (above on the right); structure without roof elements and cladding panels (below on the left); and cross section of roof elements (below on the right).

As shown in Figure 3.35, the runways simply supported by the columns and the overhead crane are modelled; the stiffness of the runways is determined by imposing

a limit of 1/500 for the deformed shape as the configuration corresponding to the worst load conditions.

The damping between the applied load and the overhead crane is neglected. The roof elements and the lateral precast cladding panels (2,4x0,2x8m) are modelled as elastic beam elements connected isostatically to the main structure: roof element hinged to the support beam and cladding panels hinged to the columns at the bottom connection and connected with a cart at the top connection.

Different non-linear dynamic analyses are performed in order to analyse the seismic response in terms of the top displacements and maximum curvature of the columns. The seismic input adopted was the main shock registered at Mirandola on May 20th in 2012 during the Emilian seismic sequence (Figure 3.36). Both the directions of the earthquake are considered, in particular the East-West direction of the earthquake is assumed as the direction along the X-axis of the fem model while the North-South direction of the earthquake corresponds to the direction along the Y-axis of the fem model.

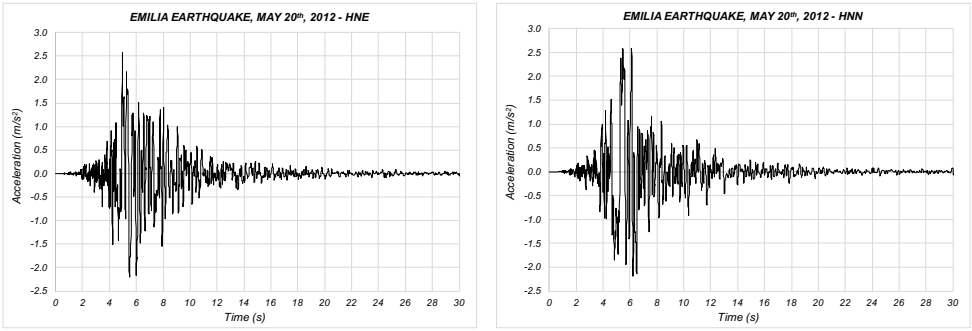

a) *b)*

Figure 3.36 Accelerogram of the horizontal components registered at Mirandola along the East-West (a) and the North-South (b) directions of the Emilia earthquake on May 20th, 2012

Different configurations for the building layout are considered: initially, the overhead crane is added to the building at the central column (3rd column), and subsequently it is placed in the middle of the last bay (between the 4th and the 5th columns) (see Figure 3.37).

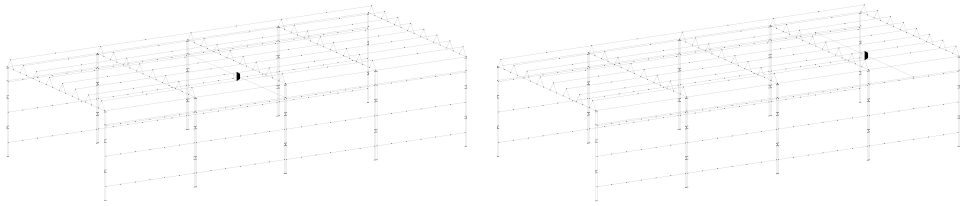

Figure 3.37 Different configurations of the building layout depending by the position of the overhead crane.

At the beginning the hanging load is neglected for both cases. Afterwards, the aforementioned configurations are examined considering the presence of the hanging load, taken equal to the maximum load capacity declared. All the analyses are carried out considering both the flexible and the rigid roof diaphragm (see Figure 3.38) in which the latter configuration is obtained by providing suitable rigid links on the roof floor of the structure that inhibit in-plane relative displacements between nodes.

Figure 3.39 shows the results in terms of top displacements of the columns in both X and Y directions and in terms of maximum curvature experienced at the base of the columns.

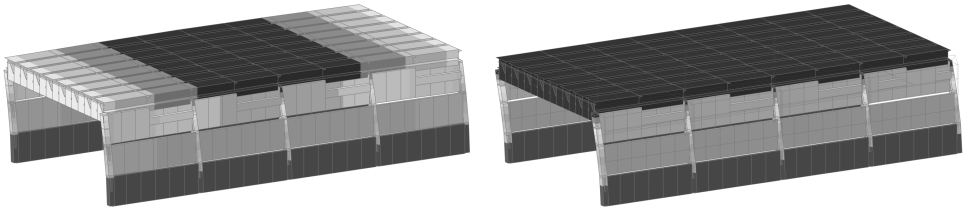

a) *b)*

Figure 3.38 Different behaviour of the roof floor in the case of: a) flexible diaphragm; b) and rigid diaphragm.

In these figures, the term "Reference" indicates the model without the overhead crane and then without the hanging load, the term "No_Pendulum" indicates the model with the overhead crane but without the hanging load, the term "Pendulum" indicates the configuration with the overhead crane and the hanging load.

In the case of flexible roof diaphragm, the results show an increase of the displacements along the longitudinal direction (X-axis) when there is the presence of the overhead crane; the displacements increment along the transverse direction (Y-axis) is seen especially in the case of eccentric overhead crane without the hanging load; regarding the curvature at the base of the columns, in the configuration with

the presence of the overhead crane but without a hanging load are observed the higher values.

In the case of rigid roof diaphragm, the results show an increase of the displacements along the longitudinal direction (X-axis). No significant increases of the displacements are observed along the transverse direction (Y-axis) while, only considering the configuration with the overhead crane located close to the 3rd column and without the hanging load, it is seen an increment of the values of the curvature related to the 3rd column itself.

In conclusion, the non-linear time history analyses of a portal structure with multiple bays show that, in the longitudinal direction, the addition of the mass of the crane leads to an increase of the roof displacements independently by the presence of a hanging load.

In the transverse direction, the response is different in the case of absence or presence of a roof diaphragm: in the first case the increase of displacement is found especially when the crane is at the end of the longitudinal plan dimension and no hanging load is present; in the second case, no significant increase of the roof displacements is recorded. Regarding changes in the curvature demand at the base of the columns, the higher increase is observed when the overhead crane is added without the hanging load. However, the aforementioned conclusions are obtained by considering a specific case study composed by a single portal and four bays. Additional research is required to allow for generalization. Although, the modelling strategy for the suspended load is suitable independently by the case study.

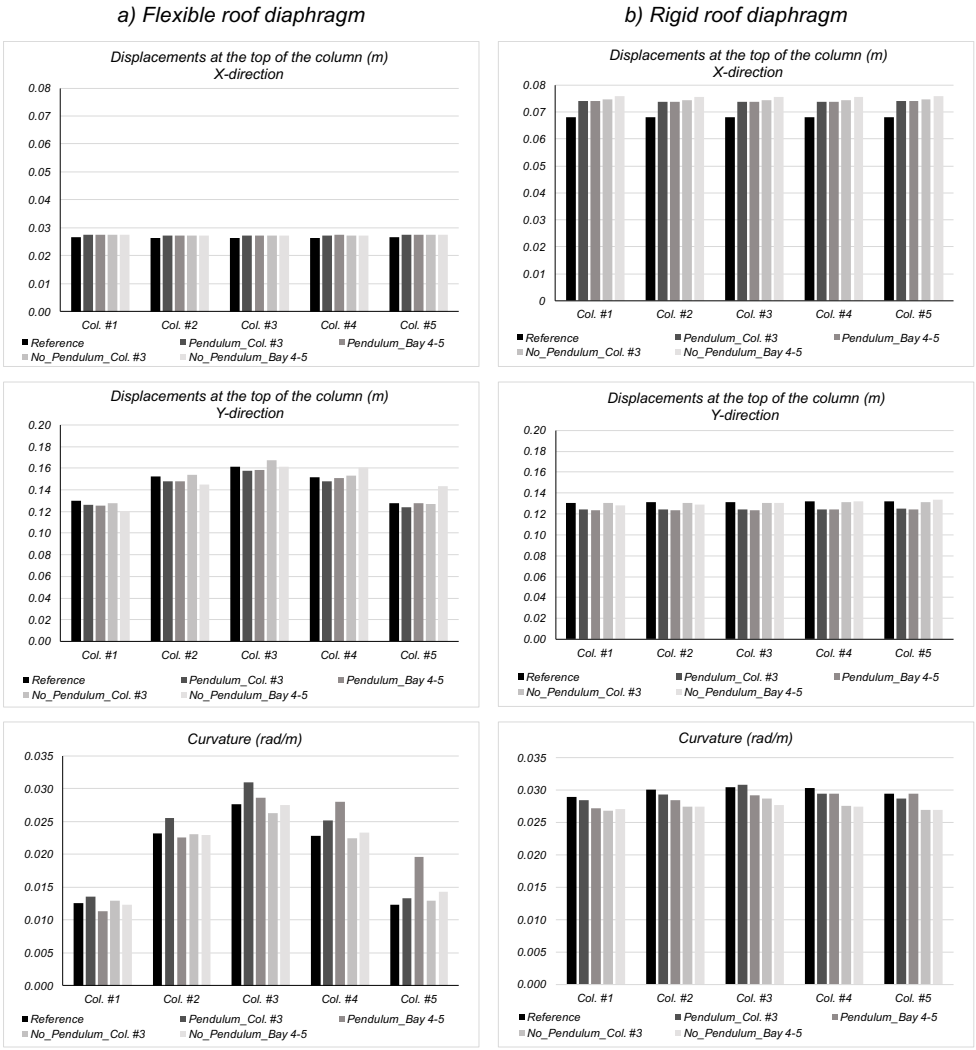

Figure 3.39 Comparison of the results in terms of top displacements of the columns and the maximum curvature experienced at the base of the columns in the case of both flexible (left) and rigid roof diaphragm (right).

3.4 Loss of support

In this Chapter, the aim is to investigate through a sensitivity analysis how the variability of parameters such as the coefficient of friction and the stiffness of the neoprene pad can influence the seismic response of a RC precast industrial building with connections between structural elements relying only on friction. This work can be considered as a preliminary study that should be the basis for the development of future research studies aimed to analyse in detail the probability to reach structural collapses due to loss of support of structural elements.

In Italy, most of the RC precast industrial buildings that were built before current Italian technical standards for construction in areas not previously classified as seismic zones [NTC, 2008] are typically supported by connections relying only on friction between the structural elements. This structural solution was adopted for both beam-to-column connections and roof-to-beam connections and the practice of construction also involved the insertion of a neoprene pad between the two structural elements.

In order to carry out a proper assessment of the vulnerability of such structures and therefore the estimation of the monetary losses (see Chapter 4), it is necessary to know the value of the coefficient of friction for the characterization of the behaviour of such connections in a finite element software.

Some recent scientific studies have been developed to meet this need; the determination of the exact value of the coefficient of friction is possible with a closed-form expression provided by [Magliulo *et al.*, 2010] alternately to what is currently proposed by the main technical standards in this field, such as [CNR 10018, 1999], [Schrage, 1991], [PCI Design Handbook, 1985] and the [UNI-EN 1337:3, 2005].

As a consequence, most of these structures exhibited local or global collapse mainly related to the loss of support of beams or roof elements causing significant economic losses and casualties. Since this kind of vulnerability was dominant in the observed collapses of buildings during the last recent earthquakes in Emilia that happened on May 29th, 2012 [Ercolino *et al.*, 2016], the current research investigates also the sensitivity analyses of the loss of support at the beam-to-column joint to selected parameters. The considered parameters include: the coefficient of friction and the stiffness of the neoprene pad where the beams are connected to columns, and the intensity measure of the horizontal and vertical components of the earthquake.

The sensitivity analysis is performed both on a single and double-bay portal in a 2-dimensional model, through the [OpenSees, 2007] software. The portal considered is

7,3m tall and the size of the cross sections of the structural elements are assumed 50x50cm for the two columns and 35x125cm for the horizontal beam (as a simplification of the fem model, the value 125cm is selected as the medium height between the lowest value of 80cm and the highest value of 180cm). These structural elements are modelled as "beam" finite elements. According to the structural scheme of hinged frame adopted in the past design of precast industrial buildings, the columns are fixed at the base and the rotational degree of freedom at the ends of the horizontal beams is released (Figure 1.3).

The structural materials adopted are C40/50 for concrete and B450 for steel. For performing the non-linear analyses, the characteristic values of such materials are considered to describe the non-linear behaviour of the plastic hinges (with a length of 50cm) at the base of the columns, in particular a Takeda trilinear behaviour is adopted [Takeda *et al.*, 1970]. The considered loads acting at the top of the column are equal to the self-weight of the beam plus the weight of the roof floor estimated to be 247,5kN for each column. The roof elements are simply modelled as nodal lumped masses. As mentioned before, the beam-to-column frictional connection is modelled with the "flat slider bearing" element in Figure 1.3 on the left, and for modelling the coefficient of friction as a function of the sliding velocity, the "Coulomb friction" model is considered (Figure 1.3, right, below). The peculiarity and the advantage offered by the "flat slider bearing" is given by the capacity of this element to evaluate the effective frictional force at each single time step as a function of the axial vertical force (Figure 1.3, left, below).

It is clear how this kind of finite element allows to catch the variation of the friction force when the seismic vertical component during an earthquake is not negligible. The characteristics of the neoprene pad assumed within the [OpenSees, 2007] software for modelling the "flat slider bearing" are the following: size of neoprene equal to 23x15x1cm, vertical modulus of Young equal to 30E10N/m^2 and shear modulus taken as 1,15E6N/m^2, the initial lateral stiffness is equal to 3'967'500N/m^2 (assessed in according to [Akogul and Celik, 2008]) and the coefficient of friction μ is equal to 0,10535, evaluated according to the latest formulas proposed in the literature [Magliulo *et al.*, 2010].

The sensitivity analysis is carried out by means of non-linear time history analyses in order to capture the non-linear behaviour of the joints relying only on friction which is dependent on vertical loading. As shown in [Ercolino et al., 2016], the vertical component of an earthquake is very important to properly assess the collapse of roof

elements due to loss of support. In this preliminary study, however, the hysteresis of the columns is not considered, being the main purpose of the sensitivity analysis the evaluation of the influence of the connection parameters: coefficient of friction and stiffness of the neoprene pad.

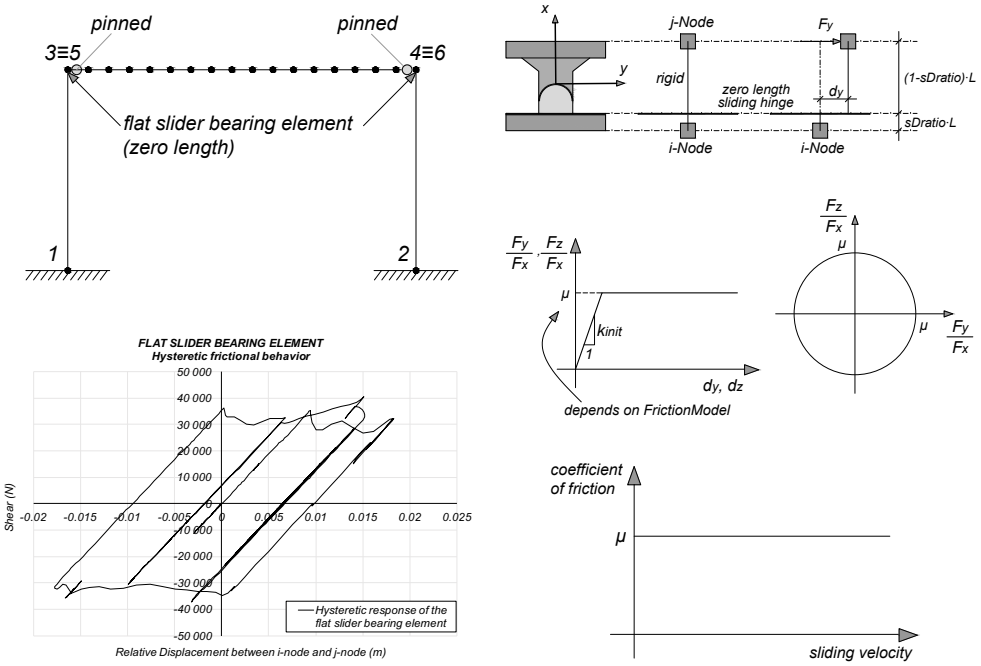

Figure 3.40 Structural 2D model of a single-bay frame considered in the sensitivity (left, above); "flat-slider bearing" element considered for the modelling of the connection and "Coulomb-friction" model adopted for the characterisation of the coefficient of friction as a function of the sliding velocity (right); and example of the hysteretic response of the "flat slider bearing" (left, below).

The loss of support at the beam-to-column joints is then investigated with both Emilia (May 29th, 2012) and L'Aquila earthquakes (April 6th, 2009).

The variation of the parameters is assumed in this range of values:

- for the coefficient of friction: [0,0025 0,0050 0,0075 0,01 0,015 0,02 0,025 0,075 0,1 0,105 0,15 0,225];
- for the stiffness of the neoprene pad: [1 2,5 4 8 20 39,675 60 80 100] E5N/m^2;
- and for the multiplier factor of the intensity measure (for both horizontal and vertical components): [0,25 0,5 0,75 1 1,25 1,5 1,75 2 2,25 2,5].

The results of the sensitivity analysis in terms of maximum relative displacement achieved are shown in Figure 3.41 and Figure 3.42 for both Emilia and L'Aquila

earthquakes. These values are referred to the single-bay frame and they are obtained performing the linear time history analysis with a time step *dt* equal to 0,01s. Figure 3.43 and Figure 3.44 also report the hysteretic cycles of the "flat slider bearing" element experienced during the sensitivity analysis and the step-by-step variation of the activation frictional force as a function of the vertical earthquake component can be appreciated.

From the previous figures, it can be observed how the relative displacements obtained for the two above referenced earthquakes are slightly different. For the sensitivity analysis carried out on the friction coefficient, the trend of the results is almost parabolic. The maximum peak of the curve is on the left side of the graph and the concavity is downwards; the lower values of the relative displacement are obtained by increasing the value of the coefficient of friction. In the case of L'Aquila earthquake, it was observed that the application of the minimum value of the coefficient of friction (0,0025) leads to an explosion of the result (the value of the relative displacement reached 2,6m), while for the maximum value of the coefficient of friction herein considered (0,225), there is an increase in the value of the relative displacement contrary to what is seen in the case of Emilia earthquake. Regarding the variability of the coefficient of friction, it can be said that a variation of the seismic input considering both the horizontal and vertical components leads to different structural responses in terms of maximum relative displacement.

As regards the variability of the stiffness of the neoprene pad, the resulting trend is similar between the two earthquakes, although few differences in terms of maximum and minimum values or the relative displacement reached are noted. The Emilia earthquake shows a greater difference between the maximum and minimum values reaching 0,142m and 0,011m respectively in comparison with the results obtained with L'Aquila earthquake equal to 0,106m and 0,064m.

When the multiplier factor is applied on the horizontal component only, and on both horizontal and vertical components at the same time, the results obtained do not show differences in the shape of the trend. The shape of the trend is a straight line with positive slope.

An interesting and distinct pattern of the values is observed when the multiplier factor is applied on the vertical component only and the horizontal component is kept fixed. For the Emilia earthquake case, it is noted that the minimum value of the relative displacement is achieved when the unit value of the multiplier factor is assumed. Any changes in this value lead to an increase of the relative displacement.

The result of the sensitivity analysis provides only a qualitative evaluation of the influencing parameters, which do not allow generalization nor design recommendations. Such results represent a starting point for the development of future research aimed to assess the loss of support between structural elements in RC precast industrial buildings. In addition, future studies will be directed towards assessing the seismic behaviour of complete 3D models in which the roof elements are provided and the beam-to-roof elements connections are based on friction.

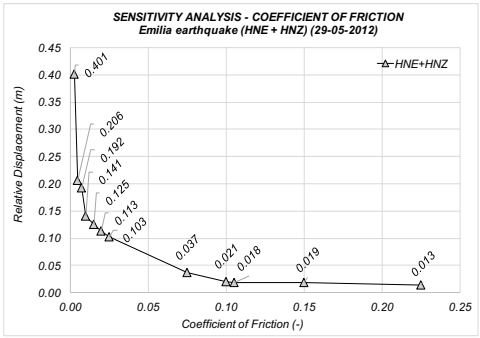

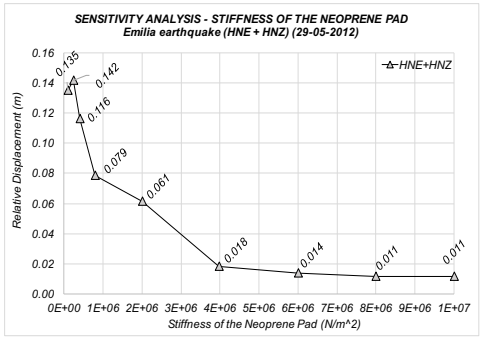

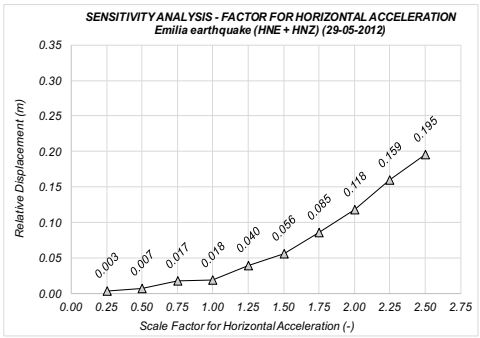

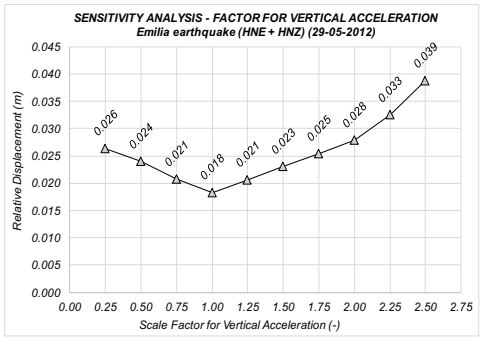

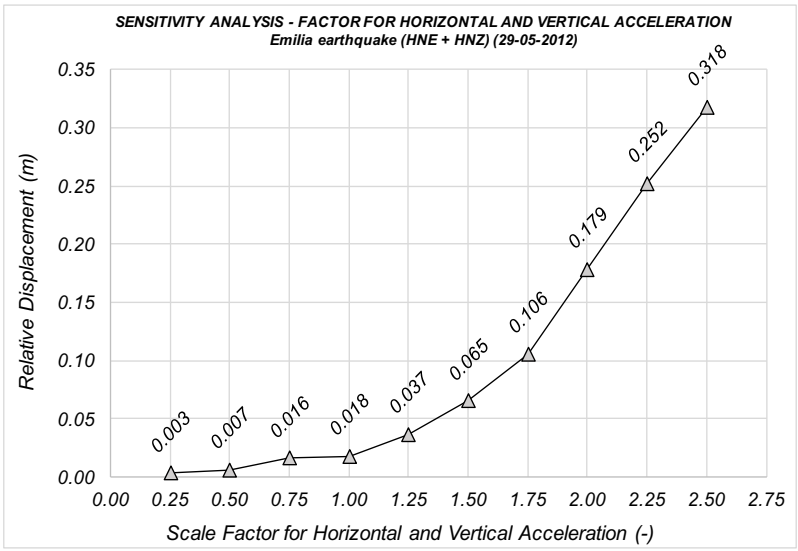

Figure 3.41 Values of the relative displacement experienced during the sensitivity analysis on different parameter considering the Emilia earthquake (May 29th, in 2012).

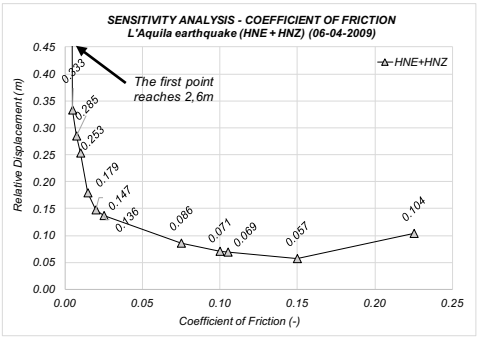

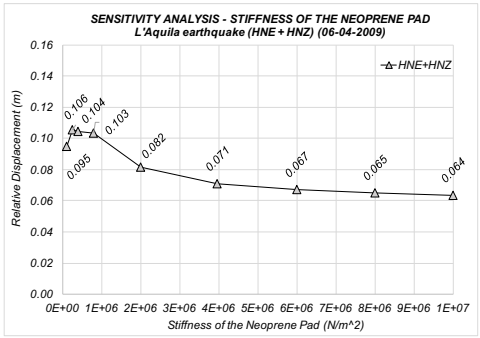

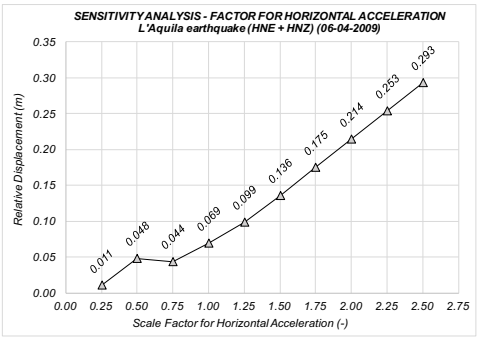

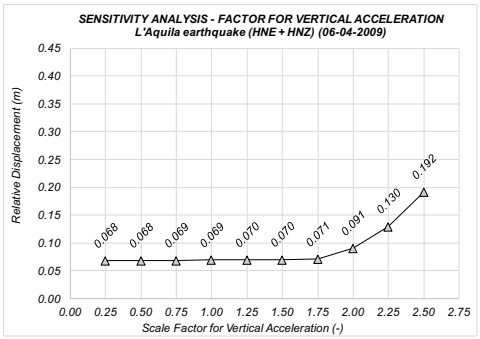

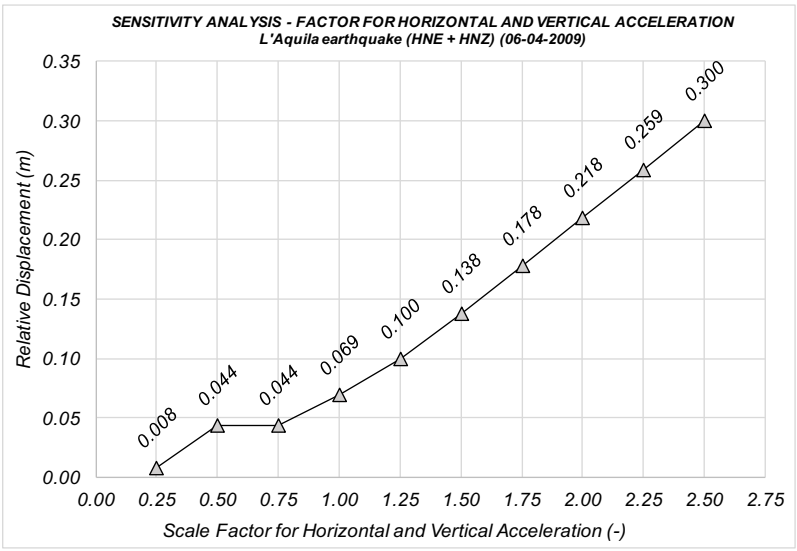

Figure 3.42 Values of the relative displacement experienced during the sensitivity analysis on different parameter considering the L'Aquila earthquake (April 6th, in 2009).

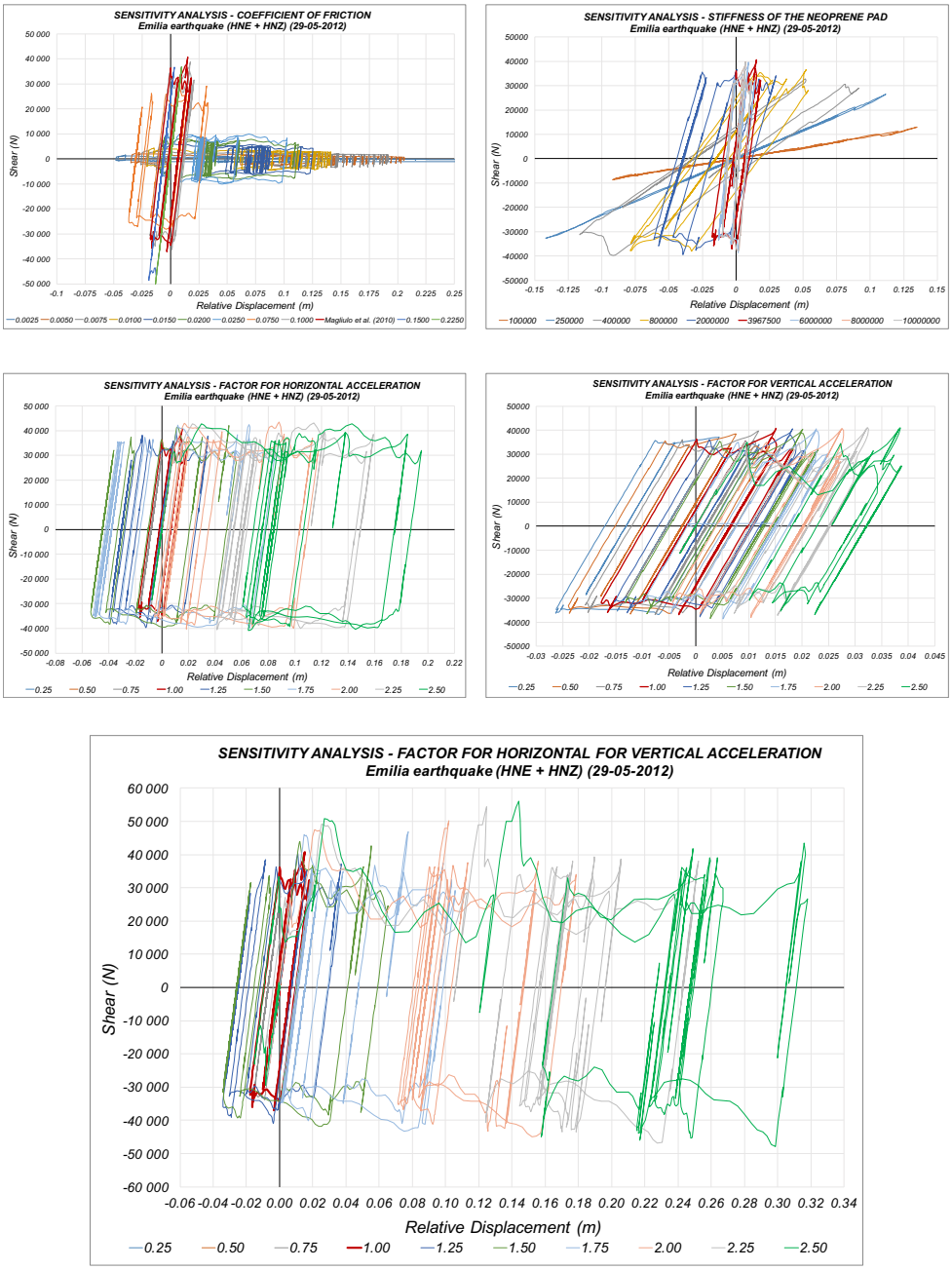

Figure 3.43 Hysteretic response of the "flat slider bearing" element for the sensitivity analysis performed with Emilia earthquake (May 29th, in 2012) on: the coefficient of friction (left, above); the stiffness of the neoprene pad (right, above); the multiplier factor for horizontal and vertical seismic acceleration and for both of them (in the middle and below).

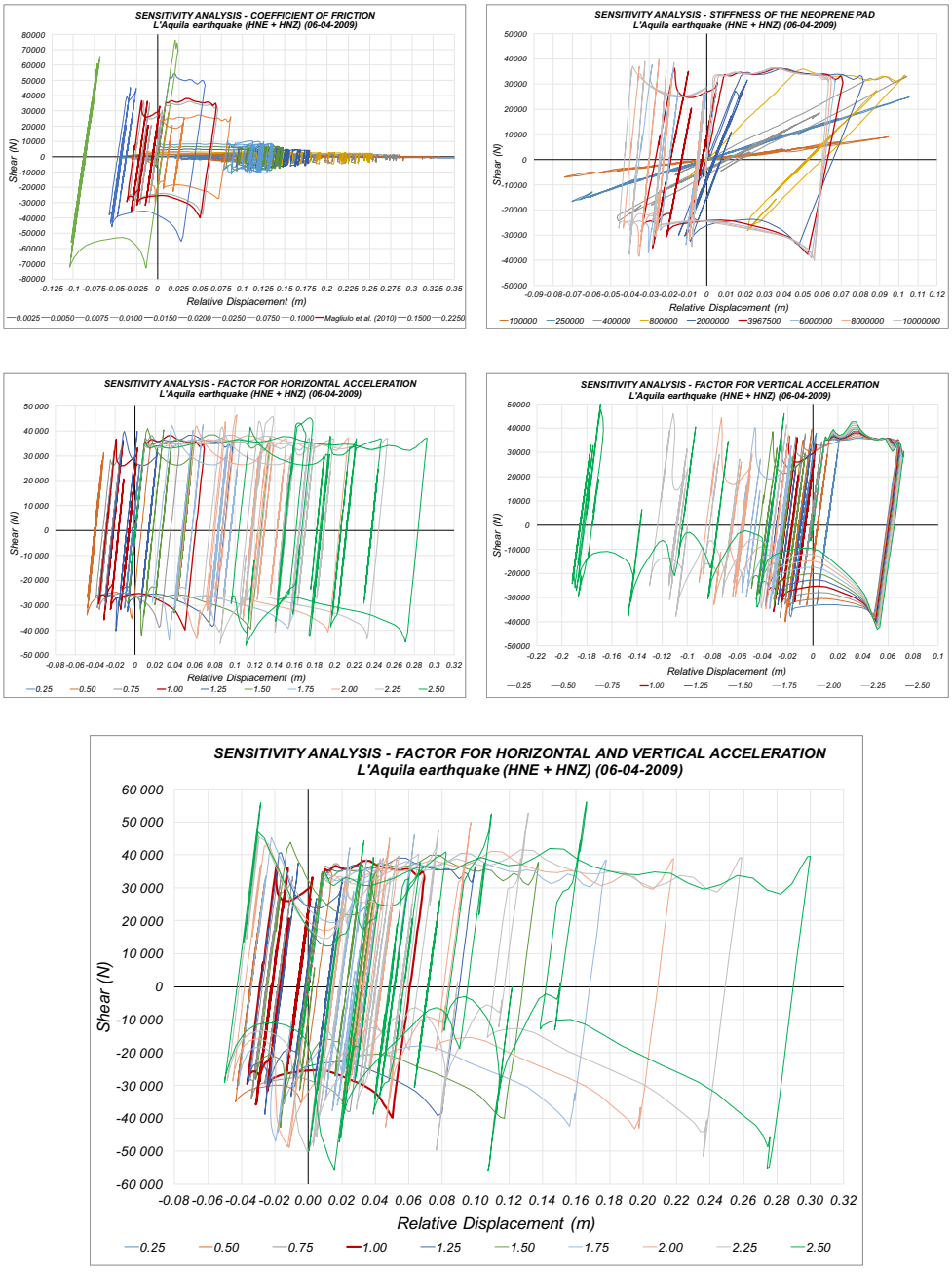

Figure 3.44 Hysteretic response of the "flat slider bearing" element for the sensitivity analysis performed with L'Aquila earthquake (April 6th, in 2009) on: the coefficient of friction (left, above); the stiffness of the neoprene pad (right, above); the multiplier factor for horizontal and vertical seismic acceleration and for both of them (in the middle and below).

3.5 References

Akkar, S., Özen, Ö. [2005] "Effect of Peak Ground Velocity on Deformation Demands for SDOF Systems", Earthquake Engineering and Structural Dynamics, Vol. 34, No.13, pp. 1551–1571.

Akkar, S., Sucuoğlu, H., Yakut, A. [2005] "Displacement-Based Fragility Functions for Low- sand Mid-rise Ordinary Concrete Buildings", Earthquake Spectra, Vol. 21, No.4, pp. 901–927.

Akogul, C., Celik, O. [2008] "Effect of Elastomeric Bearing Modeling Parameters on the Seismic Design of RC Highway Bridges with Precast Concrete Girders", The 14th World Conference on Earthquake Engineering, Beijing, China.

Arnold, C. [1989] "Cladding Design: Architectural Trends and Their Influence on Seismic Design. Proceedings: Architectural Precast Concrete Cladding – It's Contribution to Lateral Resistance of Buildings", Architectural Precast Concrete Cladding, November 8-9, Chicago.

ASCE/SEI 7-10. [2010] Minimum Design Loads for Buildings and Other Structures, American Society of Civil Engineers, Reston, Virginia, USA, pp. 1–658.

Belleri, A., Brunesi, E., Nascimbene, R., Pagani, M., Riva, P. [2014] "Seismic Performance of Precast Industrial Facilities Following Major Earthquakes in the Italian Territory", Journal of Performance of Constructed Facilities, pp. 1–10.

Belleri, A., Marini, A. [2016] "Does Seismic Risk Affect the Environmental Impact of Existing Buildings?", Energy & Buildings, Elsevier B.V., Vol. 110, pp. 149–158.

Belleri, A., Riva, P. [2012] "Seismic Performance and Retrofit of Precast Concrete Grouted Sleeve Connections", PCI journal.

Belleri, A., Torquati, M., Marini, A., Riva, P. [2016] "Horizontal cladding panels: in-plane seismic performance in precast concrete buildings", Bulletin of Earthquake Engineering, Vol. 14, No.4, pp. 1103–1129.

Belleri, A., Torquati, M., Riva, P. [2014] "Seismic Performance of Ductile Connections Between Precast Beams and Roof Elements", Magazine of Concrete Research, Vol. 66, No.11, pp. 553–562.

Belleri, A., Torquati, M., Riva, P., Nascimbene, R. [2015] "Vulnerability Assessment and Retrofit Solutions of Precast Industrial Structures", Earthquake and Structures, Vol. 8, No.3, pp. 801–820.

Bellotti, D., Bolognini, D., Nascimbene, R. [2009] "Response of Traditional RC Precast Structures Under Cyclic Loading", Environmental Semeiotics, Vol. 2, No.2, pp. 63–79.

Biondini, F., Dal Lago, B., Toniolo, G. [2013] "Role of Wall Panel Connections on the Seismic Performance of Precast Structures", Bulletin of Earthquake Engineering, Vol. 11, No.4, pp. 1061–1081.

Bournas, D.A., Negro, P., Taucer, F.F. [2014] "Performance of Industrial Buildings During the Emilia Earthquakes in Northern Italy and Recommendations for Their Strengthening", Bulletin of Earthquake Engineering, Vol. 12, No.5, pp. 2383–2404.

Brunesi, E., Nascimbene, R., Bolognini, D., Bellotti, D. [2015] "Experimental Investigation of the Cyclic Response of Reinforced Precast Concrete Framed Structures", PCI Journal, Vol. 60, pp. 57–79.

Casotto, C., Silva, V., Crowley, H., Nascimbene, R., Pinho, R. [2015] "Seismic fragility of Italian RC precast industrial structures", Engineering Structures, Elsevier Ltd, Vol. 94, pp. 122–136.

Chopra, A.K. [2012] Dynamics of Structures - Theory and Applications to Earthquake Engineering.

CNR 10018. [1999] "Apparecchi di Appoggio per le Costruzioni. Istruzioni per l'Impiego (CNR 10018)", Roma.

CNR 10021-85. [1985] Strutture di Acciaio per Apparecchi di Sollevamento. Istruzioni per il Calcolo, l'Esecuzione, il Collaudo e la Manutenzione.

Colombo, A., Negro, P., Toniolo, G. [2014] "The Influence of Claddings on the Seismic Response of Precast Structures: The Safecladding Project", Second European conference on earthquake engineering and seismology, Istanbul, pp. 1–12.

Colombo, A., Negro, P., Toniolo, G., Lamperti, M. [2016] "Design Guidelines for Precast Structures with Cladding Panels", JRC Technical Reports.

EN 1993-6. [2007] Design of Steel Structures - Part 6: Crane Supporting Structures, Eurocode 3, Brussels, Belgium.

EN 1998-1. [2004] Design of Structures for Earthquake Resistance - Part 1: General Rules, Seismic Actions and Rules for Buildings, Brussels, Belgium.

Ercolino, M., Magliulo, G., Manfredi, G. [2016] "Failure of a Precast RC Building due to Emilia-Romagna Earthquakes", Engineering Structures, Elsevier Ltd, Vol. 118, pp. 262–273.

Ferrara, L., Felicetti, R., Toniolo, G., Zenti, C. [2011] "Friction Dissipative Devices for Cladding Panels in Precast Buildings", European Journal of Environmental and Civil Engineering, Vol. 15, No.9, pp. 1319–1338.

Fischinger, M., Zoubek, B., Isakovic, T. [2014] "Seismic Response of Precast Industrial Buildings", Perspectives on European Earthquake Engineering and Seismology, A. Ansal, ed., Springer, Berlin, pp. 131–177.

Isaković, T., Zoubek, B., Lopatič, J., Fischinger, M. [2014] "Experimental Research of Typical Cladding Panel Connections in Industrial Buildings", Second European conference on earthquake engineering and seismology, Istanbul, pp. 1–10.

Liberatore, L., Sorrentino, L., Liberatore, D., Decanini, L.D. [2013] "Failure of industrial Structures Induced by the Emilia (Italy) 2012 Earthquakes", Engineering Failure Analysis, Elsevier Ltd, Vol. 34, pp. 629–647.

Lourenco, R. [2011] "Design, Construction and Testing of an Adaptive Pendulum Tuned Mass Damper," University of Waterloo.

Magliulo, G., Capozzi, V., Fabbrocino, G., Manfredi, G. [2010] "Neoprene-concrete friction relationships for seismic assessment of existing precast buildings", Engineering Structures, Elsevier Ltd, Vol. 33, No.2, pp. 535–538.

Magliulo, G., Ercolino, M., Cimmino, M., Capozzi, V., Manfredi, G. [2014] "FEM Analysis of the Strength of RC Beam-to-column Dowel Connections Under Monotonic Actions", Construction and Building Materials, Vol. 69, pp. 271–284.

Magliulo, G., Ercolino, M., Manfredi, G. [2015] "Influence of Cladding Panels on the First Period of One-story Precast Buildings", Bulletin of Earthquake Engineering, Vol. 13, No.5, pp. 1531–1555.

Magliulo, G., Ercolino, M., Petrone, C., Coppola, O., Manfredi, G. [2014] "The Emilia Earthquake: Seismic Performance of Precast Reinforced Concrete Buildings", Earthquake Spectra, Vol. 30, No.2, pp. 891–912.

Marzo, A., Marghella, G., Indirli, M. [2012] "The Emilia-Romagna Earthquake: Damages to Precast/Prestressed Reinforced Concrete Factories", Ingegneria Sismica, Vol. 29, No.2, pp. 132–147.

Medina, R.A., Sankaranarayanan, R., Kingston, K.M. [2006] "Floor Response Spectra for Light Components Mounted on Regular Moment-resisting Frame Structures", Engineering Structures, Vol. 28, No.14, pp. 1927–1940.

Metelli, G., Beschi, C., Riva, P. [2011] "Cyclic Behaviour of a Column to Foundation Joint for Concrete Precast Structures", European Journal of Environmental and Civil Engineering, Vol. 15, No.9, pp. 1297–1318.

Midas GEN (v1.2). [2014] "MIDAS Information Technologies Co., Ltd.".

Minghini, F., Ongaretto, E., Ligabue, V., Savoia, M., Tullini, N. [2016] "Observational Failure Analysis of Precast Buildings After the 2012 Emilia Earthquakes",

Earthquake and Structures, Vol. 11, No.2, pp. 327–346.

Negro, P., Bournas, D.A., Molina, F.J. [2013] "Pseudodynamic Tests on a Full-scale 3-storey Precast Concrete Building: Global Response", Engineering Structures, Vol. 57, pp. 594–608.

NIST GCR 95-681. [1995] "Literature Review on Seismic Performance of Building Cladding Systems", Report Nist Gcr; 95-681., Emeryville, California.

NTC. [2008] Decreto Ministeriale del 14 Gennaio 2008: Norme Tecniche per le Costruzioni.

OpenSees. [2007] "Open System for Earthquake Engineering Simulation", University of California, Berkeley, California.

Osanai, Y., Watanabe, F., Okamoto, S. [1996] "Stress Transfer Mechanism of Socket Base Connections with Precast Concrete Columns", ACI Structural Journal, Vol. 93, No.3, pp. 266–276.

Pantoli, E., Hutchinson, T.C., Mcmullin, K.M., Underwood, G.A., Hildebrand, M.J. [2016] "Seismic-drift-compatible Design of Architectural Precast Concrete Cladding: Tieback Connections and Corner Joints", PCI journal, pp. 38–52.

Paultre, P. [2011] Dynamics of Structures, (iSte and Wiley, eds.).

PCI Design Handbook. [1985] Precast and Prestressed Concrete.

Petrone, C., Magliulo, G., Manfredi, G. [2015] "Seismic Demand on Light Acceleration-sensitive Nonstructural Components in European Reinforced Concrete Buildings", Earthquake Engineering & Structural Dynamics, Vol. 44, pp. 1203–1217.

Politopoulos, I. [2010] "Floor Spectra of MDOF Nonlinear Structures", Journal of Earthquake Engineering, Vol. 14, No.5, pp. 726–742.

Psycharis, I.N., Mouzakis, H.P. [2012] "Shear Resistance of Pinned Connections of Precast Members to Monotonic and Cyclic Loading", Engineering Structures, Vol. 41, pp. 413–427.

Riva, P., Franchi, A., Tabeni, D. [2001] "Welded Tempcore Reinforcement Behaviour for Seismic Applications", Materials and Structures.

Ruaumoko. [2007] "Athol J. Carr, Ruaumoko - The Maori God of Volcanoes and Earthquakes", University of Canterbury, Christchurch, New Zealand.

Savoia, M., Mazzotti, C., Buratti, N., Ferracuti, B., Bovo, M., Ligabue, V., Vincenzi, L. [2012] "Damages and Collapses in Industrial Precast Buildings After the Emilia Earthquake", Ingegneria Sismica, Vol. 29, No.2–3, pp. 120–131.

Schrage, I. [1991] "Anchoring of Bearings", Concrete Institute Publication SP-70. Joint Seal Bear Syst Concrete Struct, No.1, pp. 197–215.

Scotta, R., De Stefani, L., Vitaliani, R. [2015] "Passive control of precast building response using cladding panels as dissipative shear walls", Bulletin of Earthquake Engineering.

Senel, S.M., Kayhan, A.H. [2010] "Fragility Based Damage Assessment in Existing Precast Industrial Buildings - A Case Study for Turkey", Structural Engineering and Mechanics, Vol. 34, No.1, pp. 39–60.

Sullivan, T.J., Calvi, P.M., Nascimbene, R. [2013] "Towards Improved Floor Spectra Estimates for Seismic Design", Earthquake and Structures, Vol. 4, No.1, pp. 109–132.

Takeda, T., Sozen, M.A., Nielsen, M.N. [1970] "Reinforced Concrete Response to Simulated Earthquakes", Journal of the Structural Division, pp. 2557–2573.

Toniolo, G., Colombo, A. [2012] "Precast Concrete Structures: The Lessons Learned from the L'Aquila Earthquake", Structural Concrete, Vol. 13, No.2, pp. 73–83.

UNI-EN 1337:3. [2005] Appoggi Strutturali - Parte 3: Appoggi Elastomerici, Milano, Italia.

Vanmarcke, E.H., Gasparini, D.A. [1976] "Simulated Earthquake Motions Compatible with Prescribed Response Spectra", Department of Civil Engineering, Massachusetts Institute of Technology, Cambridge, Massachusetts.

Zoubek, B., Fischinger, M., Isakovic, T. [2015] "Estimation of the cyclic capacity of beam-to-column dowel connections in precast industrial buildings", Bulletin of Earthquake Engineering, Springer Netherlands, pp. 2145–2168.

4. EVALUATION OF THE EXPECTED ANNUAL LOSS FOR PRECAST CONCRETE INDUSTRIAL STRUCTURES

In the current Chapter, the purpose is to investigate the endorsability of Performance-Based Earthquake Engineering (PBEE) methodology ([Porter, 2003] and [Günay and Mosalam, 2012]) developed by the Pacific Earthquake Engineering Research (PEER) Center at the University of California, Berkeley (USA) on one-storey precast reinforced-concrete (RC) industrial buildings, typical of the Italian national territory. Currently there are no studies in the literature that have been examined with PEER PBEE framework applied to Italian RC precast industrial buildings. As demonstrated by the effects suffered by the companies after the earthquakes that hit the Emilian region in Italy in 2012, the importance of being able to predict the expected monetary losses due to an earthquake can be a useful tool for all of those entrepreneurs whose business is located in RC precast buildings. This Chapter also investigates the applicability of the PEER PBEE as a method to assess the savings in terms of expected annual loss (EAL) after a retrofit measure made to fix a local vulnerability (rupture of the top column fork). Considerations about each phase of the PEER PBEE are reported and a special attention is given to different calculation methods that can be adopted to carry out the structural analysis in both a refined and simplified way, as: incremental dynamic analysis (IDA), static pushover-to-incremental dynamic analysis tool (SPO2IDA) and displacement-based assessment (DBA). All of them are applied to a case study and observations about the use of these methods as well as a critical comparison between them are shown and discussed. Furthermore, in the last part of the Chapter, the assessment of the expected annual loss is probabilistically evaluated and the results are discussed as well as the lacks and critical aspects of the PEER PBEE framework applied to such structures are highlighted.

Herein, the assumed benchmark structure is a precast one-storey RC industrial building, located in L'Aquila (Abruzzo, Italy). This building is a hypothetical structure that was designed before current Italian technical standards for construction [NTC, 2008]. The plan, the frontal and lateral elevation views of the building are given in Figure 2.1. The global external size of the perimeter of the structural scheme in plan view (Figure 2.1, above) is 60x40m and the interior height of the facility is 7m. The structure is made up by 11 double-portals spaced apart by 6m along the X-direction whereas the total extension along the Y-direction is equal to 40m (labels from 1 to 11 in the Figure 2.1, above, indicate the double-portals).

The structure is composed by a total of 33 precast RC columns aligned along three rows (A, B, C labels in plan view of the Figure 2.1) 8,3m high and fixed at the base with isolated socket foundations. The cross section of the columns is 0,45x0,45m and

the longitudinal rebars are 12ϕ14. The structure is closed by 9m high vertical cladding panels along the frontal sides (Y-direction) and by four alignments of horizontal cladding panels along the lateral sides (X-direction) with a height of 1,8m. In the X-direction, the columns are connected at the top by precast prestressed beams (main beams) with variable cross-section (see Figure 2.1, centre), whereas along the X-direction the columns are connected by girders with U cross-section. The roof is composed by precast elements and transparent plastic elements (2 for each portal) for allowing the internal lighting of the building.

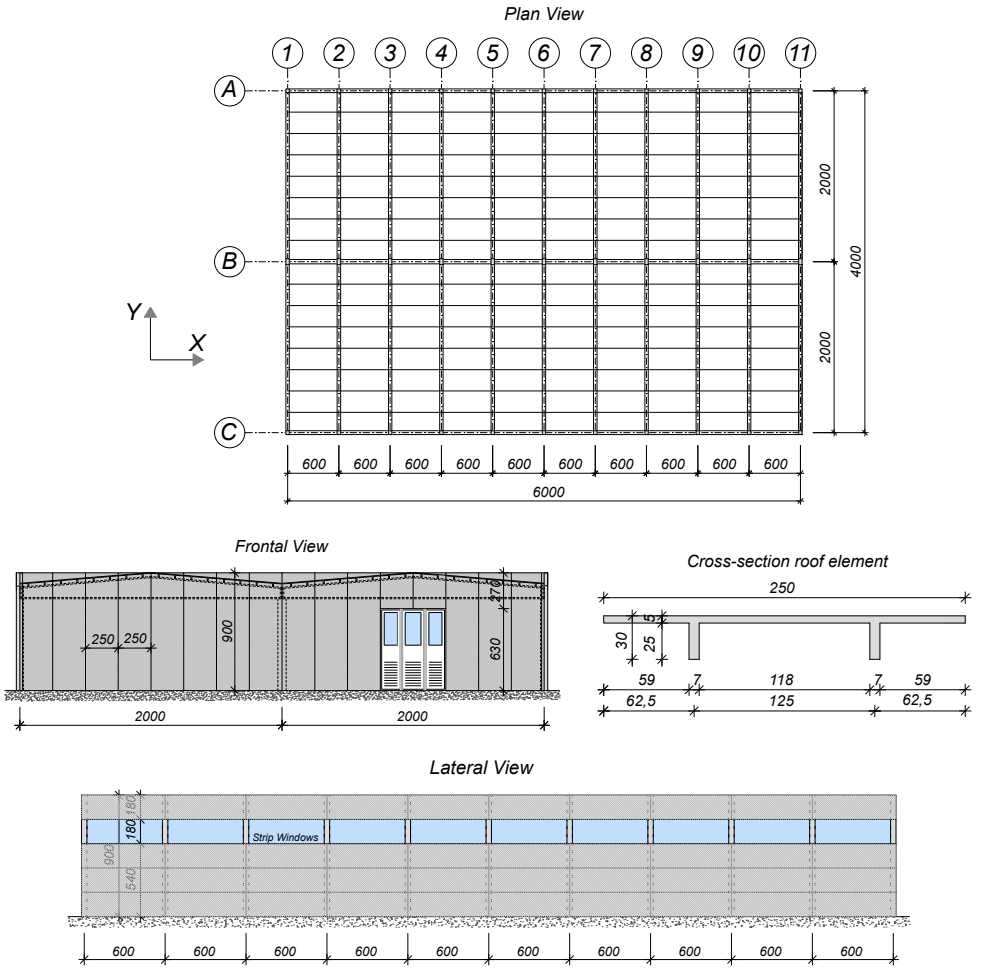

Figure 4.1 Plan view (above), frontal view (middle) and lateral view (below) of the case study, measures in centimetres.

The cross-section of the main beams varies along their longitudinal axis (global Y-axis) in terms of both cross-section shape and height. They have an I-shaped cross-section at the mid-span and a rectangular shape cross-section at their ends, corresponding to the connection with the columns; the height increases from 1m, at the ends, to a maximum value of 1,8m at the mid-span. The girders are U-shaped elements with a base of 0,65m and a total height of 0,45m. The roof elements are characterized by a TT-shape cross-section as shown in the Figure 2.1 (centre).

For all structural elements, the adopted concrete is C50/60 and the reinforcement steel is B450C. The characteristics of such materials are shown in Table 2.1.

Table 4.1 Characteristics of the assumed structural materials within the fem model.

Concrete C50/60	**Steel for rebars B450C**
$f_{ck} = 50 MPa$	$f_{yk} = 450 MPa$
$f_{ct} = f_{ctm} = 0,3 f_{ct}^{2/3} = 4,07 MPa$	
$E_{cm} = 22000 \cdot \left(\frac{f_{ck} + 8}{10} \right)^{0,8} = 37278 MPa$	$E_s = 205000 MPa$
$G_{cm} = \frac{E_c}{2 \cdot (1 + \nu)} = 15532 MPa$	

The investigated industrial building has the typical features of an Italian twenty-century one-storey precast RC structure, not designed for seismic actions. The connections between the structural elements (roof elements, beams and columns) are friction connections relying only on the friction between the connected elements. Between the main beams and the columns, a neoprene pad (23x15x1cm) is provided as a frictional connection whereas the connection between girders and columns provide bolted steel angles with a low rotational strength, for this reason the girder-to-column connections can be adopted in the modelling as hinged.

The site for the benchmark building is selected to represent a typical location in a highly seismic region of Italian territory (zone 1); the chosen site is the city of L'Aquila, Abruzzo (coordinates 13,3944° longitude, 42,366° latitude).

4.1 Application of the refined PEER PBEE method

The application of PEER PBEE methodology described in Chapter 2 is applied to the case study for the assessment of the EAL through the PACT software provided by [FEMA P-58, 2012a]. Each phase of this framework is analysed and critical aspects and considerations related to the adoption to precast reinforced concrete industrial building are shown and discussed.

4.1.1 Structural analysis

The modelling of the structure of a precast RC building requires taking into account some important considerations and precautions. Although in most cases these constructions are mainly simple one-storey structures, when the fem model is being built the presence of local vulnerabilities should be taken into account (see Chapter 3), such as the lack of connections between structural elements. These vulnerabilities cannot be ignored if the final purpose is to carry out a proper assessment of the probability of collapse and they were proven with different local collapses observed after the earthquakes that hit the Emilian region on May in 2012.

At this stage of the research, the main goal is to apply and validate the PEER PBEE methodology to precast RC industrial buildings for achieving the assessment of the EAL due to earthquake. For this reason, the adopted benchmark structure is an equivalent simplified scheme of a SDOF (Figure 4.2, a). The scheme consists of a cantilever beam fixed at the base with a point mass m at the top of the column, which represents the portion of the roof acting on each single column. The characteristics of the SDOF system modelled within [Ruaumoko, 2007] are the following: tributary mass at the top equal to m = 26,338t, height of the column equal to h = 8,3m and the size of the column is 0,45x0,45m. The non-linearities are modelled by considering a tri-linear [Takeda *et al.*, 1970] constitutive relationship in the cross-section at the base of the columns (*IHYST* model number 57 adopted in [Ruaumoko, 2007], see Figure 4.2, c), according to the hysteretic behaviour observed as a result of several experimental tests carried out for similar precast columns (Figure 4.2, b).

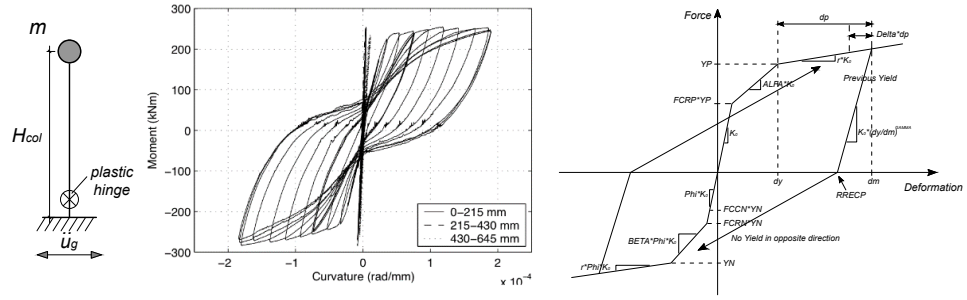

Figure 4.2 a) Simple initial SDOF system modelled within [Ruaumoko, 2007]; b) hysteretic behaviour observed performing experimental tests on precast columns; c) hysteretic model "IHYST=57 - Revised Takeda Degrading Tri-Linear Hysteresis" adopted within [Ruaumoko, 2007].

The adopted model ability to grasp the degradation of the stiffness of the column is shown in Figure 4.3, where the multiplier of the yield moment is expressed as a function of curvature ductility (ϕ_{ult}/ϕ_y).

As mentioned, precast RC industrial buildings are characterized by multiple local vulnerabilities which need more in-depth studies to allow a proper use of the probability of partial collapse (e.g. the fall of some roof elements instead the entire roof floor) within the assessment of the EAL.

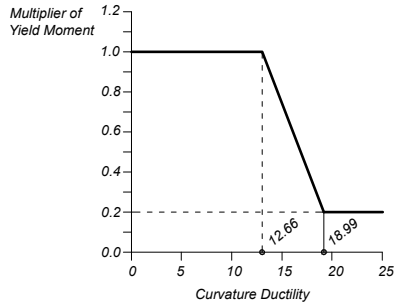

Figure 4.3 Model adopted to describe the degradation of the stiffness of the column in terms of reduction of curvature ductility.

As shown in Chapter 3, where the main vulnerabilities typical of existing RC precast industrial buildings are presented and some of them are investigated in depth, it can be said that many studies are still needed to better understand and define the structural seismic response of the existing facilities (e.g. analyses aimed to investigate about the uncertainty in the seismic response in the case of connections between structural elements relying only on friction). At this point, for this reason, the seismic retrofit measures (or improvements) classified as "first level retrofit interventions"

and envisaged by [Protezione Civile *et al.*, 2012] guidelines (drawn up following the earthquakes that hit the Emilia region (Italy) in 2012) are herein adopted.

In particular, in order to fulfil this purpose and to simplify the time history analyses, the following assumptions have been made in the fem models:

- the existence of metallic connections between roof elements and beams, opportunely designed to withstand the stressing forces and able to inhibit vulnerabilities linked to the lack of support and therefore possible collapses (Figure 4.26);
- the existence of a steel pin between the main beam and the forks at the top of the column, which is able to ensure a hinged constraint between these two structural elements (as an alternative of this solution can be considered the solution provided by [Doneux *et al.*, 2006], see Figure 4.5, b), in accordance to the hypothesis of hinged frame adopted during the design phase (Figure 4.5);
- friction connections are not taken into account;
- the metallic connections are evaluated with capacity of V_{Rd} as a product between the acceleration a^*_{SLV} and the mass of the structural element m, where a^*_{SLV} is computed considering a value equal to 2/3 of the acceleration related to the *SLV* (life safety) limit state.

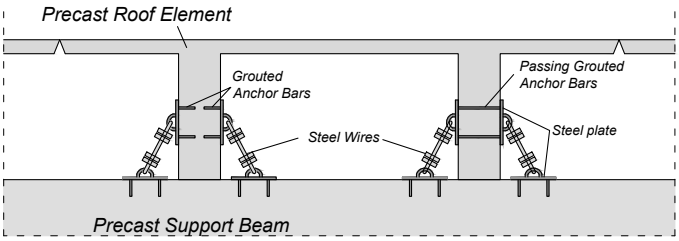

Figure 4.4 Assumed connections between roof elements and main beam.

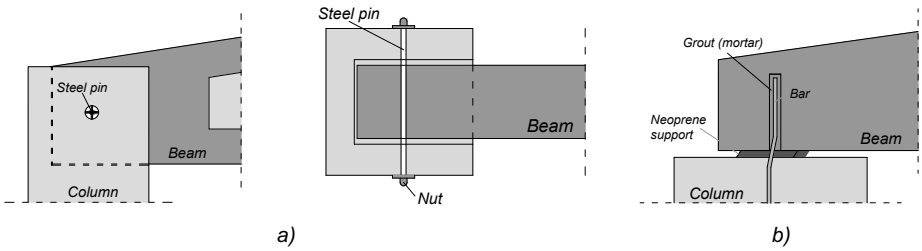

Figure 4.5 a) Beam-to-column connection with steel pin adopted in the finite element model; b) different solution of the beam-to-column connection provided by [Doneux et al., 2006].

To perform the assessment of the EAL, the first input needed to proceed with PACT is the total replacement cost (RC) of the facility.

The total replacement cost (900'000€) is obtained multiplying the total surface area of 2'400m^2 times an average construction cost of 375€/m^2. In addition, the value of the internal equipment and machineries is assumed as 1'100'000€, equalling to a total amount of 2'000'000€. Precisely, the cost per square meter for a new Italian industrial precast building is determined by considering an average cost in reference to the data provided by an Italian real estate in the year 2013 [Tecnocasa Group, 2013]. This cost is related to a new building built in the Po Valley area in Lombardy region.

4.1.1.1 Refined structural analysis with incremental dynamic analysis (IDA)

To successfully carry out the structural analysis phase, sets of ground motions must be selected for each intensity to conduct the non-linear time history analyses (NLTHA). For this work, sets of ground motion are selected for the site located in L'Aquila (Abruzzo, Italy) and A-type soil (rock) [EN 1998-1, 2004] in order to represent a site of high seismicity. IDA [Vamvatsikos and Cornell, 2002] is then performed with 90 NLTHA: ten accelerograms are taken into account for each of the nine seismic intensities corresponding to return periods (T_R) of 30, 50, 72, 101, 140, 201, 475, 975 and 2475 years.

The selected ground motions have been taken from the [RELUIS, 2013] project [Sullivan and Calvi, 2015]. Each ground motion has been selected by the authors according to the hazard information provided by "Istituto Nazionale di Geofisica e Vulcanologia" [INGV, 1999] (*http://esse1-gis.mi.ingv.it/s1_en.php*). For each hazard level and conditioning period, 10 ground-motions have been selected and scaled to match the conditional spectrum; equal weight have been provided in matching the target mean and matching the target variance. The ground motions are taken from the pan-European SHARE (*http://www.share-eu.org*) strong-motion database.

In Figure 4.6, the elastic response spectra of the accelerograms assumed for the selected site of L'Aquila and which are adopted to perform the IDAs for the eight return periods (T_R = 30, 50, 72, 101, 140, 201, 475 and 975yrs) are shown as well as the mean spectrum for each intensity measure. Concerning the ninth return period (2475yrs), the accelerograms are obtained by scaling the accelerograms associated to T_R = 975yrs by a scale factor equal to 1,46; this value is calculated in order to have the same value of $S_a(T_1)$ equal to what assessed with the formula suggested by [NTC, 2008] in *§ 3.2.3.2.1*."

The IDAs are carried out by taking into account a 2-D fem model in [Ruaumoko, 2007] from which it is possible to proceed to the evaluation of the EDPs such as interstorey drifts and accelerations at the top of the column, which are necessary before passing through the implementation of the damage and loss analyses with PACT software. The fem model is characterized by unreinforced forks at the top of the column, anyway considering the previously connections. This scenario wants to simulate the condition of an existing building. Subsequently, a retrofit procedure on the forks at the top of the column is taken as an example for the evaluation of the convenience in terms of EAL (Chapter 4.1.2).

The first important issue that must be taken into account is linked to the uncertainty due to the assumptions assumed in the modelling of the structure within the fem software. Different results of EDPs can be obtained depending on how the structure is modelled, and also on how the final results in terms of EAL can be affected.

Two different fem models are taken into account to see how different modelling may affect the values of EDPs. In this way, it is possible to have a better idea of the goodness and reliability of the adopted finite element model.

Initially, the simplest fem model is adopted: the fork is modelled as an added single *beam* element at the top of the column (Figure 4.7, a). The capacity and flexural strength are evaluated through a sectional analysis carried out on a single element of the fork, which is characterized by a cross-section of 12x45cm, 120cm height and 4ϕ8 longitudinal rebars. The vertical load due to the roof weight is applied directly at the top of the column.

A second more refined model is built for evaluating the variability of the EDPs, in this case, the main difference is that the fork at the top of the column is modelled with two *beam* elements instead of one. The capacity and flexural strength are assumed to be the same as in the previous fem model. In this model, a *beam* element is provided and placed between the two elements of the forks in order to represent the physical size of the main beam connected at the top of the column. The upper node of the beam is connected to the top of the fork through two *"compression-only"* spring elements, which can be activated only when the existing physical gap (set to 2cm) between the beam and the fork is achieved.

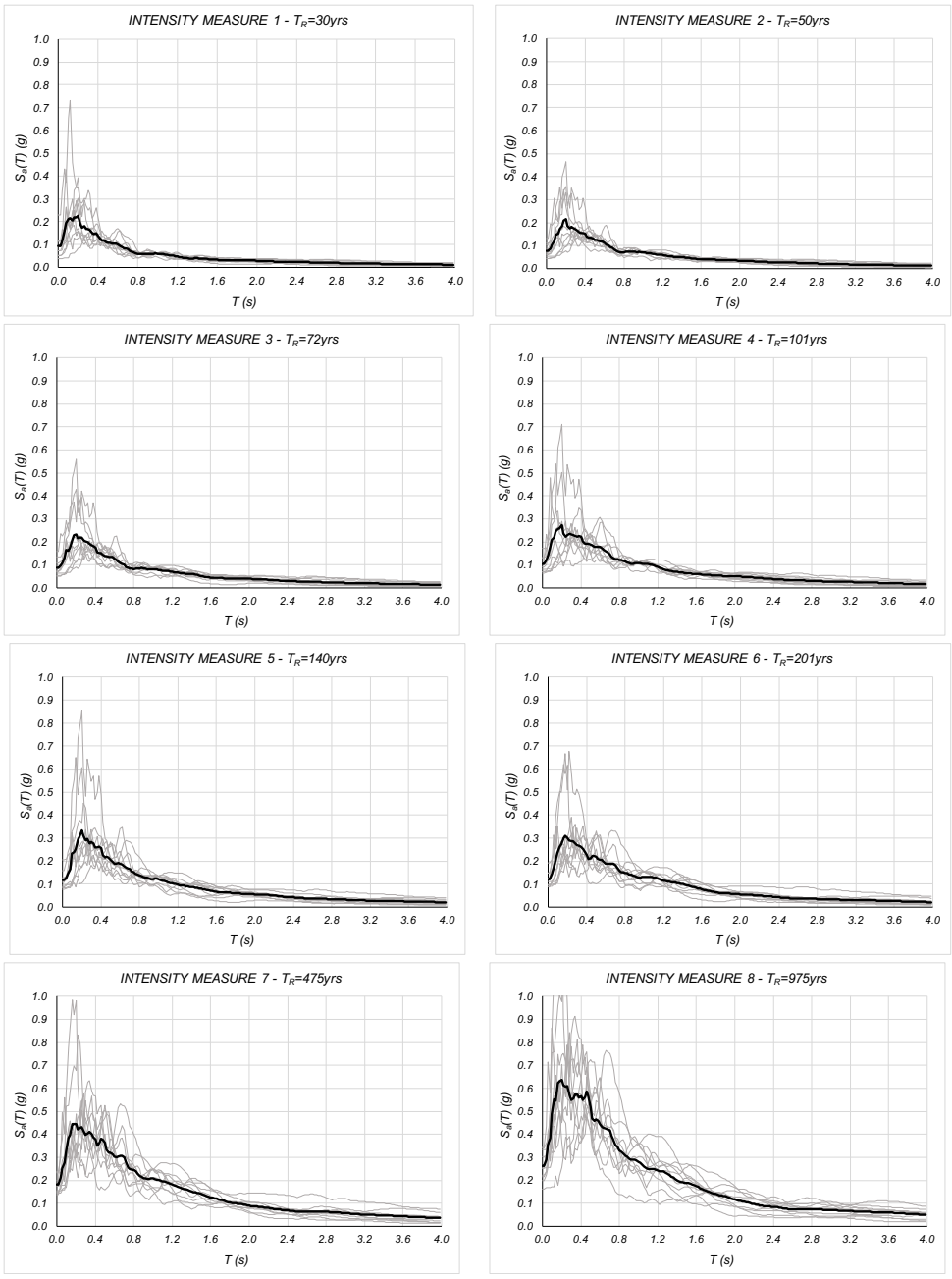

Figure 4.6 Elastic response spectra of the accelerograms for the selected L'Aquila site assumed to perform the IDA for T_R = 30, 50, 72, 101, 140, 201, 475 and 975yrs.

A vertical load equal to the weight of the roof is also applied at this upper node. For the characterization of the spring response, two different non-linear constitutive behaviours are investigated and compared: the former consists of a *"bi-linear with slackness hysteresis"* model and the latter consists of a *"Hertzian contact spring hysteresis rule"* model, both provided in [Ruaumoko, 2007] as *IHYST* model number 5 and 19 respectively (Figure 4.7, b).

In order to catch any possible differences in the response due to the activation of the elastic spring at the time of the closing of the gap between the main beam and the fork, the comparison of results obtained adopting the two constitutive behaviours is carried out performing a non-linear time history analysis with a selected accelerogram. The results are then compared in terms of moment-curvature response, moment at the base of the fork and the column and displacement of the upper node of the main beam (Figure 4.8). This comparison shows no differences in the structural response. Given the non-variability of the results, the *IHYST* constitutive behaviour number 5 (*"bi-linear with slackness hysteresis"*) is then adopted as a simpler constitutive relationship for modelling the structure and performing the next IDAs phase.

As mentioned before, the IDAs phase is carried out by performing 90 non-linear time history analyses. For both models shown in Figure 4.7 (a and b solutions), the probability of collapse is estimated by taking into account the number of cases that lead to the failure of the fork at the top of column (as the weaker element existing in the structure). Given the maximum capacity of the fork in terms of ultimate curvature, the maximum values of the curvature reached at the base of the fork for each analysis performed in IDAs are extracted and compared with this limit value in order to determine the cases of collapse.

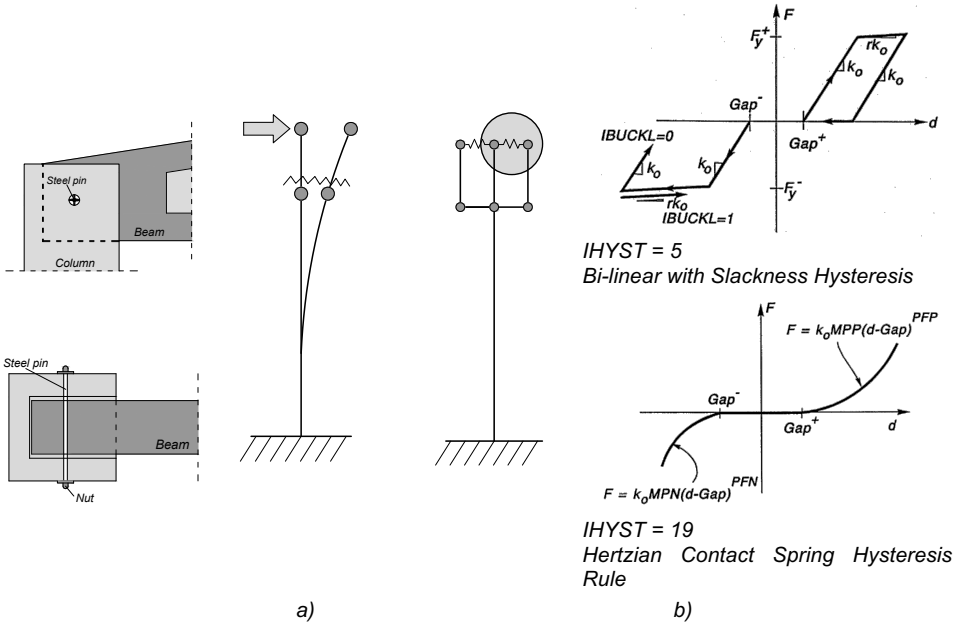

Figure 4.7 Fem models adopted in [Ruaumoko, 2007]: a) the fork at the top of the column is modelled with one beam element; b) the fork at the top of the column is modelled with two beam elements plus a contact element between the fork and the main beam.

Considering the number of non-linear analyses performed and the number of collapses reached during the IDAs, the mean spectral acceleration, $S_a(T)_{COLLAPSE}$, for which occurs the local collapse associated to the failure of the fork as well as the standard deviation, $\beta_{COLLAPSE}$, linked to the mean value are determined using the "*Collapse Fragility Tool*" implemented by Jack Baker for the ATC-58 project and then provided within [FEMA P-58, 2012a]. This tool allows to generate the collapse fragility curve by assuming a lognormal distribution of the result collected as output from IDAs.

Regarding the model of the fork modelled with a single added element at the top of the column, as shown in Figure 4.9 (a) and Table 4.2, for each of the nine intensities is taken into account in the IDAs, the number of the analysis and the number of collapses observed at a specific intensity is reported in "*Collapse Fragility Tool*" in order to fit and generate the collapse fragility curve.

The obtained $S_a(T)_{COLLAPSE}$ and $\beta_{COLLAPSE}$ are equal to 0,0986g and 0,22 respectively. Again, with "*Collapse Fragility Tool*", the $S_a(T)_{COLLAPSE}$ and $\beta_{COLLAPSE}$ are assessed for the other structural fem model previously described, obtaining values equal to 0,2457g and 0,37 respectively (Figure 4.9, b, and Table 4.2).

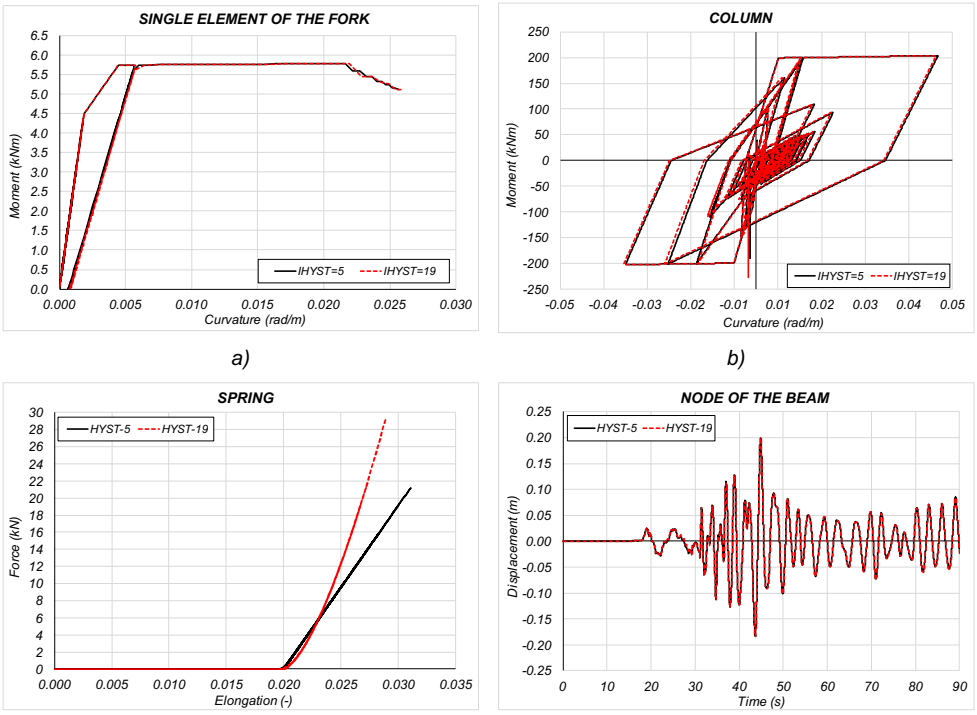

Figure 4.8 Comparison of the results obtained adopting two different hysteresis behaviour models, HYST=5 and HYST=19: a) moment-curvature relationship of the cross-section at the base of the single element of the fork; b) moment-curvature relationship of the cross-section at the base of the column; c) axial force-elongation relationship of the spring element; d) displacement-time relationship of the superior node of the main beam.

As it can be seen, the values of $S_a(T)_{COLLAPSE}$ and $\beta_{COLLAPSE}$ obtained for the two solutions of modelling analysed are different. A higher value of $S_a(T)_{COLLAPSE}$ is reached for the second solution and also the dispersion $\beta_{COLLAPSE}$ increases in comparison to the first considered fem model. Therefore, it can be said that, a difference in the modelling assumptions within the fem software can affect the results of $S_a(T)_{COLLAPSE}$ and $\beta_{COLLAPSE}$ and then the EAL assessed with PEER PBEE.

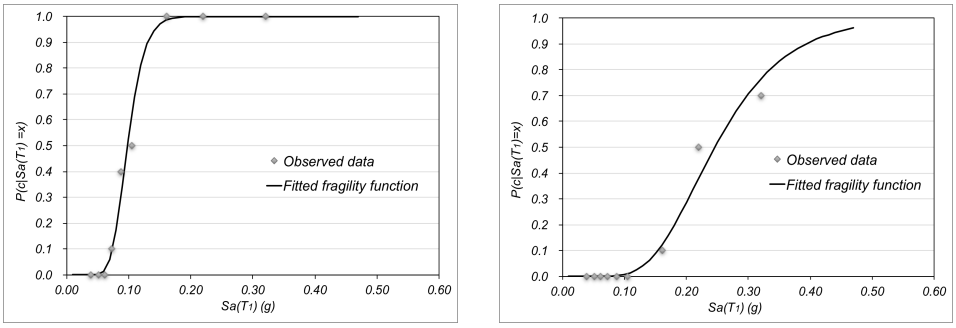

Figure 4.9 Results are obtained according to the "Collapse Fragility Tool" provided by [FEMA P-58, 2012a]. Fitting of the collapse fragility curve, for: a) fork modelled with a single element; b) fork modelled with two elements.

Such a difference in the value of $S_a(T)_{COLLAPSE}$ should lead to a high decrease of the EAL when the fork is modelled with two elements in the fem model, but this high decrease of EAL is not shown from the performed analyses. As shown in Figure 4.33 (see Chapter 4.3), the decrease of EAL with respect to the case of fork modelled with a single *beam* element only equals to -6,2% (first and third cases in Figure 4.33), a very small noticeable difference of EAL compared to the difference observed for the $S_a(T)_{COLLAPSE}$.

Table 4.2 Values of the $S_a(T)$ assumed for performing the IDA and number of collapses reached for each intensity for the fork modelled with one and two beam elements.

Fork modelled with one element			**Fork modelled with two elements**		
$S_a(T)$ (g)	Number of analysis	Number of collapses	$S_a(T)$ (g)	Number of analysis	Number of collapses
0,038690	10	0	0,038690	10	0
0,051192	10	0	0,051192	10	0
0,061666	10	0	0,061666	10	0
0,073035	10	1	0,073035	10	0
0,087574	10	4	0,087574	10	0
0,105323	10	5	0,105323	10	0
0,160568	10	10	0,160568	10	1
0,219303	10	10	0,219303	10	5
0,321243	10	10	0,321243	10	7

Looking at the results of the EDPs obtained by performing the IDAs on both fem models, a considerable difference of the values in terms of maximum interstorey drift and maximum acceleration at the top of the column can be seen (treated as an average value assessed for the 10 analyses performed for each intensity measure). The fem model with the fork built with two *beam* elements permits reaching much higher

values of the EDPs compared to the simpler model with the fork built with only one *beam* element. The trend of this difference is manifested both in terms of interstorey drift and acceleration for both the mean value, σ, and standard deviation, β (Figure 4.10 and Figure 4.11).

In order to carry out a proper assessment of the EAL, an important consideration to be noted is that in the case of fork modelled with two beam elements, the result of the EAL due to the collapse is lower than in the case of fork modelled with a single beam element (Figure 4.29); in fact, the spectral acceleration of collapse ($S_a(T)_{COLLAPSE}$) is higher in the former case ($S_a(T)_{COLLAPSE,\ 2\ ELEM}$ = 0,2457g in the case of fork modelled with two elements and $S_a(T)_{COLLAPSE,\ 1\ ELEM}$ = 0,0986g for the fork modelled with one element). Given the large difference of $S_a(T)_{COLLAPSE}$ observed by comparing both models, $S_a(T)_{COLLAPSE,\ 2\ ELEM}$ is more than double of $S_a(T)_{COLLAPSE,\ 1\ ELEM}$, a larger difference of EAL should also be expected but, on the contrary to expectations, the difference of EAL is not so large, it is equal to 6,24% (see Figure 4.29). In the case of fork modelled with two elements, the higher value of $S_a(T)_{COLLAPSE}$ leads to lower monetary losses due to collapse but, at the same time, higher values of EDPs as the inter-story drift and acceleration are reached, as shown in Figure 4.10 and Figure 4.11. For the assumed case study, the decrement of EAL due to collapse is almost equivalent to the increase of EAL due to the worst damages suffered by all vulnerable elements adopted in the assessment of EAL that are directly linked to the values of the aforementioned EDPs (see Chapter 4.1.2 and Chapter 4.1.4). For this reason, the difference of EAL is not large. It is noted that in this study, the assumed vulnerable elements in the evaluation of EAL are: grouted sleeve columns, cladding panels, strip windows and the caulking (Chapter 4.1.4 and Chapter 6). All the EDPs are expressed as a function of the interstorey drift or acceleration, for this reason, an increase in the interstorey drift and acceleration as shown in Figure 4.10 and Figure 4.11 led to an increase in the final value of monetary losses.

These results show that the use of a more refined modelling of the top column fork is able to more accurately grasp the value of the EDP which in this specific case reaches higher values both in terms of interstorey drift and acceleration. It can be therefore affirmed that a difference in the modelling lead to a difference of EDPs and then of EAL.

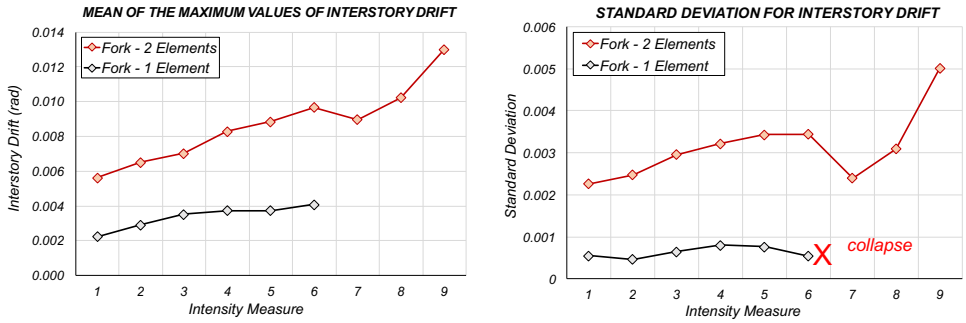

a) b)

Figure 4.10 Comparison of the result of the EDPs in terms of interstorey drift obtained from IDAs in the case of fork modelled with one and two elements: a) mean of the maximum values; b) standard deviation.

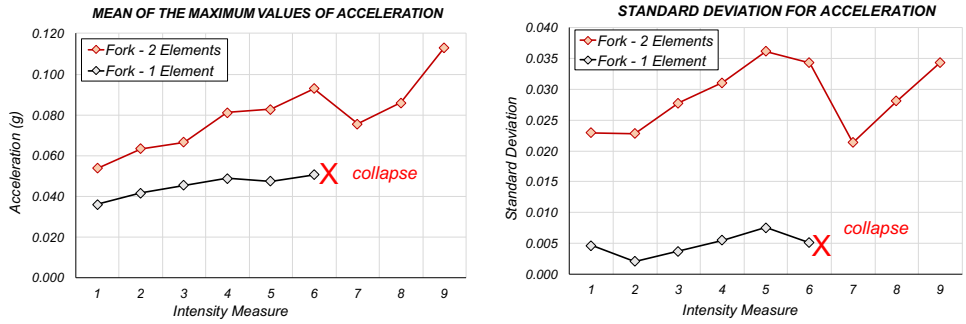

a) b)

Figure 4.11 Comparison of the result of the EDPs in terms of acceleration obtained from IDAs in the case of fork modelled with one and two elements: a) mean of the maximum values; b) standard deviation.

4.1.1.2 Simplified structural analysis with SPO2IDA tool

As an alternative to the structural analysis carried out with the refined method based on the IDAs, two different procedures for determining the EAL are investigated. The purpose of the adoption of these new procedures it to use a simplified procedure in order to prevent the computational cost required by performing the IDAs. Although nowadays the software used for the calculations have become more efficient and powerful, IDAs are not commonly used by engineers in the professional field, at least not in the way required in PEER PBEE framework. The development and validation of an alternative simplified procedure to the IDAs is essential. In this Chapter, the application of a simplified procedure to the assumed case study is shown.

The first alternative suggested procedure is based on the use of the SPO2IDA tool provided within [FEMA P-58, 2012a]. With SPO2IDA, once the pushover analysis is

performed and the pushover curve is known, the output data form IDAs are estimated in a simplified manner as specified by [Vamvatsikos and Cornell, 2006].

The analysis with the SPO2IDA tool as well as the evaluation of the EAL is carried out for the cases before and after the retrofit procedure on the fork at the top of the column. In this way, it is possible to compare the new results in terms of EAL with those obtained by performing the structural analysis with the IDAs as shown in Chapter 4.1.1.1.

In the configuration with the unreinforced fork, it is necessary to consider two possible causes that could lead to a partial local collapse: the former case is given by the failure of the fork for the achievement of the maximum capacity in the out-of-plane in terms of bending moment (Figure 4.12, a); the latter is given by the rupture of the steel pin in the beam-to-column connection due to the axial force transferred by the beam and evaluated according to [Doneux *et al.*, 2006] (Figure 4.12, b). Between these two possible mechanisms of collapse, the one that occurs with a lower shear value at the base of the column is chosen.

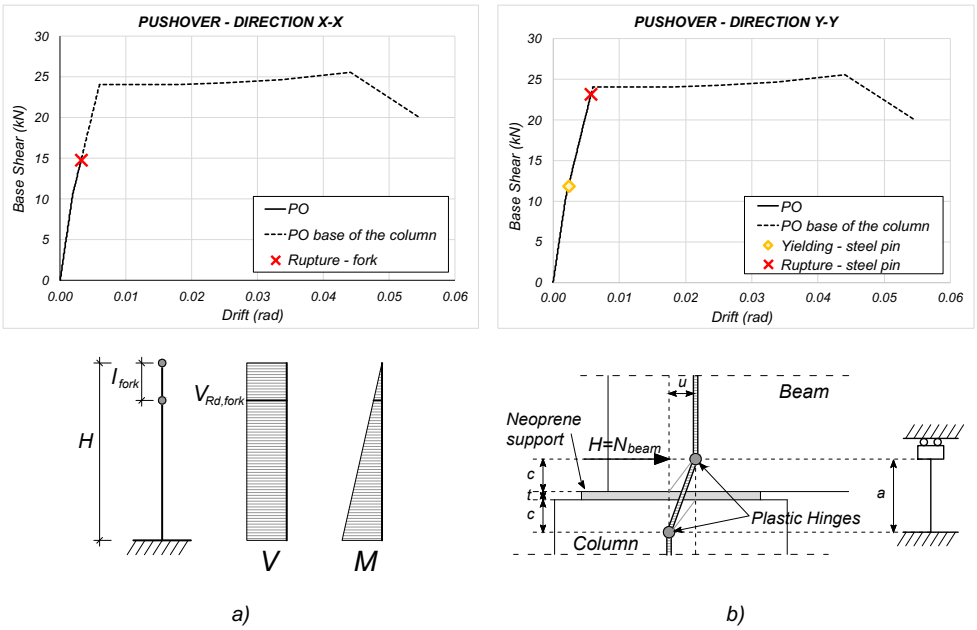

Figure 4.12 Different cases of collapse of the fork at the top of the column due for: a) achievement of the maximum out-of-plane capacity in terms of bending moment (X-direction); b) achievement of the maximum deformation of the steel pin element in the beam-to-column connection (Y-direction).

The pushover curve for which the shear value at the base of the column leads to the rupture of the fork (for the achieving of the maximum bending capacity) is taken into account, as reported in Figure 4.12 (a).

A necessary step with SPO2IDA tool is to determine and fit the main points that characterize the pushover curve obtained and imported from the analysis performed with [Ruaumoko, 2007], such as the points that define the end of the elastic behaviour, the part of the curve with hardening, the softening part and the residual plateau at the end of curve. Figure 4.13 shows the fitting of the two pushover curves made for the cases before and after the retrofit measure on the fork at the top of the column.

The results assessed with SPO2IDA tool are an estimation of the IDAs curves which are provided in the form shown in Figure 4.14. In this tool, the simplified estimate of the IDAs curves is achieved by setting the values of the interstorey drift associated with the user-selected values of $S_a(T)$, as long as these last ones are between 0 and $S_a(T)_{COLLAPSE}$. Such interstorey drift values can be adopted and directly implemented as EDP within PACT. SPO2IDA also provides the value of the $S_a(T)_{COLLAPSE}$, it is equal to 0,0560g and 0,7575g for the case before and after the retrofit intervention on the fork at the top of the column respectively, thus allowing to compare the results with those calculated through the refined IDAs (see Chapter 4.1.1.1), in which the aforesaid values of $S_a(T)_{COLLAPSE}$ are equal to 0,0986g and 0,5401g respectively. By comparing the latter values, it can be observed how the SPO2IDA tool underestimates by about 43% the $S_a(T)_{COLLAPSE}$ linked to the case of unreinforced fork and overestimates for 40% the $S_a(T)_{COLLAPSE}$ in the case of retrofitted fork.

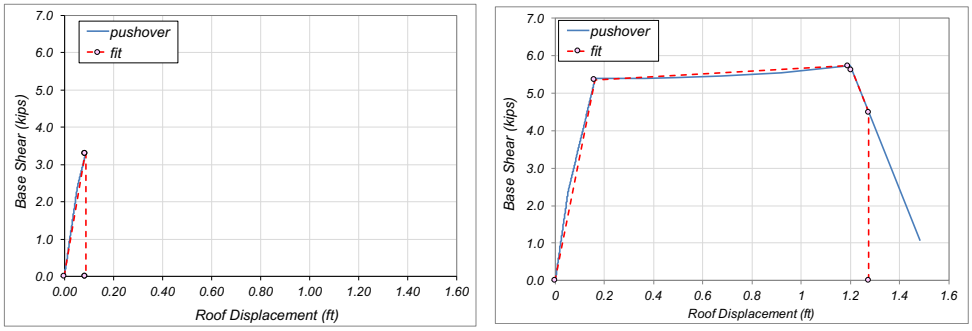

a) b)

Figure 4.13 Fitting of the pushover curve within the SPO2IDA tool in the case of: a) unreinforced fork; b) retrofitted fork.

Following the simplified method, the dispersion associated to the collapse, $\beta_{COLLAPSE}$, can be assumed as suggested by [FEMA P-58, 2012b] in *§ 6.3 -Simplified Nonlinear Analysis*, and then it can be taken equal to 0,6.

The evaluation of the EDPs required as input data within PACT for the assessment of the EAL is achieved in a simplified manner according to the formulations suggested by [FEMA P-58, 2012b] in *§ 5.3.2 - Simplified Analysis Procedure*, with the exception of the interstorey drift values, which are directly available as output from SPO2IDA tool. However, the formulas suggested by [FEMA P-58, 2012b] permit to calculate the interstorey drift, as well as the floor-velocity and floor-acceleration at the height of interest.

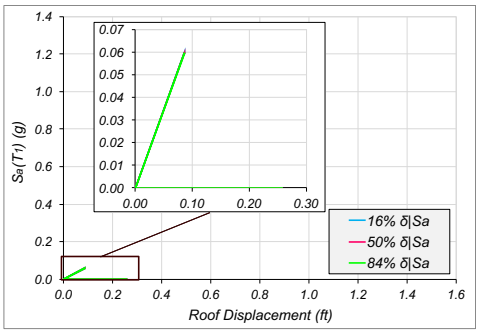

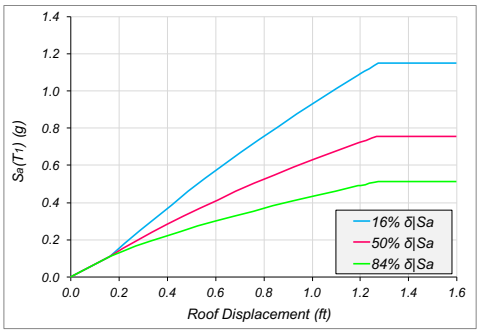

Sa	δ16%	δ50%	δ84%	mean δ	mean CR	beta δ
0.0098	0.014	0.014	0.014	0.014	1.000	0.000
0.0196	0.028	0.028	0.028	0.028	1.000	0.000
0.0295	0.043	0.043	0.043	0.043	1.000	0.000
0.0393	0.057	0.057	0.057	0.057	1.000	0.000
0.0491	0.071	0.071	0.071	0.071	1.000	0.000
0.0560	0.081	0.081	0.081	0.081	1.000	0.000

Sa	δ16%	δ50%	δ84%	mean δ	mean CR	beta δ
0.0387	0.056	0.056	0.056	0.056	1.000	0.000
0.0512	0.074	0.074	0.074	0.074	1.000	0.000
0.0617	0.089	0.089	0.089	0.089	1.000	0.000
0.0730	0.105	0.105	0.105	0.105	1.000	0.000
0.0876	0.126	0.126	0.126	0.126	1.000	0.000
0.1053	0.152	0.152	0.152	0.152	1.000	0.000
0.1606	0.206	0.224	0.258	0.225	0.973	0.115
0.2193	0.259	0.304	0.391	0.310	0.982	0.207
0.3212	0.353	0.455	0.659	0.478	1.031	0.313
0.5400	0.569	0.831	#N/D	0.893	1.146	0.379
0.7575	0.803	1.275	#N/D	1.419	1.299	0.462

a) *b)*

Figure 4.14 Estimation of the IDAs curves through the SPO2IDA tool at the 16th, 50th (median), 84th fractile and values of $S_a(T)$, displacement and dispersion in the case of: a) unreinforced fork; b) retrofitted fork.

Regarding the floor acceleration at the level of interest (first floor, roof…), e.g. in this case at the height corresponding to the top of the column, the formula in Eq. 3.2 is taken into consideration (equations 5-12 and 5-13 from [FEMA P-58, 2012b]):

$$a_i^* = H_{ai}\left(S,T,h_i,H\right)\cdot PGA \qquad for\ i = from\ 2\ to\ N+1 \qquad Eq.\ 4.1$$

where

$$\ln(H_{ai}) = a_0 + a_1 T_1 + a_2 S + a_3 \frac{h_i}{H} + a_4 \left(\frac{h_i}{H}\right)^2 + a_5 \left(\frac{h_i}{H}\right)^3 \qquad for\ S \geq 1,\ i = from\ 2\ to\ N+1 \qquad Eq.\ 4.2$$

with reference to the next Table 4.3 for the determination of the coefficients a_0, a_1, a_2, a_3, a_4 and a_5.

Table 4.3 Corrections factors for the storey drift ratio, floor velocity and floor acceleration for 2-storey to 9-storey buildings (Table 5-4, [FEMA P-58, 2012b]).

Demand	Frame Type	a_0	a_1	a_2	a_3	a_4	a_5
Storey drift ratio	Braced	0,900	-0,120	0,012	-2,650	2,090	0
	Moment	0,750	-0,044	-0,010	-2,580	2,300	0
	Wall	0,920	-0,036	-0,058	-2,560	1,390	0
Floor velocity	Braced	0,150	-0,100	0	-0,408	0,470	0
	Moment	0,025	-0,068	0,032	-0,530	0,540	0
	Wall	-0,033	-0,085	0,055	-0,520	0,470	0
Floor acceleration	Braced	0,660	-0,270	-0,089	0,075	0	0
	Moment	0,660	-0,250	-0,080	-0,039	0	0
	Wall	0,660	-0,150	-0,084	-0,260	0,570	0

Within PACT, the ground acceleration (a_g) for each IM is assumed equal to the peak ground acceleration computed according to the standard for construction on the Italian territory [NTC, 2008] for the site of L'Aquila. It is noted that the values of the interstorey drift supplied from SPO2IDA tool are obtainable for each of $S_a(T)$ entered in the SPO2IDA tool itself. Related to the case of the model with retrofitted fork at the top of the column, the selected $S_a(T)$ for the SPO2IDA tool are those provided for all 9 IMs on which the hazard curve is constructed and assessed according to [INGV, 1999] and [NTC, 2008]. For the case of the unreinforced fork, a critical issue linked to the fact of having a vulnerable element at low IMs is highlighted. Given the low value of the $S_a(T)_{COLLAPSE}$ obtained from the pushover analysis (0,0560g) in the case of unreinforced fork, it is not possible to adopt the same 9 values of $S_a(T)$ adopted in the previous case (retrofitted fork) as input data for the SPO2IDA tool. In this case, instead, it is necessary to assume different values of $S_a(T)$, which must preferably be chosen between the values of 0 and $S_a(T)_{COLLAPSE}$ and possibly spaced with a regular interval.

The value of $S_a(T)_{COLLAPSE}$ determined by SPO2IDA tool is very close to the value of $S_a(T)$, equal to 0,051g, provided by [NTC, 2008] for a T_R of 50yrs, considering the site of L'Aquila and soil type A.

Being the values of $S_a(T)$ lower than $S_a(T)_{30yrs}$, the actual standard of construction [NTC, 2008] does not give any guideline regarding the determination of the response spectrum parameters (a_g, F_0, T_C^*), the selection of a suitable criterion for the calculation of the values of a_g necessary for the implementation of the inputs within PACT tool is crucial. In order to have a value of $S_a(T)$ lower than the value which correspond to $S_a(T)_{30yrs}$ for the site of L'Aquila (equal to 0,039g), a possible solution is to proceed by keeping constant the value of the ratio between a_g and $S_a(T)$ computed for those seismic intensity levels for which [NTC, 2008] provide the aforementioned characteristic parameters of the response spectrum. This proposed solution is taken into account for the determination of the EAL in the case of unreinforced fork.

The results of the EAL and the comparison with the results obtained with other methods are shown in Chapter 4.3.2 and Chapter 4.3.4.

4.1.1.3 Simplified structural analysis with DDBD

This research also wanted to investigate also the endorsability of the Displacement-Based Assessment (DBA) methodology applied to RC precast industrial buildings in accordance to what is shown by [Sullivan *et al.*, 2014] as a simpler alternative to the refined PEER PBEE framework. Following this simplified method, the phase of the structural analysis provided within PEER PBEE framework is carried out with the Direct Displacement-Based Design (DDBD) proposed by [Priestley *et al.*, 2007] in which the main assumption is to characterize the multi-storey building as an equivalent SDOF system. For the adopted case study, this first step is neglected because the RC precast building is already assumed as a simplified single column and the DDBD can be directly applied. Subsequent to this first step, it is necessary to identify the limit states of interest (or of some specific damage states of interest) on which it is possible to develop the DBA procedure for determining the input values for PACT (PGA, $S_a(T)$, interstorey drift, peak floor velocity, peak floor acceleration…).

By using several hypotheses on the selection of the limit states of interest, it is noted how this step has fundamental importance and can strongly characterize the final result in terms of EAL, typically expressed in €/year (or $/year). This aspect appears to be one of the biggest issue detected during the implementation of the DBA method: basically, the selection of the limit states affects the discretization of the EAL curve in the MAFE-Direct Loss graph, see Figure 4.15. An increase in the number of points for which the curve is discretized corresponds to an increase in the precision of the final assessment of the EAL as determined through the IDA (see Chapter

4.1.1.1), in contrast, a reduced number of points that discretize the real curve may lead to an excessive approximation of the real MAFE-Direct Loss curve in Figure 4.15 with a consequent considerable difference of the final value of EAL.

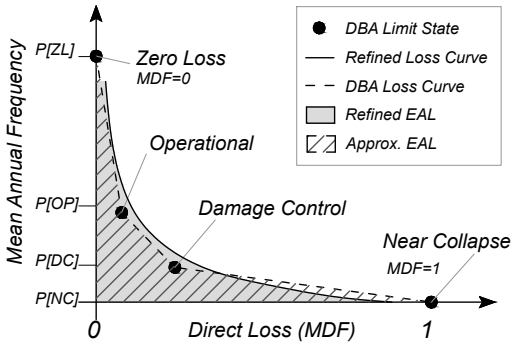

Figure 4.15 Comparison of the curves of the Expected Annul Loss built in a continuously way and discretized with four points which identify the 4 limit states, from [Welch et al., 2012].

As it is seen from the comparison of the results obtained by performing various analyses, a correct estimation of the EAL can be achieved by choosing the limit states in correspondence with the damage states (DS1, DS2, DS3, DS4, …) chosen for those vulnerable elements for which the fragility curves are constructed and the EALs are computed. This means that the choice of the limit states should be made by assuming the values of EDPs (interstorey drift, PGA, peak ground velocity, peak ground acceleration…) that identify the different damage states of all those damageable elements which contribute to the assessment of monetary losses.

In the present research, the study of the application of the DBA method is carried out considering the fem model with reinforced fork, for which it is possible to guarantee the structural collapse mechanism based on the formation of the plastic hinge at the base of the column. This aspect is much more restrictive than what is seen with the application of the simplified method based on the use of SPO2IDA tool (see Chapter 4.1.1.2). Furthermore, within the DBA procedure, it is necessary to ensure the development of a specific mechanism of collapse of the real structure which is not always determined "a priori", especially as in the case of precast RC buildings characterized by different types of structural vulnerabilities (Chapter 3).

As previously mentioned, another critical issue detectable during the application of the DBA procedure is linked to how to carry out the initial choice of the limit states and that it must be done as a function of those determined values of the interstorey drift (or other EDPs) for which a proper level of damage of the vulnerable elements is expected (structural and non-structural). The fact of having to make a correlation

between a certain value of the interstorey drift and the damage experienced by any vulnerable element, one consequence that is observed is that this involves a strong limitation in the predictability of the damage states for those elements whose fragility curves are expressed in terms of others EDPs (peak floor velocity, peak floor acceleration, PGA …). Given the pushover curve expressed as a shear-interstorey drift relationship, for those vulnerable elements, whose fragility curves are expressed with a different EDP instead of the interstorey drift, the damage state can be checked only at the end of the DBA process, i.e. just when all values of the EDPs for each interstorey drift (initially imposed and linked to them) are derived. Therefore, to obtain a correct relationship between the selected limit state and the value of the interstorey drift, it is necessary to proceed with several attempts in the selection of the initial values of interstorey, until the final values of the EDP of interest corresponds to the limit state that one wants to describe.

The assessment of the EAL with the DBA method is herein carried out with four main points that identify the limit states corresponding to the following damage states of the adopted vulnerable elements:

- LS-1: total absence of the damage for each of the vulnerable element taken into account in the computation of the EAL; the interstorey drift at the top of the column is equal to 0,0007rad;
- LS-2: limit state for which the following damage states levels are reached: DS-1 for the strip windows and a DS-2 regarding the caulking of the cladding system; the interstorey drift at the top of the column is equal to 0,001rad;
- LS-3: limit state in which almost all vulnerable elements reached the DS-2 damage state level; the interstorey drift at the top of the column is equal to 0,003rad;
- LS-4: limit state in which almost all vulnerable elements reached the last damage state level (DS-3 or DS-4); the interstorey drift at the top of the column is equal to 0,01rad.

A representation of these damage states on the pushover curve is shown in Figure 4.16, while the intermediate steps of the DDBD for each of the aforementioned selected limit states are carried out in accordance to the prescriptions shown by [Priestley *et al.*, 2007] and [Sullivan *et al.*, 2014] and they are reported in Table 4.4. Some notes must be specified concerning the calculation of these individual steps and the assumptions.

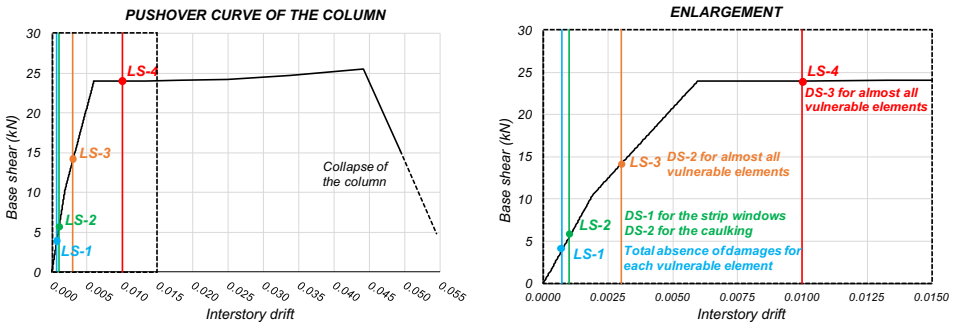

Figure 4.16 Pushover curve of the column adopted within the DBA procedure in order to define the structural capacity and identification of the four points corresponding to the selected limit states.

The determination of the effective first period of vibration is done by assuming the stiffness k equal to the slope of the line between the origin point of the graph and the first yielding point identified in correspondence of an interstorey drift value equal to 0,00594rad (i.e. Δ_y = 0,0494m if a total height of the column equal to 8,3m is assumed) and a value of the base shear (V_y) equal to 24kN. Assuming an effective seismic mass at the top of the column equal to 26338,25kg, estimated by taking into consideration the portion of the roof acting on a single central column of the case study shown in Figure 2.1, the obtained value of the initial period of vibration is T_i = 1,46s.

For completeness, it is specified that the formulas used to calculate the ductility demand, μ, equivalent viscous damping, ξ and the spectral-scaling factor, η, are the same proposed by [Sullivan *et al.*, 2014], [Welch *et al.*, 2014] and [Priestley *et al.*, 2007] and reported in Eq. 4.3, Eq. 4.4 and Eq. 4.5.

$$\mu = \frac{\left(\frac{T_{EFF}}{T_i}\right)^2 (1-r)}{\left(1-r\left(\frac{T_{EFF}}{T_i}\right)\right)} \qquad \text{Eq. 4.3}$$

$$\xi = 0{,}05 + C\left(\frac{\mu_i - 1}{\mu_i \cdot \pi}\right) \qquad \text{Eq. 4.4}$$

$$\eta = \sqrt{\frac{0{,}1}{0{,}05+\xi}} \qquad \text{Eq. 4.5}$$

where r is the post-yield stiffness ratio assumed equal to 0,001 that characterizes the pushover curve, C is a coefficient dependant on the hysteresis rule and adopted equal to 0,565.

Table 4.4 Intermediate step of the DBA procedure applied for four limit states.

Limit State	θ (rad)	$S_{D,\,INEL}$ (m)	V (kN)	k_{EFF} (kN/m)	T_{EFF} (s)	μ	ξ	η^*	$S_{D,\,EL}$ (m)	θ_{EL} (rad)	$S_{A,\,EL}$ (T_{EFF}) (g)
LS-1	0,0007	0,0058	2,82	485,50	1,46	1,00	0,05	1,00	0,0058	0,0007	0,0109
LS-2	0,0010	0,0083	4,03	485,50	1,46	1,00	0,05	1,00	0,0083	0,0010	0,0156
LS-3	0,0030	0,0249	12,09	485,50	1,46	1,00	0,05	1,00	0,0249	0,0030	0,0468
LS-4	0,0100	0,0830	24,00	289,16	1,90	1,68	0,12	0,76	0,1091	0,0132	0,1221

**Determined with Eq. 2.9 from [Priestley et al., 2007]*

The parameters obtained through the DBA method for the two models analysed (two different solutions of the fitting of the hazard curve) are reported in Table 4.5, in which it can be noted that the only difference in terms of input data for PACT is given by the different values of MAFE.

Table 4.5 Output data values obtained with DBA method and directly implemented as input in PACT.

Limit State	θ (rad)	β_{SD}	PGA (g)	$S_a(T_1)$ (g)	$a_{g,\,top}$ (g)	β_{FA}	MAFE* hyp (b)	MAFE** hyp (c)
LS-1	0,0007	0,292	0,0256	0,0109	0,03272	0,430	0,03333	0,09527
LS-2	0,0010	0,292	0,0364	0,0156	0,04640	0,430	0,03333	0,07968
LS-3	0,0030	0,292	0,1062	0,0468	0,13160	0,430	0,02022	0,02384
LS-4	0,0100	0,391	0,2956	0,1583	0,33289	0,472	0,00163	0,00227

** constant value of MAFE for all of T_R lower than 30yrs, see hypothesis b) in § 4.2.2.*
*** MAFE curve fitted according to the hypothesis c) in § 4.2.2.*

For the assessment of EAL, the following assumptions are adopted within PACT in order to be consistent with the choice to perform the calculation of EAL in the simplest possible way:

- regarding the structural collapse, in accordance with a simplified procedure for the assessment of EAL and therefore in order to obtain a considerable saving of time, the value of $S_a(T)_{COLLAPSE}$ previously obtained with the SPO2IDA tool (see Chapter 4.1.1.2) and equal to 0,7575g is assumed (since this is the simplest and fastest way to get $S_a(T)_{COLLAPSE}$), as well as the dispersion, $\beta_{COLLAPSE}$, adopted equal to 0,6, as suggested by [FEMA P-58, 2012b] in *§ 6.3 - Simplified Nonlinear Analysis*;
- the values of the acceleration at the top of the column is evaluated according to that exposed in Chapter 4.1.1.2;
- within PACT software, the selected analysis-type option is the *"Simplified (Linear)"*;
- the computation of the residual interstorey drift is neglected.

To remain consistent with the choice to proceed in the assessment of EAL in a simplified way, the evaluation of the dispersions linked to the interstorey drift, β_{SD}, and the floor acceleration, β_{FA}, is made in accordance with the suggestions provided by [FEMA P-58, 2012b] in *§ 5.3.2 - Simplified Analysis Procedure*, in which these formulations are proposed:

$$\beta_{SD} = \sqrt{\left(\beta_{a\Delta}^2 + \beta_m^2\right)} \quad \text{for interstory drift}$$
$$\beta_{FA} = \sqrt{\left(\beta_{aa}^2 + \beta_m^2\right)} \quad \text{for acceleration} \qquad \textit{Eq. 4.6}$$
$$\beta_{FV} = \sqrt{\left(\beta_{av}^2 + \beta_m^2\right)} \quad \text{for velocity}$$

where $\beta_{a\Delta}$, β_{aa}, β_{av} and β_m are the dispersions provided by [FEMA P-58, 2012b] and shown in Table 4.8 and expressed as a function of the period of vibration linked to the first mode of shape, T_1, and the value of $S=(S_a(T_1)\cdot W)/V_{y1}$. This last term, S, is a function of: the spectral acceleration at the first period of vibration obtained from the DDBD procedure, $S_a(T_1)$; the weight assumed at the top of the column, W; and the value of the shear at the base for which the first yield strength is achieved, V_{y1}.

In the current research, the enforceability of the DBA methodology to RC precast industrial buildings is also investigated for nine new limit states. The choice of nine limit states is done in order to make a direct comparison to what has been achieved with IDA performed on nine different seismic intensity levels (see Chapter 4.1.1.1). Coherently to this reason, the selection of these limit states within DDBD is made by assuming the same value of $S_a(T_1)$ to that given within IDA at each intensity measure. Since within DDBD the $S_a(T_1)$ is available only at the last step, matching of values was possible to get only through an iterative process.

The intermediate steps of the DDBD performed for nine limit states and the results are reported in Table 4.6 and Table 4.7 respectively.

EAL are then assessed with PACT and results and comparisons are shown in Chapter 4.3.3. As can be seen, the choice of the number of points that discretize the MAFE-Direct Loss curve in Figure 4.15 can influence the value of EDPs and then the final result of EAL. An increase in the number of points which discretize the MAFE-Direct Loss curve leads to a more accurate EAL result. However, using fewer number of points to fit the real MAFE-Direct Loss curve leads to a not so accurate EAL result, which can be acceptable if the computational time saved compared to the refined method is taken into account.

Table 4.6 Intermediate step of the DBA procedure applied for nine limit states.

Limit State	θ (rad)	$S_{D,\,INEL}$ (m)	V (kN)	k_{EFF} (kN/m)	T_{EFF} (s)	μ	ξ	η^*	$S_{D,\,EL}$ (m)	θ_{EL} (rad)	$S_{A,\,EL}$ (T_{EFF}) (g)
LS-1	0,00220	0,0183	8,87	485,50	1,46	1,00	0,05	1,00	0,0183	0,0022	0,0343
LS-2	0,00300	0,0249	12,09	485,50	1,46	1,00	0,05	1,00	0,0249	0,0030	0,0468
LS-3	0,00350	0,0291	14,10	485,50	1,46	1,00	0,05	1,00	0,0290	0,0035	0,0546
LS-4	0,00425	0,0353	17,13	485,50	1,46	1,00	0,05	1,00	0,0353	0,0043	0,0663
LS-5	0,00510	0,0423	20,55	485,50	1,46	1,00	0,05	1,00	0,0423	0,0051	0,0796
LS-6	0,00610	0,0506	24,00	474,03	1,48	1,02	0,05	0,98	0,0517	0,0062	0,0949
LS-7	0,00920	0,0764	24,00	314,30	1,82	1,54	0,11	0,78	0,0976	0,0118	0,1188
LS-8	0,01450	0,1204	24,00	199,42	2,28	2,44	0,16	0,70	0,1728	0,0208	0,1334
LS-9	0,02700	0,2241	24,10	107,54	3,11	4,53	0,19	0,65	0,3473	0,0418	0,1446

**Determined with Eq. 2.9 from [Priestley et al., 2007]*

Table 4.7 Output data values obtained with DBA method and directly implemented as input in PACT.

Limit State	θ (rad)	β_{SD}	PGA (g)	$S_a(T_1)$ (g)	$a_{g,\,top}$ (g)	β_{FA}	MAFE* hyp (b)
LS-1	0,00220	0,292	0,07944	0,03432	0,09954	0,430	0,03333
LS-2	0,00300	0,292	0,10528	0,04680	0,13051	0,430	0,02022
LS-3	0,00350	0,292	0,12057	0,05460	0,14846	0,430	0,01470
LS-4	0,00425	0,292	0,14221	0,06630	0,17335	0,430	0,00984
LS-5	0,00510	0,292	0,16482	0,07956	0,19864	0,430	0,00675
LS-6	0,00610	0,292	0,18963	0,09601	0,22533	0,430	0,00458
LS-7	0,00920	0,391	0,25977	0,14765	0,29525	0,472	0,00188
LS-8	0,01450	0,430	0,33346	0,20812	0,35977	0,515	0,00092
LS-9	0,02700	0,484	0,44733	0,30721	0,44315	0,541	0,00041

** constant value of MAFE for all of T_R lower than 30yrs, see hypothesis b) in § 4.2.2.*

By comparing the results in terms of interstorey drift, PGA, top column acceleration and dispersions obtained through IDA and DBA methodology and shown in Figure 4.17, it can be affirmed that:

1. the imposed interstorey drift at the beginning of the DBA procedure, have been chosen with care in order to have values close to that obtained with IDA;
2. top column accelerations calculated with the simplified formula proposed within the [FEMA P-58, 2012b] in *§ 5.3.2 - Simplified Analysis Procedure* greatly overestimate the values of the same EDP obtained by IDA;

3. dispersions assessed using simplified formula proposed by [FEMA P-58, 2012b] and reported in Eq. 4.6 can be accepted as approximate values of the IDA results as long as the latter are assessed considering the modelling dispersion of the structure (β_m, see Chapter 4.1.3) as represented in Figure 4.17 with orange line.

In conclusion, the value of monetary losses may be very different from that obtained with refined IDA procedure, when within the evaluation of EAL, the main part of losses is given by the damages suffered by all of those vulnerable elements whose fragility curves have the top column acceleration as EDP. Conversely, in absence of damageable elements sensitive to the top column acceleration, a significant difference of EAL will not occur because the slight difference of interstorey drift values obtained through DBA and IDA. [FEMA P-58, 2012b] formulas can however be adopted to assess the accelerations but at the same time this allows to accept that a significant approximation is made and that the EAL may be affected if there are damageable elements sensitive to accelerations within the assessment of the monetary losses.

The results in terms of EAL obtained with the DBA method and the comparison of the results achieved with other methods are shown in Chapters 4.3.3 and 4.3.4 respectively.

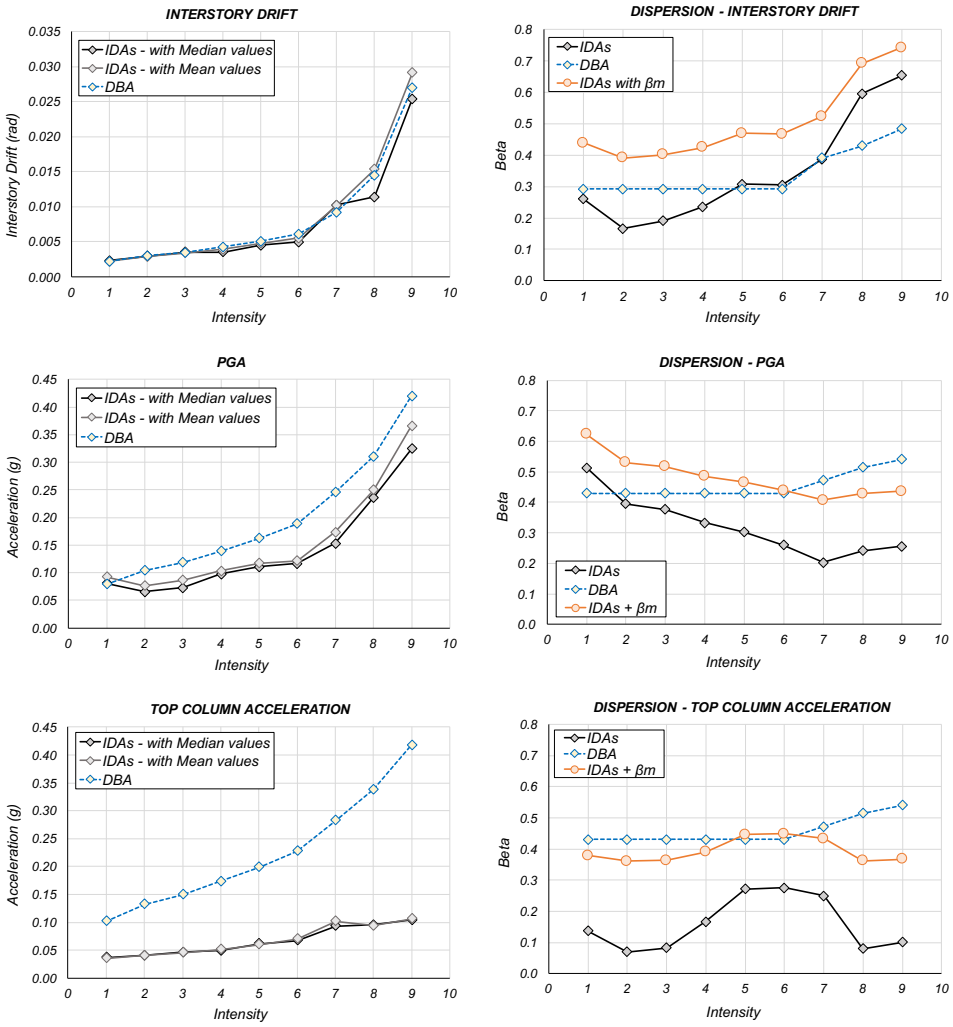

Figure 4.17 Comparison of results in terms of interstorey drift, PGA, top column acceleration and dispersions linked to them obtained through IDA and DBA methodology.

Table 4.8 Values of the dispersion $\beta_{a\Delta}$, β_{aa}, β_{av} and β_m as a function of S and T_1 (Table 5-6, [FEMA P-58, 2012b].

T_1 (s)	$S = S_a(T_1)\,W / V_{y1}$	$\beta_{a\Delta}$	β_{aa}	β_{av}	β_m
0,20	≤ 1,0	0,05	0,10	0,50	0,25
	2	0,35	0,10	0,51	0,25
	4	0,40	0,10	0,40	0,35
	6	0,45	0,10	0,37	0,50
	≥ 8	0,45	0,05	0,24	0,50
0,35	≤ 1,0	0,10	0,15	0,32	0,25
	2	0,35	0,15	0,38	0,25
	4	0,40	0,15	0,43	0,35
	6	0,45	0,15	0,38	0,50
	≥ 8	0,45	0,15	0,34	0,50
0,50	≤ 1,0	0,10	0,20	0,31	0,25
	2	0,35	0,20	0,35	0,25
	4	0,40	0,20	0,41	0,35
	6	0,45	0,20	0,36	0,50
	≥ 8	0,45	0,20	0,32	0,50
0,75	≤ 1,0	0,10	0,25	0,30	0,25
	2	0,35	0,25	0,33	0,25
	4	0,40	0,25	0,39	0,35
	6	0,45	0,25	0,35	0,50
	≥ 8	0,45	0,25	0,30	0,50
1,00	≤ 1,0	0,15	0,30	0,27	0,25
	2	0,35	0,30	0,29	0,25
	4	0,40	0,30	0,37	0,35
	6	0,45	0,30	0,36	0,50
	≥ 8	0,45	0,25	0,34	0,50
1,50	≤ 1,0	0,15	0,35	0,25	0,25
	2	0,35	0,35	0,26	0,25
	4	0,40	0,30	0,33	0,35
	6	0,45	0,30	0,34	0,50
	≥ 8	0,45	0,25	0,33	0,50
≥ 2,00	≤ 1,0	0,25	0,50	0,50	0,25
	2	0,35	0,45	0,45	0,25
	4	0,40	0,45	0,45	0,35
	6	0,45	0,40	0,40	0,50
	≥ 8	0,45	0,35	0,35	0,50

4.1.2 *Retrofit measure on the top column forks*

One of the main advantages in the use of PEER PBEE methodology is the fact that it can be employed as a useful tool for engineers in the assessment of possible seismic improvements and/or retrofit measures on existing buildings, according to the will and the opinion of the stakeholders.

As discussed in Chapter 3, there are many different vulnerabilities in the most common single-storey precast RC industrial buildings spread on the Italian territory. For this reason, the possible detectable vulnerabilities are identified and classified; for each of them, the monetary cost necessary for the execution of the retrofit measures is defined, according to what is provided by [Protezione Civile *et al.*, 2012]. In Table 3.1, a brief reference to the elements of interest is reported.

Table 4.9 List of possible retrofit measures for the inhibition of the main local vulnerabilities in one-storey precast RC industrial buildings, from [Protezione Civile et al., 2012].

Description of the main retrofit measure	***€ / unit***
Confinement at the base of the column with RC jacketing	*398,79*
Confinement at the base of the column with HPFRC jacketing	*281,57*
Beam-to-column connection with steel dowel and improvement of the stiffness of the RC forks by providing a steel beam (UPN 200) at each side	*313,32*
Beam-to-column connection by means of steel dowel	*88,00*
Beam-to-roof element connection by steel wires connected at the base of the roof elements	*117,03*
Insertion of connectors made with bolted steel elements	*106,09*
Connection of the horizontal cladding panels by steel wires (price for panel installed)	*214,65*
Insertion of steel wires for the prevention of the out-of-plane falling of the horizontal cladding panels	*147,00*
Connection between vertical cladding panels by means of steel wires (price for panel installed)	*192,65*
Connection between vertical cladding panels using steel brackets	*299,20*

The influence of a retrofit measure on an existing industrial building in terms of variation of the value of EAL is investigated in the current research. For achieving the aforementioned investigation and to test this kind of application for precast RC industrial buildings, the execution of a reinforcing seismic retrofit measure on the fork at the top of the column is take into account. The hypothesized retrofit intervention is based on the installation of two UPN 200 steel profiles at each side of the fork at the top of the column. These two profiles are equipped with an appropriate slotted hole in the highest part, to allow the accommodation of the steel pin, in order to guarantee a hinged constraint in the beam-to-column connection. By

the introduction of these lateral elements, the premature and not desired failure of the fork is then inhibited (inhibition of a partial collapse). Therefore, in the new configuration, the collapse is governed by the development of the plastic hinge at the base of the column.

A fem model able to consider this retrofit measure is carried out by providing a column in which the previous fork elements now replaced by an elastic element having an equivalent stiffness computed by the contribution of both the fork and steel profiles stiffness. In this way, the collapse is estimated at the ultimate capacity of the base section of the column (Figure 4.18).

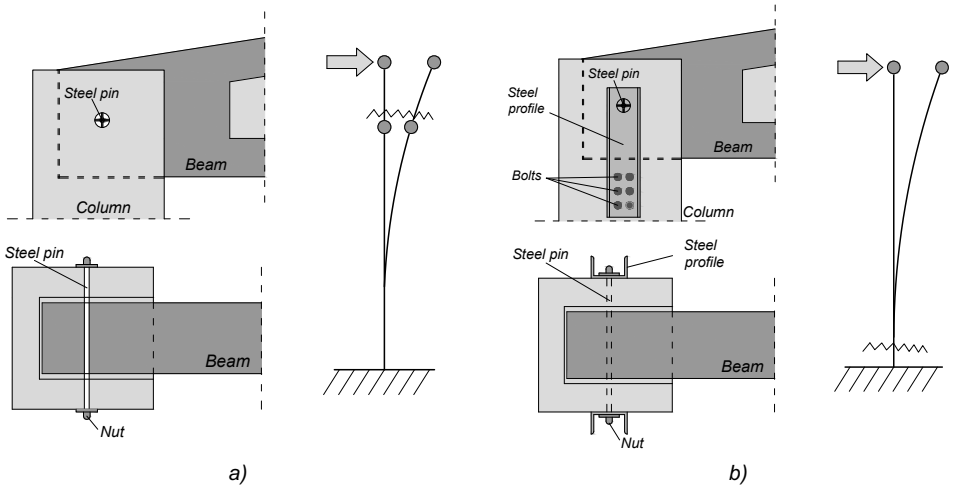

Figure 4.18 a) Structural model with the unreinforced fork; b) structural model with the reinforced fork with two lateral UPN 200 steel profiles.

By performing the IDAs for this new structural configuration, only one case of collapse is observed when the value of the ultimate curvature at the base section of the column is exceeded. Due to the high strength of the precast columns, the number of the collapses that occurred linked to the IDAs performed on the retrofitted structure do not allow correct estimation of the $S_a(T)_{COLLAPSE}$ and the related dispersion, $\beta_{COLLAPSE}$ (the maximum mean spectral acceleration assessed at the first period of vibration, $S_a(T_1 = 1{,}33s)$, on the accelerograms provided by [INGV, 1999] and associated to a T_R = 2475yrs for the site of L'Aquila is equal to 0,32g). To overcome this difficulty especially related to the high-resistance structures, as the precast RC buildings, new IDAs are made using the accelerograms provided for the maximum return period, T_R = 2475yrs, but scaled for having a gradually increasing values of $S_a(T_1)$, assumed to be equal to: 0,05g, 0,15g, 0,25g, 0,45g, 0,51g, 0,76g, 0,91g and 1,15g. Even though the result obtained is approximated, since the use of scaled

accelerograms, it is possible to have a reference indication for the new value of the collapse capacity of the column. With this arrangement, a greater number of collapses are reached for an increasing seismic intensity (see Table 4.10 and Figure 4.19). The results of the $S_a(T)_{COLLAPSE}$ and $\beta_{COLLAPSE}$ are determined as before using the "*Collapse Fragility Tool*" provided within [FEMA P-58, 2012a]. The values are equal to 0,54g and 0,36 respectively.

Table 4.10 Values of the $S_a(T)$ assumed for performing the IDA and number of collapses reached for each intensity in the case of reinforced fork with two lateral UPN 200 steel profiles.

Fork modelled with a single element		
$S_a(T)$ (g)	Number of analysis	Number of collapses
0,0500	10	0
0,1500	10	0
0,2500	10	0
0,4500	10	4
0,5118	10	4
0,7575	10	8
0,9000	10	9
1,1475	10	10

At the end of the IDAs phase, once the values of the EDPs of interest are known, it is possible to proceed with the evaluation of the EAL through PACT software. The numeric results as well as the comparisons between different modelling solutions adopted are shown in Chapter 4.3.

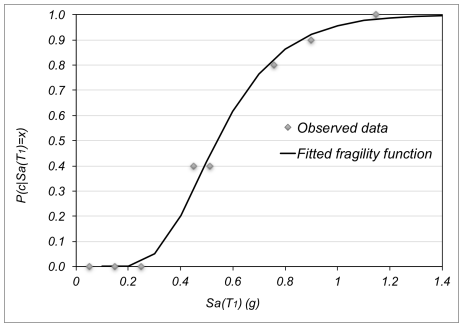

Figure 4.19 Results are obtained according to the "Collapse Fragility Tool" provided by [FEMA P-58, 2012a]. Fitting of the collapse fragility curve in the case of reinforced fork with two lateral UPN 200 steel profiles.

Here, an important mention about how to consider the monetary amount of the cost due to the retrofit measure within the PEER PBEE framework should be done. The possible ways that can be pursued are two. A first mode would be to provide the monetary amount of the retrofit measure as an additional share of the total cost of construction of the building, given the fact that the latter value is required as an initial

data within PACT. A second mode is based by computing within the PACT the monetary amount of the retrofit measure as the average value of the cost linked to the first damage state, DS1, of the UPN 200 steel profile adopted. This solution can be pursued by setting a very low value of the EDP for the DS1, by doing so, the activation of this cost is obtained for each of the intensity measure (Figure 4.20), even at low intensities. This second way is adopted in the current research for carrying out the analysis and the later comparisons of the results.

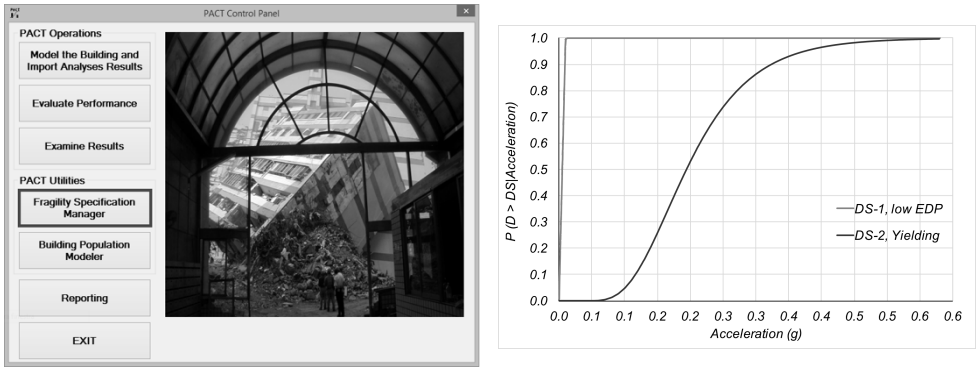

Figure 4.20 a) Screenshot of the PACT software for the access to the "Fragility Specification Manager" tool; b) creation of the fragility curves for the two damage states DS1 and DS2 of the UPN 200 steel profile.

4.1.3 Modelling dispersion, β_m

In order to perform the assessment of the EAL with PACT software provided within [FEMA P-58, 2012a], one of the inputs required is the modelling dispersion, β_m. Such input entry is provided within the program for considering the uncertainty and/or imprecisions and/or lacks linked to the assumptions made during the modelling phase of the facility, as for example the choice which falls back on the type of finite element assumed (*truss, beam, wall, spring, …*) or the damping and the seismic masses considered. The evaluation of β_m is made specifically considering the uncertainty associated with the level of the building and the quality which it was made, β_c, and the uncertainty linked to the quality and the level of completeness of the model adopted for performing the non-linear analyses, β_q. According to the *§ 5.2.5 - Uncertainty* of the [FEMA P-58, 2012b], with particular reference to the expression *5-1*, the total modelling dispersion, β_m, can be estimated as $\beta_m = \sqrt{(\beta_c^2 + \beta_q^2)}$. The β_c and β_q dispersions are assumed according to the Table 4.11 and the Table 4.12 respectively. An average level in both the cognitive and production quality of the

building, and in the quality of the realization of the finite element model are assumed, then, β_c and β_q are chosen with a value of 0,25.

Table 4.11 Dispersion associated to the level in the definition of the building and the reliability concerning to the quality with which the same has been realized, β_c (Table 5-1 [FEMA P-58, 2012b]).

Building definition and Construction Quality Assurance	β_c
Superior Quality, New Buildings: The building is completely designed and will be constructed with rigorous construction quality assurance, including special inspection, materials testing, and structural observation. *Superior Quality, Existing Buildings: Drawings and specifications are available and field investigation confirms they are representative of the actual construction, or if not, the actual construction is understood. Material properties are confirmed by extensive materials testing.*	*0,10*
Average Quality, New Buildings: The building design is completed to a level typical of design development; construction quality assurance and inspection are anticipated to be of limited quality. *Average Quality, Existing Buildings: Documents defining the building design are available and are confirmed by visual observation. Material properties are confirmed by limited materials testing.*	*0,25*
Limited Quality, New Buildings: The building design is completed to a level typical of schematic design; or other similar level of detail. *Limited Quality, Existing Buildings: Construction documents are not available and knowledge of the structure is based on limited field investigation. Material properties are based on default values typical for buildings of the type, location, and age of construction.*	*0,40*

The obtained value of β_m is equal to $\beta_m = \sqrt{(0{,}25^2 + 0{,}25^2)} = 0{,}3536$. As an alternative of this value, in order to see how a variation of only this input can affect the final result in terms of EAL, the assessment of the EAL is made for the same building model but taking into account a limited quality in the building definition and construction quality assurance, the modelling dispersion is assumed equal to $\beta_m = \sqrt{(0{,}40^2 + 0{,}25^2)} = 0{,}4717$. In Chapter 4.3, the results obtained considering different assumptions in the input value for PACT are shown, and some comments are made.

It is worth noting that the dispersions provided by [FEMA P-58, 2012b] and here shown in Table 4.11 and Table 4.12 are proposed by the same standard with validity to buildings built on American territory. In future research, it would make sense to make a dedicated parametric study in relation to the Italian context in order to determine whether the values in the aforementioned tables are good to be used or not in a conservatively way also for Italian RC precast industrial buildings.

Table 4.12 Dispersion associated to quality of the adopted analytical model, β_q (Table 5-2 [FEMA P-58, 2012b]).

Quality and Completeness of the Analytical Model	β_q
Superior Quality: The numerical model is robust over the anticipated range of response. Strength and stiffness deterioration and all likely failure modes are explicitly modelled. Model accuracy is established with data from large-scale component test through failure. Completeness: The mathematical model includes all structural components and non-structural components in the building that contribute to strength or stiffness.	0,10
Average Quality: The numerical model for each component is robust over the anticipated range of displacement or deformation response. Strength and stiffness deterioration is fairly well represented, though some failure modes are simulated indirectly. Accuracy is established through a combination of judgment and large-scale component tests. Completeness: The mathematical model includes most structural components and non-structural components in the building that contribute significant strength or stiffness.	0,25
Limited Quality: The numerical model for each component is based on idealized cyclic envelope curves from ASCE/SEI 41-06 or comparable guidelines, where strength and stiffness deterioration and failure modes are not directly incorporated in the model. Completeness: The mathematical model includes structural components in the seismic-force-resisting system.	0,40

4.1.4 Damageable elements

For the assessment of the EAL, in the present research the monetary losses are evaluated by taking into account the damage suffered by:

- the base of the column due to the development of a plastic hinge;
- the precast cladding panels mainly due to the out-of-plane (acceleration as the reference EDP) and the in-plane failure (interstorey drift as the reference EDP);
- the strip windows (for cost and repair time [Hunt and Stojadinovic, 2010]);
- the caulking on the perimeter of the windows and between the cladding panels (for cost and repair time [Hunt and Stojadinovic, 2010]).

Obviously, these vulnerable elements are taken as an example for studying the applicability of the PEER PBEE procedure to precast RC industrial buildings. Figure 4.21 shows by way of example the fragility curves provided by [Hunt and Stojadinovic, 2010] regarding the caulking in cladding system and the strip windows successively adopted in PACT. In Table 4.13 and Table 4.14 the mean and standard deviation for different damage state are reported.

Table 4.13 Damage states for caulking in cladding system, from [Hunt and Stojadinovic, 2010].

Damage State	**Description**	**λ (rad)**	**β**
DS-0	Initial cracking	0,0048	0,15
DS-1	Failure	0,0096	0,25

Table 4.14 Damage states for strip windows, from [Hunt and Stojadinovic, 2010].

Damage State	Description	λ (rad)	β
DS-0	Glass pane contact and small cracking at perimeter	0,006	0,12
DS-1	Glass translational and gasket pull-out	0,011	0,20
DS-2	Observable cracking in glass	0,016	0,19
DS-3	Major cracking and glass fallout	0,020	0,16

According to [Hunt and Stojadinovic, 2010], the repair procedures necessary for each damage state of the caulking in the cladding system and strip windows are shown in the Table 4.15.

Table 4.15 Elements required for the repair operations at each limit state, as regards to the interstorey drift sensitive elements: caulking in cladding system and strip windows. From [Hunt and Stojadinovic, 2010].

Damage State	Repair Item	Quantity
DS1	Glass pane contact	
	Provide rigging/staging to access caulking (EA)	1
	Remove and replace caulking in cladding (LF)	25% of caulking length
DS2	Caulking failure	
	Provide rigging/staging to access caulking (EA)	1
	Remove and replace caulking in cladding (LF)	25% of caulking length
	Deglaze and reposition window (EA)	5% of windows
	Replace gaskets for repositioned windows (LF)	5% of gasket length
DS3	Glass translation and gasket pull-out	
	Provide rigging/staging to access caulking (EA)	1.5
	Remove and replace caulking in cladding (LF)	50% of caulking length
	Deglaze and reposition window (EA)	10% of windows
	Replace gaskets for repositioned windows (LF)	10% of gasket length
	Replace gaskets that have become dislodged (LF)	10% of gasket length
DS4	Observable cracking in glass	
	Provide rigging/staging to access caulking (EA)	1.5
	Remove and replace caulking in cladding (LF)	50% of caulking length
	Deglaze and reposition window (EA)	20% of windows
	Remove and replace window (EA)	20% of windows
	Replace gaskets for repositioned windows (LF)	20% of gasket length
	Replace gaskets that have become dislodged (LF)	15% of gasket length
DS5	Major cracking and glass fallout	
	Provide rigging/staging to access caulking (EA)	2
	Remove and replace caulking in cladding (LF)	75% of caulking length
	Deglaze and reposition window (EA)	30% of windows
	Remove and replace window (EA)	40% of windows
	Replace gaskets for repositioned windows (LF)	30% of gasket length
	Replace gaskets that have become dislodged (LF)	20% of gasket length
DS∞	Complete replacement of all components	
	Provide rigging/staging to access caulking (EA)	2
	Remove and replace caulking in cladding (LF)	100% of caulking length
	Deglaze and reposition window (EA)	30% of windows
	Remove and replace window (EA)	70% of windows
	Replace gaskets for repositioned windows (LF)	30% of gasket length

The library of the vulnerable elements provided inside PACT (editable with the *"Fragility Specification Manager"* utility) could be expanded as desired with respect to what is done here. So, the professional engineers have the option to provide additional and specific vulnerable elements of interest in order to achieve a better

and accurate assessment of the EAL. Better evaluations may thus be made to get the target agreed with the stakeholders.

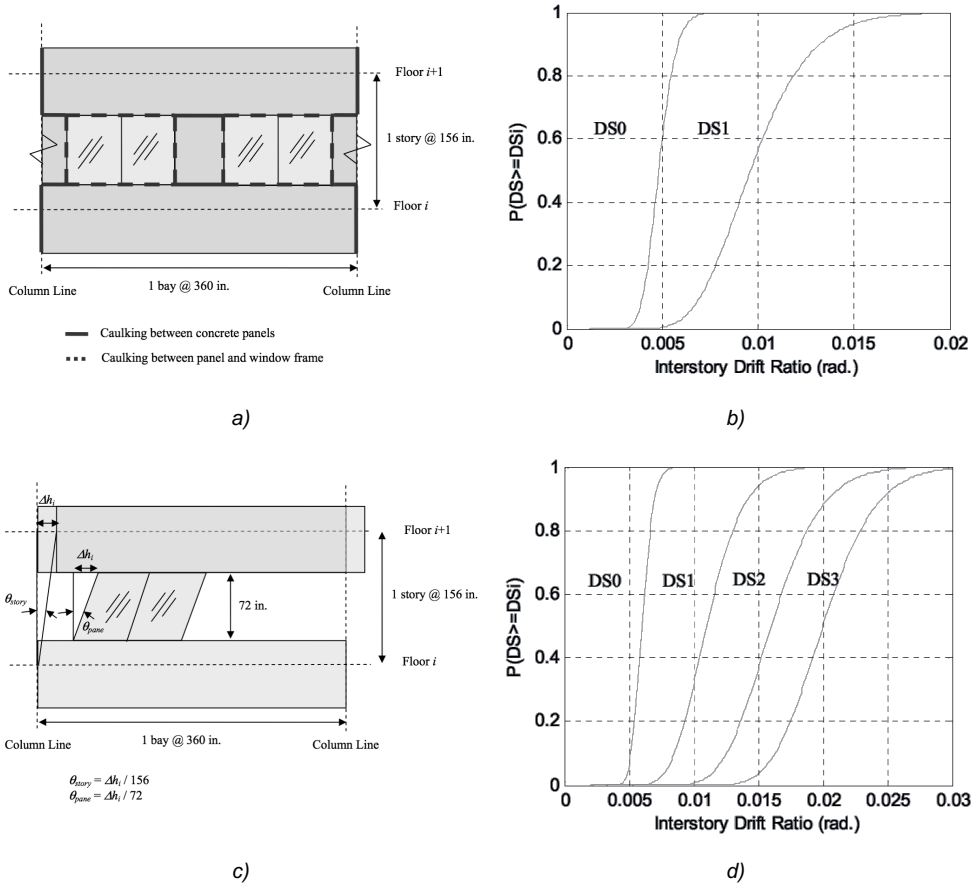

Figure 4.21 a) Identification of the caulking on a typical view of the perimetral facade; b) fragility curves for caulking; c) the rotation suffered by the strip windows is greater than what suffered by the cladding panels: at the same interstorey drift, the height of the strip window is much lower than the interstorey height; d) fragility curves for strip windows. Images and fragility curves from [Hunt and Stojadinovic, 2010].

It is also true, however, that any precast RC industrial building is characterized by its own specifications and it is equipped with special vulnerable elements usually with unique design and for which there is not much information in the literature about their fragility curves.

It is enough to think about the possible different types of systems and internal equipment typically installed in industrial buildings (see Figure 4.22, Figure 4.23 and Figure 4.24).

a) b)

Figure 4.22 Example of non-structural elements installed in industrial facilities: a) control panels of the electrical and network system; b) control panel of a specific machinery without any seismic restraints at its base.

Currently, a large branch of the research in the field of civil engineering is focused on the development and the creation of new fragility curves and researchers are doing a lot of effort in their studies for scheduling different types of non-structural vulnerable elements.

a) b)

Figure 4.23 Example of non-structural elements installed in industrial facilities: a) heater and piping system; b) fan coil units installed in the offices.

a) b)

Figure 4.24 Different lighting systems: a) in the laboratories of the industrial facility; b) in the offices.

In the actual literature, some good indications oriented to prevent damages on non-structural elements in case of earthquake can be found within [FEMA 74-FM, 2005], [FEMA 460, 2005] and [FEMA E-74, 2012]. For those non-structural elements for which there are no data available concerning the fragility curves at each damage state, recommendations and suggestions from the aforementioned standards can be adopted to determine the values of different EDPs analytically and then the fragility curves indispensable to carry out the assessment of EAL. Some EDPs that can be calculated are e.g.: accelerations; minimum force at the centre of gravity that leads to overturning of a not-fixed non-structural element (machineries in Figure 4.22, heating systems only supported on column shelves as shown in Figure 4.23, lighting systems as in Figure 4.24, or not-fixed inner content in general as shelving, racks, storage equipment); interstorey drift for piping systems as shown in Figure 4.23 (a) etc.

In regards to the structural elements, the current research defines in Chapter 6.1 the damage states and assesses the related repair cost for the main structural elements in Italian RC precast industrial buildings as: column, top column fork, beam-to-roof element joint and structure-to-cladding panel connection.

4.2 Considerations about PEER PBEE framework

4.2.1 Residual interstorey drift in PACT

Related to the precast RC industrial buildings, a note should be made about the residual interstorey drift required for the implementation of the PEER PBEE framework in PACT. Unlike the ordinary RC buildings, it is observed that the precast RC buildings are generally characterized by a higher slenderness, flexibility and a lower vertical axial load acting on the columns. For this reason, the adoption of the limit values of residual interstorey drift usually adopted for the ordinary RC structures is not suitable for the precast RC buildings. As can be seen from the results of laboratory tests [Belleri and Riva, 2012] performed on a precast column-to-foundation node in a scale of 1 to 1 (Figure 4.25), the damage at the base section of the column at 1% of residual drift is not such as to justify total reconstruction of the structural element. The economic damage suffered by the structure is very slight, certainly much less than the damage expected to be observed for the non-structural elements for the same level of residual interstorey drift.

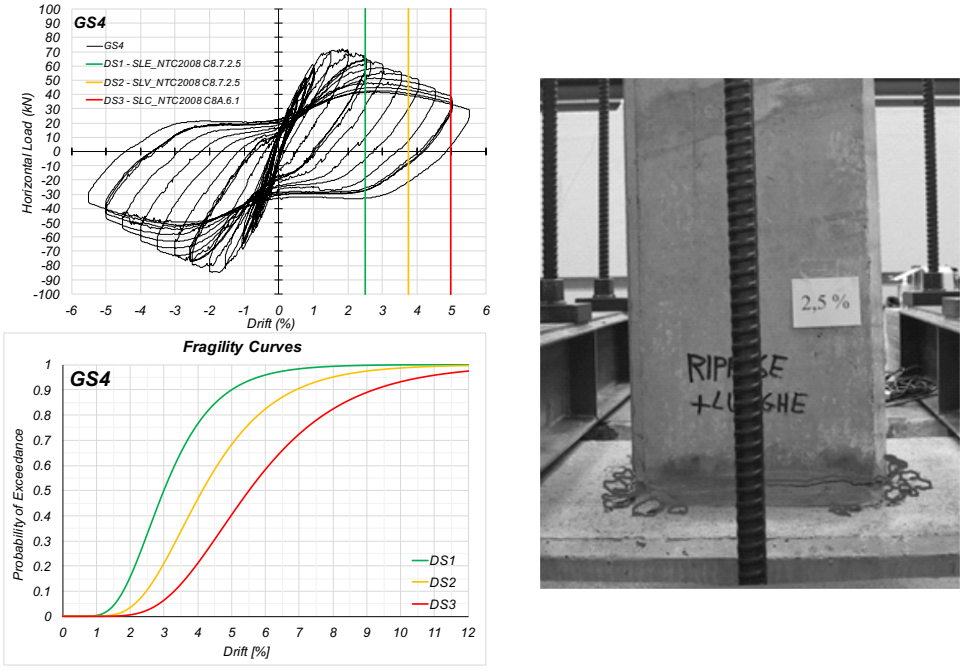

a) b)

Figure 4.25 Laboratory test performed on a precast column-to-foundation node [Belleri and Riva, 2012]: a) results in terms of horizontal load-drift relationship and fragility curves in comparison with the fragility curves of socket foundations; b) damage state for a drift equal to 2,5%.

Nevertheless, the issue of the residual interstorey RC precast industrial building should be further investigated with appropriate analyses focused to evaluate both the resilience level of a damaged structure when a new earthquake happens and the capability of the existing structure hit by an earthquake and characterized by a residual drift of 1% to support the static vertical loads. Most likely, it might be thought that given the low values of the vertical loads acting on the columns of a typical one-storey RC precast industrial building, it is expected that the presence of residual interstorey drift assumed equal to 1% does not affect too much the value of the bending moment at the base of the column and then the damage level of the column itself. Further studies are needed to investigate this issue. Meanwhile, based on what has just been said and looking forward to see more specific studies in this way, the evaluation of EAL linked to the damages assessed from the level of residual interstorey drift can be neglected.

4.2.2 Hazard analysis

Some fundamental things must be taken into account or considered regarding the determination of the hazard curve. It has already been mentioned how some limitations can arise when there is the necessity and the desire to evaluate the monetary losses for low intensities, i.e. for T_R lower than 30yrs.

Currently, the "*Istituto Nazionale di Geofisica e Vulcanologia*" [INGV, 1999] in Italy provides data for the construction of the hazard curve for only 9 levels of seismic intensity, which are expressed by the following values of the return period, T_R: 30, 50, 71, 101, 140, 201, 475, 975 and 2475yrs. When there is the necessity to consider values of the return period below 30 and above 2475yrs respectively, the current standard for construction for the Italian territory [NTC, 2008] does not provide any information regarding the determination of additional points located outside of the domain of the given hazard curve. This means that there are no available values of the MAFE and the related $S_a(T)$ for T_R lower than 30yrs and greater than 2475yrs. However, in the absence of specific data and for low intensities, [INGV, 1999] gives a suggestion to solve this issue. It suggests that the limit value is equal to the rate of occurrence, μ, of the earthquakes at the site of which the MAFE value (λ) constitutes a fraction.

This aspect is of fundamental importance if one wants to proceed in the evaluation of the EAL for low seismic intensities, as in the case of unreinforced fork for which the $S_a(T)_{COLLAPSE}$ was equal to 0,056g. In order to remedy this lack and to be able to

predict the values of MAFE for those seismic intensities outside the domain of the hazard curve, the current research also investigates the variability of the results in terms of EAL for different solutions of the fitting of the hazard curve.

In particular, the following hypothesis for making the fitting of the hazard curve in different ways are take into account and proposed:

a. a straight line in the log-log domain obtained by performing the fitting on all known points of the hazard curve provided by [NTC, 2008], similar to what is suggested by the [SAC-FEMA-350, 2000] procedure and as discussed also by [Dolsek and Fajfar, 2007] and [Fajfar and Dolsek, 2012] (Figure 4.26, a);

b. a straight line in the log-log domain obtained by performing the fitting on all known points of the hazard curve provide by [NTC, 2008] when the assessment of the MAFE for $S_a(T)_{30yrs} < S_a(T) < S_a(T)_{2475yrs}$ is required, whereas for values of $S_a(T) < S_a(T)_{30yrs}$ the values of the MAFE is considered constant and equal to what is determined for a $S_a(T)_{30yrs}$ ($MAFE = \lambda = 1/30 = 0{,}03333$);

c. a portion of parabola built on the first three points of the hazard curve (linked to T_R = 30, 50, 72yrs) for the determination of the values of the MAFE which correspond to $S_a(T) < S_a(T)_{30yrs}$, whereas for $S_a(T)$ between two values provided by [NTC, 2008], the definition of the MAFE is defined by considering the point at the intersection between the outgoing vertical line from the value of $S_a(T)$ assessed for the return period of interest and the straight line that connects the two known points of the hazard curve for which the values of the $S_a(T)$ are known from [NTC, 2008] (Figure 4.26, b).

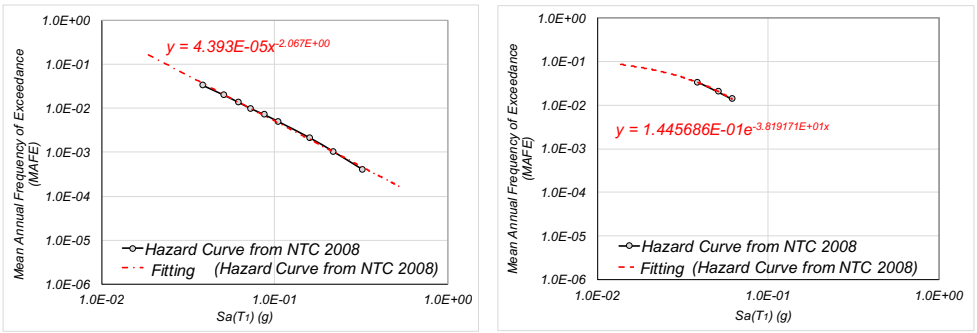

a) b)

Figure 4.26 Hypothesized hazard curve solutions: a) straight line fitted on each point of the existing hazard curve, for each T_R; b) parabola fitted on the first three point of the hazard curve linked to the lower intensities.

The values of the MAFE linked to $S_a(T) < S_a(T)_{30yrs}$ and assessed according to the different hypotheses of fitting of the hazard curve are shown in Table 4.16.

The current research shows how the final value of the EAL (see Chapter 4.3) can be strongly affected by the selection of the values of the MAFE associated to the low intensities. In particular, it is possible to see that the final value of the EAL is more sensitive to the variability of MAFE related to $T_R < 30$yrs rather than the variability of the value of MAFE related to $T_R > 2475$yrs. From this, it is clear how the EAL resulting from the damage suffered by vulnerable elements for low damage states have a greater influence in the calculation of the final value rather than the EAL assessed for high intensities. This aspect is mainly due to the fact that in the computation of the monetary losses for low intensity, a small difference in the values of the MAFE associated with low $S_a(T)$ leads to a high increase in the area under the curve of EAL. The increase of the losses in some cases is so big that it makes the final result of EAL unreliable. As can be observed from the plots shown in Figure 4.27, the position of the point determined by the intersection between the curve of EAL and the vertical axis can greatly influence the final results: a higher value of the point on the vertical axis corresponds to a greater area under the curve of EAL which corresponds to a greater value of the economic losses.

Table 4.16 Values of the MAFE assessed for different solutions of fitting of the hazard curve.

$S_a(T)$ (g)	**Mean Annual Frequency of Exceedance (MAFE)**		
	Type of fitting of the hazard curve		
	Straight line on each point	Straight line on each point with limit	Parabola on the first three points
0,0098	0,623587	0,0333333	0,0994321
0,0196	0,148822	0,0333333	0,0683879
0,0295	0,063920	0,0333333	0,0468569
0,0393	0,035331	0,0333333	0,0323956
0,0491	0,022300	0,0223000	0,0215819
0,0560	0,016992	0,0169920	0,0167750

Following the results obtained in terms of EAL in the case of unreinforced fork (see Chapter 4.3), the best solution for the fitting of the hazard curve is given by the hypothesis *b*, which leads to a value of EAL equal to 16273€/yr, very close to what is obtained with IDA (10185€/yr, see Figure 4.37 and Figure 4.33). However, this difference is mainly due to the dispersion associated to the collapse, $\beta_{COLLAPSE}$, equal to 0,6 when the simplified procedure is adopted (following the suggestion by [FEMA

P-58, 2012b]) and 0,22 in the case of the structural analysis performed with refined method.

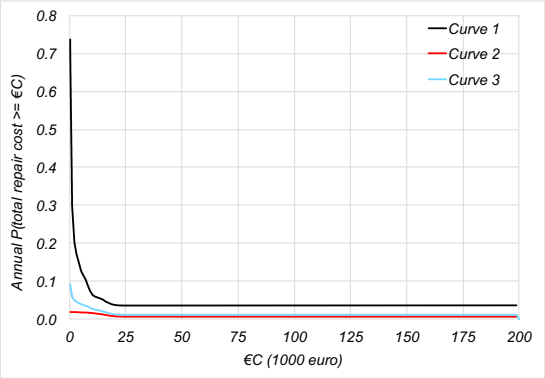

Figure 4.27 Results of the EAL obtained by adopting different hypothesis for the fitting of the hazard curve in the log-log plan: straight line fitted on each point of the existing hazard curve, and then for each T_R (Curve 1); straight line fitted as in the previous case but a limit value of the MAFE = 0,03333 is adopted for all of those intensity measures lower than T_R = 30yrs (Curve 2); parabola fitted on the first three points of the hazard curve linked to the lower intensities, T_R = 30, 50, 72yrs (Curve 3).

4.2.3 Loss analysis and decision variables

The PEER PBEE framework considers different types of Decision Variables (DVs) for the assessment of the EAL, such as:

- casualties and/or injuries; even if the DV is not incisive and dominant for the category of precast RC industrial buildings;
- economic losses and repair costs: e.g. due to the damages suffered by expensive machinery that are installed inside the facility caused by the collapse of the roof elements; are very important DV for the category of precast RC industrial buildings;
- downtimes or delays of the production chain due to the restoration of the security of the facility and for allowing the repair and/or the replacement of the vulnerable elements damaged by the earthquake; is also an important DV for precast RC industrial building.

In the current research, the selected DV for performing the PEER PBEE framework is the EAL in terms of direct losses computed through the PACT software. This software is able to assess the monetary losses due to the damage suffered for each intensity measure by the vulnerable elements taken into account.

Currently, despite the PEER PBEE framework allowing the computation of the repair time, an important limitation is the inability to evaluate the indirect losses due to downtime, which are not negligible in the assessment of the monetary losses of precast RC industrial buildings.

In addition to this, it is known that most of the precast buildings are intended for industrial activities and the frequent presence of expensive machinery and furniture inside them makes the phase of the loss analysis more delicate.

It is worth noting that for this category of buildings, the greatest losses are linked to the damage suffered by elements located inside the facility and the indirect losses due to downtime. The need to quantify the probability of damage suffered by the machinery is one of the aspect that should be addressed as a continuation of this research. The correlation that exists between the position of the expensive machinery and the probability of being under the roof element that loses the support and falls down should be investigated and analysed. In order to satisfy this aspect, a possible proposal would be to compute the monetary loss due to the damage suffered by the expensive machinery by considering different classes of damageable groups for those roof elements which are located above the expensive furniture. These specific damageable groups should be created by including the price of the machinery located under the collapsed roof element in addition to the cost of repair and/or replacement of the roof elements itself (Figure 4.28).

Moreover, given the importance that downtime has on the industrial activity of a company, it is important to investigate the probability that the collapse of some roof elements located in specific areas in plan can cause a total (or partial) stopping of the industrial activity. In the assessment of the economic losses due to an earthquake, it would be useful to investigate also the possibility to have a scenario in which the building needs to be restored while the interior machinery and furniture's are completely undamaged and functioning. In this case, the company could transfer its expensive machinery to another building in order to continue the activity and avoid (or reduce) the monetary losses due to downtime.

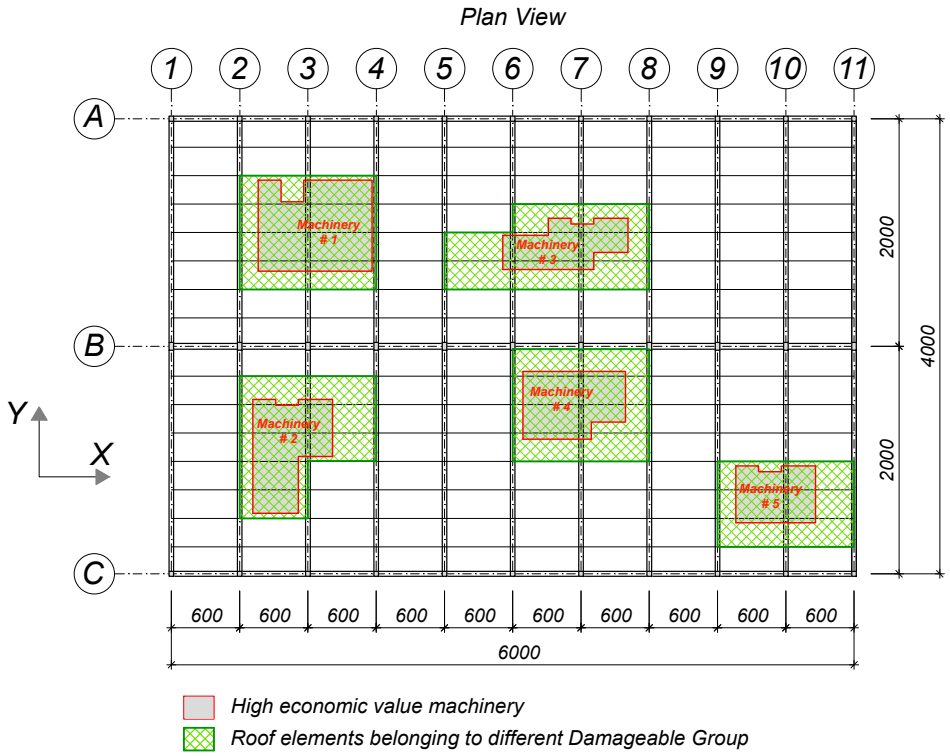

Figure 4.28 Hypothesis of the internal disposition of the machinery and identification of possible roof elements associated to different damageable groups.

4.2.3.1 Indirect losses

As previously mentioned, it is known that the major effects which determine the bigger monetary losses for a company after an earthquake are due to indirect losses. This fact has been confirmed by the experience that the affected companies on the Emilian territory had after the seismic events in May 2012.

The PEER PBEE framework does not allow a computation of this type of loss, which are mainly attributable to:

a. losses in the *immediate period* related to: the accounting write-off of the property and/or of the installations contained within the facility; the disposal of the debris and waste; the restoration of the damaged areas to the net of any insurance compensation;

b. losses in the *short-term (transient)* such as: missed gain of the company in the transient period; the impact on the working capital due to the customers and suppliers' reaction (expressed as a function of the length of the transient period); the impact on the cost of debt due to the reaction of the banking system;

c. loss in the *long-period* related to the possible loss of market share and/or to the possible loss of technological know-how.

Some studies on the determination of indirect losses due to downtime have already been done and are available in literature as [Patterson, 2002], [Iron Mountain, 2004], [Fox *et al.*, 2008], [VISION Solutions, 2014a] and [VISION Solutions, 2014b] but many more studies should be addressed in this direction. In particular, future research should investigate regarding the inclusion of the indirect losses linked to downtime within the PEER PBEE framework. As demonstrated by the effects suffered by all companies from Emilian region in Italy which were affected by an earthquake in 2012, this kind of loss plays an important role in the assessment of the monetary losses endured by the owners of RC precast industrial buildings because the greater damage that a company can experience is given by a possible stop of the production activity localized inside the facility, more than the direct losses due to the damages suffered by all structural and non-structural elements (internal content and machineries necessary for the production excluded).

4.3 Comparison of the results obtained

In the current section, a comparison of results in terms of EAL obtained through refined and simplified procedures and by choosing different assumptions for the inputs data needed in PACT (e.g. dispersion, type of analysis, $S_a(T_1)_{COLLAPSE}$, hazard analysis etc.) is presented. It is worth noting that the results of this sensitivity analysis are valid for the case study defined at the beginning of the current Chapter. In the end, the shape of the loss-intensity measure curve as well as the application of the closed formula proposed by [Sullivan, 2016] for the assessment of the value of EAL are investigated and applied to the case study.

4.3.1 EAL assessed with the refined PEER PBEE framework

As a first analysis and comparison, the sensitivity analysis is carried out on the variability of the expected annual loss assessed through the refined PEER PBEE framework which provides that the structural analysis is performed by means of the incremental dynamic analysis.

In Figure 4.29, the results obtained by performing the structural analysis with the IDA are shown in terms of EAL, for the cases of: unreinforced top column fork modelled with only one single element; unreinforced top column fork modelled with two elements; and retrofitted top column fork with two UPN 200 steel profiles laterally installed. For each case, $S_a(T)_{COLLAPSE}$ and the dispersion related to it ($\beta_{COLLAPSE}$) are assessed as shown in Chapter 4.1.1.1, the obtained values are reported in Table 4.17.

Table 4.17 Results of $S_a(T)_{COLLAPSE}$ and the dispersion related to it ($\beta_{COLLAPSE}$) for the different models adopted to perform the structural analysis and the comparison of EAL.

Histogram in Figure 4.30	Features of the fem model	$S_a(T)_{COLLAPSE}$ (g)	$\beta_{COLLAPSE}$
1	Unreinforced top column modelled with 1 element	0,0986	0,22
2	Unreinforced top column modelled with 2 elements plus spring elements	0,2457	0,37
3	Reinforced top column fork	0,5401	0,36

As can be seen from Figure 4.29, the PEER PBEE framework is a useful tool to predict the saving of EAL consequently to a retrofit measure that in this case is due to the reinforcement of the top column fork but it may also concern other vulnerabilities shown in Chapter 3.

From Figure 4.29, it can be noted how the execution of a retrofit measure on the fork at the top of the column clearly leads to a decrease of the value of EAL, which passes from a value of 10185€/yr in the case of unreinforced top column fork modelled with

one element (9550€/yr if the unreinforced top column fork is modelled with two *beam* elements plus *spring* elements, see Chapter 4.1.1.1 for more details) up to a value of 8808€/yr after the execution of the retrofit intervention on the top column fork.

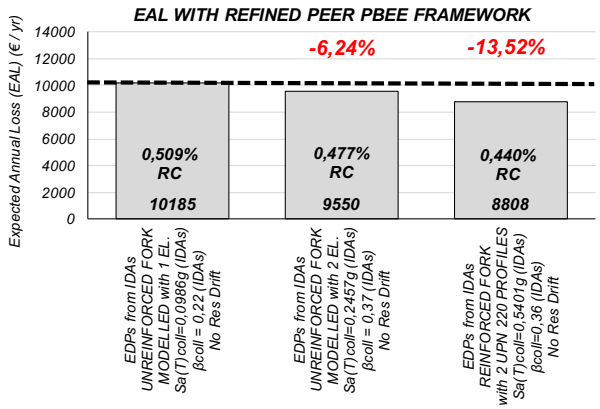

Figure 4.29 Comparison of EAL assessed through refined PEER PBEE framework for the cases of: unreinforced top column fork modelled with one element (first column in the chart); unreinforced top column fork modelled with 2 elements (second column in the chart); reinforced top column ford (third column in the chart).

A difference of -6,24% of EAL is reached from the fem model with the unreinforced top column fork built with one element to the case of unreinforced top column fork modelled with two elements plus *spring* elements. A refinement of the fem model used to assess the seismic response of the facility during the structural analysis affects the final value of EAL. In this specific case study, with the damageable elements assumed according to what is shown in Chapter 4.1.4, a reduction of EAL is observed. Furthermore, when a retrofit action is provided, a reduction of the EAL equal to 13,52% is observed according to initial expectations (given an initial financial investment aimed to improve the seismic response of the structure), confirming that the PEER PBEE methodology is a useful tool to assess the convenience or not of a retrofit measure and/or to compare different retrofit solutions between themselves. More details about the difference of the two models adopted are shown in Chapter 4.1.1.1.

After this first study, the sensitivity analysis has investigated the value of EAL as a function of the variability of different parameters required within the PEER PBEE framework and then within PACT. By taking as a reference the model with reinforced top column fork, the sensitivity analysis is carried out considering the cases reported in Table 4.18. Values of EAL assessed for each case are summarized and compared in Figure 4.30.

Table 4.18 Features of the fem models adopted in the comparison shown Figure 4.30. The values of $S_a(T)_{COLLAPSE}$, $\beta_{COLLAPSE}$ and the residual interstorey drift assumed in the assessment of EAL with PACT are reported.

Histogram in Figure 4.30	Features of the fem model	$S_a(T)_{COLLAPSE}$ (g)	$\beta_{COLLAPSE}$	Residual drift
1	EDPs assessed through IDA	0,5401	0,36	-
2	EDPs assessed through IDA $\beta_{MODELLING}$ assumed equal to 0,47 (see Chapter 4.1.3) instead of 0,35 as adopted in all the other cases	0,5401	0,36	-
3	EDPs assessed through IDA Residual interstorey drift is taken into account within PACT	0,5401	0,36	σ = 1% β = 0,3
4	EDPs assessed through IDA Residual interstorey drift is taken into account within PACT	0,5401	0,36	σ = 0,5% β = 0,3
5	EDPs assessed through IDA $\beta_{COLLAPSE}$ is calculated in a simplified manner as suggested by [FEMA P-58, 2012b]	0,5401	0,60	-
6	EDPs assessed through IDA $S_a(T)_{COLLAPSE}$ and $\beta_{COLLAPSE}$ are chosen equal to what is evaluated in a simplified manner through SPO2IDA and as suggested by [FEMA P-58, 2012b] respectively	0,7575	0,60	-
7	EDPs assessed through IDA $S_a(T)_{COLLAPSE}$ and $\beta_{COLLAPSE}$ are chosen equal to what is evaluated in a simplified manner through SPO2IDA and as suggested by [FEMA P-58, 2012b] respectively	0,7575	0,60	-
8	EDPs assessed through IDA but a "Linear analysis" type is chosen in PACT: the mean and dispersions are manually calculated on IDAs values $S_a(T)_{COLLAPSE}$ and $\beta_{COLLAPSE}$ are chosen equal to what is evaluated in a simplified manner through SPO2IDA and as suggested by [FEMA P-58, 2012b] respectively	0,7575	0,60	-

Results of EAL shown in Figure 4.30 demonstrate that the value of EAL can be influenced in a different way by the initial assumptions chosen within PACT.

In particular, the comparison is made by considering these different combinations of the input parameters, such as:

- dispersion β_m linked to the accuracy of the fem model assumed and the reliability regarding the definition of the building and the construction quality itself (see Chapter 4.1.3); chosen equal to 0,35 (average quality for both building definition and completeness of the analytical model) for all cases except the second case in Figure 4.30 for which it is selected 0,47 (average and limited quality for building definition and completeness of the analytical model respectively or vice-versa);
- the median value of the spectral acceleration for which the collapse occurs, $S_a(T)_{COLLAPSE}$, evaluated in a refined way through the IDAs and in a simplified

manner with the SPO2IDA tool; this to see how the use of $S_a(T)_{COLLAPSE}$ evaluated in a simplified manner can influence the EAL;

- the dispersion $\beta_{COLLAPSE}$ related to the median value of the spectral acceleration, $S_a(T)_{COLLAPSE}$, which is defined with the value calculated using the "*Collapse Fragility Tool"* provided within [FEMA P-58, 2012a], or by the value suggested by [FEMA P-58, 2012b] in *§ 6.3 - Simplified Nonlinear Analysis*, equal to 0,6;
- the contribution or non-contribution of the residual interstorey drift (see Chapter 4.2.1);

For example, by keeping the same values of EDPs calculated through IDAs for all the cases, a low difference of EAL (+0,9%) is observed in this case study when the β_m is assumed as 0,47 instead of 0,36.

If the 1% of residual interstorey drift is taken into account within PACT (see Chapter 4.2.1), case belonging to the third histogram in Figure 4.30, for this case study the difference in the outcome of EAL is low, reaching only +0.9%. This is due to the fact that at the end of the IDA process, the observed values of residual interstorey drift are very low compared to the imposed median value of the interstorey drift set at 1%. Low residual deformation and then values of residual interstorey drift are observed because the column behaves mostly elastically. However, if a lower median value of the residual interstorey drift is selected, e.g. 0,5% (fourth histogram in Figure 4.30), the rate of EAL linked to the residual interstorey drift is no longer negligible because a higher increase of EAL equal to 8,6% is noted.

For this case study, an overestimation of 2,9% of EAL (fifth histogram in Figure 4.30) is observed if the only value of the $\beta_{COLLAPSE}$ passes from the value calculated using the "*Collapse Fragility Tool"* (implemented by Jack Baker for the [ATC, 2012] project and then provided within [FEMA P-58, 2012a]), equal to 0,36, to the value calculated in a simplified manner as suggested by [FEMA P-58, 2012b] at the paragraph *6.3 - Simplified Nonlinear Analysis*, equal to 0,6. On the contrary, the variability of the $S_a(T)_{COLLAPSE}$ ($\beta_{COLLAPSE}$ is kept equal to the value evaluated with rigorously, equal to 0,36) does not affect the result of EAL which are assessed by using the $S_a(T)_{COLLAPSE}$ calculated in a simplified manner with SPO2IDA, equal to 0,7575g, and the $S_a(T)_{COLLAPSE}$ calculated in a rigorous manner with "*Collapse Fragility Tool"*, equal to 0,5401g. An underestimation of 0,5% is observed. Another model (sixth histogram) shows the $S_a(T)_{COLLAPSE}$ and the $\beta_{COLLAPSE}$ calculated both in a simplified manner with SPO2IDA tool and as suggestions provide by [FEMA P-58, 2012b] respectively. This assumption takes into account the possibility that the data which describe the

structural collapse are both estimated in a simplified way in order to obtain a saving of computational time. For this case study, the observed difference is only of +0,4%.

Contrary to all the other cases, in which the EDPs are inserted within PACT individually and according to what is obtained by IDAs for each accelerogram, in the last case shown in Figure 4.30 (seventh histogram), the selected type of analysis within PACT is the *"Simplified (Linear)"*, as shown in Figure 4.31. With this kind of analysis related to the values of EDPs, PACT simply requires the insertion of the median value and the dispersion linked with it. The computation of the median value and the dispersion of the EDPs of interest is made with the results from IDA for each seismic intensity which are not characterized by a structural collapse. The advantage of this procedure is given by the time saved for the insertion of the value one by one in PACT. The final result obtained is very close to what is evaluated with the classical procedure that involves the insertion of EDP achieved for each individual accelerogram.

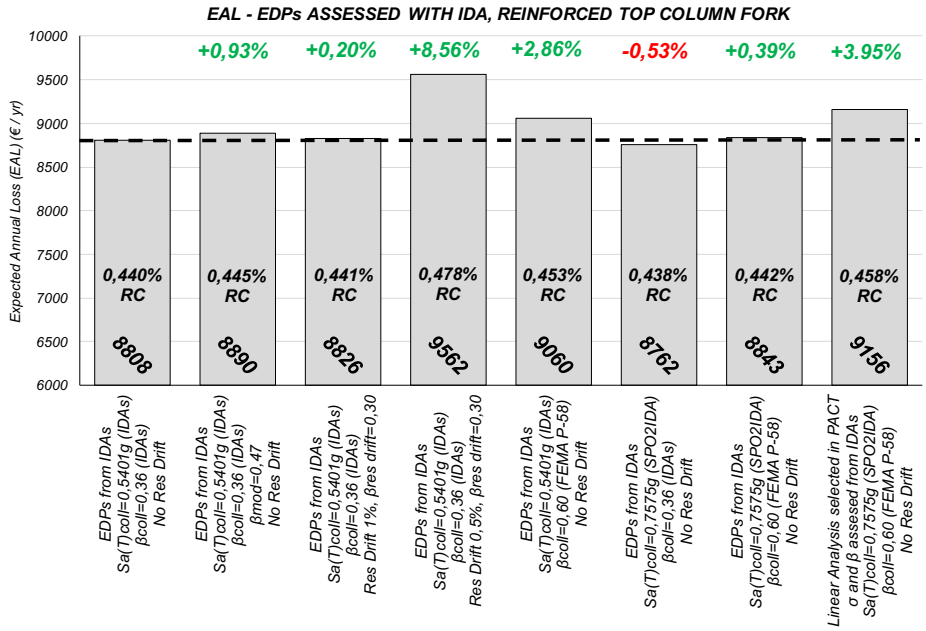

Figure 4.30 Results of the EAL obtained through the refined PEER PBEE procedure by taking into account different solutions in the values of the input data required within PACT.

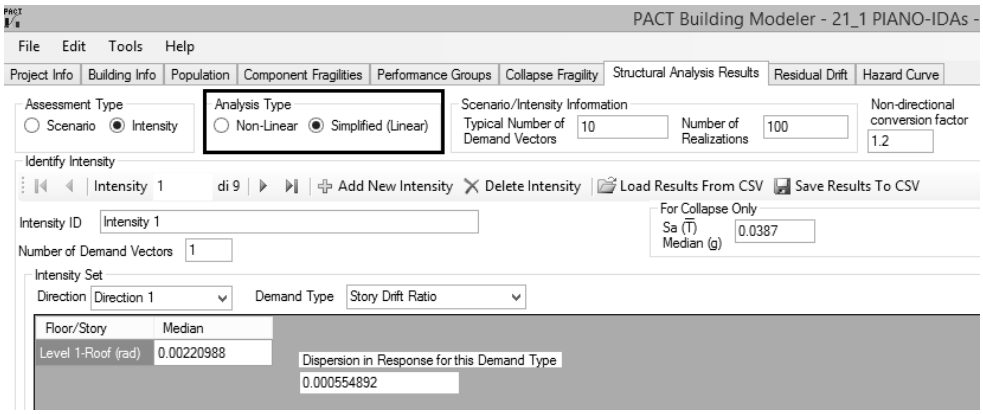

Figure 4.31 Screenshot of the "Structural Analysis Result" window in PACT in which it is possible to select the analysis type as "Simplified (Linear)".

4.3.2 EAL assessed using the SPO2IDA tool for performing the structural analysis

In the current section, the results of EAL calculated using the SPO2IDA tool for performing the structural analysis are shown.

In Figure 4.32, the comparison of EAL evaluated for both the unreinforced and reinforced top column fork is illustrated with histogram showing the comparison in terms of percentage of replacement cost (RC) and the variation in percentage of EAL compared to the reference case. For both cases, $S_a(T)_{COLLAPSE}$ is assessed with SPO2IDA tool and $\beta_{COLLAPSE}$ is assumed as suggested by [FEMA P-58, 2012b] in *§ 6.3 - Simplified Nonlinear Analysis*, equal to 0,6 (see Chapter 4.1.1.2).

As can be seen from Figure 4.32, through the simplified procedure using SPO2IDA to perform the structural analysis, it is possible to predict the saving of EAL consequently to a retrofit action but it is fundamental to get the pushover curve needed within SPO2IDA that is able to represent the local collapse linked to the selected local structural vulnerability. A retrofit action on the fork at the top of the column clearly leads to a decrease of the value of EAL (equal of 54,85%), which passes from a value of 16273€/yr (0,814% of RC) in the case of unreinforced top column fork (first column in the chart) up to a value of 7348€/yr (0,367% of RC) after the execution of the retrofit actions on the top column fork (second column in the chart).

It is interesting to observe the comparison between the EAL obtained with the refined procedure (see Chapter 4.3.1), for the cases with top column fork modelled with one

beam element and with two *beam* plus *spring* elements, and the simplified method with SPO2IDA.

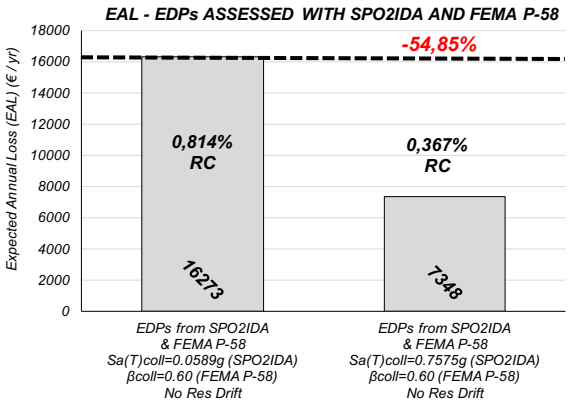

Figure 4.32 Comparison of EAL assessed using the SPO2IDA tool for performing the structural analysis for the cases of unreinforced (left column) and reinforced (right column) top column fork.

In Figure 4.33 and Figure 4.34, the comparisons of EAL calculated with both refined and the simplified method and for both cases before and after the retrofit intervention on the top column fork are shown.

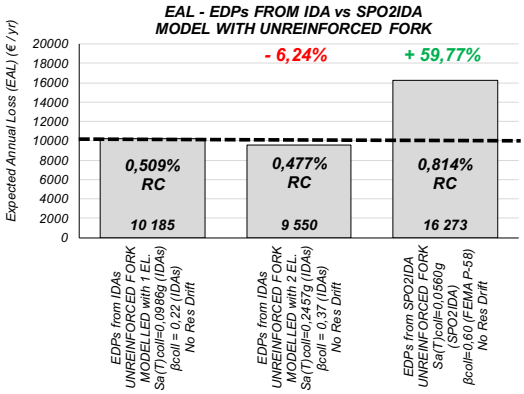

Figure 4.33 EAL assessed for both cases when the structural analysis is performed through IDA and with SPO2IDA in the scenario with unreinforced top column fork and hazard curve for the simplified procedure assumed according to the assumption b as defined in Chapter 4.2.2.

From the comparison carried out for the case of unreinforced top column fork, it can be observed how the use of EDPs obtained by the simplified manner in the assessment of the monetary losses leads to an overestimation of the value of EAL (of almost 60%) compared to what is assessed in a refined manner. This great difference of EAL between these two options should be sought mainly in the fact that the IDA

has been recreated in a simplified way (through SPO2IDA tool) starting from a truncated pushover curve (see Chapter 4.1.1.2) which has been approximated in SPO2IDA on significant points and also to the fact that the EDPs were assessed in a simplified way as well.

With reference to the case of reinforced top column fork, from Figure 4.34 it is possible to observe how the assessment of EAL using the EDPs evaluated in a simplified manner with SPO2IDA led to an underestimation of 16,58% compared to the case with the EDPs assessed through IDA. The value expressed in percentage terms of RC passes from 0,440% to 0,367%.

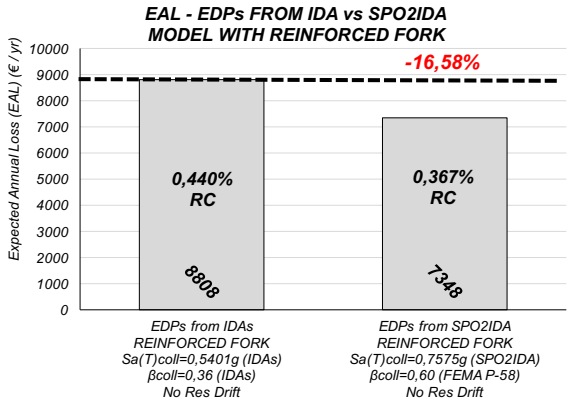

Figure 4.34 Comparison of the EAL assessed for both cases when the structural analysis is performed through IDA and with SPO2IDA in the scenario with retrofitted fork at the top of the column.

In Figure 4.35 and Figure 4.36, the results of EAL obtained with different assumptions are illustrated for the cases of unreinforced and retrofitted top column fork respectively, both assessed using the EDPs calculated through SPO2IDA tool and following the formulations provided by [FEMA P-58, 2012b] in *§ 6.3 - Simplified Nonlinear Analysis*.

As can be observed in the case of unreinforced top column fork in Figure 4.35, a variability of only $\beta_{COLLAPSE}$ can affect a lot the value of EAL leading to a difference in values equal to 30,8%. The comparison is carried out by taking into account in the former case (first column in the chart) the value suggested by [FEMA P-58, 2012b] in *§ 6.3 - Simplified Nonlinear Analysis*, equal to 0,6, and in the latter case the value calculated using the *"Collapse Fragility Tool"* (implemented by Jack Baker for the [ATC, 2012] project and then provided within [FEMA P-58, 2012a]), equal to 0,22 (see Chapter 4.1.1.1). For this case study, a considerable difference of EAL is observed by keeping all the other parameters fixed.

Therefore, a particular attention should be paid on the selection of the $\beta_{COLLAPSE}$, because, when the value suggested by [FEMA P-58, 2012a] is chosen, a consequent overestimation of EAL should be expected.

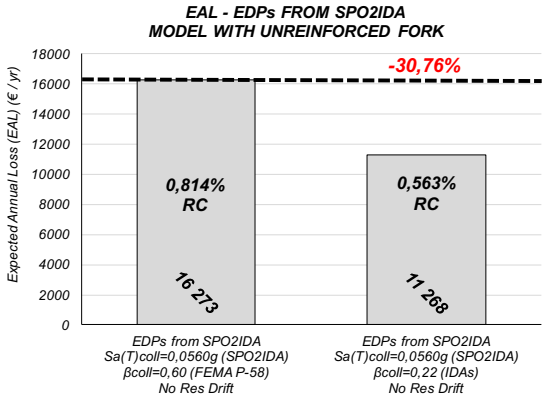

Figure 4.35 Results of EAL in the case of model with unreinforced top column fork. Two different values of the dispersion linked to the collapse ($\beta_{COLLAPSE}$) are assumed in PACT.

In Figure 4.36, it can be observed how different solutions of modelling are taken into account within PACT, obtained by adopting different assumptions for the input data needed, such as:

- the contribution or non-contribution of the 1% residual interstorey drift (Chapter 4.2.1), in which the value of the $S_a(T)_{COLLAPSE}$ in the fifth column is evaluated in a simplified manner with the SPO2IDA tool;
- adopting the median value of the spectral acceleration for which the collapse occurs, $S_a(T)_{COLLAPSE}$, evaluated in a simplified manner with the SPO2IDA tool, equal to 0,7575g (first column in the chart), and in a refined way through the IDAs, equal to 0,5401g (fourth column in the chart);
- adopting the $\beta_{COLLAPSE}$ related to $S_a(T)_{COLLAPSE}$ and selected according to the value suggested by [FEMA P-58, 2012b] in *§ 6.3 - Simplified Nonlinear Analysis*, equal to 0,6 (first column in the chart), or by the value calculated using the "*Collapse Fragility Tool*" provided within [FEMA P-58, 2012a], equal to 0,36 (third column in the chart).

The biggest difference in terms of EAL is given when the value of $S_a(T)_{COLLAPSE}$ is calculated through IDA that is equal to 0,5401g in comparison to a higher value of $S_a(T)_{COLLAPSE}$ assessed with SPO2IDA, equal to 0,7575g. The observed increase of EAL

(equal to 3,54%) is due to a higher contribution of monetary losses linked to the collapse.

In addition to the results seen for the two cases of the unreinforced and retrofitted top column fork, the variability of the EAL is also investigated for different assumptions linked to the typology of the fitting adopted for the hazard curve, as shown in Chapter 4.2.2. This study on the variability of the EAL due to the different assumptions for the fitting of the hazard curve is undertaken in the case of unreinforced top column fork.

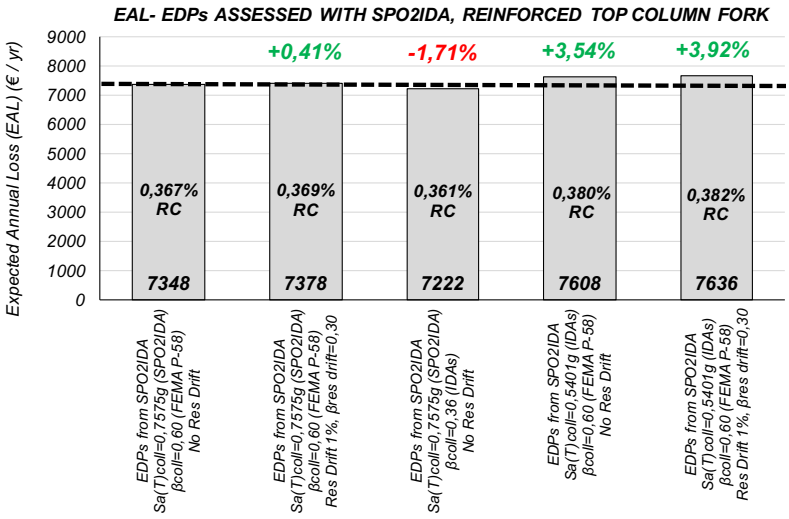

Figure 4.36 Results of EAL for different assumptions in PACT in the case of model with the retrofitted top column fork.

Figure 4.37 shows the comparison of the results. The best hypothesis for the fitting of the hazard curve is the case with a constant value of the MAFE when $S_a(T) < S_a(T)_{30yrs}$. In this case, the assumed value of the MAFE is equal to $\lambda = 1 / (T_R = 30\text{yrs}) = 0{,}03333$. The result obtained is able to guarantee a very close estimation to what is assessed through adopting the refined PEER PBEE method in the case of unreinforced top column fork (EAL = 10185€/yr, 0,509% of RC).

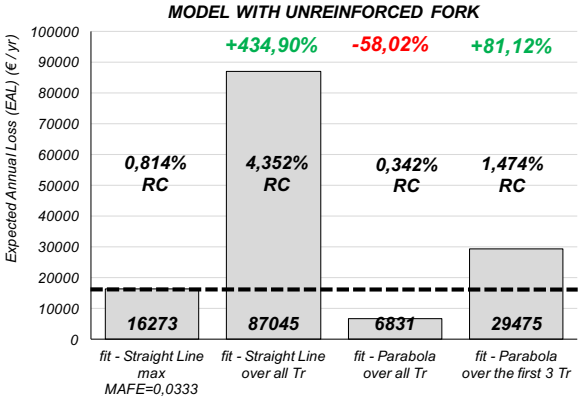

Figure 4.37 Results in terms of EAL obtained through the simplified method based on the using of the SPO2IDA tool for models with different fitting of the hazard curve, according to the assumptions described in Chapter 4.2.2.

4.3.3 *EAL assessed using the DBA approach for performing the structural analysis*

As shown in Chapter 4.1.1.3, DDBD procedure is investigated as a simpler and faster alternative than IDA to perform the structural analysis in PEER PBEE framework for RC precast industrial buildings. In Figure 4.38, a comparison of EAL between what is achieved by performing the structural analysis with both IDAs and the DDBD method for the structural model with retrofitted top column fork are shown. In this comparison, the referring value of EAL is given by the value obtained through IDA and some results achieved by DBA are compared by taking into account different hypotheses in assumptions relating to the values of MAFE (see Chapter 4.2.2) and the number of the selected limit states on which settle the DDBD procedure according to [Priestley *et al.*, 2007], [Sullivan *et al.*, 2014] and [Welch *et al.*, 2014].

It is worth noting that the second and the third models in Figure 4.38, differ in the hypothesis made regarding the fitting of the hazard curve: the former model follows the hypothesis defined according to the point *b* illustrated in Chapter 4.2.2; the latter adopts the hypothesis *c* defined in the same paragraph, in which the hazard curve for T_R < 30yrs is fitted with a parabola built on the first three points of the curve provided by [NTC, 2008]. As can be seen in Figure 4.38, the adoption of the hypothesis *c* for the determination of MAFE for T_R < 30yrs leads to an excessive overestimation of EAL of +88,95% (third column) in contrast to what is obtained with the assumption of the hypothesis *b* that still led to an overestimate of EAL but with a lower percentage equal to +19,13% (second column). As specified in Chapter 4.1.1.3,

this last difference of 19,13% should be sought in the fact that the real MAFE-Direct Loss curve is approximated to a discretized MAFE-Direct Loss curve built only on 4 points thus leading to a consequent approximation of the final result of EAL. An increase in the number of the limit states assumed in DBA leads to a closer value of EAL compared to what is obtained through the refined method. However, the use of DBA does not allow the exact calculation of the EAL: despite an increasing in the number of the limit states adopted there is difference of EAL equal -8,44% and -8,64% in the case with nine and 17 limit states respectively. It can still claim that it is a reliable method to estimate the EAL quickly.

Based on the results of EAL observed in Figure 4.38 for the assumed analysed case study, it can be said that the DBA method can be applied to Italians RC precast industrial buildings as an alternative to the refined procedure (which involves the carrying out of structural analysis with IDA) as long as the initial choice of the limit states as regards on both their number and the value of the interstorey drift associated to each of them is made very carefully as explained in Chapter 4.1.1.3. The adoption of hypothesis *b* according to Chapter 4.2.2 ($MAFE$ = 0,03333 in case of T_R < 30yrs) is also recommended in absence of more specific data.

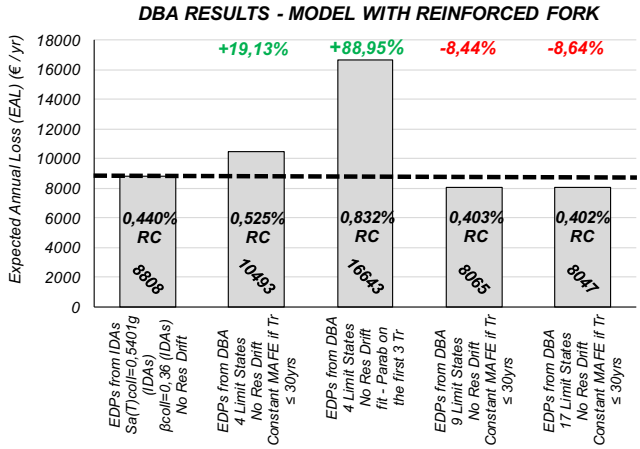

Figure 4.38 Comparison of EAL computed by performing the structural analysis with IDA and with DBA in different configuration regarding the values of MAFE and the number of the adopted limit states.

4.3.4 *Comparison between the all procedures*

In the end, a comparison of the results of EAL assessed with three methods investigated for performing the structural analysis are presented in Figure 4.39. The model used as a reference for the comparison is the one that adopts the retrofit measure on the fork at the top of the column. As can be seen, the use of EDPs evaluated through SPO2IDA tool and with the simplified formula provided by [FEMA P-58, 2012b] leads to an underestimation of EAL for an amount of 16,58% compared to what is obtained in the case of structural analysis performed with IDA. As the considerable amount of time is saved by carrying out the analysis with a simplified method, the final result can be quite satisfactory.

The assessment of EAL with the DBA procedure leads to an overestimation of 19,13% compared to the result reached with the structural analysis performed with IDA. This difference is mainly due to the fitting of the EAL curve which is built for points as illustrated by [Welch *et al.*, 2012] and shown in the previous Figure 4.15. The construction of the EAL curve by points implies a greater area under the curve in the graph compared to the continuous curve, and this means (to reach) a greater value of the economic losses since the assessment of the EAL is made by solving the integral extended to the EAL curve itself.

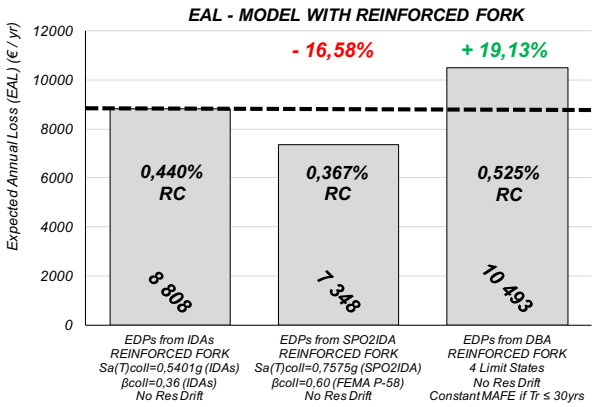

Figure 4.39 Results of EAL obtained for the three procedures adopted for carrying out the structural analysis: IDA (left histogram), SPO2IDA (central histogram) and DBA (right histogram).

4.4 Influence of modelling in the assessment of EAL

In the current section, different equivalent finite element models are adopted and non-linear time history analyses conducted in order to investigate the influence of modelling in the assessment of EAL. In particular, the RC top column fork is modelled in different ways, also considering the seismic retrofit. The EDPs obtained from the analyses are used within the PEER-PBEE methodology for the assessment of the expected losses (EL) under a scenario-based earthquake.

The assumed benchmark structure is the same illustrated at the beginning of the current Chapter and shown in Figure 2.1, with structural layout and details typical of the Italian practice before the enforcement of anti-seismic regulations. In this case, only the vertical cladding panels (2,5x9x0,15m) are assumed to surround the whole building. The panels are connected with the structure at their top through metallic fastenings reported in Figure 6.2 in Chapter 6.1.4, which the characteristics are adopted equal to what is shown in [Anže and Dolšek, 2016] for "Fastenings B" is shown in Figure 4.40 (b). The roof elements are made by prestressed double-T beams. The connections between the structural elements (roof elements, beams and columns) rely only on friction for transferring lateral loads. For all structural elements, the considered concrete cylindrical strength is 60MPa and the steel yield stress 450MPa.

The finite element modelling affects the PEER-PBEE results in terms of expected losses. Four models with increasing complexity are considered herein and represented in Figure 4.40. The first model ("*Model 1*") considers a single column as a cantilever beam fixed at the base, as illustrated in Chapter 4.1.1, with a tip mass (26338kg) corresponding to the roof tributary mass (total roof mass divided by the number of columns). The non-linearity is modelled by a plastic hinge at the column's base according to what is shown in Figure 4.2. Such model represents the structural performance after retrofitting of the RC forks at the column's top by means of steel profiles, as indicated in Chapter 4.1.2. The second and third models ("*Model 2*" and "*Model 3*") take into account the influence of the RC top column fork modelled as shown in Chapter 4.1.1.1. In *Model 2*, one beam element is provided with a plastic hinge at the fork's base according to [Takeda *et al.*, 1970] (see Figure 4.7, a); the plastic hinge considers the influence of a single fork element, owing to the absence of mechanical connections assuring a bilateral behaviour. *Model 3* considers the presence of both fork's elements (see Figure 4.7, b). In this model, a vertical beam element is provided to represent the main beam connected at the top of the column.

The upper node of the beam is connected to the top of the fork's elements through two compression-only springs with an initial gap of 1cm. An additional model ("*Model 4*") has been defined to catch a closer seismic response of the real structure and the activation of local vulnerabilities and it is represented in Figure 4.40 (a); the model considers two portals and one bay and it represents a portion of the central part of the facility shown Figure 2.1. The columns and the RC forks have been modelled as described in the third model. The roof elements and the double-tapered beams are included as beam elements. The cladding panels are modelled as point masses.

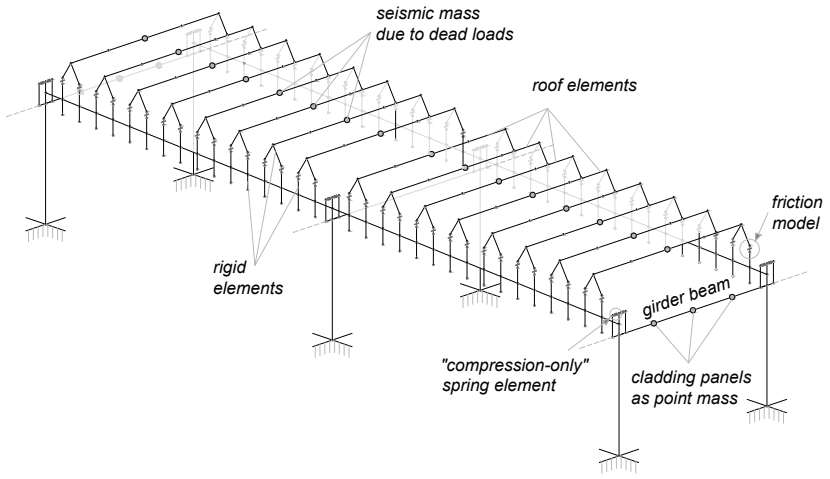

Figure 4.40 Considered 3D finite element model for the 4th model.

The following damageable elements are considered in the assessment of expected loss (EL): column, RC top column fork, roof element, and cladding panel. The damage related to the building content, as machineries and plants, is not considered herein. Table 4.19 reports the fragility, in terms of EDP, at each damage state and the related repair cost for each damageable element. The values are expressed as median values following a lognormal distribution with dispersion 0,6 for the fragility and 0,4 for the repair cost.

The expected loss in terms of repair cost is evaluated following the PEER-PBEE methodology under a scenario-based approach. The second main shock of the Emilia's seismic sequence (May 29th, 2012) is considered, whose ground motions are shown in Figure 3.36. Non-linear time history analyses have been conducted with the finite element software [Midas GEN (v1.2), 2014] including the three components of

the earthquake. The EDPs obtained from the analyses have been recorded and included as input value in the PACT software.

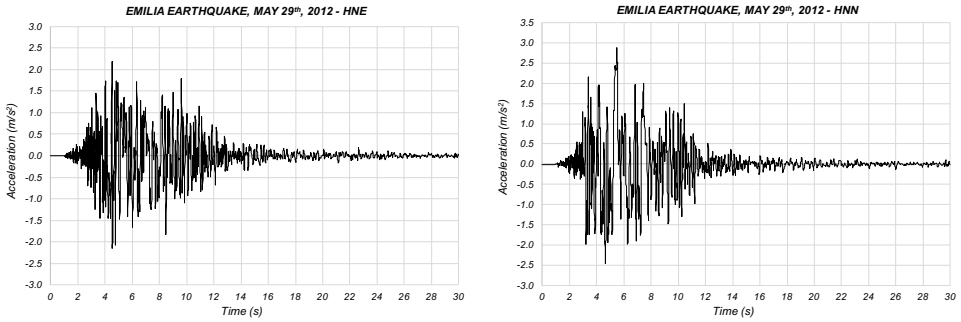

a) b)

Figure 4.41 Accelerogram of the horizontal components registered at Mirandola along the East-West (a) and the North-South (b) directions of the Emilia earthquake on May 29th, 2012.

Table 4.19 Damage states, repair actions, EDP values, and repair cost of the selected damageable groups.

Damageable element	Damage state	EDP	EDP value	Unit repair cost (€)
Column	DS-1: Slight cracking at the base (Injection with epoxy resin)	curvature (rad/m)	0,00094	126
	DS-2: Spalling of the cover at the base (RC jacketing)		0,00958	286
	DS-3: Collapse of the column (Restore collapsed elements)		0,06859	50175
RC fork	DS-1: Slight cracking at the base (Injection with epoxy resin + UPN 200 at each side)	curvature (rad/m)	0,00189	325
	DS-2: Spalling of the cover at the base (RC jacketing + UPN 200 at each side)		0,03083	599
	DS-3: Fork's failure (Restore collapsed elements		0,23378	38165
Beam-to-roof element joint	DS-1: Small relative displacement (Restore of sealant in 25% of perimeter + steel wire connection to avoid extra displacements)	Relative displacement (cm)	3	151
	DS-2: Intermediate relative displacement (Restore of sealant in 100% of perimeter + steel wire connection to avoid extra displacements)		6	200
	DS-3: High relative displacement and loss of the support		8	1237
Structure-to-cladding panel connection	DS-1: Yielding of the top connections (Restore of sealant in 25% of perimeter + steel brackets to avoid overturning)	Relative displacement (cm)	1	197
	DS-2: Rupture of the connections and fall of the cladding panel (Provision of a new panel)		4	1963

The results of the probabilistic simulation are represented in Figure 4.42 and they show how the cladding panels represent the most vulnerable element of the

considered case study and how they significantly impact the estimation of the total repair cost. In addition, it is observed how in *Model 2*, RC forks modelled with a single element, highly overestimates the cost related to forks' failure.

The comparison between *Model 3* and *Model 4* shows very similar results between the two models. Therefore, a good estimation of the repair costs could be obtained with *Model 3*, in which each fork's element is modelled with a nonlinear beam and the contact between the main beam and the fork is provided by compression-only springs. No significant differences are obtained between the simple one column model (*Model 1*) and the three-dimensional model (*Model 4*); therefore, such model could be adopted to estimate the repair costs. Further research is required to evaluate the parameters affecting the loss of support of the roof elements from the supporting beam.

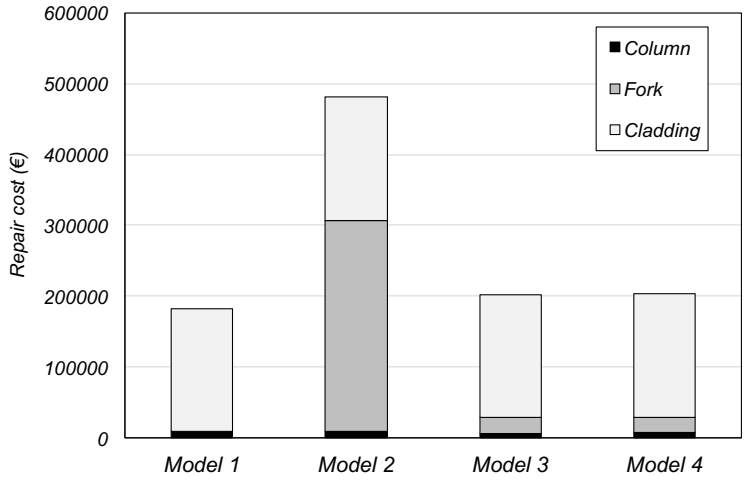

Figure 4.42 Expected loss as a function of the considered finite element models.

4.5 *Application of a new simplified procedure as an alternative to the PEER PBEE method*

The application of a further simplified procedure that has been developed and proposed by [Sullivan, 2016] is analysed in case of precast RC industrial buildings. In particular, this procedure calculates the EAL through the use of a closed formula applied to the schematization of the loss-intensity curve as a bilinear simplified curve (Figure 4.43). The final result obtained expresses the EAL as a percentage of the replacement cost.

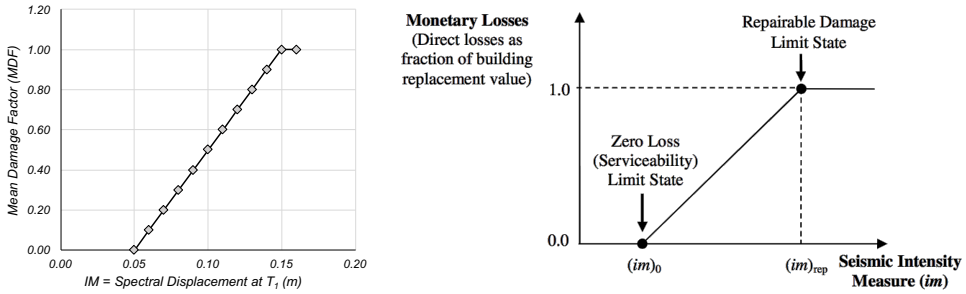

a) b)

Figure 4.43 a) Loss results as a function of seismic intensity, for a hypothetical case study building; b) bilinear loss versus intensity model for simplified loss assessment purpose, from [Sullivan, 2016].

According to identification of the points as shown in Figure 4.43 (b), the closed form formulation proposed by [Sullivan, 2016] for the assessment of the EAL is the following:

$$EAL = \frac{\left(\lambda_0 - \lambda_{rep}\frac{(IM)_{rep}}{(IM)_0}\right)}{\left(1 - \frac{\ln\left(\frac{(IM)_{rep}}{(IM)_0}\right)}{\ln\left(\frac{\lambda_0}{\lambda_{rep}}\right)}\right)\left(\frac{(IM)_{rep}}{(IM)_0} - 1\right)} - \frac{\left(\lambda_0 - \lambda_{rep}\right)}{\left(\frac{(IM)_{rep}}{(IM)_0} - 1\right)} + \lambda_{rep} \qquad \text{Eq. 4.7}$$

where λ_0 and λ_{rep} are the mean annual rates of exceeding the zero-loss and replacement loss states respectively, and the ratio $(IM)_{rep}/(IM)_0$ is the ratio of the intensity values expected to cause the two key loss states to exceed.

In order to investigate the accuracy of the result obtained by applying Eq. 4.7 to the assumed case study, the loss-intensity curves are built by referring to the results of EAL obtained for each intensity and evaluated with both IDA and DBA method,

where the latter method is performed on nine limit states (Figure 4.44, a). The choice of the nine selected limit states is made to allow a direct comparison of the shape of the curve with the one obtained in the case of structural analysis performed with IDA, in which the nine intensities provided by [INGV, 1999] according to [NTC, 2008] are chosen (Table 4.20). The assumed limit states are selected in order to have similar values of the ratio $S_a(T_1)/S_a(T_1)_{SLV}$ compared to what is taken into account for performing the IDA, which for the site of L'Aquila we have: $S_a(T_1)_{SLO}$ = 0,0387g, $S_a(T_1)_{SLD}$ = 0,0512g, $S_a(T_1)_{SLV}$ = 0,1606g, $S_a(T_1)_{SLC}$ = 0,2193g. In both procedures, the value of the EAL results approximately equal to 0,4% of the construction cost of the building which is equal to 2'000'000€ (Chapter 4.3.4).

Although the value of the EAL is almost equal, from Figure 4.44 (a) it can be observed how the loss-intensity curves do not perfectly overlap each other, especially for high intensities, as the eighth and ninth IM. This result is justified by the fact that the EDPs resulting from both procedures are not perfectly the same (see Chapter 4.1.1.3). By the way, the damages suffered by all the vulnerable elements within the facility (Chapter 4.1.4) are due to the low intensities, for which there is a close proximity between the two loss-intensity curves, as it can be seen from Figure 4.44 (a). The determination of the zero-loss and replacement points is necessary to allow the application of the formulation in Eq. 4.7 defined according to [Sullivan, 2016]. A first limitation is observed during the application of the aforementioned formula: the loss-intensity curves constructed and shown in Figure 4.44 (a) are not sufficient to define the point for which a value of MDF=1 is achieved as well as the point with MDF=0.

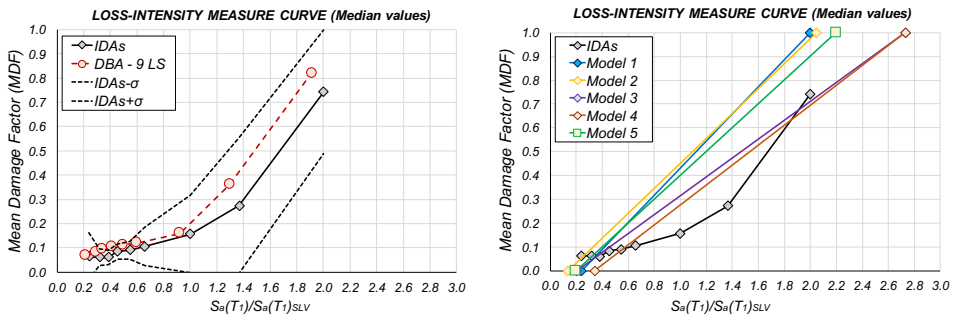

a) b)

Figure 4.44 a) Loss-intensity curve built for the cases of: IDA; IDA with uncertainty and the DBA performed on 9 limit states; b) different assumptions of the loss-intensity curve.

At this point and with the loss-intensity curves thus defined, it is difficult to accurately determine EAL through Eq. 4.7. As it can be seen from Figure 4.44 (b) and Table 4.21, the effect on the result in terms of EAL due to the choice of the points λ_0,

λ_{rep}, $S_{a,0}(T_1)$ and $S_{a,rep}(T_1)$ is investigated. This is because the choice of these points can greatly affect the final result of EAL and sometimes it can lead to unreliable values compared to what is obtained with PEER PBEE.

Table 4.20 Limit states taken into account for performing the simplified DBA procedure with 9 intensities and input data for PACT.

Limit State	θ_C (rad)	PGA (g)	$S_a(T_1)$ (g)	MAFE*	$a_{g,top}$ (g)	β_{SD}	β_{FA}
LS-1	0,00220	0,07944	0,03432	0,03333	0,09954	0,292	0,430
LS-2	0,00300	0,10528	0,04680	0,02022	0,13051	0,292	0,430
LS-3	0,00350	0,12057	0,05460	0,01470	0,14846	0,292	0,430
LS-4	0,00425	0,14221	0,06630	0,00984	0,17335	0,292	0,430
LS-5	0,00510	0,16482	0,07956	0,00675	0,19864	0,292	0,430
LS-6	0,00610	0,18963	0,09601	0,00458	0,22533	0,292	0,430
LS-7	0,00920	0,25977	0,14765	0,00188	0,29525	0,391	0,472
LS-8	0,01450	0,33346	0,20812	0,00092	0,35977	0,430	0,515
LS-9	0,02700	0,44733	0,30721	0,00041	0,44315	0,484	0,541

** constant value of MAFE for all of T_R lower than 30yrs, see hypothesis b) in § 4.2.2.*

The result of the survey in term of EAL is shown in Table 4.21; as previously said, the value of EAL is affected even for small variations in the locations on the graph of the points λ_0, λ_{rep}, $S_{a,0}(T_1)$ e $S_{a,rep}(T_1)$. Therefore, it is evident that the choice of these points cannot be done randomly and so the definition of the entire curve is necessary and crucial in order to proceed to the assessment of the position of the points with MDF=0 and MDF=1, and then for the calculation of the EAL with Eq. 4.7.

Table 4.21 EAL (as a percentage of the replacement cost) assessed with the formula proposed by [Sullivan, 2016] for different assumptions of the values of λ_0, λ_{rep}, $S_{a,0}(T_1)$ e $S_{a,rep}(T_1)$.

Model	λ_0	λ_{rep}	$im_0=S_{a,0}(T_1)$ (g)	$im_{rep}=S_{a,rep}(T_1)$ (g)	EAL (%)
Model-1	0,03297451	0,00045947	0,0387	0,3212	0,39
Model-2	0,06256525	0,00043737	0,0219 ($0,1 \cdot S_a(T_1)_{SLC}$)	0,3290 ($=1,5 \cdot S_a(T_1)_{SLC}$)	0,48
Model-3	0,04115880	0,00024133	0,0329 ($0,15 \cdot S_a(T_1)_{SLC}$)	0,4386 ($2 \cdot S_a(T_1)_{SLC}$)	0,31
Model-4	0,01781238	0,00024133	0,0548 ($0,25 \cdot S_a(T_1)_{SLC}$)	0,4386 ($2 \cdot S_a(T_1)_{SLC}$)	0,21
Model-5	0,03333333	0,00030967	0,0321	0,3533	0,31

Another critical point is due to the lack of data for determining the last part of the curve (high intensities). In fact, through the nine intensities provided by [NTC, 2008] and used for performing the IDA, it is not possible to define the curve in a

comprehensive and detailed manner. For this reason, the DBA procedure is chosen and applied to the reinforced top column fork fem model in order to investigate quickly the economic losses at higher intensity compared to those provided by [NTC, 2008] and used in the IDA. The structural analysis with the simplified DBA method is then carried out on 17 limit states considering the following assumptions, that are applicable also to the construction of the loss-intensity curve: in a log-log domain, the hazard curve has a linear pattern for the seismic intensities between $(im)_{30yrs}$ and $(im)_{2475yrs}$; the relationship between the MAFE (λ) and IM can be expressed as $\lambda(im) = k_0 \cdot im^{-k}$; λ is assumed as a constant value, equal to 1/30, for all of those intensities with $T_R < T_{R,\ 30yrs}$; the relationship $\lambda(im) = k_0 \cdot im^{-k}$ is assumed also for the assessment of those points with $T_R > T_{R,\ 2475yrs}$. The values of the interstorey drift adopted for each limit state and the output data in terms of EDPs are shown in Table 4.22.

Table 4.22 Limit states taken into account for performing the simplified DBA procedure with 9 intensities and input data for PACT.

Limit State	θ_c (rad)	PGA (g)	$S_a(T_1)$ (g)	MAFE	$a_{g,\ top}$ (g)	β_{SD}	β_{FA}
LS-1	0,00220	0,07917	0,03432	0,03333	0,09920	0,292	0,430
LS-2	0,00300	0,10484	0,04680	0,02022	0,12996	0,292	0,430
LS-3	0,00350	0,12005	0,05460	0,01470	0,14783	0,292	0,430
LS-4	0,00425	0,14164	0,06630	0,00984	0,17266	0,292	0,430
LS-5	0,00510	0,16427	0,07956	0,00675	0,19797	0,292	0,430
LS-6	0,00610	0,18916	0,09601	0,00458	0,22477	0,292	0,430
LS-7	0,00920	0,25973	0,14765	0,00188	0,29520	0,391	0,472
LS-8	0,01450	0,33588	0,20812	0,00092	0,36238	0,430	0,515
LS-9	0,01800	0,37567	0,24020	0,00069	0,39427	0,484	0,541
LS-10	0,02200	0,41623	0,27247	0,00053	0,42486	0,484	0,541
LS-11	0,02600	0,45314	0,30102	0,00043	0,45131	0,484	0,541
LS-12	0,03000	0,49074	0,32881	0,00036	0,47721	0,484	0,541
LS-13	0,03400	0,52788	0,35436	0,00031	0,50215	0,484	0,541
LS-14	0,03800	0,56727	0,37855	0,00027	0,52850	0,532	0,570
LS-15	0,04200	0,61272	0,40162	0,00024	0,55961	0,532	0,570
LS-16	0,04600	0,67810	0,42526	0,00021	0,60685	0,532	0,570
LS-17	0,05000	0,77276	0,44508	0,00019	0,67987	0,532	0,570

Through PACT, the EAL is calculated for each of the IM taken into account based on the values of EDPs and MAFE entered. In this manner, it is possible to construct the missing right part of the loss-intensity curve and then to proceed to the determination

of the exact limit of the curve for which a value of MAFE=1 is reached (Figure 4.45, a). According to the shape of the derived loss-intensity curve, the construction of the simplified bilinear line (Figure 4.45, b) is made by adopting the values of 0,03333333, 0,00030967, 0,03212g and 0,35332g for the points λ_0, λ_{rep}, $S_{a,\,0}(T_1)$ and $S_{a,\,rep}(T_1)$ respectively. By taking into account the bilinear line just created, the EAL are then computed with the Eq. 4.7 and the final result is equal to 0,37%, a value closed to what reached through PEER PBEE framework (0,44%).

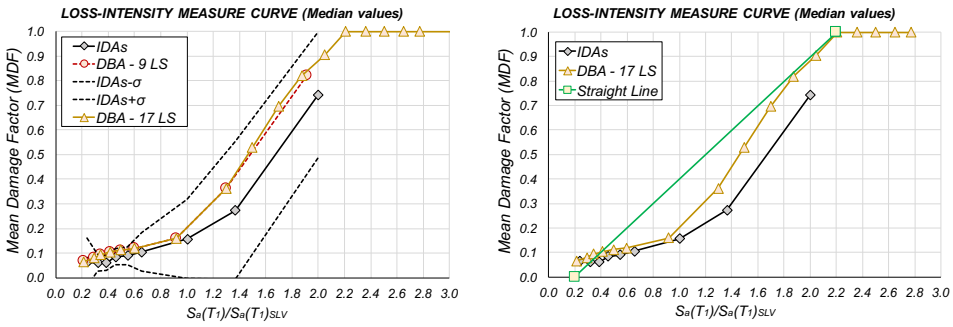

Figure 4.45 a) Loss-intensity curve built for the case of DBA performed on 17 limit states and comparison with the other loss-intensity curves obtained for the IDA (and IDA with uncertainty) and the DBA assessed on 9 limit states; b) bilinear loss-intensity curve fitted based on the real loss-intensity curve.

As it can be seen from Figure 4.46, the difference in the EAL results obtained is due to difference between the shape of the real curve (built with DBA performed on 17 limit states) and the shape of the simplified curve (bi-linear) which is not suitable to describe the real case. In fact, the bilinear curve adopted is not able to predict the pronounced concavity of the real loss-intensity curve for intermediate values of IM as well as is not able to help evaluate MDF when it is different from a zero value for the lowest intensity, as in the case study herein taken into account (note the left lower part of the real loss-intensity curve in Figure 4.45 (a), where the value of MDF is equal to 0,05). In the creation of the simplified bilinear curve, a value of MDF equal to zero is assumed as the starting point (left lower part of the continuous bilinear line in Figure 4.45, b), a hypothesis that clearly admits an intrinsic approximation of the final result.

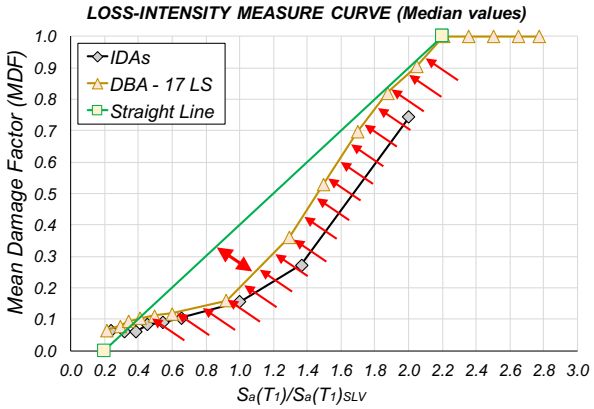

Figure 4.46 Gap between the real loss-intensity curve and the simplified bilinear curve for the assessment of EAL according to [Sullivan, 2016].

The aim is to achieve a simplified curve that would better represent the real curve for this case study. To obtain a better fitting of the new simplified curve, different solutions are studied and the variability of EAL is then investigated.

Initially, a curve with trilinear shape is adopted, where the middle point is selected as a point located on the real loss-intensity curve in correspondence to a MDF value equal to 0,5, as shown in Figure 4.47 (a). In this case, the EAL can be assessed by applying the formulation of Eq. 4.7 on the two areas under the curve identified in Figure 4.47 (a) and then by summing the individual results obtained as an integral evaluated on each area. The final value of EAL is equal to 0,33%, still far compared to what is computed with the PEER PBEE framework (0,44%), this is due to the fact that once again the simplified curve is not accurate enough and optimized for predicting the shape of the real loss-intensity curve.

Afterwards, it is interesting to see how the initial part (bottom left) and the final part (top right) of the curve can affect the value of EAL in order to proceed to an optimal fitting of the simplified curve.

In this new case, the top right part of the curve is investigated. Compared to the previous solution, the difference lies in that the new curve takes into account a constant value of the ratio $S_a(T)/S_a(T)_{SLV}$ in correspondence to a MDF equal to 0,5. A vertical straight line is adopted from this point (Figure 4.47, b). It is observed that the variation of the EAL is not affected with this change, as the final value is equal to 0,32%, quite similar compared to what was previously obtained. This is mainly due to the fact that the sum of the EAL has reached 90% of the total value of EAL at the 9th limit state within the DBA process (9th of 17 limit states), as shown in Figure 4.48

(b) in which the progressive value of EAL is represented with histograms as a function of an increasing value of the seismic intensity. This means that the contribution of the last eight IMs does not considerably affect the final value of EAL much (only 10%). For this case study, greater losses are generated at low intensities and they are mainly due to the damages suffered by non-structural elements and the assessment of the EAL does not take into account the inner content and the equipment but rather only the vulnerable elements referred to Chapter 4.1.4.

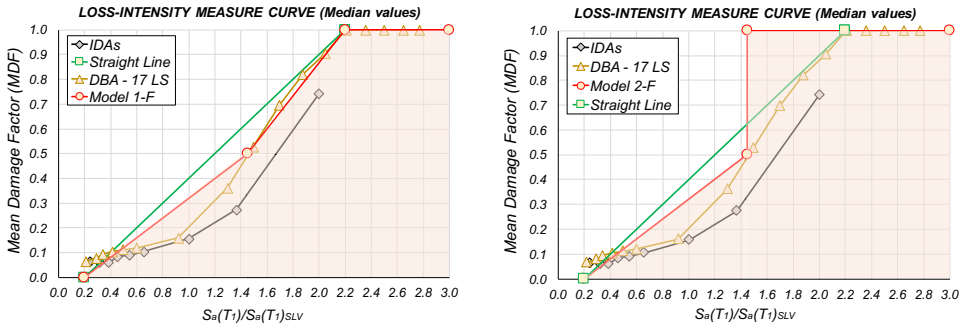

a) b)

Figure 4.47 a) Trilinear curve proposed as an alternative to the bilinear curve proposed by [Sullivan, 2016]; b) modified trilinear simplified curve with a vertical line adopted in correspondence to MDF=0,5.

Future research could investigate whether these deductions may be extended or not to the entire class of RC precast industrial buildings.

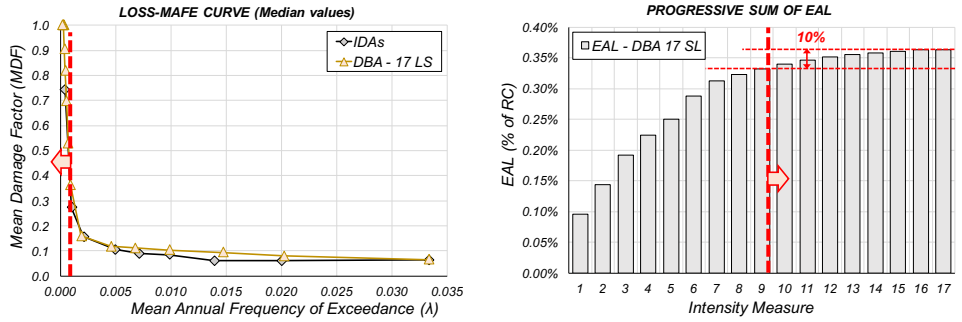

a) b)

Figure 4.48 a) The points of the MDF-MAFE curve are extrapolated for proceeding in the assessment of EAL by evaluating the integral of the area under the curve; b) progressive value of EAL with increasing of the intensity.

As previously mentioned, the evaluation of the EAL by the integral is very sensitive to the shape of the curve itself. Until now, the simplified calculation of the EAL has been done considering a value equal to zero for $S_{a,0}(T_1)$, but this assumption does not appear to be representative of the real shape. For this reason, a new trilinear shape of

the simplified curve is investigated, where the first point of the curve in correspondence of $S_{a,0}(T_1)$ is related to a value of MDF equal to 0,05 (Figure 4.49, a). With this new solution, the result of EAL undergoes an increase from 0,33% (first case of the adopted trilinear curve) to 0,47%, thus proving that even this solution is not appropriate to represent the correct loss-intensity curve. This happens because in this case also there is a difference between the trilinear simplified curve and the real curve, especially concerning the central part where the concavity of the real curve is not caught by the simplified solution.

A final proposal for a simplified loss-intensity curve is shown in Figure 4.49 (b) and even here the assessment of EAL is made by solving the integral of the shaded area under the curve. Contrary to the previous cases, with this solution, the addition of a further point in the bottom left part of the curve is provided in order to fit better the shape of the initial part and the concavity of the curve in correspondence of the middle-low intensity. The value obtained is equal to 0,41%, almost identical to what is obtained with the PEER PBEE framework (0,44%).

For this case study, the last chosen model of the loss-intensity measure curve proves to be effective for the assessment of EAL but as it can be seen, it was necessary to proceed with a refined calibration in order to obtain a better fitting of the simplified loss-intensity measure curve. Other structural configurations need to be analysed to investigate the applicability of this simplified curve to other typologies of precast RC industrial buildings, which are characterized by differences related to the type of external cladding (rigid infills or RC precast panels), the type of roof elements, the type of beams among others.

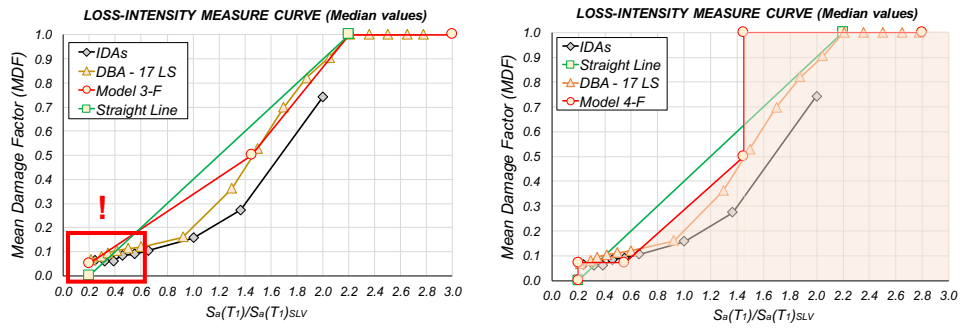

Figure 4.49 a) Third hypothesis of simplified trilinear curve with the initial point, $S_{a,0}(T_1)$, associated to MDF=0,05; b) final shape of the simplified loss-intensity curve for the analysed case study.

4.6 References

Anže, B., Dolšek, M. [2016] "Seismic Fragility Functions of Industrial Precast Building Classes", Engineering Structures, Vol. 118, pp. 357–370.

ATC. [2012] Applied Technology Council - Development of Next Generation Performance-Based Seismic Design Procedures for New and Existing Buildings.

Belleri, A., Riva, P. [2012] "Seismic Performance and Retrofit of Precast Concrete Grouted Sleeve Connections", PCI journal.

Dolsek, M., Fajfar, P. [2007] "Simplified probabilistic seismic performance assessment of plan-asymmetric buildings", Earthquake Engineering & Structural Dynamics, Vol. 41, No.11, pp. 1549–1568.

Doneux, C., Hausoul, N., Plumier, A. [2006] "Risk Mitigation for Earthquakes and Landslides Integrated Project, pages 60-75".

EN 1998-1. [2004] Design of Structures for Earthquake Resistance - Part 1: General Rules, Seismic Actions and Rules for Buildings, Brussels, Belgium.

Fajfar, P., Dolsek, M. [2012] "A practice-oriented estimation of the failure probability of building structures", Earthquake Engineering & Structural Dynamics, Vol. 41, No.11, pp. 1549–1568.

FEMA 460. [2005] Seismic Considerations for Steel Storage Racks Located in Areas Accessible to the Public, p. 174.

FEMA 74-FM. [2005] Earthquake Hazard Mitigation for Nonstructural Elements - Field Manual, p. 55.

FEMA E-74. [2012] Reducing the Risks of Nonstructural Earthquake Damage – A Practical Guide, p. 885.

FEMA P-58. [2012a] Seismic Performance Assessment of Buildings, Volume 3 - Supporting Electronic Materials and Background Documentation.

FEMA P-58. [2012b] Seismic Performance Assessment of Buildings, Volume 1 - Methodology.

Fox, J.P., Brammall, J.R., Yarlagadda, P.K. [2008] "Determination of the Financial Impact of Machine Downtime on the Australia Post Large Letters Sorting Process", 9th Global Congress on Manufacturing and Management (GCMM2008), Surfers Paradise, Australia, pp. 12–14.

Günay, M., Mosalam, K. [2012] "PEER Performance Based Earthquake Engineering Methodology, Revisited", Journal of Earthquake Engineering, Lisboa, Vol. 17, No.6, pp. 829–858.

Hunt, J.P., Stojadinovic, B. [2010] Seismic Performance Assessment and Probabilistic Repair Cost Analysis of Precast Concrete Cladding System for Multistory Buildings.

INGV. [1999] Istituto Nazionale di Geofisica e Vulcanologia, Roma, Italy, http://www.ingv.it/it/.

Iron Mountain. [2004] "The Business Case for Disaster Recovery Planning: Calculating the Cost of Downtime", pp. 1–12.

NTC. [2008] Decreto Ministeriale del 14 Gennaio 2008: Norme Tecniche per le Costruzioni.

Patterson, D. [2002] "A Simple Way to Estimate the Cost of Downtime", Proceedings of LISA '02: Sixteenth Systems Administration Conference, Philadelphia, PA, pp. 185–188.

Porter, K.A. [2003] "An Overview of PEER's Performance-Based Earthquake Engineering Methodology", Ninth International Conference on Applications of Statistics and Probability in Civil Engineering (ICASP9), San Francisco.

Priestley, M.J.N., Calvi, G.M., Kowalsky, M.J. [2007] Displacement-Based Seismic Design of Structures, IUSS Press.

Protezione Civile, Reluis, CNI, ASSOBETON. [2012] "Prezziario di Riferimento per gli Interventi Locali e Globali su Edifici Industriali Monopiano non Progettati con Criteri Antisismici di cui alle Linee di Indirizzo del 19.06/2012, v.1.0", Ufficio Tecnico del Genio Civile di Area Vasta Arezzo, Firenze, Prato e Pistoia, Regione Toscana, Italia.

RELUIS. [2013] Consorzio della Rete dei Laboratori Universitari di Ingegneria Sismica.

Ruaumoko. [2007] "Athol J. Carr, Ruaumoko - The Maori God of Volcanoes and Earthquakes", University of Canterbury, Christchurch, New Zealand.

SAC-FEMA-350. [2000] Recommended Seismic Design Criteria for New Steel Moment-frame Buildigns.

Sullivan, T., Calvi, G.M. [2015] "Developing Information Relevant to Simplified Displacement-Based Loss Assessment and Retrofit Approaches".

Sullivan, T.J. [2016] "Use of Limit State Loss versus Intensity Models for Simplified Estimation of Expected Annual Loss", Journal of Earthquake Engineering, Vol. 2469, No. May, pp. 1–21.

Sullivan, T.J., Welch, D.P., Calvi, G.M. [2014] "Simplified seismic performance assessment and implications for seismic design", Earthquake Engineering and

Engineering Vibration, Vol. 13, No. Suppl. 1, pp. 95–122.

Takeda, T., Sozen, M.A., Nielsen, M.N. [1970] "Reinforced Concrete Response to Simulated Earthquakes", Journal of the Structural Division, pp. 2557–2573.

Tecnocasa Group. [2013] "Mercato Immobiliare non Residenziale - Industriale: Capannoni", <http://www.tecnocasa.it/mediaObject/approfondimenti/ufficio-stampa/comunicatistampa/2013/10-ottobre/Mercato-immobiliare-CAPANNONI-Isem2013---Tecnocasa/original/Mercato immobiliare CAPANNONI Isem2013 - Tecnocasa.pdf.>.

Vamvatsikos, D., Cornell, C.A. [2002] "The Incremental Dynamic Analysis and Its Application to Performance-Based Earthquake Engineering", European Conference on Earthquake Engineering, p. 10.

Vamvatsikos, D., Cornell, C.A. [2006] "Direct Estimation of the Seismic Demand and Capacity of Oscillators with Multi-linear Static Pushovers Through IDA", Earthquake Engineering and Structural Dynamics, Vol. 35, No.9, pp. 1097–1117.

VISION Solutions. [2014a] "Assessing the Financial Impact of Downtime".

VISION Solutions. [2014b] "Business Continuity and Disaster Recovery Workbook: How to Assess the Financial Impact of Downtime".

Welch, D.P., Sullivan, T.J., Calvi, G.M. [2012] "Towards a Direct Displacement-Based Loss Assessment Methodology for RC Frame Buildings".

Welch, D.P., Sullivan, T.J., Calvi, G.M. [2014] "Developing Direct Displacement-Based Procedures for Simplified Loss Assessment in Performance-Based Earthquake Engineering", Journal of Earthquake Engineering, Vol. 18, No. April 2014, pp. 290–322.

5. CONCLUSIONS AND FUTURE DEVELOPMENTS

The principal aim of this research has been to investigate the suitability of *Performance-Based Earthquake Engineering (PBEE)* methodology developed by the *Pacific Earthquake Engineering Research (PEER) Center* at the University of California, Berkeley (USA) on the Italian one-storey precast reinforced-concrete (RC) industrial buildings, in order to assess the expected annual loss (EAL) due to earthquakes. This procedure provides the expected annual loss (EAL) linked to the damages suffered by all vulnerable elements within the facility. As demonstrated by the effects suffered by the companies after the earthquakes that hit the Emilian region in Italy in 2012, the importance of being able to predict the expected monetary losses due to an earthquake can be a useful tool for all stakeholder of RC precast buildings. Currently, no studies are available in the literature regarding a direct application of the PEER PBEE to the aforementioned structural typology, probably due to the probabilistic approach involvewd, the complexity of the PEER PBEE framework, and the multidisciplinary nature of the knowledge required.

In order to carry out a proper assessment of the economic losses and then of EAL, the knowledge of the seismic behaviour as well as the understanding of how local vulnerabilities can affect the seismic structural response and lead to possible collapses is required. For this reason, at first, the research focused its attention to examine, identify and investigate some of the main typical vulnerabilities and structural weaknesses observed from the recent earthquakes that hit the Italian territory (L'Aquila, 2009 and Emilia, 2012) and which characterized RC precast industrial buildings. Appropriate suggestions and considerations for each analysed vulnerability that can be helpful during the assessment of damages and thus monetary losses are provided in the current research.

In particular, an important contribution of this research is the assessment of the out-of-plane seismic response of the horizontal cladding panels in the one-storey precast buildings. At the state of the art, the formulations suggested by the current codes for construction at Italian [NTC, 2008], European [EN 1998-1, 2004] and American [ASCE/SEI 7-10, 2010] level do not estimate accurately the seismic load demand on precast cladding panels of single-storey buildings. The behaviour of these non-structural elements and the interaction between them and the structure has been investigated and analysed with linear and non-linear analyses. Results obtained from time history analyses are compared to the results calculated through formulae provided by current standards in order to show the inadequacy of the latter in the

estimation of the forces acting on the structure-to-cladding panel connections. What was observed from the parametric study helped developing a new refined procedure that is able to predict the values of the out-of-plane seismic loads on the horizontal cladding panels in one-storey RC precast structures, as an alternative to the formulations provided by current standards for non-structural elements. A direct application of this new formula is shown in a step-by-step example.

Furthermore, the interaction between the overhead crane and the bare structure and the influence of the overhead crane in the seismic response of a typical RC precast industrial building are studied in terms of difference on both top displacements and curvature at the base of the column. The importance of this study lies in the fact that possible differences of engineering demand parameters might affect the value of EAL, for this reason it is important to understand how the presence of the overhead crane in a RC precast industrial building can influence the seismic response of the structure especially since most of Italian precast RC industrial buildings are equipped with overhead crane. Usually, at the design stage, this element is assumed as a non-structural component and it is not taken into account as an interacting component with the structure. However, in reality, under the seismic excitation, this element is not completely isolated from the structural response. The interaction between the overhead crane and the structure is investigated starting from the derivation of the equations of motion. In particular, the equivalent stiffness and the equivalent coefficient of damping are defined. Laboratory tests are also conducted to determine the damping factor considering different configurations of the overhead crane. Once these parameters are defined, different modelling solutions are taken into account and compared. Optimal modelling solutions are suggested. Non-linear time history analyses of a 3D portal structure with multiple bays have shown that in the longitudinal direction, the addition of the mass of the crane leads to an increase of the roof displacements independently by the presence of a hanging load. On the contrary, in the transverse direction, the response is different in the case of absence or presence of a roof diaphragm: in the first case the increase of displacements is associated to a crane placed at the end of the longitudinal plan dimension and no hanging load present; in the second case, no significant increase of the roof displacements is recorded. Regarding changes in the curvature demand at the base of the columns, the overhead crane without the hanging load leads to the higher increase. Overall, the differences in values of EDPs observed for the assumed case study were minimal. To simplify the structural analysis in PEER PBEE, the presence of the overhead crane can be therefore omitted during the modelling in order to

obtain a simpler fem model. However, the conclusions are obtained by considering a single case study of RC precast industrial building composed of a single portal and four bays. Further research is needed to extedn the results to other configurations.

Also, a particular attention has been placed on the beam-to-column connections that are based solely on friction, which was one of the main cause that led to the collapse of the precast RC buildings during the last two earthquakes in Italy. A preliminary sensitivity analysis has been performed in order to investigate how the variability of parameters such as the coefficient of friction and the stiffness of the neoprene pad can influence the seismic response of a RC precast industrial building with friction connections. This work can be considered as a starting point for the development of future research aimed to analyze in detail the loss of support between structural elements and therefore to investigate the probability of collapse in RC precast industrial buildings related to the fall of structural elements horizontally oriented and simply supported. Future studies will be directed towards assessing the seismic behaviour of the structure as well as the probability of collapse in a complete 3D model. Furthermore, the variability of the results due to the development of plastic hinges at the column bases should be investigated.

After the investigation and the discussion of the major vulnerabilities in Italian RC precast industrial buildings, the suitability of the PEER PBEE framework applied to a case study representing an Italian RC precast building has been investigated in Chapter 4. Each phase within this methodology (Hazard Analysis, Structural Analysis, Damage Analysis and the Loss Analysis) was carried out and critically analysed in order to understand what in PEER PBEE can affect the assessment of the EAL and if this procedure can be easily used by professional engineers, engineering companies and/or insurance companies to evaluate the monetary losses. In the current research, the critical issues are identified and alternative solutions are proposed with the aim to facilitate the direct application in the professional field. For this reason, major problems in PEER PBEE were analysed and suggestions have been proposed to simplify the procedure.

It has been observed that in the Hazard Analysis, the choice of the mean annual frequency of exceedance (MAFE) values for low intensities is a critical issue, because small increments of MAFE correspond to large increments of EAL. It is suggested that in the absence of specific data, the value provided by [INGV, 1999] might be taken as a limit value to solve this issue. Such value is equal to the rate of occurrence, μ, of the earthquakes at the site under consideration. In the Structural Analysis, it has

been seen that the result of EAL can be influenced by the assumptions made in the fem model of the structure, because this can lead to different values of $S_a(T)_{COLLAPSE}$ and $\beta_{COLLAPSE}$ which are required within the *Performance Assessment Calculation Tool* (PACT) for the evaluation of the EAL. A key point in this step is related to the determination of the residual drift: unlike conventional RC buildings, for precast structures the residual drift may be due to rotations of the column at the foundation and then there is the possibility to recover the initial vertical position mechanically. For such high values of rotation at the base of the column, the largest share of the EAL is due to the damages suffered by non-structural elements and by the collapse of the roof elements caused by high values of relative displacements (in the case of connections based only on friction). The damages linked to the residual interstorey drift can be neglected. Regarding the Damage Analysis, a complete library of fragility curves related to all vulnerable elements is needed. Currently, the lack of fragility curves is one of the main issue for achieving this phase, especially for non-structural components in RC precast industrial buildings due to their features and uniqueness. These curves can be found in literature (only for some elements) or they can be built according to a lognormal distribution with a median value and a known dispersion associated to it. For calculating the median value, the most appropriate method would be to perform a series of laboratory tests. An alternative procedure adopted herein is to determine the median value with analytical formulae, according to the existing formulations in the literature or in the PEER and NEES reports or in the FEMA guidelines. In the case of unique experimental tests, a solution might be to take the observed value of interest as the median and the dispersion determined according to [FEMA P-58, 2012]. Relative to the Loss Analysis phase, the assessment of EAL linked to damages suffered by the inner content (such as expensive machinery) has been identified as one of the main problems in case of RC precast industrial buildings that will require further investigation. It is herein suggested to assign different cost curves to the roof elements placed above the equipment. Another important issue concerns the assessment of the EAL due to downtime (indirect losses), which are a cause of significant economic losses suffered by precast industrial buildings. This aspect requires further study and knowledge of economics.

Nowadays the PEER PBEE methodology is applicable mainly to academic research, because of the complexity associated to the determination of the many input data needed to carry out all the phases. Different aspects of the PEER PBEE framework should be simplified to allow the direct application by professional engineers.

In order to simplify the Structural Analysis for non-academic use, two simpler approaches, the *Static Pushover Analysis to Incremental Dynamic Analysis* (SPO2IDA) tool and the *Displacement-Based Assessment* (DBA) have been considered as an alternative of the incremental dynamic analysis (IDA) and the results observed show that these methods are reliable for the assessment of the direct losses and they can be used as a method for performing the Structural Analysis.

The significant advantage of using the *Static Pushover Analysis to Incremental Dynamic Analysis* (SPO2IDA) tool is that through the pushover curve it is possible to get the simulated results of the IDA with a considerable saving of computational time. In regards to this last consideration, it is important to take into account that RC precast industrial buildings fem models are not easy to run compared to typical infilled RC residential buildings. On the contrary to typical infilled RC frames, where the non-linearity is lumped in plastic hinges and perimetral infills and the assumption of rigid in-plane diaphragm typically applies, the RC precast industrial buildings are characterized by a higher computation demand due to the model of each connection, both mechanical or relying on friction. This leads to more complex models and therefore to an increase of modelling time and computational time.

An interesting solution applicable to this type of structures is to guarantee a minimum level of structural safety and robustness by inhibiting all local vulnerabilities that may lead to partial collapses. This case leads also to a sensible reduction of the model complexity.

The research investigated also the suitability of the DBA method applied to RC precast industrial buildings as an alternative to the refined PEER PBEE framework. By assuming different hypotheses on the selection of the limit states of interest, it has been noted how this phase of the procedure is fundamental and can strongly affect the output in terms of EDPs that are needed within PACT to perform the assessment of EAL. In terms of application of the DBA method, this aspect is one of the major issues that was highlighted, because the selection of the limit states affects the discretization of the EAL curve in the MAFE-Direct Loss graph and the accuracy of the EAL result is proportional to the number of points chosen to discretize the curve. For all those vulnerable elements, which the fragility curves are expressed as a function of the interstorey drift, the procedure is directly applicable and the damage states of these elements can be chosen at the beginning; otherwise, the damage states can be checked only at the end of the DBA procedure because the other engineering demand parameters (EDPs) are available only at the end (peak floor velocity, peak

floor acceleration, PGA …). In order to choose the right damage state level for these latter elements (non-sensitive to the interstorey drift), the selection of the interstorey drift can become an iterative process. The DBA procedure is then applied to a RC precast industrial case study building assuming 4, 9 and 17 selected limit states. In particular, the comparison of EDPs obtained with both the IDA and the DBA performed with 9 limit states showed that the main differences in the values are linked to the accelerations and the dispersions (related to accelerations and interstorey drift and calculated through FEMA P-58). However, the difference of EAL for the analysed case study is not high, this is because the main vulnerable elements that contribute to generate the monetary losses are sensitive to the interstorey drift.

Differently from SPO2IDA, DBA method can not be used in the case of local vulnerabilities as for example the rupture of the top column fork. Therefore, this procedure is well suited if the local vulnerabilities are inhibited.

In the current research, also a new loss-intensity curve has been studied as a simpler alternative method for the assessment of the EAL. It allows to assess the EAL directly with a closed formula by taking into account only few input data. This proposed formulation is advantageous because the estimated EAL are similar to what obtained with the refined PEER PBEE method and the computational time saved is significant.

5.1 Future research

In the future developments, the seismic response of the connection relying only on the friction between structural elements should be studied more in depth. The sensitivity analysis should be carried out in order to estimate the probability of collapse of the roof elements due to the loss of support. Nowadays, fragility and cost curves for non-structural elements installed in precast buildings are not available broadly. For this reason, the future research and studies will be aimed to satisfy this need.

The determination of indirect losses due to downtime is not yet considered in PEER PBEE framework (and then in PACT) for the assessment of the EAL. The future development of this methodology should be directed towards the contribution of these indirect losses, to assess a more realistic value of EAL.

Finally, the PEER PBEE framework and the new studied loss-intensity curve should be tested and extended to other case studies in order to check if the conclusions reached within this research are valid for the entire category of one-storey precast RC

industrial buildings. Such studies should also evaluate the limitation of the proposed simplified loss-intensity curve.

6. APPENDIX

6.1 Evaluation of the prices for each damage state

In this Chapter, the monetary losses linked to different damage states that can be caused by the main vulnerable elements during an earthquake are evaluated. Herein the monetary losses at each DS are assessed for a column, top column fork, beam-to-roof element joint and the structure-to-cladding panel connection. The costs per unit and the total prices are then defined and this information can be utilized by engineers during the assessment of the EAL according with PEER PBEE framework (see Chapter 4).

Table 4.22 shows general cost per unit that can be used in the calculation of the individual and the total cost at each DS. One of the most important reference that can be used to evaluate the cost per unit is given by [Protezione Civile *et al.*, 2012].

Table 6.1 Main costs per unit used for the assessment of the economic cost related to each damage state.

Description	Unit of measure	€ / unit
Cost of labour, consisting of skilled workers trained and informed (average value among the possible workers)	€/h	35,00
Rental of self-propelled aerial platform, diesel engine, articulated, including the transportation to the construction site (maximum working height of 15m)	€/d	150,00
Rental of telescopic cranes, including the man at the manoeuvre, fuel, lubricant, including the transportation to the construction site (capacity of 65tons, telescopic brace of 42m, minimum duration of the rental 8h)	€/h	177,00
Charges and landfill taxes for inert waste, for which is permitted the landfill disposal (uncontaminated soil and rocks from excavation)	€/t	13,50
Landfill charges for non-hazardous special waste (not contaminated concrete in large blocks)	€/t	35,00
Only cargo on the machine and transport of waste materials from partial excavation to landfill and/or treatment-recovery authorized facilities up to 20km away (no travel expenses charges, assuming to move within 50 km)	€/m^3	18,70
Complete general excavation up to a depth of 5m, on areas not subject to reclamation, including the lifting of the material to the loading floor of the truck, the loading, the transportation and the stacking of the material within the site area (not including the backfilling and the rebars for the walls of the excavation)	€/m^3	9,05
Backfilling with suitable materials coming from the construction site, including the load, the transportation and the laying in successive layers with a maximum height of 50cm, with compacting layer by layer with a mechanical machinery used for paving and regularization (excluded any construction arrangements)	€/m^3	11,00

6.1.1 Column

Three damage states are assumed and defined in the following as DS-1, DS-2 and DS-3 for both lateral and central typical column of the case study set out in Chapter 4 (see Figure 4.1). In the third damage state, the cost to fully restore the structural layout as in the pre-earthquake configuration is evaluated by taking into account the

collapse of both the column and all the structural elements supported by the column itself (beams, roof elements and cladding panels).

In order to define the damage states for the column, the chosen EDP is the curvature and each limit value linked to its DS is obtained through a section analysis. In Table 6.2, the values of EDP at each DS are shown.

Table 6.2 Value of EDP at each damage state identified for the column.

Damage State	Description	Limit value of EDP Curvature (rad/m)
DS-1	Slight cracking at the base	0,00094
DS-2	Spalling of the cover at the base	0,00958
DS-3	Collapse of the column	0,06859

DS-1: Slight cracking at the base

The first damage state consists of a light cracking at the base of the column. The restore procedure of the first damage state is provided by injections with epoxy resin and it is the same for both lateral and central column (Table 6.3).

Table 6.3 Individual and total cost necessary to fully restore one lateral or central column in the case of DS-1.

	Description	Unit of measure	Quantity	€ / unit	Total price
Material	Epoxy resin for injections	n. of pack	2,00	28,00	56,00
Manpower	Specialized manpower	h	2,00	35,00	70,00
			Total cost of the installation		126,00

DS-2: Spalling of the cover

In this second damage state, a scenario with a significant cracking at the base of the column and a wide spalling is assumed. The column shows the beginning of a plastic rotation at its base. The restore procedure foresees an increase in the stiffness of the column through a confinement at the base of the column itself with RC jacketing and it is the same for both lateral and central column (Table 6.4).

Table 6.4 Individual and total cost necessary to fully restore one lateral or central column in the case of DS-2.

	Description	Unit of measure	Quantity	€ / unit	Total price
Material	ϕ20 connecting jacket-column rebars	kg	80,00	0,80	64,00
	ϕ8/15 stirrups	kg	18,00	0,90	16,20
	ϕ8 forks	kg	6,00	0,90	5,40
	C50/60 concrete, 10cm thick including the formwork	m^3	0,70	160,00	112,00
Rental	Sandblaster	h	1,00	18,75	18,75
Manpower	Specialized manpower	h	2,00	35,00	70,00
			Total cost of the installation		286,35

DS-3: Collapse of the column

In the third damage state, the scenario foresees that the seismic excitation leads to the collapse of the lateral column, and therefore of the supported beam and the overhead roof elements. The restore procedure is aimed to restore the collapsed structural elements in order to obtain the pre-earthquake configuration.

When the lateral column undergoes collapse, one supported main beam, 16 roof elements and 6 cladding panels undergo collapse too. The economic losses shown in Table 6.5 are then calculated considering the collapse suffered by all these vulnerable elements.

Table 6.5 Individual and total cost necessary to fully restore the structural layout in the case of collapse of the lateral column as expected for the DS-3.

	Description		**Unit of measure**	**Quantity**	**€ / unit**	**Total price**
Disposal	*Landfilling of the inert, including loading and transportation*	*Column*	*€ / m³*	*1,48*	*18,70*	*27,64*
		Beam		*6,12*		*114,44*
		Roof element		*19,68*		*368,02*
		Cladding panel		*20,25*		*378,68*
Charges	*Charges and landfill taxes for inert*		*€ / t*	*118,82*	*13,50*	*1604,08*
Subject	*RC or precast double slope beam (slope between 10 and 12%) with a double-T section along the length and a rectangular section at the ends, total length of 20m and interaxes in the range between 8 and 12m*		*m*	*20,00*	*269,92*	*5398,30*
	Precast roof element with a π-section, calculated with a simple restrain at the ends and an overload of 200kg/m2, a total length up to 10m		*m²*	*320,00*	*37,04*	*11852,80*
	Column with a square or rectangular section, including the necessary rebars and stirrups, characterized by predominant axial load acting within the central core of inertia, excluding shelves, plates, downspouts and any other interior accessories		*m*	*7,30*	*99,63*	*727,30*
	Supply and installation of precast concrete cladding panels, thickness 15cm, reinforced with a B450C welded mesh and trellis checked in the factory, covered with stone slabs (these separately measured)		*m²*	*135,00*	*82,22*	*11099,70*
				Total cost of the installation		*31570,96*

Regarding the third damage state of the central column, the number of elements supported by the central column are different in quantities compared to the lateral column (Table 6.6). In this case, the individual and total cost necessary to fully restore the structural layout are assessed by considering two main supported beams, 32 roof elements and 6 cladding panels.

Table 6.6 Individual and total cost necessary to fully restore the structural layout in the case of collapse of the central column as expected for the DS-3.

	Description		Unit of measure	Quantity	€ /unit	Total price
Disposal	Landfilling of the inert, including loading and transportation	Column	€ / m^3	1,48	18,70	27,64
		Beam		12,24		228,89
		Roof element		39,36		736,03
		Cladding panel		20,25		378,68
Charges	Charges and landfill taxes for inert		€ / t	183,32	13,50	2474,83
Subject	RC or precast double slope beam (slope between 10 and 12%) with a double-T section along the length and a rectangular section at the ends, total length of 20m and interaxes in the range between 8 and 12m		m	40,00	269,92	10769,60
	Precast roof element with a π-section, calculated with a simple restrain at the ends and an overload of 200kg/m2, a total length up to 10m		m^2	640,00	37,04	23705,60
	Column with a square or rectangular section, including the necessary rebars and stirrups, characterized by predominant axial load acting within the central core of inertia, excluding shelves, plates, downspouts and any other interior accessories		m	7,30	99,63	727,30
	Supply and installation of precast concrete cladding panels, thickness 15cm, reinforced with a B450C welded mesh and trellis checked in the factory, covered with stone slabs (these separately measured)		m^2	135,00	82,22	11099,70
				Total cost of the installation		50175,27

6.1.2 *Top column fork*

At the top of the column, the beam-to-column joint is provided with a RC fork. Three damage states are assumed and defined in the following as DS-1, DS-2 and DS-3 for both fork at the top of the lateral and central column of the case study as shown in Chapter 4 (see Figure 4.1). As for the column, in the third damage state linked to the fork, the cost to fully restore the structural layout as in the pre-earthquake configuration is evaluated by taking into account the collapse of both the fork and all the structural elements connected to the top column fork itself (beams and roof elements).

In order to define the damage states for the top column fork, the chosen EDP is the curvature and each limit value linked to its DS is obtained through a section analysis. In Table 6.7, the values of EDP at each DS are shown.

Table 6.7 Value of EDP at each damage state identified for the top column fork.

Damage State	Description	Limit value of EDP Curvature (rad/m)
DS-1	Slight cracking at the base	0,00189
DS-2	Spalling of the cover at the base	0,03083
DS-3	Collapse of the column	0,23378

DS-1: Slight cracking at the base

The first damage state consists of a light cracking at the base of the top column fork. The restore procedure of the first damage state is provided by injections with epoxy resin. In addition to this (Figure 6.1), the stiffness of the RC forks is improved by providing a steel profile (UPN 200) at each side and it is the same for both fork at the top of lateral and central column (Table 6.8).

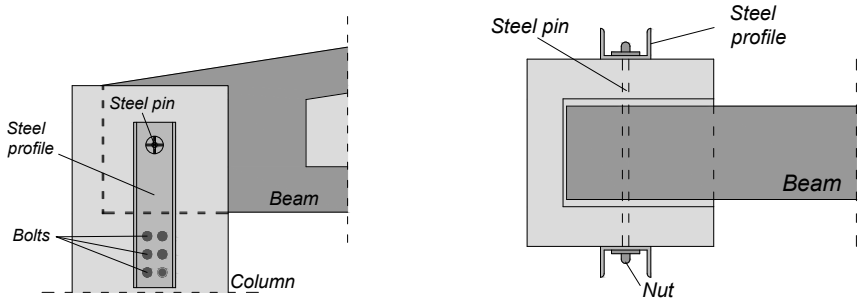

Figure 6.1 Repair of the top column fork in the case of DS-1 is provided by increasing the lateral stiffness of the fork with two lateral UPN 200 steel profiles.

Table 6.8 Individual and total cost necessary to fully restore one fork at the top of the lateral or central column in the case of DS-1.

	Description	Unit of measure	Quantity	€ / unit	Total price
Material	Epoxy resin for injections	n. of pack	1,00	28,00	28,00
	n. 2 hot galvanized UPN 200 profiles	kg	36,00	2,20	79,20
	n. (6+6) ϕ12 chemical anchors	n.	12,00	3,00	36,00
	n. 2 hot galvanized 100x10mm plates	kg	10,00	2,20	22,00
	n. 2 hot galvanized shims (3 kg/each)	kg	6,00	2,20	13,20
	ϕ18 steel pin with nuts and washers	n.	2,00	10,00	20,00
Rental	Platform for working at height	h	3,00	18,75	56,25
Manpower	Specialized manpower	h	2,00	35,00	70,00
			Total cost of the installation		324,65

DS-2: Spalling of the cover

In this second damage state, a scenario with a significant cracking at the base of the fork, a wide spalling and relative movements between the structural elements is assumed. The fork shows the beginning of a plastic rotation at its base. The restore procedure foresees an increase in the stiffness of the fork through a confinement at its base with RC jacketing and it is the same for both fork at the top of lateral and central column (Table 6.9).

Table 6.9 Individual and total cost necessary to fully restore one fork at the top of the lateral or central column in the case of DS-2.

	Description	Unit of measure	Quantity	€ / unit	Total price
Material	Concrete for restoring	m^3	1,00	160,00	160,00
	n. 2 hot galvanized UPN 200 profiles	kg	36,00	2,20	79,20
	n. (6+6) ϕ12 chemical anchors	n.	12,00	3,00	36,00
	n. 2 hot galvanized 100x10mm plates	kg	10,00	2,20	22,00
	n. 2 hot galvanized shims (3 kg/each)	kg	6,00	2,20	13,20
	ϕ18 steel pin with nuts and washers	n.	2,00	10,00	20,00
Rental	Platform for working at height	h	5,00	18,75	93,75
Manpower	Specialized manpower	h	5,00	35,00	175,00
			Total cost of the installation		599,12

DS-3: Rupture of the fork

In the third damage state, the scenario shows that the seismic excitation leads to the collapse of the fork, and therefore of the supported beam and the overhead roof elements. The retrofit procedure is aimed to restore the collapsed structural elements as in the pre-earthquake configuration.

When the fork at the top of the lateral column undergoes collapse, one supported main beam and 16 roof elements undergo collapse too. The economic losses shown in Table 6.10 are then calculated considering the collapse suffered by all these vulnerable elements.

Table 6.10 Individual and total cost necessary to fully restore the structural layout in the case of collapse of the fork at the top of the lateral column as expected for the DS-3.

	Description		Unit of measure	Quantity	€ / unit	Total price
Disposal	Landfilling of the inert, including loading and transportation	Fork	€ / m^3	0,11	18,70	2,02
		Beam		6,12		114,44
		Roof element		19,68		368,02
Charges	Charges and landfill taxes for inert		€ / t	64,77	13,50	874,40
Material	Assembled steel fork		kg	401,14	2,20	882,50
	ϕ18 steel pin with nuts and washers		n.	2,00	10,00	20,00
	n. 2 hot galvanized shims (3 kg/each)		kg	6,00	2,20	13,20
	n. (6+6) ϕ12 chemical anchors		n.	12,00	3,00	36,00
Subject	RC or precast double slope beam (slope between 10 and 12%) with a double-T section along the length and a rectangular section at the ends, total length of 20m and interaxes in the range between 8 and 12m		m	20,00	269,92	5398,30
	Precast roof element with a π-section, calculated with a simple restrain at the ends and an overload of 200kg/m2, a total length up to 10m		m^2	160,00	37,04	11852,80
				Total cost of the installation		19561,67

Concerning the third damage state of the fork at the top of the central column, the number of the elements which collapse following the collapse of the fork itself are

different in quantities compared to the fork at the top of the lateral column (Table 6.11). In this case, the individual and total cost necessary to fully restore the structural layout are assessed by considering two main supported beams and 32 roof elements.

Table 6.11 Individual and total cost necessary to fully restore the structural layout in the case of collapse of the fork at the top of the central column as expected for the DS-3.

	Description		Unit of measure	Quantity	€ / unit	Total price
Disposal	Landfilling of the inert, including loading and transportation	Fork	€ / m^3	0,11	18,70	2,02
		Beam		12,24		228,89
		Roof element		39,36		736,03
Charges	Charges and landfill taxes for inert		€ / t	129,27	13,50	1745,15
Material	Assembled steel fork		kg	401,14	2,20	882,50
	ϕ18 steel pin with nuts and washers		n.	2,00	10,00	20,00
	n. 2 hot galvanized shims (3 kg/each)		kg	6,00	2,20	13,20
	n. (6+6) ϕ12 chemical anchors		n.	12,00	3,00	36,00
Subject	RC or precast double slope beam (slope between 10 and 12%) with a double-T section along the length and a rectangular section at the ends, total length of 20m and interaxes in the range between 8 and 12m		m	40,00	269,92	10796,60
	Precast roof element with a π-section, calculated with a simple restrain at the ends and an overload of 200kg/m2, a total length up to 10m		m^2	640,00	37,04	23705,60
				Total cost of the installation		38165,98

6.1.3 *Beam-to-roof element joint*

The beam-to-roof element joint relies only on frictional forces at the interfaces between the same two structural elements. In this case, the damage states taken into account are not about the status of the structural element section (cracking, yielding, spalling or collapse) but rather they are fixed and linked to the relative displacement between the support beam and the roof element. Small relative displacement, intermediate relative displacement and high relative displacement with loss of the support are set as DS-1, DS-2 and DS-3 respectively.

In order to define the damage states for the beam-to-roof element joint, the chosen EDP is the relative displacement between the support beam and the roof element themselves. In Table 6.12, the values of EDP at each DS are shown.

Table 6.12 Value of EDP at each damage state identified for the beam-to-roof element joint.

Damage State	Description	Limit value of EDP Relative displacement (cm)
DS-1	Small relative displacement	$\Delta < 4$
DS-2	Intermediate relative displacement	$4 < \Delta < 8$
DS-3	High relative displacement and loss of support	$\Delta > 8$

DS-1: Small relative displacement

The relative displacement between the support beam and the roof element is observed. Restore procedure is given by providing a wire to reduce and avoid future relative displacements. Furthermore, on the upper face of the roof element, the restoring of the sealant and the sheath over 25% of the perimeter of the roof element itself (for a width of 50cm) must be carried out.

Table 6.13 Individual and total cost necessary to fully restore and improve the beam-to-roof element joint in the case of DS-1.

	Description	Unit of measure	Quantity	€ / unit	Total price
Material	Waterproofing layer with bitumen-polymer elastomeric membrane	m^2	2,63	6,19	16,25
	Connecting wire	n.	2,00	2,50	5,00
	Slotted steel elements	n.	16,00	0,50	8,00
	Threaded bars	n.	1,00	4,00	4,00
	Chemical resin	n. of pack	1,00	10,00	10,00
Rental	Platform for working at height	h	2,00	18,75	37,50
Manpower	Specialized manpower	h	2,00	35,00	70,00
			Total cost of the installation		150,75

DS-2: Intermediate relative displacement

In this case, a relative displacement between the support beam and the roof element is still observed and the restore procedure is the same as assumed for DS-1. An increase in surface area on the upper face of the roof element which needs to be repaired is now allowed: the sealant and the sheath to restore reach 100% of the perimeter of the roof element itself (for a width of 50cm).

Table 6.14 Individual and total cost necessary to fully restore and improve the beam-to-roof element joint in the case of DS-2.

	Description	Unit of measure	Quantity	€ / unit	Total price
Material	Waterproofing layer with bitumen-polymer elastomeric membrane	m^2	10,50	6,19	65,00
	Connecting wire	n.	2,00	2,50	5,00
	Slotted steel elements	n.	16,00	0,50	8,00
	Threaded bars	n.	1,00	4,00	4,00
	Chemical resin	n. of pack	1,00	10,00	10,00
Rental	Platform for working at height	h	2,00	18,75	37,50
Manpower	Specialized manpower	h	2,00	35,00	70,00
			Total cost of the installation		199,50

DS-3: High relative displacement and loss of the support

In the third damage state, the relative displacements between the support beam and the roof element lead to the loss of support and consequently the collapse of the roof elements themselves. The retrofit procedure includes the restoring of the collapsed roof elements and the installation of a safety system with wires.

Table 6.15 Individual and total cost necessary to fully restore and improve the beam-to-roof element joint in the case of DS-3.

	Description	Unit of measure	Quantity	€ / unit	Total price
Disposal	Landfilling of the inert, including loading and transportation Roof element	€ / m^3	1,23	18,70	23,00
Charges	Charges and landfill taxes for inert	€ / t	3,08	13,50	41,51
Material	Connecting wire	kg	2,00	10,00	20,00
	Slotted steel elements	n.	16,00	1,30	20,80
	Threaded bars	kg	1,00	8,00	8,00
	Chemical resin	n.	1,00	10,00	10,00
Subject	Precast roof element with a ⌐-section, calculated with a simple restrain at the ends and an overload of 200kg/m2, a total length up to 10m	m^2	20,00	37,04	740,80
Rental	Platform for working at height	h	2,00	18,75	37,50
	Telescopic crane	h	1,50	177,00	265,50
Manpower	Specialized manpower	h	2,00	35,00	70,00
			Total cost of the installation		1237,11

6.1.4 Structure-to-cladding panel connection

By taking into account the 2,5x9x0,15m vertical precast cladding panels of the case study as shown in Chapter 4, the damage states and the individual total cost necessary to fully restore the damaged structure-to-cladding panel connection are defined. The panels are connected with the structure at their top through metallic fastenings reported in Figure 6.2, which the characteristics are adopted equal to what is shown in [Anže and Dolšek, 2016] for "*Fastenings B*". Two damage states are defined according to the status of the top structure-to-cladding panel connection: DS-1 when the yielding of the fastening is reached; and DS-2 when the rupture of the fastening and the subsequent collapse of the cladding panel occurs.

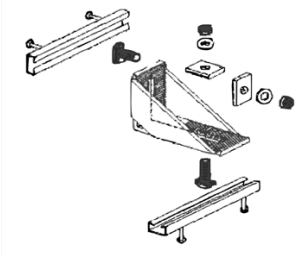

Figure 6.2 Example of fastening that can be adopted for the structure-to-cladding panel top connection. Specifications and characteristic are adopted by assuming the "Fastening B" type as shown in [Anže and Dolšek, 2016].

In order to define the damage states for the structure-to-cladding panel top connection, the chosen EDP is the relative displacement between the structure and the cladding panel assessed at its top. In Table 6.16, the values of EDP at each DS are shown.

Table 6.16 Value of EDP at each damage state identified for the structure-to-cladding panel connection.

Damage State	Description	Limit value of EDP Relative displacement (mm)* *data adopted from [Anže and Dolšek, 2016]
DS-1	Yielding of the top connection	$\Delta = 5$
DS-2	Rupture of the connection and fall of the cladding panel	$\Delta = 40$

DS-1: Yielding of the top connections

The damage is due to the yielding of the two top connections and there is no overturning of the cladding panel. The restore procedure consists of providing metal brackets, which help the yielded connections support the cladding panel.

Table 6.17 Individual and total cost necessary to fully restore the top structure-to-cladding panel connection in the case of DS-1.

	Description	Unit of measure	Quantity	€ / unit	Total price
Material	Galvanized slotted steel bracket	kg	12,00	3,50	42,00
	ϕ12 Threaded bars	m	1,50	6,00	9,00
	Plates for external side	kg	4,00	3,50	14,00
	Bolts and nuts	n.	12,00	0,35	4,20
	Chemical resin	n. of pack	2,00	10,00	20,00
Rental	Platform for working at height	h	2,00	18,75	37,50
Manpower	Specialized manpower	h	2,00	35,00	70,00
			Total cost of the installation		196,70

DS-2: Rupture of the connections and fall of the cladding panel

The damage that occurs consists of the collapse of the top connections and then the collapse of the cladding panel caused by high displacement not supported by the

existing brackets. The restore procedure consists of a cleaning operation of the yard, the disposal of the aggregates, the installation of a new panel and new connections.

Table 6.18 Individual and total cost necessary to fully restore the top structure-to-cladding panel connection in the case of DS-2.

	Description	**Unit of measure**	**Quantity**	**€ / unit**	**Total price**
Disposal	*Landfilling of the inert, including loading and transportation*	*€ / m^3*	*3,00*	*18,70*	*56,10*
Charges	*Charges and landfill taxes for inert*	*€ / t*	*7,50*	*35,00*	*262,50*
Subject	*Supply and installation of precast concrete cladding panels, thickness 15cm reinforced with a B450C welded mesh and trellis checked in the factory, covered with stone slabs (these separately measured)*	*m^2*	*20,00*	*82,00*	*1664,40*
			Total cost of the installation		*1963,00*

6.1 References

Anže, B., Dolšek, M. [2016] "Seismic Fragility Functions of Industrial Precast Building Classes", Engineering Structures, Vol. 118, pp. 357–370.

Protezione Civile, Reluis, CNI, ASSOBETON. [2012] "Prezziario di Riferimento per gli Interventi Locali e Globali su Edifici Industriali Monopiano non Progettati con Criteri Antisismici di cui alle Linee di Indirizzo del 19.06/2012, v.1.0", Ufficio Tecnico del Genio Civile di Area Vasta Arezzo, Firenze, Prato e Pistoia, Regione Toscana, Italia.